INVESTIGATION OF THE POTENTIAL SEPARATION OF ISOMERS AND RELATED COMPOUNDS USING HOST COMPOUND (2*R*,3*R*)-(−)-2,3-DIMETHOXY-1,1,4,4-TETRAPHENYLBUTANE-1,4-DIOL

P.L. POHL

Nelson Mandela University

2017

INVESTIGATION OF THE POTENTIAL SEPARATION OF ISOMERS AND RELATED COMPOUNDS USING HOST COMPOUND (2*R*,3*R*)-(−)-2,3-DIMETHOXY-1,1,4,4-TETRAPHENYLBUTANE-1,4-DIOL

by

PIETER LOURENS POHL

Submitted in fulfilment of the requirements of the degree of

PHILOSOPHIAE DOCTOR

In the Faculty of Science to be awarded at the Nelson Mandela University,

South Africa

2017

PROMOTOR: DR. B. BARTON

NELSON MANDELA UNIVERSITY

DECLARATION BY CANDIDATE

NAME: Pieter Lourens Pohl

STUDENT NUMBER: 210018372

QUALIFICATION: Ph.D Chemistry

TITLE OF PROJECT: Investigation of the potential separation of isomers and related compounds using host compound (2*R*,3*R*)-(–)-2,3-dimethoxy-1,1,4,4-tetraphenylbutane-1,4-diol

DECLARATION:

In accordance with Rule G5.6.3, I hereby declare that the above-mentioned treatise/ dissertation/ thesis is my own work and that it has not previously been submitted for assessment to another University or for another qualification.

SIGNATURE: _____

DATE: _____

Acknowledgements

The author wishes to express his sincere thanks to:

– Dr. B. Barton for her guidance, commitment, perseverance and enthusiasm throughout this project.

– Dr. E Hosten for running of SCXRD experiments.

– Mr L. Bolo for help with thermal analysis experiments.

– Mr. E. Bashman for his assistance.

– Sasha-Lee Dorfling and Daniel Jooste for their friendship and love, without which, this project would have never been.

– The financial assistance of the National Research Foundation (NRF) towards this research is hereby acknowledged. Opinions expressed and conclusions arrived at are those of the author and are not necessarily to be attributed to the NRF.

Publications and Conferences

- Chapter 3 of this thesis has been published: Barton, B., Hosten, E. C. and Pohl, P. L., Host (−)-(2*R*,3*R*)-2,3-Dimethoxy-1,1,4,4-tetraphenylbutane-1,4-diol and guests aniline, *N*-methylaniline and *N*,*N*-dimethylaniline: A Selectivity Study, *Aust. J. Chem.*, 2017, DOI: 10.1071/CH17532.

- Chapter 4 of this thesis has been published: Barton, B., Hosten, E. C. and Pohl, P. L., Discrimination between *o*-xylene, *m*-xylene, *p*-xylene and ethylbenzene by host compound (*R*,*R*)-(–)-2,3-dimethoxy-1,1,4,4-tetraphenylbutane-1,4-diol, *Tetrahedron*, 2016, *72* (49), 8099–8105.

- Chapter 4 of this thesis was presented as a poster at the 18th Tetrahedron Symposium, Asia Edition held in Melbourne, Australia, on the 24–26th July 2017. The poster title was “Discrimination between *o*-xylene, *m*-xylene, *p*-xylene and ethylbenzene by host compound (*R,R*)-(–)-2,3-dimethoxy-1,1,4,4-tetraphenylbutane-1,4-diol”.

Contents

Acknowledgements ..... **iii**

Publications and Conferences ..... **iv**

Summary ..... **x**

Abbreviations and Symbols ..... **xii**

Chapter 1: Introduction **1**

1.1 Isomers 1

1.2 Isomer Separation 4

1.3 Host-guest Chemistry 8

1.3.1 Uses of Host Compounds 9

1.3.2 Formation and Decomposition of Inclusion Complexes 11

1.3.3 Host-guest Thermodynamics 12

1.4 Host Compound Design 15

1.4.1 Cyclodextrins 15

1.4.2 Crown Ethers 21

1.4.3 Calixarenes 22

1.4.4 Fluorene Hosts 25

1.4.5 Xanthenyl Hosts 26

1.4.6 Metal-based Hosts 27

1.4.6 Diol Hosts 29

1.4.7 Wheel-and-axle Hosts 35

1.4.8 TADDOL Hosts 42

1.4.9 TETROL Hosts 44

1.5 Aims and Objectives 48

Chapter 2: Experimental **50**

2.1.1 General Analysis 50

2.2.1 General Procedure for the Grignard Reactions 51
2.2.2 (+)-(2*R*,3*R*)-1,1,4,4-Tetraphenylbutane-1,2,3,4-tetraol (**69**)..... 52
2.3.1 General Procedure for *O*-Methylation Reactions 52
2.3.2 (–)-(2*R*,3*R*)-2,3-dimethoxy-1,1,4,4-tetraphenylbutane-1,4-diol (**73**)..... 53
2.3.3 *p*-Methylanisole 54
2.3.4 *m*-Methylanisole 54
2.3.5 *o*-Methylanisole 55
2.4.1 Formation of Single Solvent Inclusion Complexes..... 56
2.4.2 Competition Inclusion Experiments 56
2.5.1 Hirshfeld Surface Analysis..... 59
2.5.2 Computational Studies..... 60
2.6.1 GC/MS Methods 60

Chapter 3: Inclusion Compounds of DMT (73) with Aniline and the *N*-Alkylated Anilines 62

3.1 Introduction 62
3.2 Individual and Equimolar Binary and Ternary Inclusion Experiments..... 63
3.3 Host Selectivity Profiles with Changing Guest Concentrations in Binary and Ternary Guest Mixtures..... 65
3.4 Thermal analysis 69
3.5 Single Crystal X-Ray Analysis..... 73
3.6 Hirshfeld Surface Analysis 92
3.7 Conclusion 95

Chapter 4: Inclusion Compounds of DMT (73) with the Xylene Isomers and Ethylbenzene 96

4.1 Introduction 96
4.2 Individual and Equimolar Inclusion Experiments 97
4.3 Host Selectivity Profiles with Changing Guest Concentrations in Binary and Ternary Guest Mixtures..... 99

4.4 Thermal Analysis 106
4.5 Single Crystal X-Ray Analysis 111
4.6 Hirshfeld Surface Analysis 126
4.7 Conclusion 128
Chapter 5: Inclusion Compounds of DMT (73) with Aniline and the Toluidine Isomers 129
5.1 Introduction 129
5.2 Individual and Equimolar Inclusion Experiments 130
5.3 Host Selectivity Profiles with Changing Guest Concentrations in Binary and Ternary Guest Mixtures 132
5.4 Thermal Analysis 139
5.5 Single Crystal X-Ray Analysis 144
5.6 Hirshfeld Surface Analysis 155
5.7 Conclusion 157
Chapter 6: Inclusion Compounds of DMT (73) with Toluene, Ethylbenzene and Cumene 158
6.1 Introduction 158
6.2 Individual and Equimolar Inclusion Experiments 159
6.3 Host Selectivity Profiles with Changing Guest Concentrations in Binary and Ternary Guest Mixtures 162
6.4 Thermal Analysis 166
6.6 Hirshfeld Surface Analysis 182
6.7 Conclusion 184
Chapter 7: Inclusion Compounds of DMT (73) with Nitrobenzene and the Nitrotoluene Isomers 185
7.1 Introduction 185
7.2 Individual and Equimolar Inclusion Experiments 186

7.3 Host Selectivity Profiles with Changing Guest Concentrations in Binary and Ternary Guest Mixtures 188
7.4 Thermal Analysis 195
7.5 Single Crystal X-Ray Analysis 200
7.6 Hirshfeld Surface Analysis 213
7.7 Conclusion 216
Chapter 8: Inclusion Compounds of DMT (73) with Anisole and the Methylanisole Isomers 217
8.1 Introduction 217
8.2 Individual and Equimolar Inclusion Experiments 218
8.3 Host Selectivity Profiles with Changing Guest Concentrations in Binary and Ternary Guest Mixtures 220
8.4 Thermal Analysis 227
8.5 Single Crystal X-Ray Analysis 232
8.6 Hirshfeld Surface Analysis 246
8.7 Conclusion 248
Chapter 9: Inclusion Compounds of DMT (73) with the Cresol Isomers 249
9.1 Introduction 249
9.2 Individual and Equimolar Inclusion Experiments 250
9.3 Host Selectivity Profiles with Changing Guest Concentrations in Binary and Ternary Guest Mixtures 252
9.4 Thermal Analysis 256
9.5 Single Crystal X-Ray Analysis 260
9.6 Hirshfeld Surface Analysis 272
9.7 Conclusion 274
Chapter 10: Miscellaneous 276
10.1 Other Inclusions 276
10.2 Computational Analysis 278

10.3 DMT Single Crystal X-Ray Analysis 281
10.4 Isostructurality of Inclusion Compounds 285
Chapter 11: Conclusion and Future Work 291
11.1 Conclusion 291
11.2 Future Work 294
References 296

Summary

In this study, we investigated the potential of a host compound, (2*R*,3*R*)-(−)-2,3-dimethoxy-1,1,4,4-tetraphenylbutane-1,4-diol (DMT), for use in the separation of isomers and related compounds using host-guest chemistry.

The title molecule, DMT, is composed of a butane chain bearing hydroxyl moieties on the terminal carbons and methoxy moieties on the two internal, chiral carbon atoms. In addition, there are two phenyl rings on each of the terminal carbons.

The synthesis of DMT was carried out by subjecting the diester of naturally-occurring optically active tartaric acid to a Grignard reaction employing phenylmagnesium bromide. Subsequent methylation of the secondary hydroxy groups with dimethyl sulfate afforded DMT.

The resulting host molecule was investigated for its inclusion abilities by crystallizing with a number of potential aromatic, aliphatic and alicyclic guests such as toluene, aniline, nitrobenzene, anisole, cyclohexane, ethyl acetate and ethanol. Host:guest ratios were determined by means of ^{1}H-NMR spectroscopy.

Of the hosts investigated, DMT favoured a host:guest ratio of 2:1 for all included guests investigated. It complexed with most non-polycyclic aromatic guests as well as cyclohexane, cyclohexene and cyclohexanone. It was not able to include short chain or branched alcohols such as methanol, ethanol or 2-propanol, or other hetero-aliphatic or hetero- cyclic compounds such as diethyl ether, acetonitrile, morpholine or dioxane.

Competition inclusion experiments were performed in which DMT was crystallized from equimolar and non-equimolar binary, ternary and quaternary mixtures of appropriate guests. The mother liquor mixtures and resultant crystals were subjected to GC-MS analysis in order to determine whether DMT showed discriminatory behaviour towards the guests from a mixture. It was observed that DMT was able to differentiate between related compounds, for example, the host preferred to include *N,N*-dimethylaniline compared with *N*-methylaniline and aniline. The host also discriminated against isomers, for example, *p*-xylene was preferentially included over

o-xylene and *m*-xylene, while *o*-cresol was included in preference to *p*-cresol and *m*-cresol.

Single crystal X-ray analysis was used to investigate the host–guest interactions responsible for guest inclusion, as well as to discern reasons for the host's selective behaviour. X-ray data for the inclusion complexes indicated that each complex was isostructural, crystallizing in the monoclinic *C*2 crystal system. A pair of 1,3- and 2,4-intramolecular hydrogen bonds, as well as intramolecular non-classic hydrogen bonds between adjacent *ortho*-aromatic hydrogens and hydroxy moieties was a significant stabilizing factor for the geometry of the host. Guests were held within discrete cavities in the crystal lattice, and experienced only π–π stacking, CH–π interactions and other short contacts.

Thermal analyses were used to determine the relative thermal stabilities of the complexes, and these data compared to the selectivity preference of DMT, obtained from the competition experiments, in order to assess the reasons for any discriminatory behaviour. Finally, Hirshfeld surface analysis data was used to determine if the thermal stability of the complexes was related to the number and type of interactions between host and guest.

Key Words:

- Host-Guest Chemistry
- Clathrate
- Isomer Separation
- Thermal Analysis
- SCXD
- Hirshfeld Surface

Abbreviations and Symbols

H	Host
G	Guest
π–π	pi–pi
CH–π	CH–pi
TADDOL	α,α,α',α'-Tetraphenyl-2,2-dimethyl-1,3-dioxolan-4,5-dimethanol
TETROL	(+)-(2*R*,3*R*)-1,1,4,4-Tetraphenylbutane-1,2,3,4-tetraol
DMT	(−)-(2*R*,3*R*)-2,3-Dimethoxy-1,1,4,4-tetraphenylbutane-1,4-diol
T_{on}	Onset temperature of mass loss
T_b	Boiling point of a pure liquid guest
T_p	Peak temperature of mass loss
T_{end}	Peak endotherm temperature
NMA	*N*-Methylaniline
DMA	*N,N*-Dimethylaniline
oX	*ortho*-Xylene
mX	*meta*-Xylene
pX	*para*-Xylene
EB	Ethylbenzene
o-TD	*ortho*-Toluidine
m-TD	*meta*-Toluidine
p-TD	*para*-Toluidine
o-NT	*ortho*-Nitrotoluene
m-NT	*meta*-Nitrotoluene
p-NT	*para*-Nitrotoluene
o-MA	*ortho*-Methylanisole
m-MA	*meta*-Methylanisole
p-MA	*para*-Methylanisole
o-CR	*ortho*-Cresol
m-CR	*meta*-Cresol
p-CR	*para*-Cresol
TG	Thermogravimetry

DSC	Differential Scanning Calorimetry
^{1}H-NMR	Proton Nuclear Magnetic Resonance
GC-MS	Gas Chromatography / Mass Spectroscopy
K	Selectivity coefficient
X	Mole fraction of guest in the mother liquor
Z	Mole fraction of guest in the crystal
PXRD	Powder X-Ray Diffraction
SCXD	Single Crystal X-Ray Diffraction
a, b, c	Unit cell axes
α	Angle between b and c unit cell axes
β	Angle between a and c unit cell axes
γ	Angle between a and b unit cell axes
V	Unit cell volume
Z	Number of formula units per cell

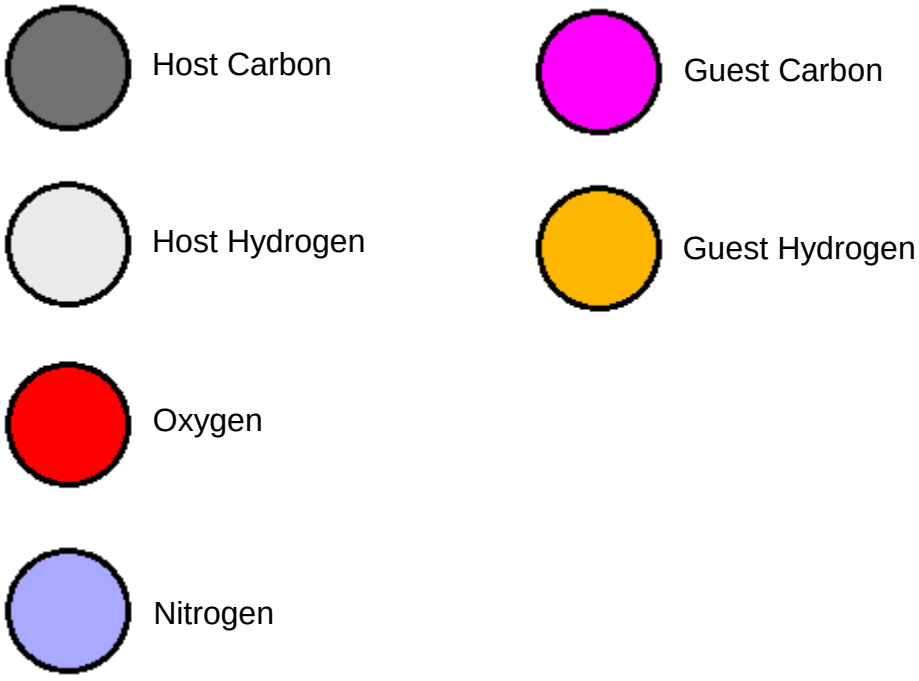

Chapter 1: Introduction

1.1 Isomers

There exists a plethora of terminology describing different isomers and their relation to one another. It is therefore important to explain and summarise the most commonly used terms.

At the top level, isomers can be separated into stereoisomers (or spatial isomers) and constitutional isomers (or structural isomers). The former can be further subdivided into enantiomers and diastereomers. The hierarchy of isomers is visualised in Figure 1.

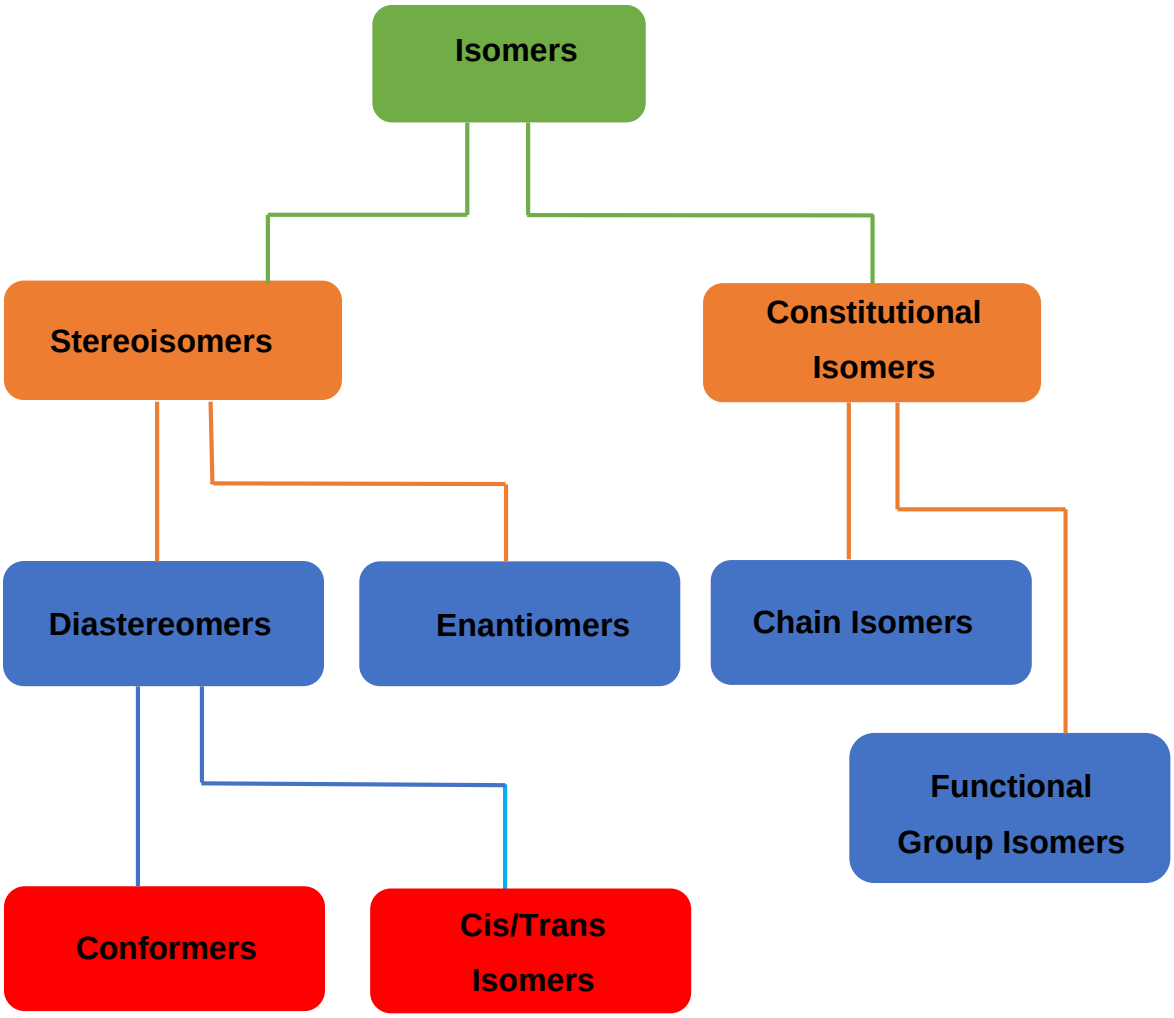

Figure 1: The hierarchy of isomers.

Stereoisomers contain chirality in most cases. Molecules containing chirality rotate the plane of plane-polarized light.[1] Chiral centres may be identified simply by the presence of four different substituents on a central carbon, sulphur or phosphorus atom (Figure 2). Furthermore, for a molecule to be chiral, it may not contain a plane, centre or rotation-reflection axis of symmetry.[2]

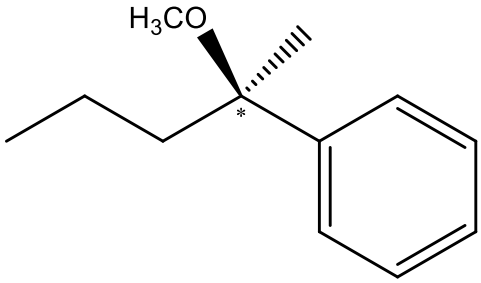

Enantiomers arise when two molecules present as non-superimposable mirror images of each other. They often, but not always, contain a chiral centre (Figure 3). Spatially, the substituents on the chiral centre are arranged in a different manner.[3]

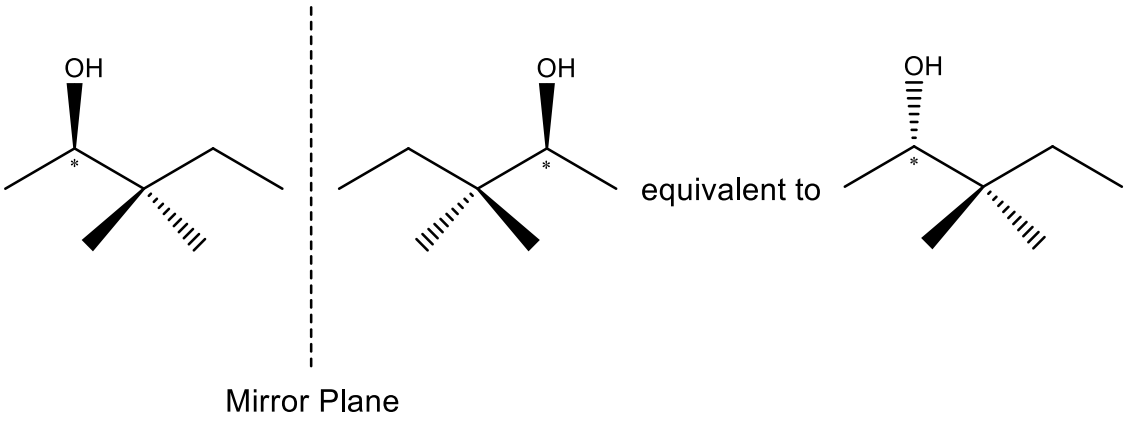

Figure 3: Enantiomers (on the left) projected across a mirror plane; these are non-superimposable mirror images.

Diastereomers are all stereoisomers that are not enantiomers – they are non-superimposable and are not mirror images of each other (Figure 4). They frequently contain a chiral centre, but not always since *cis-trans* and *E-Z* isomers are also diastereomers.[3]

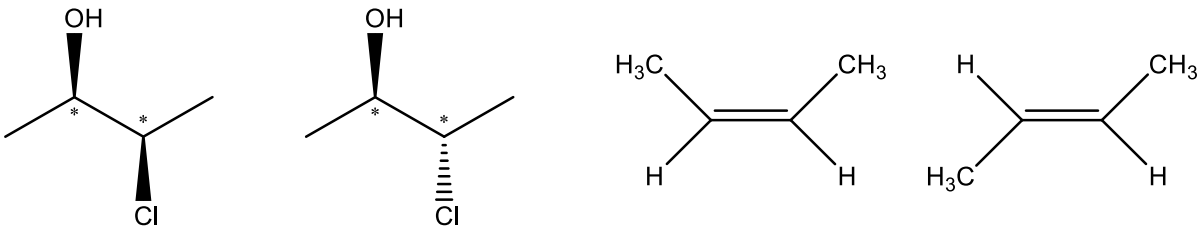

Figure 4: Examples of chiral and non-chiral diastereomer pairs.

Constitutional isomers are molecules that have the same empirical formula but different connectivity between atoms. These may take the shape of functional group isomerism (Figure 5) where the atoms that comprise one functional group are rearranged to form a different functional group.[4]

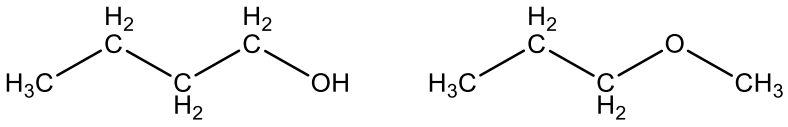

Figure 5: Functional group isomers of $C_4H_{10}O$, *n*-butanol and 1-methoxypropane.

Chain isomers contain different degrees of hydrocarbon chain branching. Simple examples are that of nonane and 3-ethylheptane (Figure 6). Both have the empirical formula C_9H_{20} but differ in the skeletal chain structure.

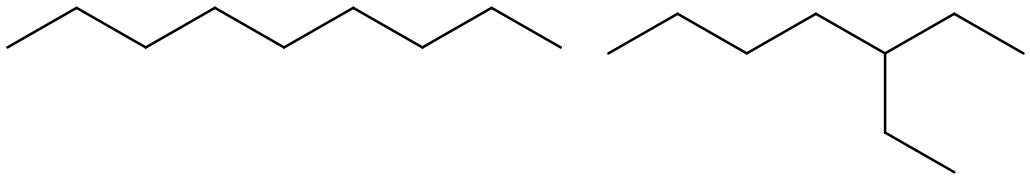

Figure 6: Two chain isomers of C_9H_{20}.

Finally, positional isomers, or regioisomers (Figure 7), differ only in the position of functional groups on the carbon backbone.[5] Positional isomers frequently have very similar physical properties such as melting points and boiling points, making their separation challenging.

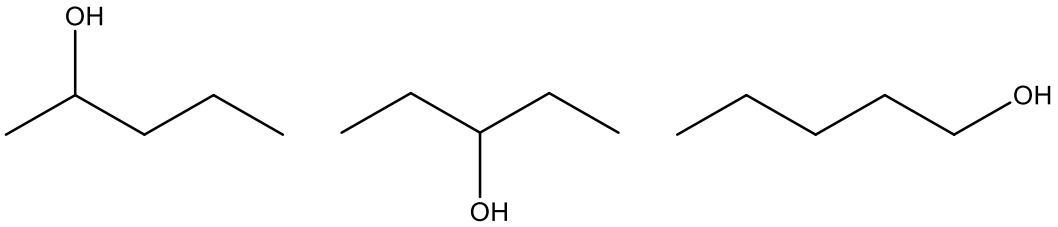

Figure 7: Three regioisomers of pentanol.

1.2 Isomer Separation

The ability to separate isomers is of vital importance to chemists. It is often necessary to obtain a compound in a pure form without the presence of any additional stereoisomers or constitutional isomers. The pharmaceutical industry has a vested interest in synthesising optically pure actives or purifying intermediates or end-products so that these are optically pure. Within a homogenous solution, enantiomers are found to possess the same chemical and physical properties, with the exception of the direction in which they rotate plane-polarized light.[6] However, *in vivo*, stereoisomers often differ in pharmacodynamic and pharmacokinetic properties. These include, but are not limited to, different absorption rates, bioavailability, distribution, metabolic rates and potency. For example, ibuprofen (Figure 8) is a

common racemic non-steroidal anti-inflammatory drug. The *S*-enantiomer is responsible for its anti-inflammatory properties, whereas the *R*-enantiomer is inactive. While the presence of the inactive enantiomer may be relatively innocuous in the case of ibuprofen, production of the single enantiomer of most drugs is still beneficial from an economic and side-effect point of view, as this would allow for the manufacture and consumption of what would essentially be a half dose.[7]

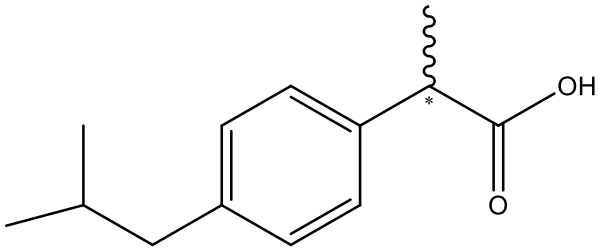

Figure 8: Racemic ibuprofen – a non-steroidal anti-inflammatory drug.

A classic example of different enantiomers bestowing beneficial and malignant effects is that of thalidomide (Figure 9). This drug was prescribed to pregnant women in the late 1950's to alleviate morning sickness. The active responsible for this therapeutic effect was the *R*-enantiomer. However, the drug was sold in racemic form, and the *S*-enantiomer was found to be teratogenic, resulting in thousands of babies being born with malformed limbs. Only 40% of these babies survived. Unfortunately, these two enantiomers interchange *in vivo* and, as such, prescription of even the pure *R*-enantiomer would not be safe for consumption during pregnancy.[8]

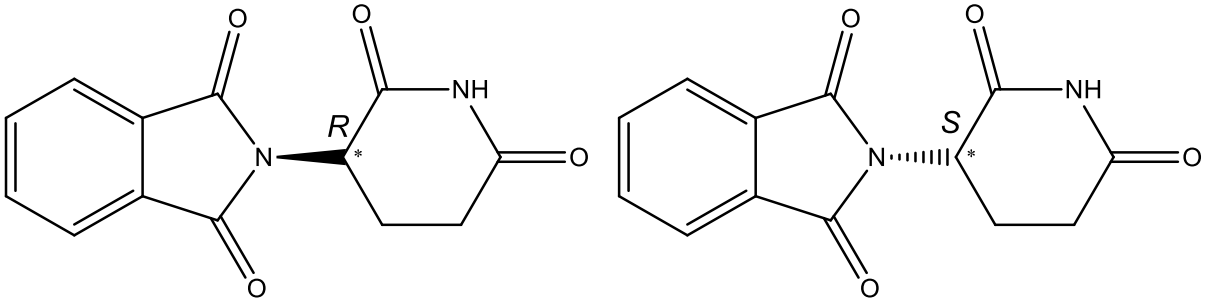

Figure 9: Thalidomide; the *R*-enantiomer (left) is a sedative and the *S*-enantiomer (right) is teratogenic.

Another such example is that of ethambutol, a drug routinely used to treat tuberculosis (Figure 10). *D*-Ethambutol is active as an anti-tuberculosis drug, whereas *L*-ethambutol is capable of causing blindness in patients.[9] This molecule also exists in the *meso* form which is not toxic but has a much lower activity than that of *D*-ethambutol.[10]

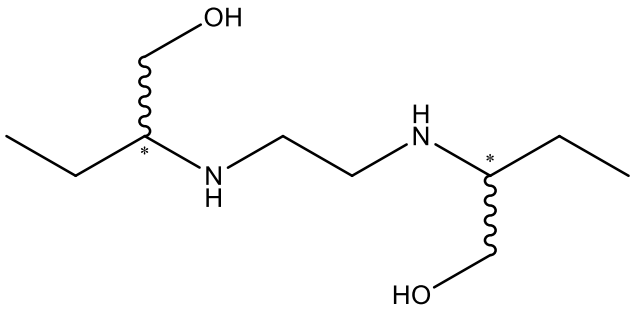

Figure 10: Ethambutol, an anti-tuberculosis drug.

Many positional isomers of aromatic and aliphatic compounds have specific, yet vastly different, uses. As such, it is necessary to isolate and purify each of these isomers. However, this may be complicated due to their similar physical properties. These include boiling points, melting points and polarities, which may complicate efforts when relying on the usual separation techniques such as distillation, crystallisation and chromatography, respectively.

To that end, many resources have been employed for effectively separating these isomers. In the case of the xylenes, the large-scale separation of the *para*- and *meta*-isomers only became feasible from the 1970's onwards as conventional fractional distillation was not economically feasible before then. Saito *et al*[11] separated *p*-xylene from *m*-xylene by continuously trans-alkylating *m*-xylene with 1,4-di-*tert*-butylbenzene while simultaneously fractionally distilling the resultant benzene and remaining *p*-xylene. Benzene was then trans-alkylated back to *m*-xylene. Scheme 1 represents the equilibrium reactions that occur simultaneously during the distillation process.

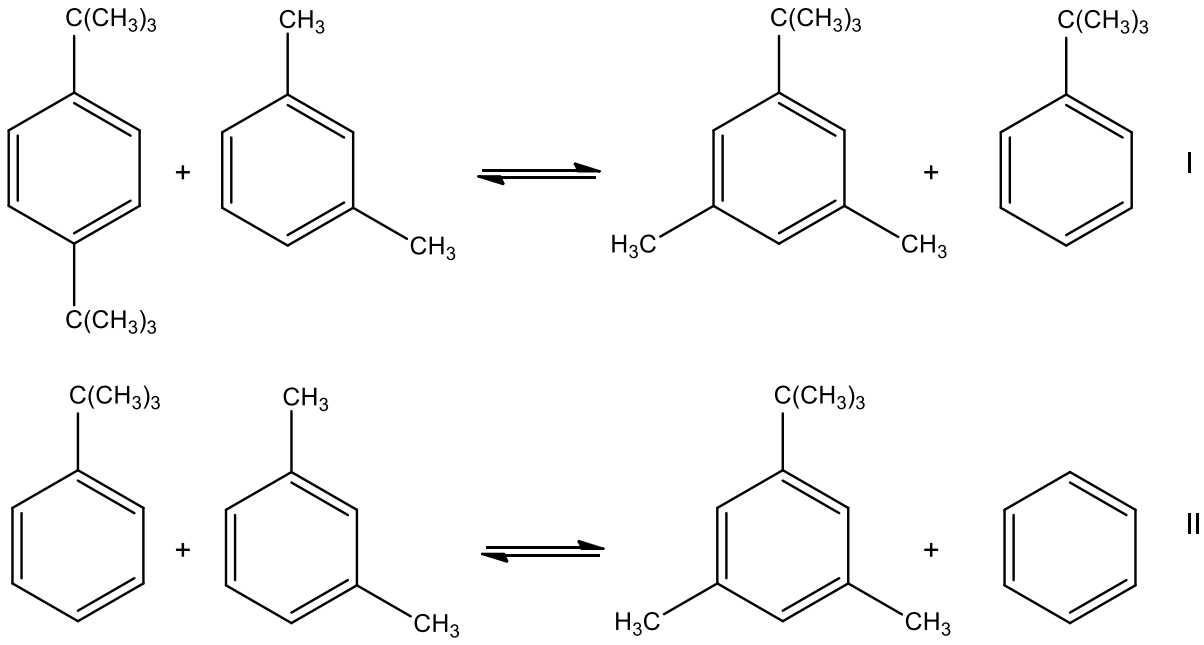

Scheme 1: Equilibrium reactions between di-*tert*-butylbenzene and *m*-xylene during fractional distillation.

More recently, the purification of *p*-xylene and *m*-xylene became feasible through a process called distillative freezing (DF). Using this technique, Shiau's research group obtained a 99.1% pure *p*-xylene sample.[12] DF works by creating triple-point conditions for the binary mixture under which the liquid mixture becomes solidified and vaporized at the same time. The solid phase consists entirely of one component of the mixture, while the vapour and liquid phases remain as mixtures. The vapour phase is removed through condensation and the process is continued until all the liquid phase disappears, leaving behind the pure, single component solid phase.[13,14]

Alternatively, metal-organic frameworks (MOFs) are experiencing a boom in interest due to their adsorption properties. These compounds are microporous crystalline coordination polymers with a predominantly organic inner surface that allows for selective adsorption of aromatic compounds within the pores.[15–18] The group of Alaerts *et al* investigated selected MOFs for their ability to discriminate between the C_8 aromatic isomers of xylene and ethylbenzene. The MOFs, Cu_3(benzene-1,3,5-tricarboxylate),[19] MIL-53[20] (aluminium-based) and MIL-47[21] (vanadium-based) were screened for their abilities to selectively adsorb these C8 aromatic isomers. Of the three, MIL-47 showed the greatest promise due to its hydrophobicity and high uptake

capacity. When packed into an HPLC column, it was able to achieve baseline separation of ethylbenzene, *m*-xylene and *p*-xylene.[22]

1.3 Host-guest Chemistry

The host-guest phenomenon can be described as the result of interactions between two or more different molecular species that are in close association with one another without forming covalent bonds. Host-guest complexes are typically held together by means of various non-covalent interactions,[23] such as:

- Van der Waals attractive forces,
- π–π interactions,
- CH–π interactions,
- Ion pairing, and
- Hydrogen bonding.

Historically, numerous terms have been used to name host-guest compounds, the most common of which are inclusion compounds, clathrates and host-guest complexes.[24] In general, hosts within the field of supramolecular chemistry are defined as the larger of the molecules involved in the complexation and having the ability to interact with the guest in a convergent manner, such as through hydrogen bond donation. Conversely, guests are traditionally seen as the smaller partner in the complex, capable of interacting with the host in a divergent manner, for example through hydrogen bond accepting interactions.[23]

Host-guest interactions may be present within the solid state and in solution. In the solid state, host-guest complexes are formed when the guest becomes entrapped within the host crystal. Before enclathration occurs, the guest may be present as a gas, liquid or solid.

1.3.1 Uses of Host Compounds

Host compounds have a wide variety of uses, the list of which is expanded upon constantly. However, there are certain fundamental uses of host compounds which exemplify the versatility of this branch of chemistry.

Some clathrate-forming compounds may be utilized in the development of molecular sensors. Host compounds based on tartaric acid, lactic acid and TADDOL have been used as vapour sensors capable of detecting ethanol, dichloromethane, tetrahydrofuran and acetone, to name a few.[25] Similarly, heterocyclic quinol-type hosts were developed as sensors that produce a change in fluorescence when subjected to the vapours of various organic solvents.[26–28] Carbon nanotubes functionalized with a host have been used as electrochemical sensors for herbicides,[29] while gold electrodes functionalized by a host have shown promise in detecting biomolecules such a dopamine through cyclic voltammetry.[30]

Host compounds may also be employed in the separation of isomers. Isomers are often difficult to separate industrially owing to their similar physical properties, such as boiling and melting points, which render distillations and selective crystallizations difficult and inefficient. A host compound may be found to selectively include one isomer over another which allows for the recovery of the included isomer by means of distillation or chromatography to separate it from the host.[31,32] More specifically, Nassimbeni *et al*[33] used host-guest chemistry to selectively enclathrate the xylene isomers. Three different host compounds **1–3** were screened during their research and found to discriminate between the xylene isomers. Host **1** had a preference for *o*-xylene when recrystallized from a binary mixture containing this isomer and *p*-xylene, despite including both *o*-xylene and *p*-xylene individually. Host **2** included *o*-xylene in preference to the other isomers from binary and ternary mixtures, while host **3** included *p*-xylene selectively.

Similarly, Caira *et al*[34] selectively formed a clathrate with xylenol isomers and host **4**. Typically, the 3,5-xylenol isomer was preferentially included by **4** when present in binary mixtures with either 2,6-xylenol or 2,3-xylenol. In the case of the latter binary mixture, 3,5-xylenol was only preferred once the concentration of 2,3-xylenol fell below 50%. Of all the isomers, 2,6-xylenol was the least preferred.

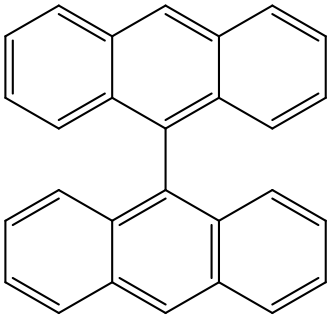

1

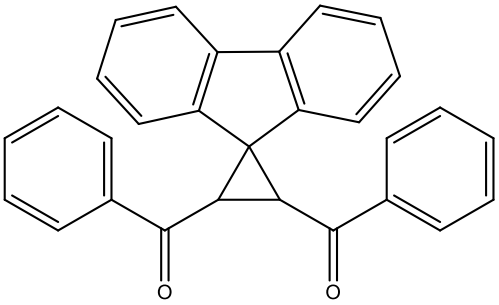

2

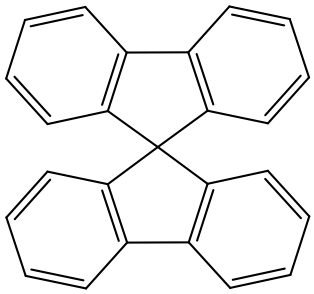

3

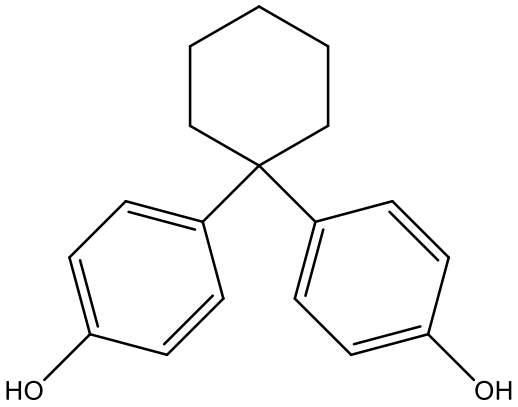

4

Furthermore, chiral and optically pure host compounds may be used to facilitate the separation of enantiomers from one another, either through the formation of complexes, or by means of the immobilization of the host on a stationary phase in chromatographic applications.[35–38]

Chiral host compounds can be utilized in NMR analysis as chiral solvating agents by forming diastereomeric complexes *in situ* with the enantiomers in question. Alternatively, chiral hosts may serve as chiral shift reagents which allow for the determination of the absolute configuration of enantiomers as well as the optical activity.[39–41]

Certain complexes may be engineered in such a way as to store volatile gases for later use. For example, hydroquinone is able to incorporate a variety of gaseous species such as CH_4, CO_2, N_2, C_2H_4 and SO_2.[42,43] The low-density β_0 polymorph of *p-tert*-butylcalix[4]arene is cable of storing CO_2, CH_4 and C_2H_4.[44] Syndiotactic

polystyrene polymer in the δ crystalline phase includes large amounts of CO_2 and C_4H_6 at room temperature, thereby forming a polymer/gas inclusion compound from which the release of gas may be controlled.[45] Hydrogen gas-storing compounds are perhaps the most sought after as a method of storage and release of the energy source of the future. Examples of hosts that enclathrate H_2 include the inorganic compound $Na_{5.5}(H_2)_{2.15}Si_{46}$ and hydroquinone.[46–48]

Macrocyclic host compounds often find use within the pharmaceutical industry as excipients for enhancing the delivery of drugs. This is especially true for the cyclodextrins which have low toxicity, good biocompatibility and are able to be functionalized, and have therefore proven themselves to be indispensable candidates for enhancing the solubility, bioavailability, stability and delivery of many drugs.[49–51]

1.3.2 Formation and Decomposition of Inclusion Complexes

The formation of solid state inclusion complexes can be accomplished relatively easily by dissolving the host as a solid in an excess of the desired solvated guest. The inclusion complex is then generated through crystal growth by means of slow evaporation of the guest solvent or through a reduction in temperature, effectively reducing the host solubility in the solvent.

It is also possible to form inclusion complexes in cases where the host is not soluble in the guest solvent, or where the guest itself is also a solid. A co-solvent (which is not included) may be added to the system to facilitate dissolution of both host and guest which, upon evaporation, may lead to complex formation. As the addition of a co-solvent significantly reduces the concentrations of both host and guest, it is recommended that crystallisation is induced under stirring conditions so as to ensure sufficient interaction between the host and guest components. In cases where the guest is present as a gas, optimal host-guest complex formation requires high pressures.[52]

The formation of inclusion compounds is promoted in the presence of thermodynamically favourable non-covalent inter- and intra- molecular forces. Upon inclusion, the guest is usually found to have lost some free vibrational and rotational

energy as well as all of its translational energy.[52] The total energy of complexation, $E_{complexation}$, can therefore be described as:[53]

$$\boldsymbol{E_{complexation} = E_{complex} - (E_{host}^{free} + E_{guest}^{free})} \qquad \textbf{Equation 1}$$

1.3.3 Host-guest Thermodynamics

The formation of inclusion complexes is exothermic in nature. The thermodynamics of host-guest complex formation is analysed by means of a variety of techniques,[54–57] the most prevalent of which are:

- Isothermal titration calorimetry,
- UV/Vis spectroscopy,
- Fluorescence spectroscopy,
- Nuclear magnetic resonance,
- Mass spectrometry, and
- Atomic force microscopy.

Menozzi *et al*[58] investigated the thermodynamic parameters of the host-guest complex formed between a phosphonate cavitand **5** and the methylpyridinium salts **6** and **7**. Through isothermal titration calorimetry experiments, the phosphonate cavitand yielded negative enthalpy and Gibbs free energy values upon complexation with the methylpyridinium guests. Enthalpy values ranged between –6.8 and –25.7 $kJ.mol^{-1}$, while Gibbs free energy values ranged between –26.3 and –39.2 $kJ.mol^{-1}$.

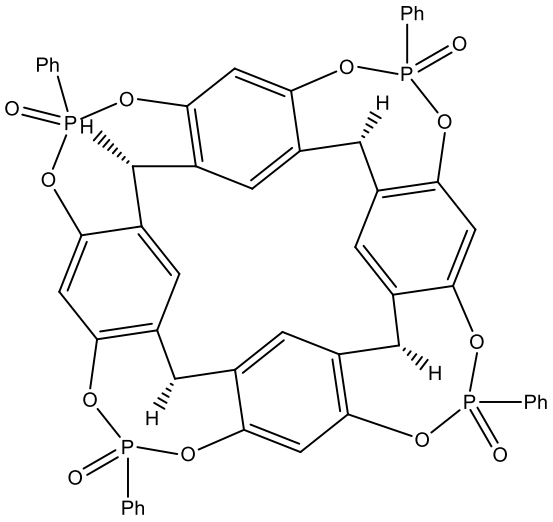

5

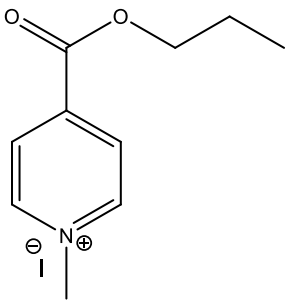

6

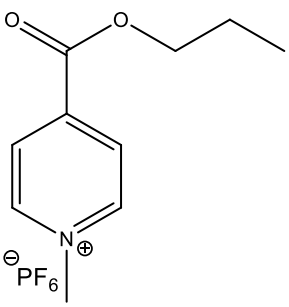

7

Similarly, the group of Schnatwinkel *et al*[59] set out to determine the thermodynamic properties of the complexes that form between pyrogallol[4]arene **8** and peralkylated ammonium cations **9–15**. Isothermal titration calorimetry was again employed to great effect to determine ΔH° values which ranged between –48 and –14 kJ.mol^{-1}, and ΔG° values ranged between –23.4 and –14.5 kJ.mol^{-1}.

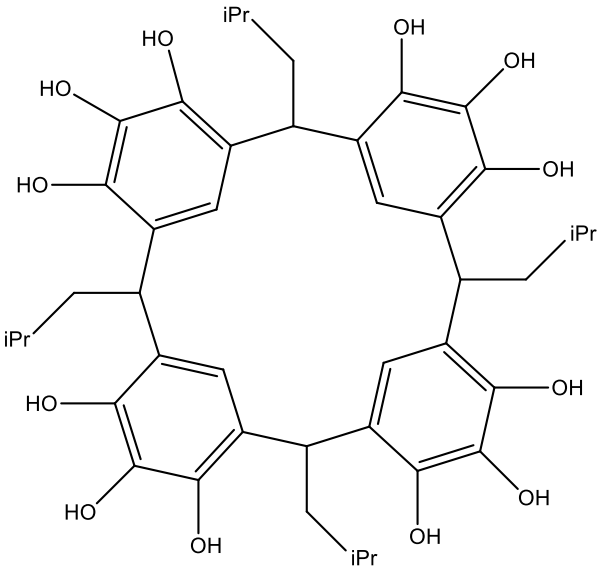

8

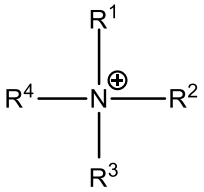

9 $R^1=R^2=R^3=R^4=CH_3$

10 $R^1=R^2=R^3=CH_3$, $R^4=CH_2CH_3$

11 $R^1=R^2=CH_3$, $R^3=R^4=CH_2CH_3$

12 $R^1=R^2=R^3=R^4=CH_2CH_3$

13 $R^1=R^2=CH_2CH_3$, $R^3=R^4=(CH_2)_2CH_3$

14 $R^1=R^2=R^3=R^4=(CH_2)_2CH_3$

15 $R^1=R^2=R^3=R^4=(CH_2)_3CH_3$

Fullerenes, or buckyballs, are spherical molecules comprised of only elemental carbon. They were speculated to exist long before Kroto *et al*[60] won a Nobel Prize for their discovery. The most abundant of the fullerenes is comprised of 60 carbon atoms forming a truncated icosahedron with 12 pentagonal faces and 20 hexagonal faces, much like a soccer ball (fullerene C_{60}, **16**). Each carbon atom has two single bonds and one double bond connecting it to 3 neighbouring carbon atoms. Fullerenes have been found to form 1:1 host:guest complexes with a curved-surface polycyclic aromatic hydrocarbon aptly named a buckycatcher (**17**). The convex nature of fullerene is complementary to the concave structure of the buckycatcher.[61,62] Isothermal titration calorimetry as well as NMR titration experiments at different temperatures indicated ΔH° values of about –1.87 and –4.61 kJ.mol^{-1} using chlorobenzene and toluene as solvents, respectively. In addition, ΔG° values in the same solvents were recorded as –3.98 and –4.77 kJ.mol^{-1}.[63]

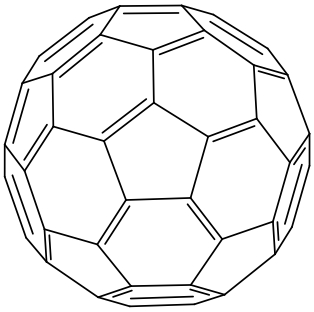

16

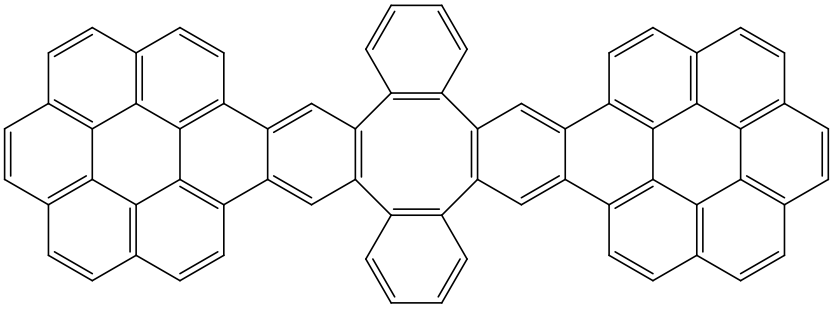

17

However, research by Green *et al*[64] into the viability of using cyclodextrin as a host for complexing chiral and achiral polycyclic aromatic hydrocarbons such as anthracene (**18**), as well as the two enantiomers of 1-(9-anthryl)-2,2,2-trifluoroethanol (TFE, **19-*S*** and **19-*R***), yielded interesting results. By utilising fluorescence spectrophotometry and multivariate regression analysis, they were able to calculate the thermodynamic properties of the inclusion complexes. The inclusions of **18** and **19-*S*** gave negative enthalpy values of –5.58 kJ.mol^{-1} and –41.62 kJ.mol^{-1}, respectively. The inclusion of **19-*R***, on the other hand, gave a positive enthalpy value of +2.75 kJ.mol^{-1}, which was attributed to the discrimination of the host against the guest based upon the chirality of the guest.

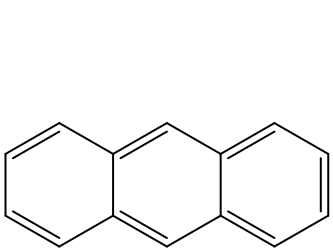

18

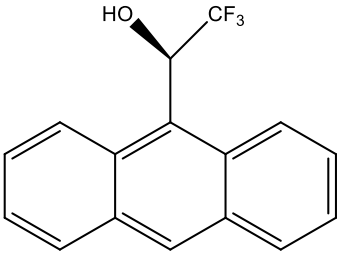

19-*S*

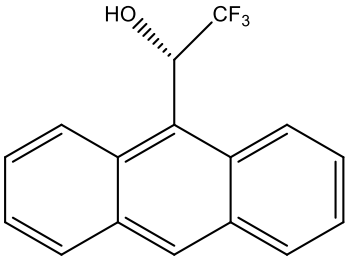

19-*R*

1.4 Host Compound Design

The number of host compounds designed to date is vast and therefore challenging to catalogue comprehensively. However, they may be categorized according to certain definite mechanistic and structural similarities.

1.4.1 Cyclodextrins

A review of host-guest chemistry would be incomplete without considering the cyclodextrins. These cylindrical molecules contain sizable hydrophobic intramolecular cavities, whilst maintaining a hydrophilic exterior.[65] Cyclodextrins are made up of *D*-glucopyranose units which are covalently bound to each other *via* α-1,4-linkages, thereby forming macrocyclic structures. The most common cyclodextrins are composed of six to eight glucopyranose residues, respectively named α-cyclodextrin **20**, β-cyclodextrin **21** and γ-cyclodextrin **22**.[66]

Table 1: Dimensional properties of α-, β- and γ- cyclodextrins.[66]

	α-CD (20)	β-CD (21)	γ-CD (22)
Number of glucopyranose residues	6	7	8
Molecular weight (g.mol^{-1})	973	1135	1297
Cavity diameter (Å)	4.7–5.3	6–6.6	7.5–8.5
Cavity height (Å)	7.9	7.9	7.9
Cavity volume (mL.mol^{-1})	174	262	472

In Table 1 is some of the physical parameters of cyclodextrins, indicating the increase in diameter and cavity volume as the number of glucopyranose units increase.

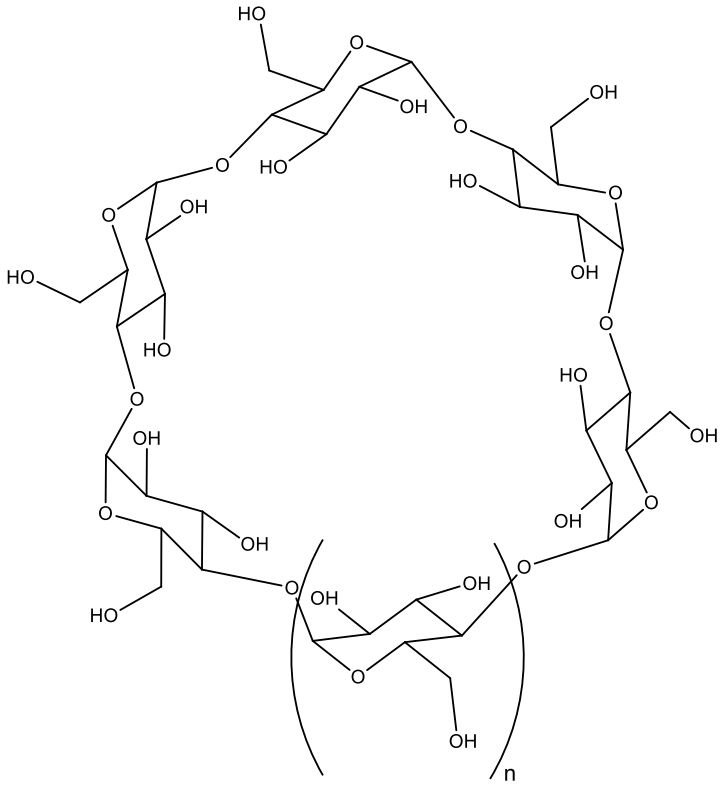

20 n = 1

21 n = 2

22 n = 3

Recent developments in the use of cyclodextrin-based host-guest chemistry include the work of Hu *et al*,[67] whose research group functionalized $CuInS_2$-based quantum dots with β-cyclodextrin. This allowed for the detection of ATP molecules *via* a

fluorescent response obtained once ATP bound to ATP-binding aptamers entered the cyclodextrin cavities during host-guest interactions (Scheme 2).

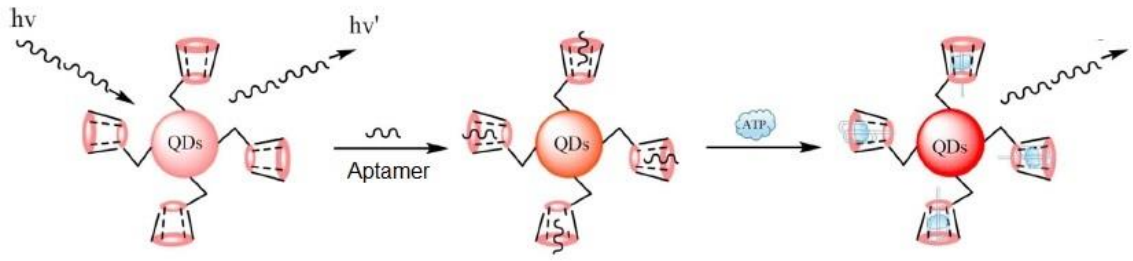

Scheme 2: Photoluminescence response brought about by aptamer-bound ATP host-guest interactions with cyclodextrin-functionalized quantum dots.[67]

Lu *et al*[68] investigated the abilities of cyclodextrins to facilitate the cellular uptake of anti-cancer drugs. The formation of a host-guest complex between 2-hydroxypropyl-β-cyclodextrin (**23**) and tetra-1,2-diethylamino-substituted zinc(II)phthalocyanine (**24**) in a 4:1 ratio resulted in increased *in vitro* anti-cancer activity as compared to the administration of **24** alone.

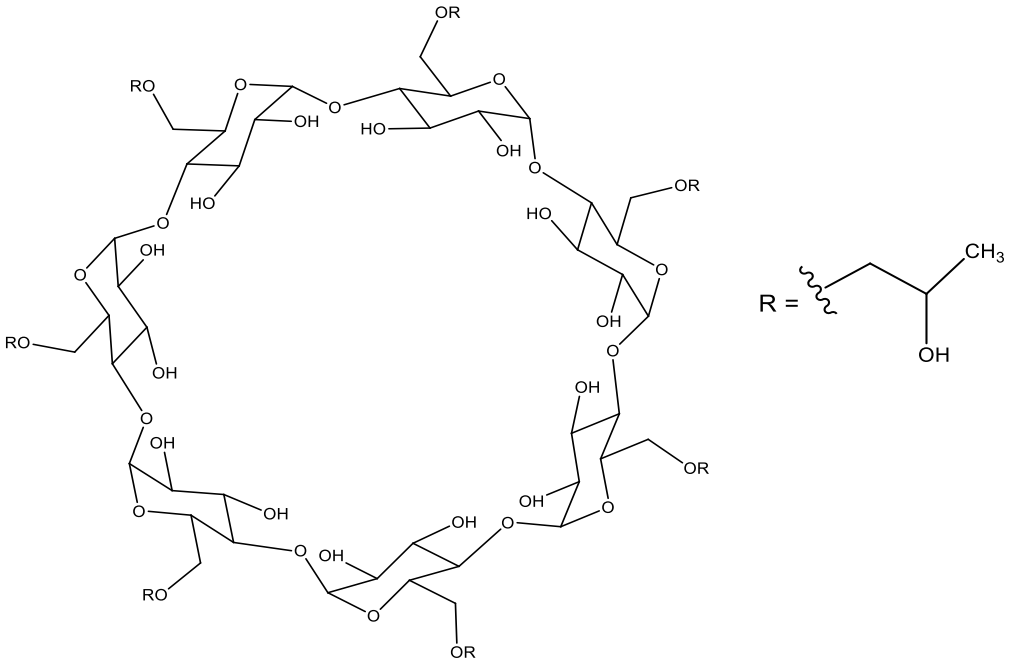

23

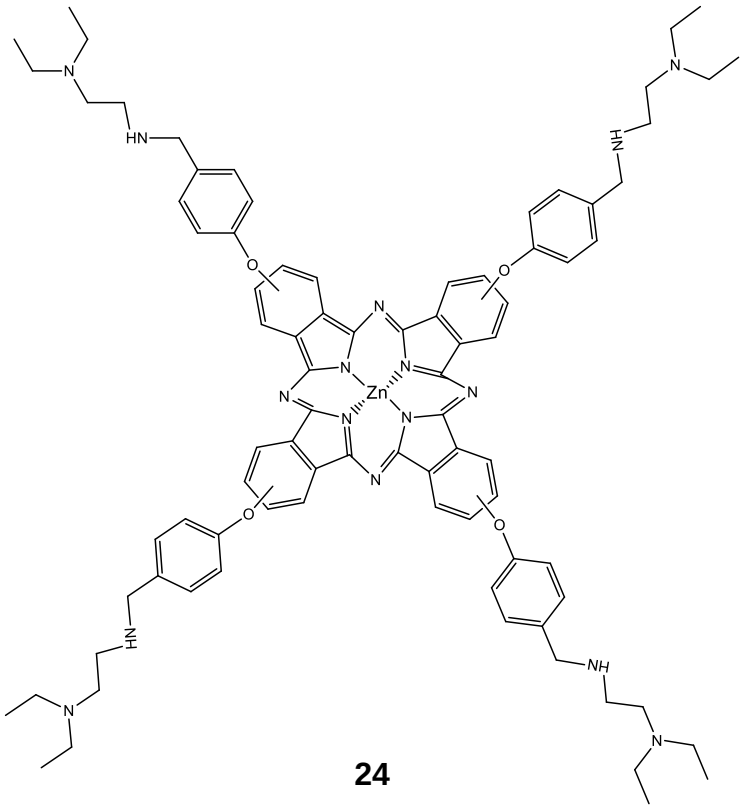

24

Similarly, Michalska *et al* used **23** to improve the aqueous solubility, pH stability and temperature resistance of the drug “ITH12674” [3-(2-isothiocyanatoethyl)-5-methoxy-1H-indole] (**25**) by forming a 1:1 host:guest complex with **23**.[69] In so doing, ITH12674 was made more effective for use in the treatment of ischemic stroke.

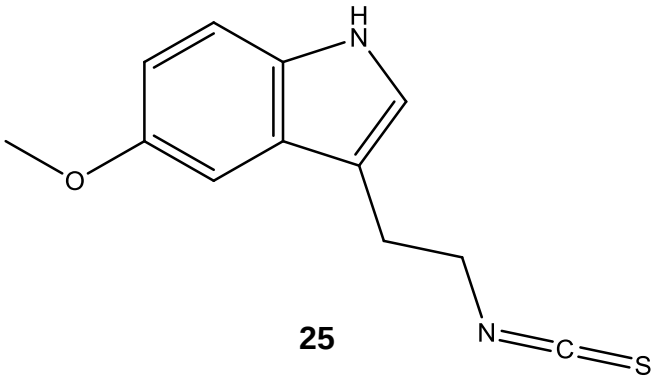

25

Furthermore, You and his team dimerised β-cyclodextrin using *p*-phenylenediamine as a bridging moiety. This cyclodextrin dimer was then used to facilitate the formation

of a supramolecular linear polyacrylamide polymer chain. Adamantane termination moieties on the polyacrylamide chains associate with each of the cyclodextrin units of the dimers through host-guest interactions, thereby elongating the polymer and creating a supramolecular chain (Scheme 3).[70]

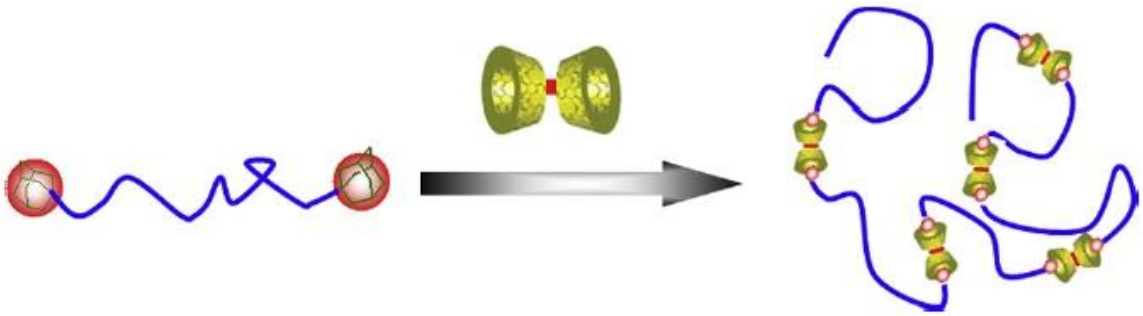

Scheme 3: Formation of supramolecular linear polyacrylamide chains through host-guest interactions.[70]

The drug *N*-methyl-2-pyridine ethanamine, commercially known as Betahistine (**26**), is routinely used in the treatment of vertigo and dizziness[71–73] (symptoms of conditions such as Ménière's disease) by increasing blood flow to the brain. Maeda and his team[74] found that β-cyclodextrin was able to form a 1:1 host:guest inclusion complex with **26**. A ROESY NMR study of the complex revealed that a part of the side chain of the drug as well as the pyridine ring were likely to reside within the cyclodextrin cavity. Of practical importance in this study was the finding that the solid inclusion complex was far less hygroscopic than the free drug. Ordinarily, the free drug would have been fully liquefied in about 100 minutes. As part of a host-guest complex, the drug failed to completely liquefy after as long as a month.

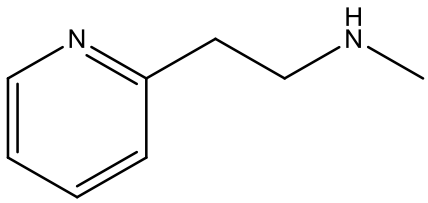

26

As a final example, β-cyclodextrin was found to include 4-acetoxy-1-(2-ethoxyethyl)-4-phenylpiperidine (**27**), a promising analgesic candidate due to lower toxicity and longer lasting therapeutic effect, with a host:guest ratio of 2:1, as discovered by Sharipov *et al.*[75] ROESY NMR spectroscopy revealed that most of the guest is situated within the cavity of the first cyclodextrin molecule, including the piperidine, acetoxy and ethoxyethyl moieties, while the second cyclodextrin molecule encapsulates part of the acetoxy moiety as well as the phenyl group. The inclusion complex, when tested on rodents, showed an anaesthetic effect of about twice that of Lidocaine and more than four times that of Novocaine, both popular numbing agents. The duration of the numbing effect of the inclusion far outweighed that of the aforementioned numbing agents, while the LD_{50} (mg.kg) was almost twice that of its nearest competitor, indicating a much lower level of toxicity.

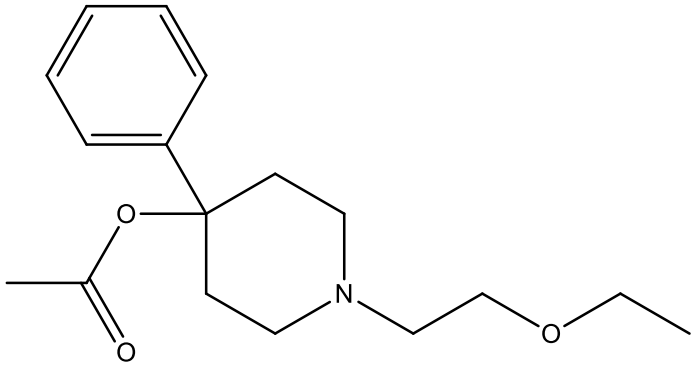

27

1.4.2 Crown Ethers

Crown ethers are cyclic polyether compounds first synthesised and reported by Charles J. Pedersen in 1967.[76] They consist of different numbers of repeating units (typically ethyleneoxy or *o*-phenylene moieties) and exhibit a hydrophobic nature around the outside of the ring, while the inside is hydrophilic. They frequently have a strong affinity for chelating biologically important cations such as Na^+, Li^+ and K^+, and the heteroatomic oxygen atoms serve as donor atoms and are capable of complexing with a variety of small organic molecules in a selective manner.[77,76]

In particular, 12-crown-4 (**28**) and dibenzo-14-crown-4 have strong affinities for complexing with lithium cations,[78–80] while 15-crown-5 (**29**) and benzo-15-crown-5 complex strongly with sodium halides and sodium salts of organic compounds.[81,82] 18-Crown-6 (**30**) predominantly includes potassium ions such as those derived from potassium halides[83] or potassium fluorenides,[84] as well as neutral organic molecules through hydrogen bonding with the available amine and hydrazine groups of the guests.[85]

The naming of crown ethers requires a special convention since the IUPAC naming system can be complicated and cumbersome. The first number in the name of a crown ether refers to the total number of atoms that comprise the main ring, while the second number indicates the number of heteroatoms in the ring. Further substituents such as benzo moieties are added as prefixes.[86]

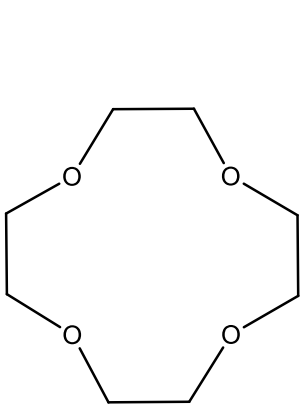

28

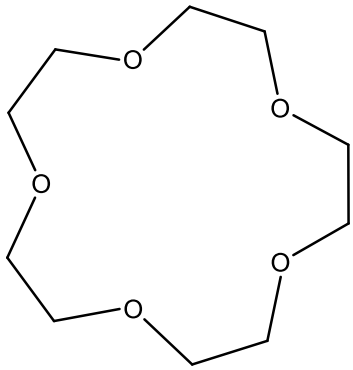

29

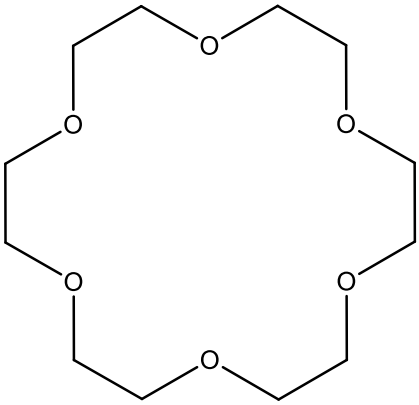

30

1.4.3 Calixarenes

Calixarenes are macrocyclic molecules, the names of which are derived from “calix crater”, a type of Greek vase. Research into the design, synthesis and use of calixarenes gained popularity throughout the 1990’s.[87] Calix[n]arenes are synthesised using a condensation reaction between a phenol and an aldehyde, and are characterised by a hydrophobic inner cavity and a hydrophilic outer surface.[88–90] Below is illustrated a basic calix[6]arene, *p*-*tert*-butyl[6]arene (**31**). Typically, ‘n’ can range from 4 to 9. A more systematic name would be calix[6]arene-37,38,39,40,41,42-hexol.

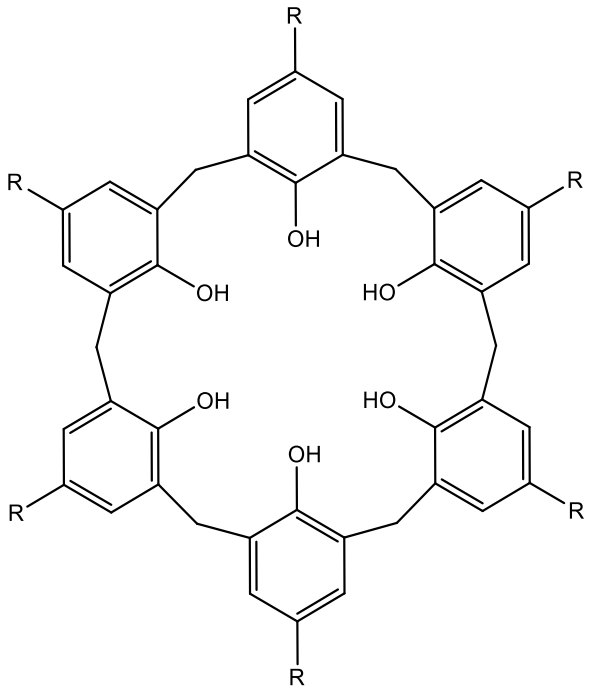

31

The OH groups are typically orientated in the *endo*- position, pointing towards the annulus of the ring (Scheme 4). Furthermore, the face bearing the hydroxyl groups is designated as the lower rim, while the face bearing the *para* substituents is designated the upper rim; however, these designations may lose their applicability when larger, more complex calixarenes are considered.[87]

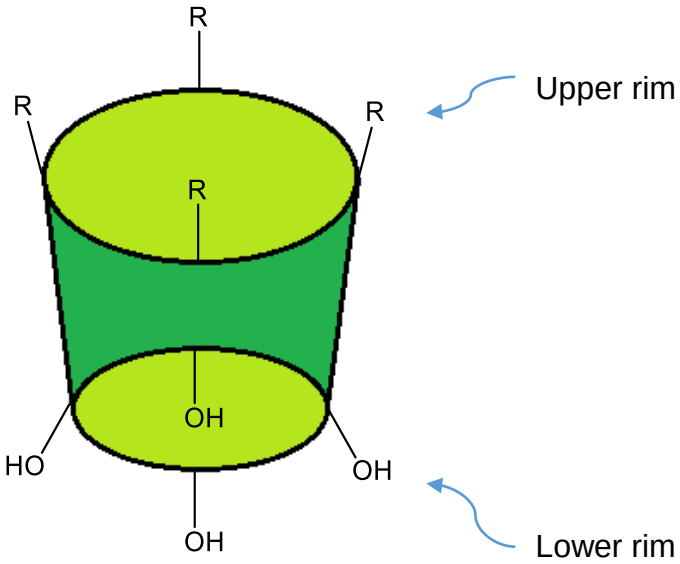

Scheme 4: Indication of the upper and lower rims of a calix[n]arene molecule.

More recently, water-soluble calixarenes such as the *p*-sulfonic calix[n]arenes (**32**) have enjoyed renewed interest due to their ability to increase the solubility of drugs in aqueous conditions, and to selectively bind metal ions, whilst being more stable in the presence of harsh conditions such as oxidising agents, heat and light.[91–96]

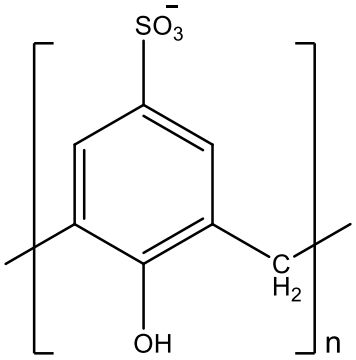

32

Chao *et al* demonstrated that *p*-sulfonatocalix[n]arenes (where n = 4, 6 or 8) formed 1:1 host:guest inclusions with ferulic acid (**33**) (a natural product found to have beneficial anti-inflammatory, anti-oxidant, anti-microbial and anti-thrombotic properties) over a range of pH values.[97,98] Furthermore, they determined that the antioxidant activity and photo- and thermal- stabilities of ferulic acid were increased upon host-guest complex formation.[99]

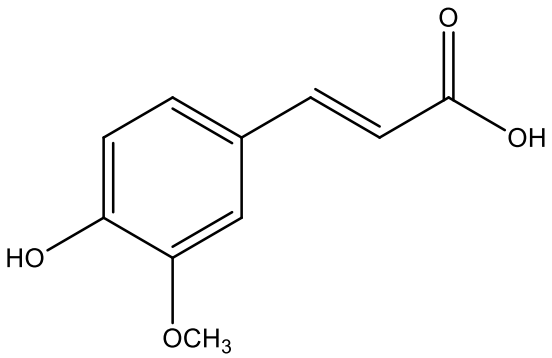

33

Interestingly, Basílio and his team investigated the existence of a ternary host-guest system involving γ-cyclodextrin which includes an *O*-alkylated *p*-sulfonatocalix[4]arene through interaction between the hydrophobic cavity of cyclodextrin and the alkyl chains of the calixarene.[100] The calixarene, in turn, is still available for further host-guest complex formation and was able to include tetramethylammonium chloride within its own cavity (Scheme 5).

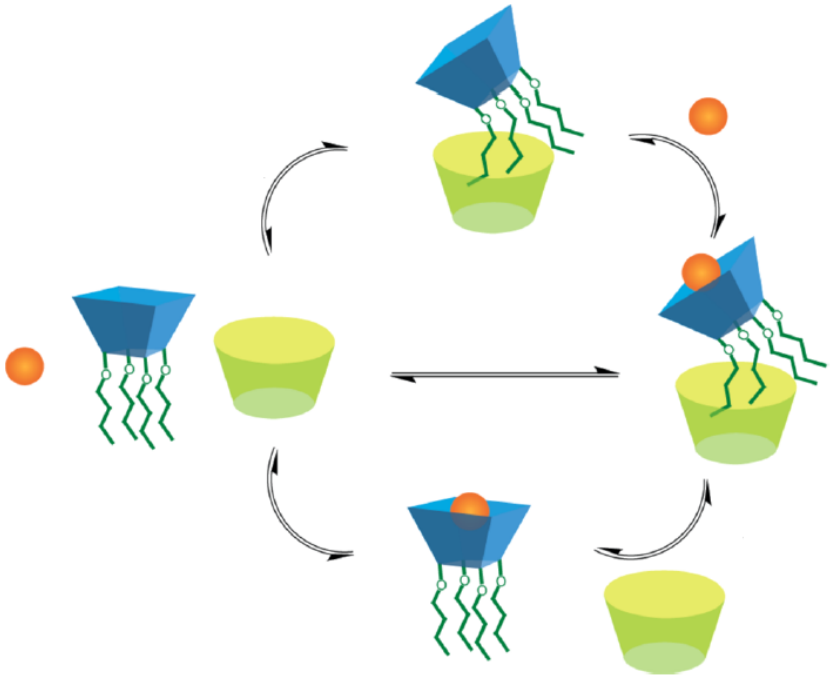

Scheme 5: The dynamic equilibrium in the ternary host-guest system between cyclodextrin, *O*-alkylated *p*-sulfonatocalix[4]arene and tetramethyl-ammonium chloride.

1.4.4 Fluorene Hosts

Many fluorene-based compounds are effective hosts, exhibiting guest-specific fluorescence. The addition of halogen atoms at the 2- and 7- positions of fluorene allows for the preparation of different derivatives with the ability to interact with each other by means of a variety of non-covalent interactions such as π–π stacking, halogen interactions and hydrogen-bonding contacts. Two such hosts (**34** and **35**) were synthesised by Hosseinzadeh *et al*.[101] Host **34** included diethylamine, triethylamine, piperidine (all with 1:1 host:guest ratios) and 1,4-dioxane (2:1), whereas host **35** included di- and tri- ethylamine (1:1) and pyridine (2:1). Both of these hosts failed to enclathrate simple alcohols and aprotic polar and dipolar guests. Interestingly, the host compounds on their own presented as yellow crystals but turned colourless when diethylamine was complexed. Through single crystal X-ray diffraction studies of the solvated and unsolvated hosts, this phenomenon was attributed to the shift from continuous stacks formed by the fluorene molecules to the formation of dimers.

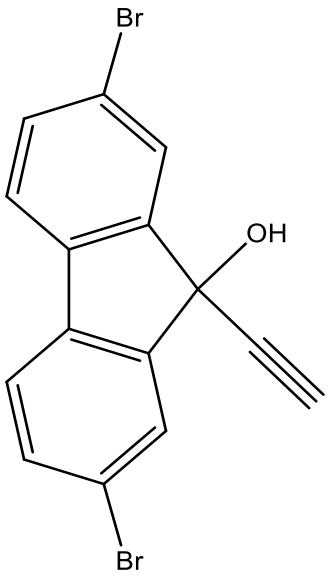

34

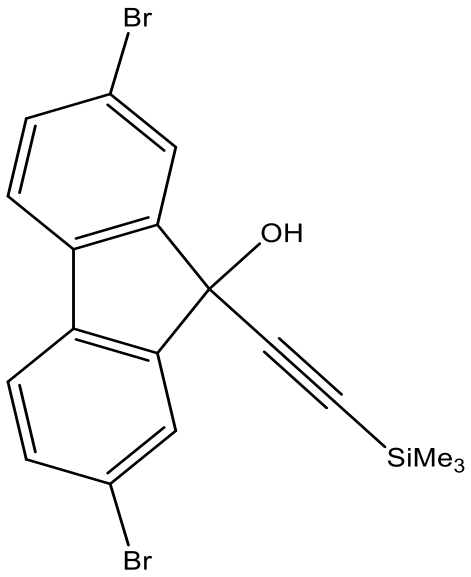

35

1.4.5 Xanthenyl Hosts

The host molecules *N*,*N*'-bis(5-phenyl-10,11-dihydro-5-dibenzo[*a,d*]cycloheptenyl)-ethylenediamine (**36**) and *N*,*N*'-bis(5-phenyl-5-dibenzo-[*a,d*]cycloheptenyl)-ethylenediamine (**37**) are characterized by the presence of two tricyclic and two phenyl moieties as bulky end-caps, linked through ethylenediamine as a non-rigid spacer.[102]

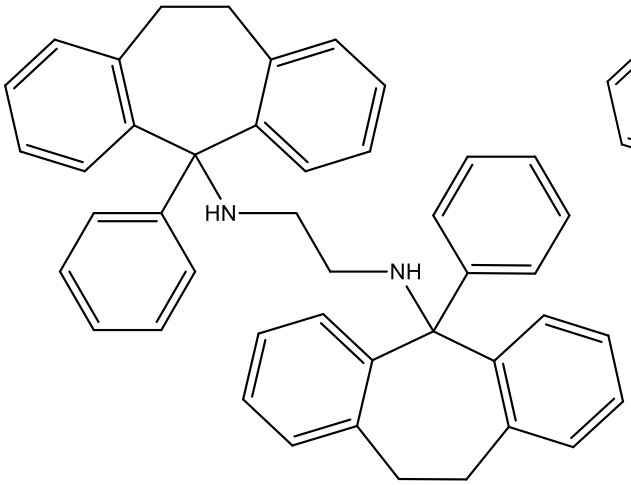

36

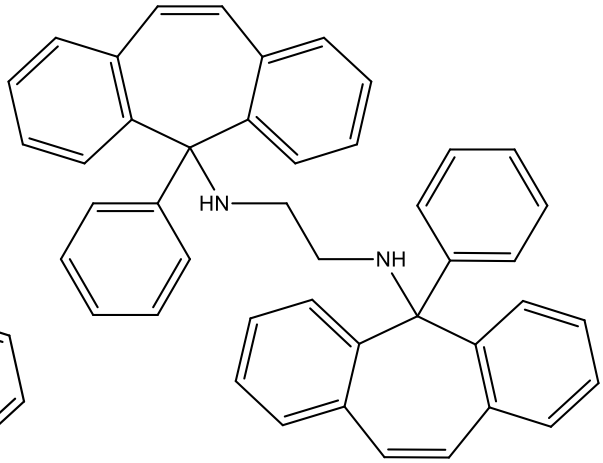

37

Both of these hosts displayed the ability to include acetone, acetonitrile and 1,4-dioxane (all 1:1), as well as DMF (1:2). Interestingly, the unsaturated host included all three common dihalomethanes in a 1:1 host:guest ratio, whereas the saturated host included the dihalomethanes in a 2:1 ratio.[102] Single crystal X-ray diffraction studies of the six dihalomethane complexes revealed that all the complexes crystallised in the monoclinic crystal system, with the exception of **36**•CH_2I_2, which crystallised in the triclinic system. In all three inclusions where **36** was present as a host, disorder of the guest was evident. Furthermore, it was found that crystals of **36**•CH_2Cl_2 and **36**•CH_2Br_2 were isostructural, with the guests occupying open channels. On the other hand, the X-ray molecular structure of **36**•CH_2I_2 indicated that the guest occupied discrete, albeit large, cavities incorporating two guests concomitantly. Usually, host-guest complexes where the guest molecules occupy channels in the host lattice are

relatively less thermally stable than guest molecules occupying discrete cavities.[103] Theoretically, the latter complex should be more thermally stable, and this was indeed confirmed by thermogravimetric analysis. Decomposition of the dichloro- and dibromo- methane complexes occurred even at room temperature, from the onset of the analysis, while the diiodomethane complex only decomposed at approximately 77 °C. All three dihalomethane guests, when complexed with **37,** resided in discrete cavities (each incorporating one guest) and, as such, their thermal stabilities were much higher than in the case of **36** (onset temperatures for the guest release processes were approximately 97, 102 and 94 °C, respectively).[102]

1.4.6 Metal-based Hosts

Host compounds may also be metal-based as demonstrated by Okeke and Soldatov.[104] Metal dibenzoylmethanates [$M(DBM)_2$] were synthesised incorporating either cobalt, zinc, cadmium or nickel as the central metal atom. Quinoline (Q) was coordinated to the metals as ligands forming the [$M(DBM)_2Q_2$] complex (**38**) with the quinoline moieties in the *trans* configuration. This metal complex was found to include non-coordinated quinoline, as well as naphthalene, substituted benzenes and cyclohexanes.

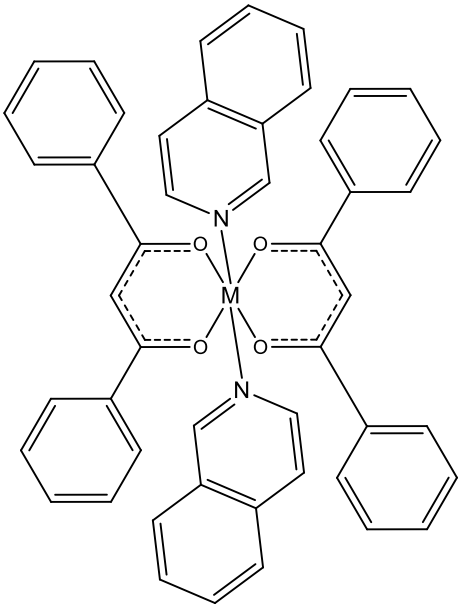

38

Metal complexes may provide a means towards the synthesis of metal-free host molecules. Shen *at al*[105] derived a macrocyclic host molecule (*E*)-H_2dmdbdptaa (**40**), from the nickel metal complex (*E*)-Nidmdbdptaa (**39**) through a demetallation reaction (Scheme 6). The demetallized host **40** was found to include toluene in a 1:2 ratio. Through single crystal X-ray diffraction, it was observed that one toluene molecule resided within the cavity formed by the host while the other guest resided outside of the cavity. Notably, in a host as rich in phenyl moieties as **40**, toluene did not experience any appreciable π–π stacking interactions. Crystal close-packing and van der Waals forces were responsible for the mode of inclusion.

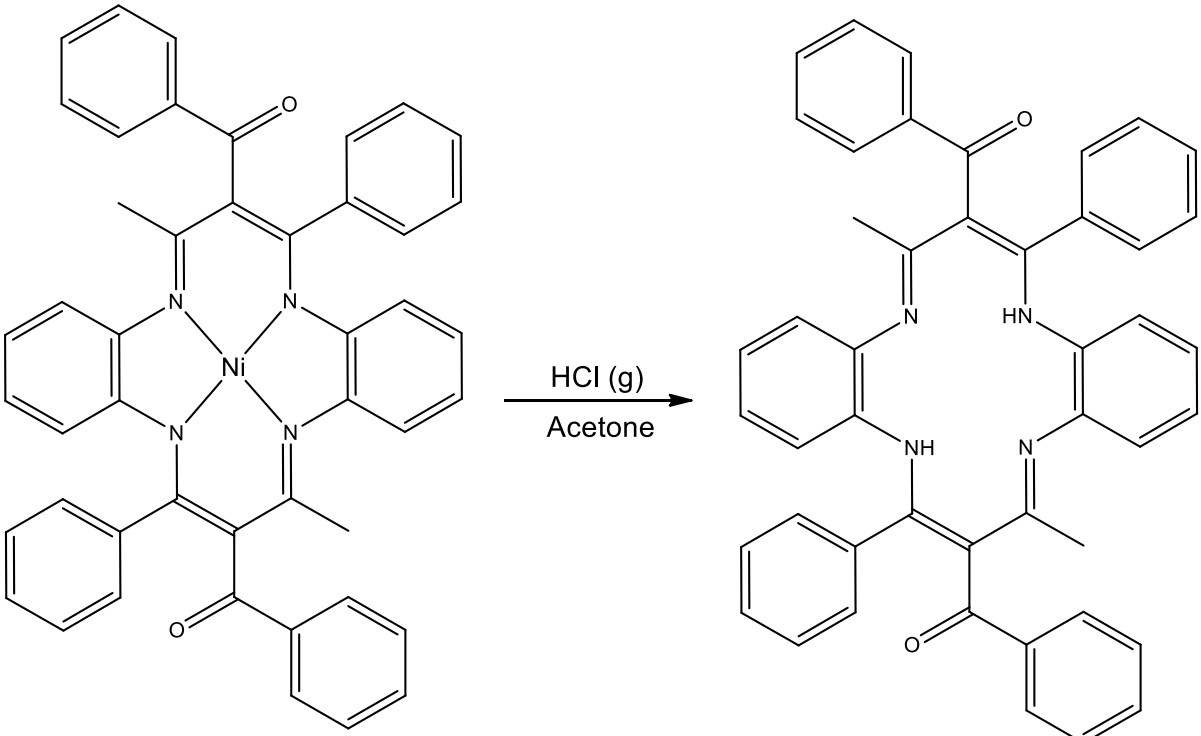

39 **40**

Scheme 6: Treatment of (*E*)-Nidmdbdptaa with $HCl_{(g)}$ in acetone leads to the formation of the metal-free host compound (*E*)-H_2dmdbdptaa.

1.4.6 Diol Hosts

A variety of different diol host structures are known, with the key structural similarity being the presence of the two alcohol moieties. One such example is *trans*-9,10-dihydroxy-9,10-diphenyl-9,10-dihydroanthracene (**41**). The host-guest properties of this molecule have been extensively investigated,[106–112] and it was found to be capable of including a large variety of hydrogen-bond forming guests such as methanol, ethanol, acetophenone, acetonitrile, 3-hydroxypropionitrile, cyclohexanone, 2- and 4-methylcyclohexanone, and 2- and 4- methylpyridine, amongst many others (Table 2).[106,107, 113,114] Acetonitrile and 3-hydroxypropionitrile were also included with nitrogen acting as a hydrogen-bond acceptor. The activation energy required for the release of acetonitrile was determined to range between 83 $kJ \cdot mol^{-1}$ and 115 $kJ \cdot mol^{-1}$, depending on the degree of decomposition.[113,108]

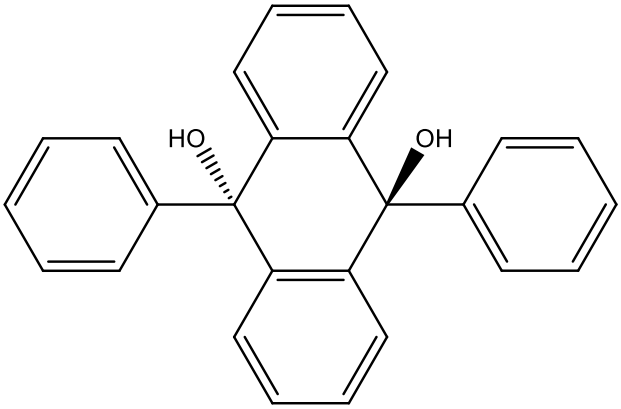

41

Table 2: Inclusions of host compound 41.

Guest	H:G
Methanol[106]	1:2
Ethanol[107]	1:1
1,4-Butanediol[109]	1:1
Cyclohexanone[114]	1:2
Acetonitrile[113]	1:2
3-Hydroxypropionitrile[113]	1:2
Acetophenone[110]	1:2
3-Methylcyclopentanone[110]	1:2
2-Methylcyclohexanone[112]	1:2
4-Methylcyclohexanone[112]	1:2
4-Vinylpyridine[111]	1:2
4-Methylpyridine[111]	1:2
2-Methylpyridine[111]	1:1
2-Butanone[111]	1:1

Other diol hosts comprise two 9-hydroxy-functionalized, bulky fluorene moieties (**42**, **43**). The fluorene units are often dimerized through phenylene or ethynylene groups, or a combination of both. These hosts may have substituents on the 2- and 7-positions and these can enhance their inclusion abilities by providing additional stabilising interactions.[115,116] These fluorenyl hosts include a wide variety of guests such as amines, alcohols, ketones, heterocyclic and aromatic compounds.

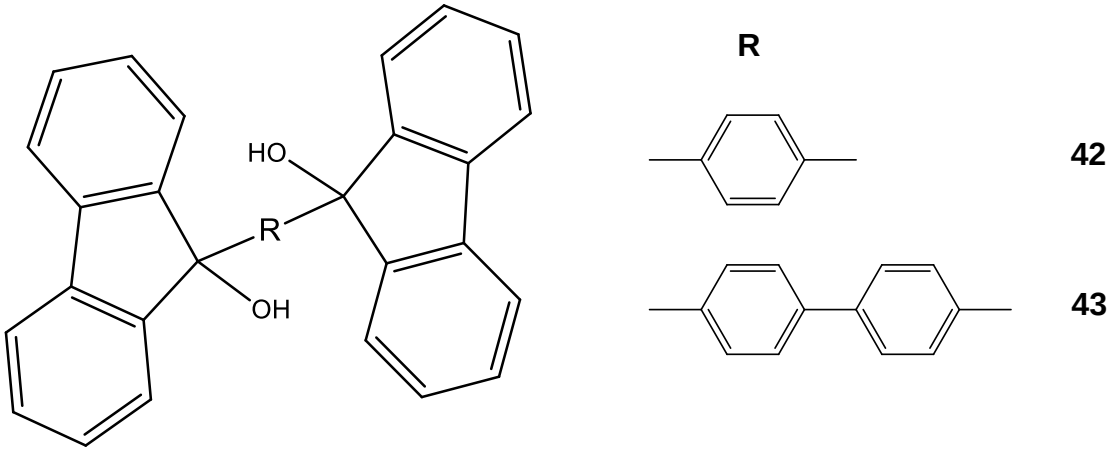

Compound **42** formed complexes with a variety of guests such as amides [dimethylformamide and dimethylacetamide (both 1:1)], tetramethylurea and hexamethylphosphoramide (both 1:2),[117] morpholine, pyridine and the isomeric methyl pyridines (all 1:2),[118] methanol and ethanol (both 2:1), and acetone (1:1).[115]

Compound **43** enclathrated guests such as methacrylic acid, diethylene glycol and bis(2-aminoethyl)amine (all 1:1), 2-cyclopenten-1-one (1:2),[119] 1-propylamine, diethylamine and trimethylamine (1:1), methanol, ethanol, cyclohexanol, dimethylformamide and nitromethane (1:2).[115,116]

BINOL (1,1'-bi-2-naphthol) (**44**), being a diol, has been shown to include a variety of guest molecules and appears to have a particular preference for forming host-guest complexes with diimine compounds such as compounds **45–51**.[120,121] Of these guests, BINOL exclusively prefers **50** when subjected to equimolar binary competition experiments containing the other diimine compounds. This phenomenon was ascribed to extensive hydrogen bonding as well as π–π interactions between host and guest that significantly outweighed the strength of similar interactions between BINOL and the other diimines.[120]

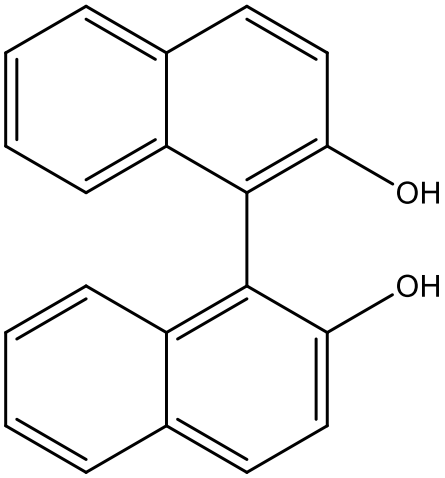

44

Table 3: Host:guest ratios of the complexes formed between 44 and diimine compounds 45–51.

Compound	H:G
45	1:2
46	1:2
47	1:2
48	2:2
49	2:2
50	1:1
51	1:2

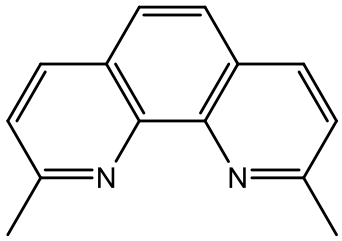

45

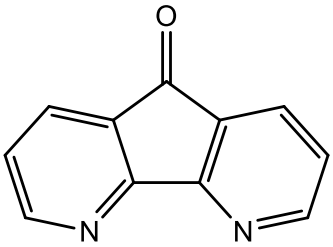

46

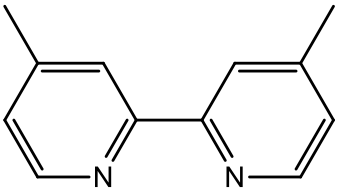

47

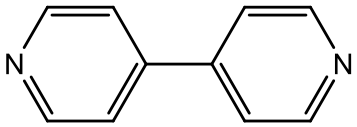

48

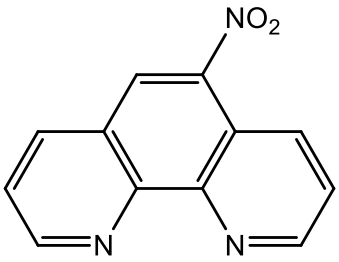

49

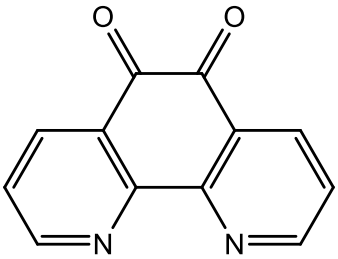

50

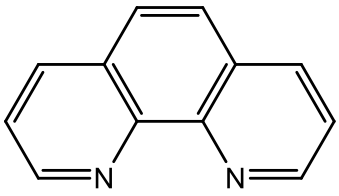

51

BINOL exhibits the ability to form inclusion complexes with molecules such as 4,4'-bipyridine (**48**) and 1,4-benzoquinone (**52**) through O-H···N or O-H···O hydrogen bonding. These complexes are then able to include a variety of additional guest molecules. In a study by Biradha and Mahata, it was found that the *rac*-BINOL•**48** complex formed inclusion compounds with toluene, benzene, biphenyl, naphthalene, *p*-xylene and anthracene and that all were stabilised through aromatic interactions. Crystallisation from 1,4-dioxane resulted in the formation of a 1:2 host:guest complex with **48** alone.[122]

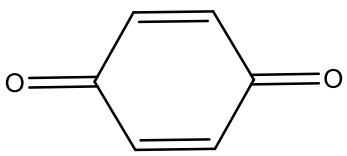

52

Structurally related to **44** is 10,10'-dihydroxy-9,9'-biphenanthryl (**53**) which has the larger π-conjugated phenanthrene rings compared to BINOL's naphthalene rings. When **53** was allowed to crystallise from different *n*-alkyl alcohols such as *n*-propanol or *n*-butanol in the presence of methylviologen (1,1'-dimethyl-4,4'-bipyridinium dichloride, **54**), a charge-transfer host-guest complex was formed. Within this complex, **53** acted as the electron donor and **54** as an electron acceptor. The colour of the crystals formed during inclusion depended on the specific alcohol used as guest. It was reported that complexes obtained from *n*-PrOH presented as red crystals, while those obtained from *n*-BuOH were blue-black. The authors used diffuse reflectance spectroscopy to characterise the colour differences of the crystals. This allowed the biphenanthryl-methylviologen host system to serve as a visual indicator for molecular recognition.[123]

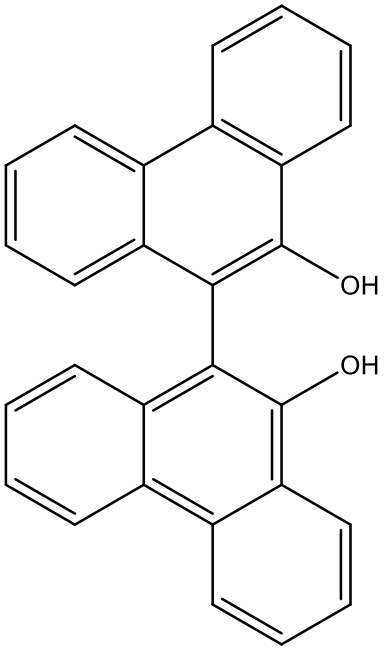

53

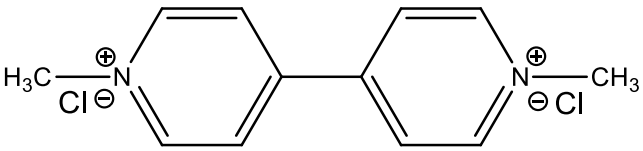

54

1.4.7 Wheel-and-axle Hosts

A well-known and versatile class of host compounds are the so-called wheel-and-axle hosts (Figure 11).[124] These are named owing to their structure which mimics the shape of two wheels, frequently made up of bulky aromatic groups, linked together by a single, long axis, traditionally made up of triple bonds. The axis may also be formed through fused, linear rings.

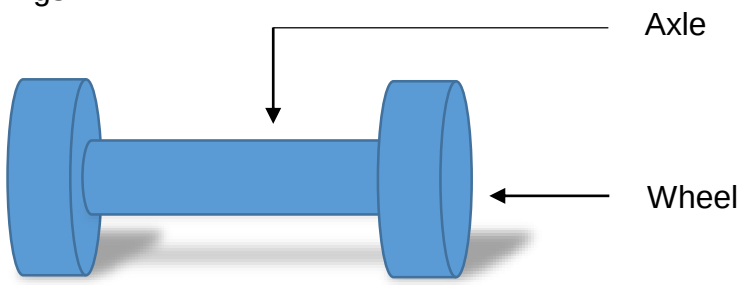

A typical example of a wheel-and-axle host is 1,1,6,6-tetraphenylhexa-2,4-diyne-1,6-diol (**55**). It dates back as far as 1968 when it was first synthesised by the well-known host-guest chemist, Toda.[125] This compound possesses ample rigidity along the axis, and bulky phenyl groups at the ends allow the compound to crystallise in such a manner to allow for the formation of channels or cavities in which guests may reside. Furthermore, the presence of hydroxy groups on the ends allows for hydrogen bonding between host and guest, when available, thereby stabilising the complex further.[126]

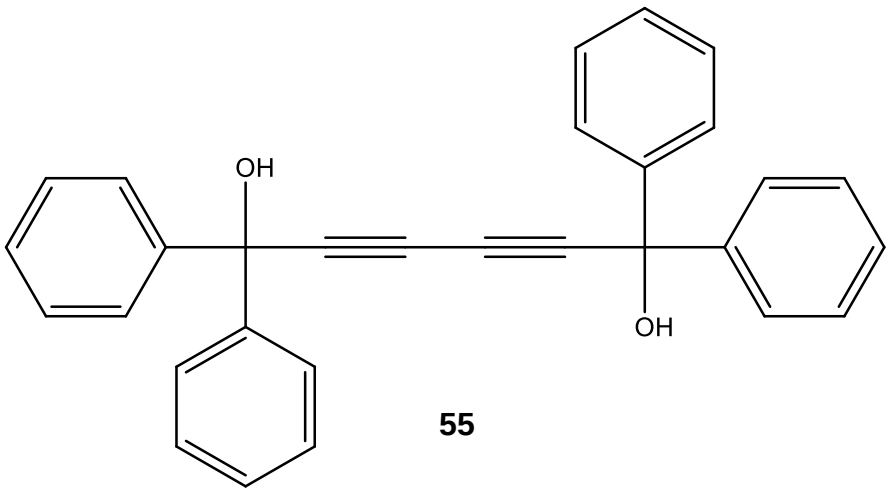

55

The work of Bacsa *et al*,[126] aimed at separating pyridine and picoline isomers from one another, revealed that host **55** formed complexes with pyridine and the 3- and 4-methylpyridine isomers with a host:guest ratio of 1:2. Furthermore, competition experiments between the different isomers and pyridine showed that the host selectivity varied depending on the mole fraction of each guest species present in the recrystallizing mixture.

In order to assess the influence of derivatising the ethynylene axle on the inclusion ability of these wheel-and-axle hosts, Weber *et al*[127] synthesised a series of analogues incorporating 1,4-phenylene and various other aromatic moieties to serve as the axle. The simplest analogue, **56**, proved to be an efficient host, complexing with a variety of solvents such as the bulky alcohol isopropanol, and DMF and DMSO, as well as acetonitrile and nitromethane (Table 4). It was also able to include some heterocyclic compounds, namely piperidine, dioxane, THF and morpholine. The host **57**, having bulkier wheel substituents, fared less well as a host, including only DMF, DMSO and the heterocyclic compounds listed in Table 4. Host **58**, with the longer axle, compared favourably to host **56**, with its ability to include ethanol replacing the inclusion of nitromethane.

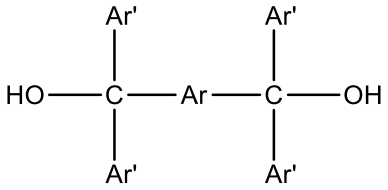

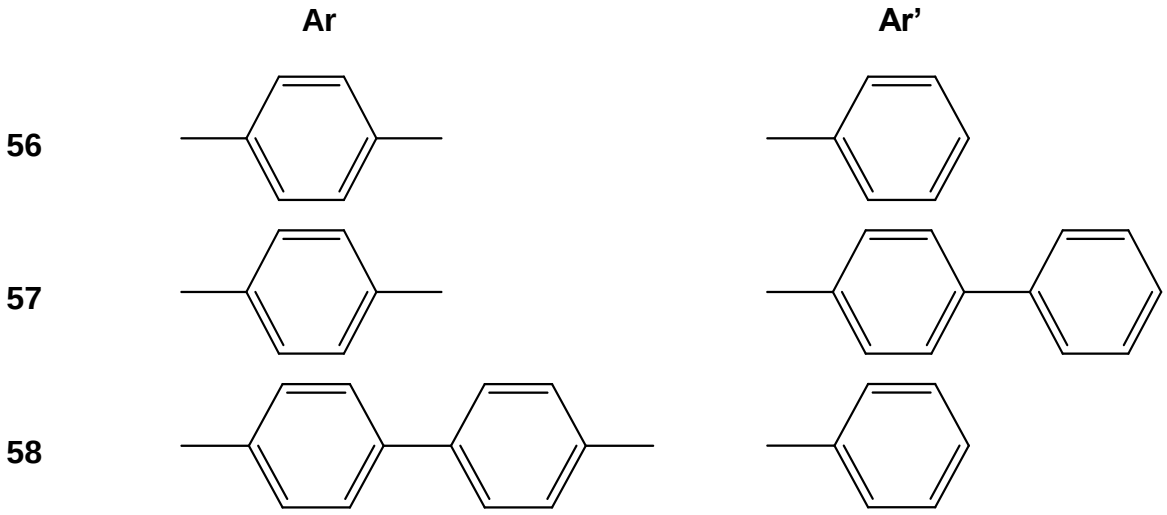

Table 4: Various host:guest ratios of the inclusion complexes of host compounds 56–58.

Guest solvents	56	57	58
Ethanol	1:0	1:0	1:2
^{i}PrOH	3:2	1:0	1:2
MeCN	2:1	1:0	1:1
$MeNO_2$	2:1	1:0	1:0
DMF	1:2	1:3	1:2
DMSO	1:2	1:3	1:2
THF	2:1	1:3	1:2
Dioxane	1:2	1:3	1:2
Morpholine	1:1	1:3	1:1
Piperidine	1:2	1:3	1:2

More recently, Katzch and Weber[128] succeeded in substituting the terminal phenyl groups of **56** with pyridyl (**59**) and thienyl (**60**) groups, thereby allowing for possible modification of inclusion behaviour. However, the inclusion ability of these hosts were negatively affected in this way in comparison to that achieved by the parent compound. The pyridyl derivative was found to include only toluene (1:2) and 1,4-dioxane (1:1). The thienyl derivative performed comparatively better by forming complexes with pyrrolidine (1:2), 1,4-dioxane (1:1), and both DMSO and acetone (2:1), and it also succeeded in complexing with *n*-butanol and *n*-propanol (both 1:2), which **58** was not able to accomplish.

Through X-ray structure analysis of the hosts, it was determined that a contributing factor to the weak inclusion ability of the pyridyl-derived host is the formation of intramolecular hydrogen bonds between the host hydroxyl groups and the pyridyl moieties. This, in effect, restricts the host's ability to interact with polar guest solvents.

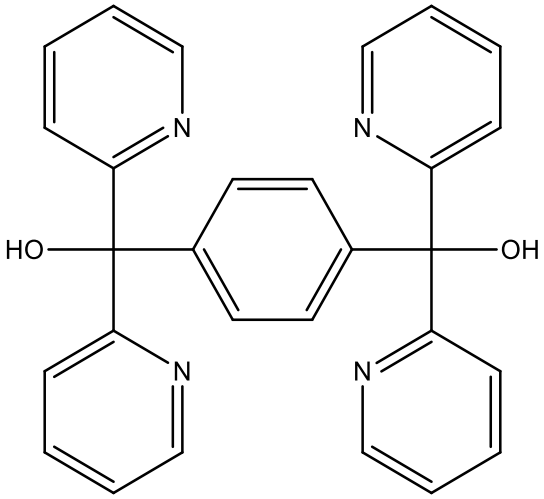

59

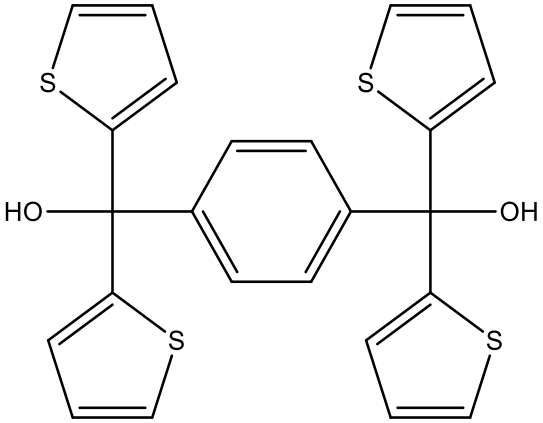

60

In an effort to increase the bulkiness of the heteroaromatic 'wheel' groups, Katzsch *et al*[129] synthesised two further wheel-and-axle hosts incorporating benzo[*b*]thiophene as the terminal groups (**61** and **62**). This led to a marked increase in host ability as compared to the thienyl derivative. Compound **61** included ethanol, diethylamine, pyrrolidine, acetone, ethyl acetate, DMSO, DMF, pyridine, THF and 1,4-dioxane (all 1:2, except ethyl acetate, where a 3:2 H:G ratio was obtained). The reintroduction of the ethynylene 'axle' moiety in **62** resulted in similar inclusion characteristics, with the exception of the additional inclusion of *n*-propanol and *n*-butanol, and of methanol instead of ethanol; the host:guest ratio of complexed ethyl acetate was determined to be 1:1.

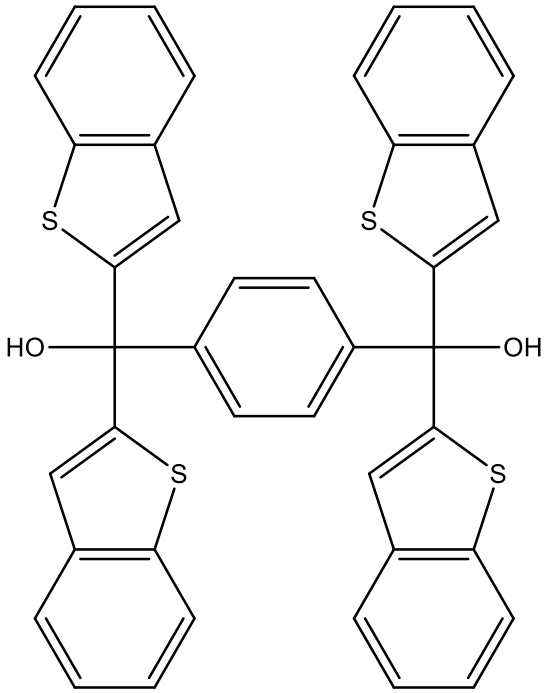

61

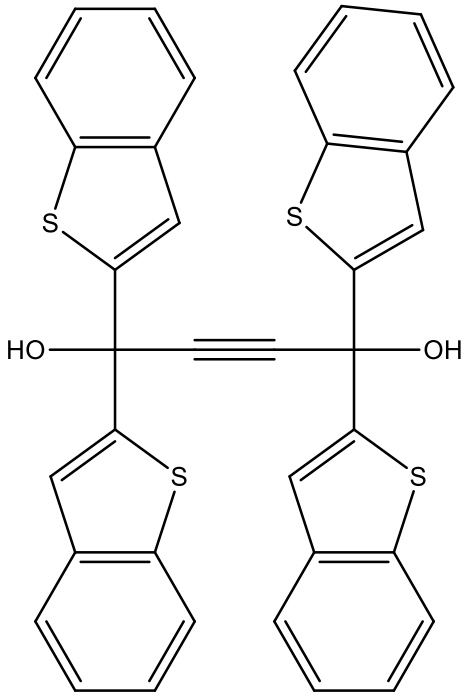

62

In an investigation into the effect of varying the molecular geometry of wheel-and-axle hosts, Skobridis and his research team[130] synthesised three regioisomers of host **58** comprising a biphenylylene ‘axle’ and two diphenylhydroxymethyl ‘wheels’. The isomers differed in terms of their position of connectivity between the ‘wheel’ and ‘axle’ (2,2’-, 3,3’- and 4,4’-, Scheme 7).

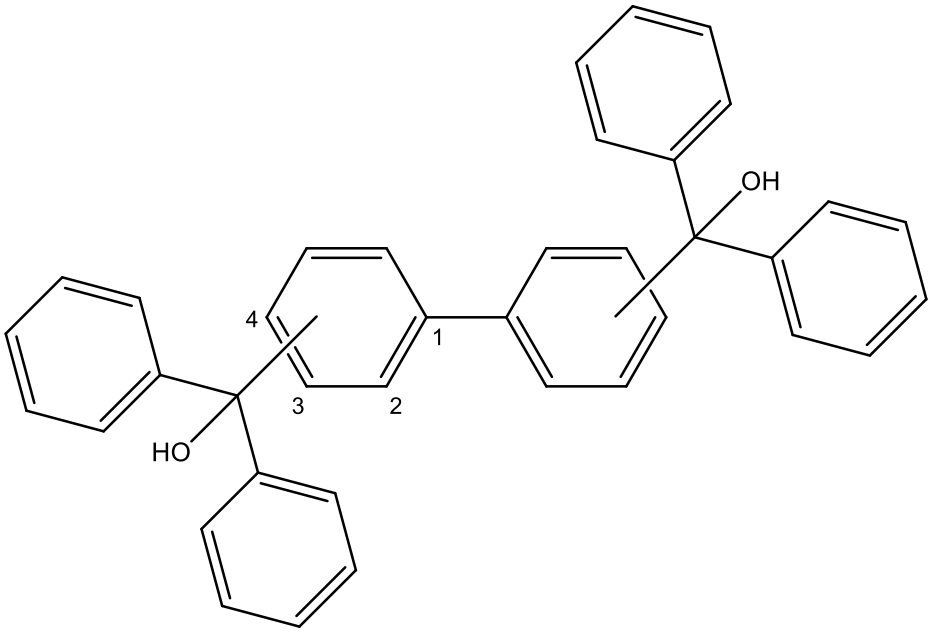

Scheme 7: Different regioisomers of host molecule 58

The result of this study indicated that the three isomers presented different inclusion behaviour. The 2,2'-isomer preferentially included alcohols compared with the 3,3'- and 4,4'-isomers. It also preferred a 2:1 host:guest ratio, in contrast to the 3,3'- (1:1) and 4,4'- (1:2) substituted compounds. The 2,2'-isomer experienced a prominent intramolecular hydrogen bond which served to lock it in a compact geometry regardless of the presence or absence of a guest. This hydrogen bonding behaviour explained the formation of cyclic hexameric host-guest aggregates and that it was solely responsible for the structural behaviour of the host. In the case of the less bent 3,3'- and linear 4,4'- isomers, the hydroxyl groups were more accessible to form intermolecular hydrogen bonds to guests, often resulting in the formation of molecular strand-structures.[130]

Jetti *et al*[131] considered synthesising the wheel-and-axle host **63** but, due to the difficulty of the synthetic route and the anticipated solubility issues of the host, they did not proceed. In its stead, the group investigated 4-(triphenylmethyl)benzoic acid (**64**), which arranges itself as a dimer in a wheel-and-axle configuration similar to **63** through hydrogen bonding interactions.

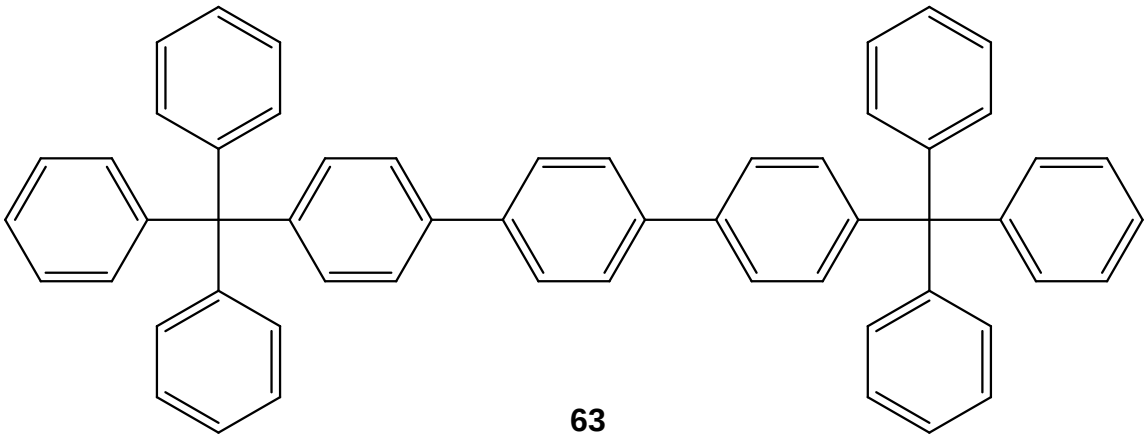

63

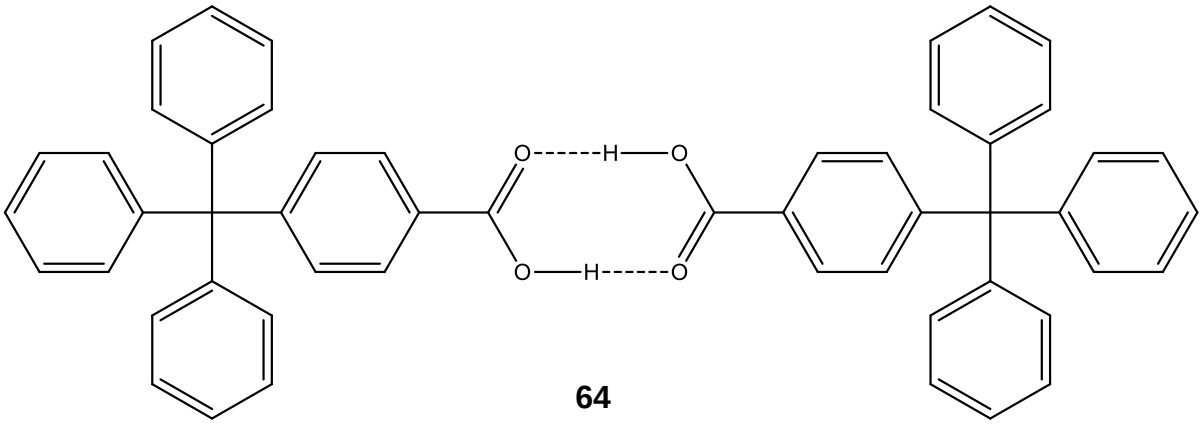

64

This dimer (**64**) was found to include the xylene isomers, anisole, mesitylene, chloro- and bromo- benzene as well as nitrobenzene, all with a host:guest ratio of 2:1. In addition, each of the host-guest complexes were isostructural.

Interestingly, asymmetric guests such as *o*-xylene and *m*-xylene showed appreciable amounts of disorder in the crystal packing. It was postulated that the disorder may have been due to the host cavity size being large enough to allow the guests to assume different orientations, or that there was a mismatch between the symmetry of the host and guests. The absence of guest disorder upon the inclusion of symmetric *p*-xylene supported this latter suggestion.[131]

1.4.8 TADDOL Hosts

TADDOL, α,α,α',α'-tetraphenyl-2,2-dimethyl-1,3-dioxolan-4,5-dimethanol (**65**), is an accomplished organic host molecule derived from naturally-occurring tartaric acid. Esterification and acetalation of tartaric acid, followed by treatment with phenylmagnesium bromide results in a solid host which readily crystallises from hydrogen-bond accepting solvents. TADDOL contains a 1,3-dioxolane ring which provides rigidity to the molecule, and two hydroxyl moieties on the terminal carbons (C4 and C5) of the butane backbone enhance its hydrogen bonding ability. Finally, terminally located, bulky phenyl groups add rigidity and aromatic interaction ability to TADDOL in the solid state.[31]

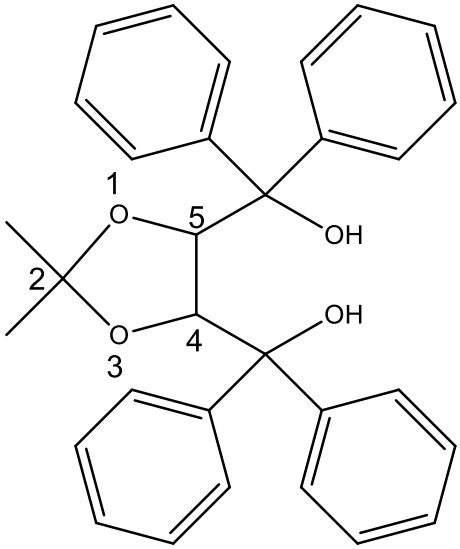

65

TADDOL and its analogues were originally used as chiral auxiliaries so as to catalytically introduce chirality within a reaction end-product.[31] In particular, the use of titanium TADDOLates has been employed in a wide variety of chiral nucleophilic addition reactions, including the addition of diethylzinc to aldehydes and Grignard reactions. Ti-TADDOLates were also successfully used in enantioselective Diels-Alder reactions.[31]

As TADDOLs are able to crystallise out readily when hydrogen-bond acceptors are present, they were naturally found to form inclusion compounds. Furthermore, due to

the inherent chiral and optically pure nature of TADDOLs, their inclusion capability has been used with much success to separate enantiomers of optically impure compounds through the selective inclusion of one enantiomer over the other.[31]

The TADDOL derivative, 2,3-*O*-cyclohexylidene-1,1,4,4-tetraphenylthreitol (**66**), was able to include a tricyclic dipeptide derived from (*S*)-proline (**67**), and the inclusion behaviour of this host compound was found to rely significantly on its optical purity.[132] When racemic **66** was heated with the amino acid derivative in benzene or toluene as co-solvent, a 2:1 host:guest complex was formed which contained the host in its racemic form. However, when the same inclusion experiment was performed using (4*R*,5*R*)-**66**, the inclusion complex that formed had a host:guest ratio of 1:1. The researchers were able to use this phenomenon to affect the disproportionation of the enantiomers of non-racemic **66**. Preparing the host-guest complex from an 80% e.e. mixture of host, where the major component was (4*R*,5*R*)-**66**, resulted in a 2:1 host:guest complex containing *rac*-**66**, and remaining in the flask was a 100% e.e. of (4*R*,5*R*)-**66**.[132] Incidentally, it was observed that *rac*-**44** included the same proline derivative in a 2:1:3 ratio of host to guest to benzene, but enantiopure **44** was unable to form an inclusion complex.[133]

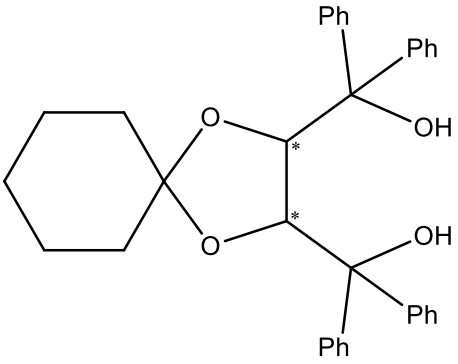

66

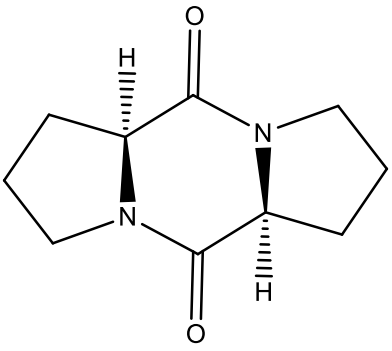

67

Host **66** was used successfully by Bagi and his team to resolve the enantiomers of 1-isopropyl-3-methyl-3-phospholene-1-oxide (**68**). The host formed a 2:1 host:guest complex from a racemic mixture of **68** which, upon separation through column chromatography and analysis by chiral gas chromatography, ultimately furnished an e.e. of 95% composed of the *S*-enantiomer.[134]

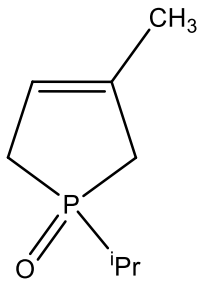

68

The ability of **65** to discriminate between different compounds through inclusion was recently investigated by Barton *et al*.[135] Of particular interest was the possible discrimination between pyridine and the three isomeric methylpyridines by optically pure (–)-**65** and *rac*-**65**. Competition experiments between pyridine and the three isomeric methylpyridines were carried out upon which it was revealed that optically pure (–)-**65** selected for the pyridines in the order 3-methylpyridine > 4-methylpyridine > pyridine > 2-methylpyridine. Interestingly, the selectivity order of *rac*-**65** changed only slightly to 3-methylpyridine > 4-methylpyridine > 2-methylpyridine > pyridine. In both cases, 3-methylpyridine was significantly preferred over the other competitors (>80% in binary and ternary mixtures; 75% in the quaternary mixture). These results are promising for the application of host-guest chemistry in the field of isomer separations.

1.4.9 TETROL Hosts

Closely related to **65** is the chiral compound TETROL [(+)-(2*R*,3*R*)-1,1,4,4-tetraphenylbutane-1,2,3,4-tetraol] (**69**). Shan *et al* investigated strategies for the synthesis of TETROL and various phenyl derivatives thereof and, in doing so, prepared TETROL in moderate yield.[136] Scheme 8 shows an alternative synthetic route towards **69**.[137] The diester of tartaric acid is treated with an excess of phenylmagnesium bromide (> 6 mole equivalent) in a Grignard reaction with anhydrous THF as solvent. An aqueous work-up with 10% ammonium chloride followed by extraction and drying of the organic phase afforded TETROL with a yield of more than 60%.

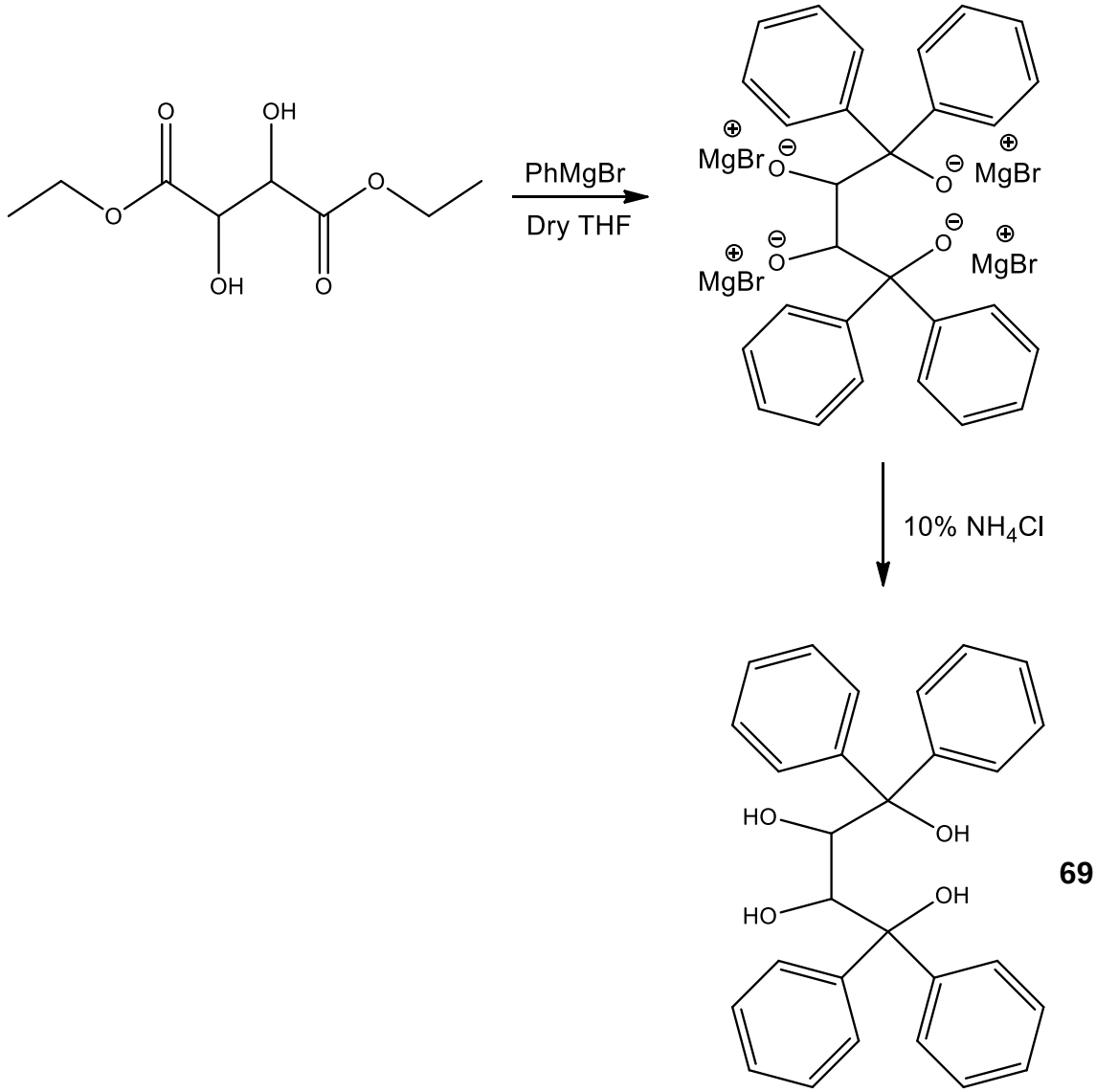

Scheme 8: The synthetic pathway to TETROL.[137]

Preceding the work of Barton *et al*,[137] no reports on **69** with respect to host-guest chemistry were found in the literature. The compound was subsequently determined to be an efficient host. Single crystal X-ray diffraction and computational studies revealed the formation of favourable 1,3- and 2,4- intramolecular hydrogen bonds which aid in the restriction of conformational mobility of the butane chain, while the butane backbone presents in the *anti*-conformation. The added rigidity due to this intramolecular hydrogen bonding, and the additional ability to form intermolecular hydrogen bonds explains the efficient host abilities of this compound.

When allowed to crystallise from pyridine and the isomeric methylpyridines, it was found that pyridine was included by **69** in a 1:2 host:guest ratio, whereas 3- and 4-

methylpyridine were included in a 1:1 ratio. 2-Methylpyridine failed to be complexed in these experiments. When **69** was subjected to competition experiments involving pyridine and the methylpyridine isomers, it showed a selectivity preference in the order of 4-methylpyridine >> 3-methylpyridine > pyridine > 2-methylpyridine. It is interesting to note that during a competition between 2- and 3- methylpyridine, the 2-isomer was included to some extent, despite not being included in the single solvent experiment.[137]

In addition, it has been reported that **69** forms complexes with cyclohexanone and the three isomeric methylcyclohexanones, each with a 1:1 host:guest ratio.[138,139] Thermal stability studies of these complexes showed that cyclohexanone, 2-methylcyclohexanone and 4-methylcyclohexanone were released in a stepwise fashion, while the complex containing 3-methylcyclohexanone desolvated in a single step. Upon calculating the packing indices for these inclusion complexes, it became clear that higher packing indices correlated with higher desolvation onset temperatures.[138] Interestingly, analysis of single crystal X-ray diffraction data of the 3- and 4- methylcyclohexanone complexes revealed that these guests were present exclusively in their energetically-disfavoured axial methyl conformations, while the 2-methyl derivative preferred the more conventional conformation with the alkyl group in the equatorial position. The '3-alkylketone effect' was denoted as responsible for the loss of one of the destabilising 1,3-diaxial alkyl hydrogen interactions and, as a result, multiple weaker attractive forces between the host and guest resulted in the axial methyl conformation being favoured.[139]

As **69** is a chiral compound, it may have the potential to resolve racemates through enantioselective inclusion. Complexes prepared using various chiral guests were subjected to chiral gas chromatography, and **69** showed a preference for the (*R*)-enantiomer of 2- and 3- methylcyclohexanone (e.e.'s of 21.7% and 16.7%, respectively).[140] The (*S*)-enantiomer of synthetic camphor was slightly preferred with an e.e. of 3.8%, while the (*R*)-enantiomer of methyl phenyl sulfoxide was favoured (e.e. 17.8%). In an attempt to better the enantiomeric selectivity of **69**, derivatives were synthesised by substituting various groups on the aromatic moieties. Racemic 2- and 3- methylcyclohexanones were separated to some degree in this way, with e.e's of 44.3% and 20.4%, respectively, by the *p*-anisylTETROL derivative (**70**) (where the *S*-enantiomer was favoured). The e.e. of methyl phenyl sulfoxide was improved

to 29.2% through inclusion with *o*-tolylTETROL (**71**), whereas the (*R*)-isomer of 2-butanol was preferred by *p*-tolylTETROL (**72**) with an e.e. of 23.5%.[140]

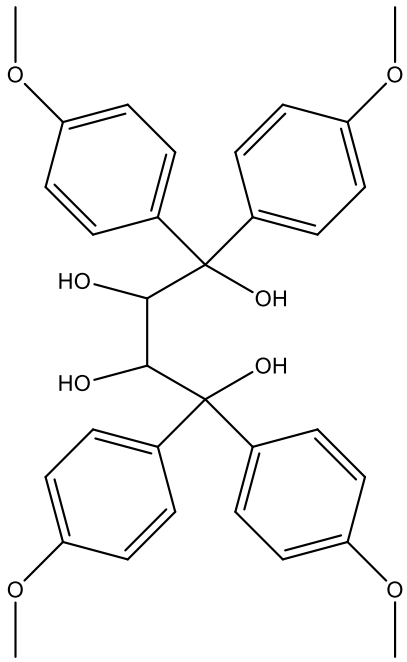

70

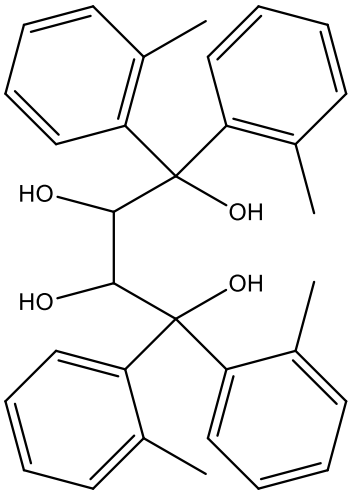

71

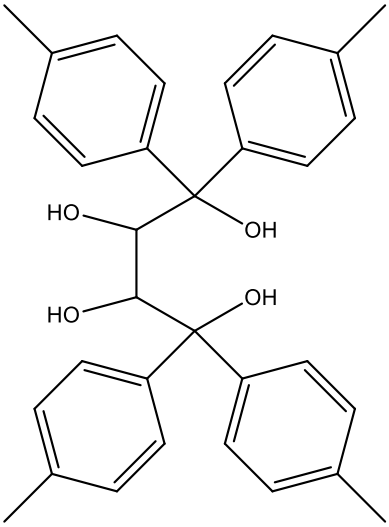

72

Compound **69** may also be modified by considering the reactivity of the four hydroxyl groups. The secondary hydroxyl groups situated vicinally on each of the interior chiral carbons are facile etherification targets. Upon deprotonation and subsequent methylation of these groups, the resultant potential host molecule 2,3-dimethoxy-1,1,4,4-tetraphenylbutane-1,4-diol (**73**) was isolated. A literature review on **73** yielded very little, but the initial synthesis can be ascribed to Seebach *et al* in 1977.[141] They employed sodium hydride as a base and dimethyl sulfate as methylation agent in diethyl ether. A more recent application was the efforts of Teller *et al*,[142] who attempted to modify **73** as a phosporamidite-gold chiral catalyst (**74**) with much success. When screened in a [2+2] cycloaddition reaction, the catalyst was able to furnish an e.e. of 94% for the required product.

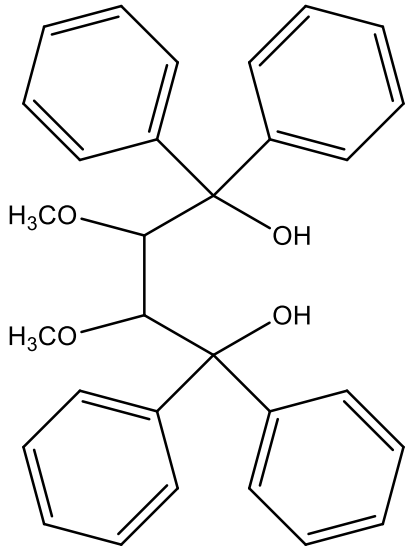

73

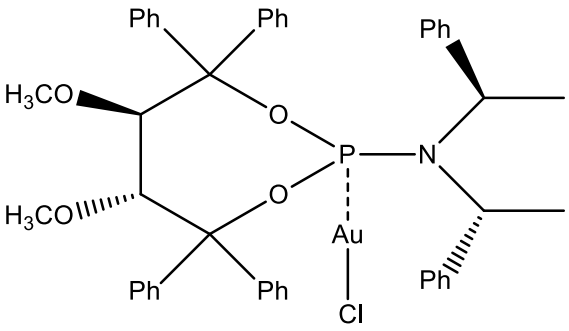

74

The only reported host-guest application found for **73** was that reported by Toda *et al*[143] in 1993, who found that inclusion complexes formed between **73** and cyclohexane as well as *rac*-limonene, toluene, cyclohexanol, diethyl ether and diethylamine. The favoured host:guest ratio was 2:1 in each case. The host was described as having "very low guest-inclusion ability" ascribed to the intramolecular hydrogen bonds formed between the hydroxy and methoxy groups. However, preliminary screening results from a variety of substituted aromatic and cyclic aliphatic compounds by our research team revealed that **73** is an extremely accomplished host in its own right.

1.5 Aims and Objectives

Compound **73** has never been assessed for its potential application in isomer and related guest separations. Therefore, due to the relative novelty of compound **73** as a host, and the industrial importance of effective isomer separation, it was deemed prudent to perform an in-depth investigation into the inclusion capabilities of the host, with a specific interest in the separations of related guests.

In this current work, the inclusion ability of host **73** will be extensively investigated by, first, assessing which organic compounds are suitable guests for this host and, then, subjecting the resultant complexes to available analytical methods such as:

- Proton and carbon NMR analysis,
- Thermal analysis, including thermogravimetric analysis and differential scanning calorimetry,
- Single crystal X-ray diffraction analysis,
- Hirshfeld surface analysis, and
- Gas chromatography coupled to mass spectroscopy.

The host's ability to selectively include one guest in preference to another with the aim of separating similar guests from each other will be investigated in much detail. Related guests that will be assessed include:

- Aniline, *N*-methylaniline and *N,N*-dimethylaniline,
- Ethylbenzene and the xylene isomers,
- Aniline and the toluidine isomers,
- Toluene, ethylbenzene and cumene,
- Nitrobenzene and the nitrotoluene isomers,
- Anisole, and the methylanisole isomers, and
- The cresol isomers.

In this work, attempts will be made to explain any selective behaviour revealed by the host by utilizing data obtained from the aforementioned analytical techniques.

2.1.1 General Analysis

Melting points were recorded on a Stuart SMP10 melting point apparatus and are uncorrected.

Infrared spectra were recorded on a Bruker Tensor 27 Fourier Transform Infrared Spectrometer.

^{1}H-NMR and ^{13}C-NMR spectra were recorded on a 400 MHz Bruker Avance Ultrashield Plus 400 Spectrometer with the chloroform peak of $CDCl_3$ used as internal standard.

Thermogravimetric (TG) and differential scanning calorimetry (DSC) traces were obtained using a TA SDT Q600 module system and analysed using TA Universal Analysis 2000 data analysis software. High purity nitrogen was used as purge gas. An open platinum pan containing the sample and an empty platinum pan as reference was used during these thermal experiments. The heating rate was 10 °C.min^{-1} from room temperature to 250 °C.

Single-crystal X-ray diffraction studies were performed using a Bruker Kappa Apex II diffractometer with graphite-monochromated Mo Kα radiation (λ = 0.71073 Å). The studies were performed at 200K. APEXII[144] was used for data collection and SAINT[144] for cell refinement and data reduction. The structures were solved using SHELXT-2014[145] and refined by least-squares procedures using SHELXL-2016[146] with SHELXLE[147] as graphical interface. Non-hydrogen atoms were refined anisotropically. Hydrogen atoms were placed in idealized geometrical positions in a riding model. Data were corrected for absorption effects using the SADABS[144] numerical method. For ease of reference, the crystallographic information files (.cif) for each single crystal X-ray diffraction experiment is located on the attached CD-ROM at the back of this document.

Gas chromatography was performed using an Agilent Technologies 7890 A gas chromatograph system connected to an Agilent Technologies 5975 C VL MSD mass spectrometer with a triple-axis detector. High purity helium gas was used as the carrier

gas. Column parameters and thermal programs used for each guest mixture are listed in Section 2.6.1.

2.2.1 General Procedure for the Grignard Reactions

Grignard reactions were carried out by charging a 500 mL two-necked round-bottomed flask with magnesium turnings, an iodine crystal and stirrer bar. The turnings were covered with anhydrous THF and the flask fitted with a condenser, $CaCl_2$ drying tube and a dropping funnel. To the flask was added a portion of the required bromobenzene diluted in anhydrous THF. The reaction was initiated through gentle heating while stirring, until the mixture became colourless. Heating was then ceased, and an exothermic reaction occurred. After the reaction subsided somewhat, the remainder of the bromobenzene was added dropwise so as to maintain a steady reflux. Upon completion of the addition of the bromobenzene, the mixture was heated under reflux for 1 h. Thereafter, the mixture was cooled in an ice-water bath. The carbonyl compound, in anhydrous THF, was added dropwise to the stirred solution after which it was, once more heated, under reflux for 1 h. The mixture was subsequently cooled and added into 200 mL of a 10% NH_4Cl solution, poured into a separatory funnel and extracted with ethyl acetate (3 x 50 mL). The combined organic extracts were dried over anhydrous Na_2SO_4. The solvent was removed under reduced pressure to afford a viscus orange oil which crystallized and was recrystallized from ethanol.

2.2.2 (+)-(2*R*,3*R*)-1,1,4,4-Tetraphenylbutane-1,2,3,4-tetraol (**69**) (See general procedure in Section 2.2.1)

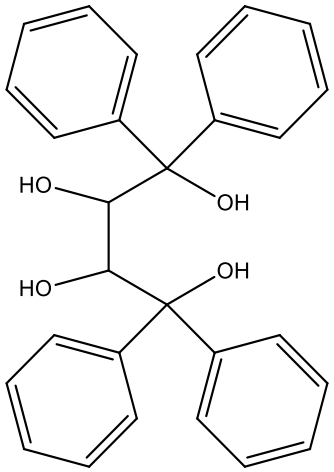

69

Magnesium turnings (8.0571 g, 0.3339 mol), bromobenzene (46.2486 g, 0.2945 mol) and (+)-diethyl L-tartrate (10.4116 g, 0.05049 mol), in dry THF, yielded (+)-(2*R*,3*R*)-1,1,4,4-tetraphenylbutane-1,2,3,4-tetraol (**69**) as a white solid (13.9977 g, 0.03282 mol; 65%), mp 148–150 °C (lit.,[136] mp 150–151 °C); $[\alpha]_D^{23}$ +163° (*c*. 3.18 CH_2Cl_2) {lit.,[136] $[\alpha]_D^{23}$ +154° (*c*. 1.2 $CHCl_3$)}; ν_{max}(solid)/cm^{-1} 3525–3380 (br, OH), 3392–3146 (br, OH), 3057 (Ar), 3031 (Ar), 1597 (Ar) and 1493 (Ar); δ_H($CDCl_3$)/ppm 3.82 (4H, br, 2HCOH and 2CPh_2OH), 4.31 (2H, s, 2HCOH) and 7.05–7.30 (20H, m, Ar); δ_C($CDCl_3$)/ppm 72.10 (HCOH), 81.71 (CPh_2OH), 124.97 (Ar), 126.06 (Ar), 127.14 (Ar), 127.27 (Ar), 128.37 (Ar), 128.55 (Ar), 143.85 (quaternary Ar) and 144.17 (quaternary Ar).

2.3.1 General Procedure for *O*-Methylation Reactions

Methylation reactions were carried out by adding to a two-necked round-bottomed flask anhydrous THF, excess sodium hydride and a stirrer bar. The flask was then fitted with a dropping funnel, condenser and $CaCl_2$ drying tube. The flask was cooled in an ice bath and the hydroxy-containing compound slowly added. Upon completion of this addition, a stoichiometric amount of dimethyl sulfate was added slowly, with

great care. The mixture was allowed to stir for 24 h whereafter it was poured into an ice cold saturated solution of $NaHCO_3$ and stirred for an additional hour. The mixture was poured into a separatory funnel and extracted with ethyl acetate (3 x 50 mL). The combined organic extracts were dried over anhydrous Na_2SO_4, and solvent removed under reduced pressure to afford the desired product.

2.3.2 (–)-(2*R*,3*R*)-2,3-dimethoxy-1,1,4,4-tetraphenylbutane-1,4-diol (**73**, DMT) (See General Procedure in Section 2.3.1)

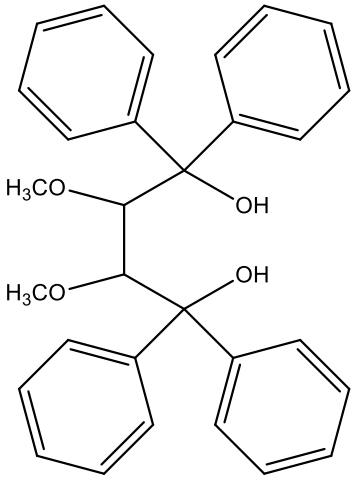

73

(+)-(2*R*,3*R*)-1,1,4,4-Tetraphenylbutane-1,2,3,4-tetraol (**69**) (6.0514 g, 0.01419 mol), excess sodium hydride (6.1424 g, 55–65% suspension in mineral oil) in dry THF and dimethyl sulfate (3.5796 g, 0.02838 mol) produced a gum which was crystallized from petroleum ether (40–60 °C) and recrystallized from ethanol to yield (–)-(2*R*,3*R*)-2,3-dimethoxy-1,1,4,4-tetraphenylbutane-1,4-diol (**73**, DMT) as a white solid (4.6456 g, 0.01022 mol, 72%), mp 124–126 °C (lit.,[143] mp 125–126 °C); $[\alpha]_D^{23}$ –154.5° (*c*. 0.27, CH_2Cl_2) {lit.,[143] –153° (*c*. 0.8, $CHCl_3$)}; ν_{max}(solid)/cm^{-1} 3576–3271 (br, OH), 3025 (Ar), 2836 (CH_3) and 1567 (Ar); δ_H($CDCl_3$)/ppm 2.60 (6H, s, 2OC<u>H</u>$_3$), 4.46 (2H, s, 2<u>H</u>COCH$_3$), 4.87 (2H, s, 2CPh$_2$O<u>H</u>), 7.17 (2H, m, Ar), 7.26 (4H, m Ar), 7.32 (2H, m, Ar) 7.46 (4H, m, Ar) and 7.63 (8H, m, *ortho*-Ar); δ_C($CDCl_3$)/ppm 61.00 (O<u>C</u>H$_3$), 80.09 (<u>C</u>Ph$_2$OH), 85.27 (H<u>C</u>OCH$_3$), 125.89 (Ar), 126.05 (Ar), 126.79 (Ar), 127.22 (Ar), 127.95 (Ar), 128.46 (Ar), 144.92 (quaternary Ar) and 145.64 (quaternary Ar).

2.3.3 *p*-Methylanisole (See General Procedure in Section 2.3.1)

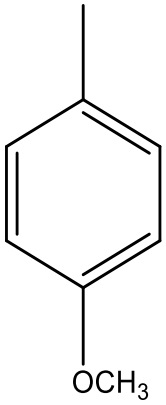

p-Methylphenol (17.2010 g, 0.1591 mol), excess sodium hydride (7.6342 g, 55–65% suspension in mineral oil) in dry THF and dimethyl sulfate (20.1808 g, 0.1600 mol) were refluxed for 2 hours and stirred overnight to produce a yellow liquid which was fractionally-distilled to afford *p*-methylanisole as a colourless liquid (17.7285 g, 0.1451 mol, 91%), b.p. 59–61 °C/12 mmHg (lit.,[148] 65 °C/14 mmHg); ν_{max}(liquid)/cm^{-1} 3102 (weak, Ar), 3064 (weak, Ar), 2956 (CH_3), 2903 (CH_3) and 1581 (Ar); δ_H($CDCl_3$)/ppm 2.40 (3H, s, PhC<u>H</u>$_3$), 3.87 (3H, s, PhOC<u>H</u>$_3$), 6.89–6.94 (2H, m, Ar) and 7.18–7.21 (2H, m, Ar); δ_C($CDCl_3$)/ppm 20.48 (Ph<u>C</u>H$_3$), 55.25 (PhO<u>C</u>H$_3$), 113.79 (Ar), 129.85 (quaternary Ar), 129.96 (Ar) and 157.60 (quaternary Ar).

2.3.4 *m*-Methylanisole (See General Procedure in Section 2.3.1)

m-Methylphenol (25.1412 g, 0.2325 mol), excess sodium hydride (10.1594 g, 55–65% suspension in mineral oil) in dry THF and dimethyl sulfate (30.2838 g, 0.2401 mol) were refluxed for 2 hours and stirred overnight to produce a yellow liquid which was fractionally-distilled to afford *m*-methylanisole as a colourless liquid (21.7868 g, 0.1783 mol, 77%), b.p. 69–71 °C/22 mmHg (lit.,[148] 65 °C/14 mmHg); ν_{max}(liquid)/cm^{-1} 3050 (Ar), 3029 (Ar), 2952 (CH_3), 2835 (CH_3) and 1586 (Ar); δ_H($CDCl_3$)/ppm 2.44 (3H, s, PhC<u>H</u>$_3$), 3.87 (3H, s, PhOC<u>H</u>$_3$), 6.81–6.88 (2H, m, Ar) and 7.27 (2H, t, Ar); δ_C($CDCl_3$)/ppm 21.64 (Ph<u>C</u>H$_3$), 55.07 (PhO<u>C</u>H$_3$), 111.03 (Ar), 115.00 (Ar), 121.71 (Ar), 129.41 (Ar), 139.57 (quaternary Ar) and 159.94 (quaternary Ar).

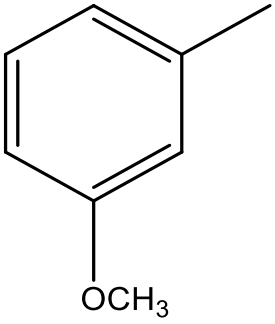

2.3.5 *o*-Methylanisole (See General Procedure in Section 2.3.1)

o-Methylphenol (30.5913 g, 0.2829 mol), excess sodium hydride (14.1502 g, 55–65% suspension in mineral oil) in dry THF and dimethyl sulfate (36.6408 g, 0.2905 mol) was refluxed for 2 hours and stirred overnight to produce a yellow liquid which was fractionally-distilled to afford *o*-methylanisole as a colourless liquid (29.9414 g, 0.2451 mol, 86%), b.p. 55–57 °C/12 mmHg (lit.,[148] 64 °C/14 mmHg); ν_{max}(liquid)/cm^{-1} 3065 (weak, Ar), 3024 (weak, Ar), 2947 (CH_3), 2835 (CH_3) and 1591 (Ar); δ_H($CDCl_3$)/ppm 2.33 (3H, s, PhC<u>H</u>$_3$), 3.91 (3H, s, PhOC<u>H</u>$_3$), 6.90–6.97 (3H, m, Ar) and 7.22–7.28 (1H, m, Ar); δ_C($CDCl_3$)/ppm 16.43 (Ph<u>C</u>H$_3$), 55.28 (PhO<u>C</u>H$_3$), 110.16 (Ar), 120.58 (Ar), 126.79 (quaternary Ar), 127.12 (Ar), 130.89 (Ar) and 158.04 (quaternary Ar).

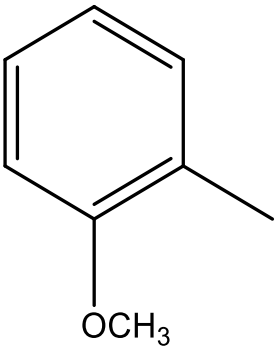

2.4.1 Formation of Single Solvent Inclusion Complexes

The host compound was dissolved in the guest with heating if necessary. A co-solvent was added in those cases where the guests were solids. The co-solvent required careful selection since it should not be included by the host material. Upon standing at ambient temperature and pressure, a solid crystallized out. The crystals were filtered, washed with cold ethanol and petroleum ether (40–60 °C), and dried using vacuum filtration. The crystalline material was then analysed by NMR spectroscopy in order to determine whether inclusion had occurred and, if so, the host:guest (H:G) ratio. This was achieved by integrating the relevant host and guest signals in the ^{1}H-NMR spectra.

2.4.2 Competition Inclusion Experiments

Competition experiments were performed in order to determine whether the host displayed any selectivity when recrystallized from a mixture of two or more guests. Initially, approximately 0.2 g of the host was dissolved in equimolar and non-equimolar binary mixtures of the guest compounds. In cases where the major guest component was a solid, a carefully selected co-solvent was added in order to facilitate dissolution. The crystals thus formed were filtered and washed as with the single solvent guest inclusion experiments. These crystals and their respective mother liquors were analysed by means of gas chromatography to determine the mole fraction of guests A and B in the mother liquor (X_A and X_B) and the crystal (Z_A and Z_B). This allowed for the construction of selectivity curves where Z_A (or Z_B) was plotted against X_A (or X_B) (Figure 12). The selectivity coefficient as a measure of selectivity is defined by:

$$\boldsymbol{K_{A:B} = (Z_A/Z_B) \times (X_B/X_A)} \text{ where } \boldsymbol{X_A + X_B = 1} \qquad \textbf{Equation 2}$$

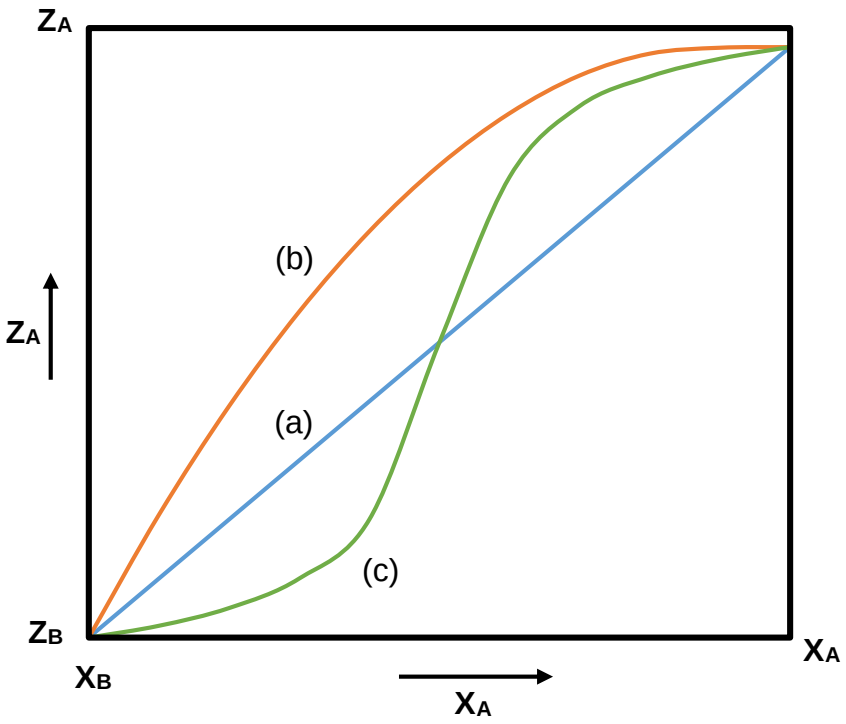

Figure 12: Representative selectivity curves obtained from selectivity experiments. X_A is the mole fraction of guest A in the mother liquor, and Z_A is the mole fraction of guest A in the crystal; a) no selectivity (K = 1); b) positive selectivity for guest A (K > 1) and c) selectivity is guest concertation-dependent.

Ternary competition experiments were also carried out in a similar manner to the binary competitions by recrystallizing a known amount of host from equimolar and non-equimolar mixtures of three different guests. Analysis of the resultant crystal content and mother liquor composition from these ternary mixtures allowed for the construction of ternary plots as provided in Figure 13. The apices of the triangular plot represent pure guest compositions, and guest compositions of A, B and C increase according to the direction shown. As a descriptive example, point 4' has a composition of 0.2A, 0.2B and 0.6C (where A + B + C = 1).

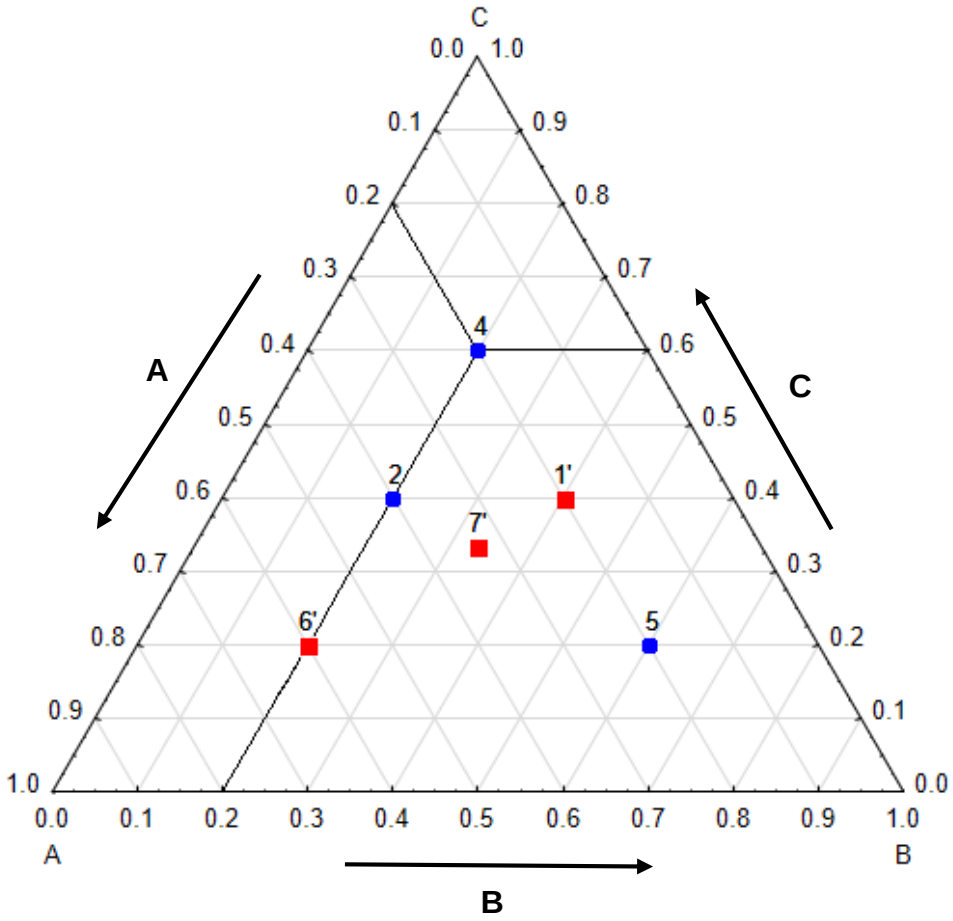

Figure 13: Example of a ternary plot using three hypothetical guest compounds in the recrystallization process. A data point labelled with an apostrophe signifies the guest content of a complex, while a point without an apostrophe indicates the composition of the mother liquor.

2.5.1 Hirshfeld Surface Analysis

In order to explore the types of intermolecular interactions between host and guest in inclusion complexes quantitatively, the Hirshfeld surface around the guest was modelled using the software Crystal Explorer.[149] The Hirshfeld surface depicts the interactions between the guest molecule internal to this surface and the rest of the molecules external to the surface. This allows for the intermolecular interactions to be shown quantitatively in a graphical manner, permitting simplified identification and interpretation of the significant interaction differences in various host-guest complexes. A two-dimensional fingerprint plot of external distance (d_e) *vs* internal distance (d_i) may be generated, providing information about the intermolecular interactions between host and guest. Each point on the plot thus corresponds to a unique (d_e,d_i) value, the colour of which is relative to the surface area contributing to that (d_e,d_i). points coloured blue signify smaller contributions, while green to red indicate greater contributions. Figure 14a shows a typical Hirshfeld surface, and Figure 14b the two-dimensional fingerprint plot generated from the surface.

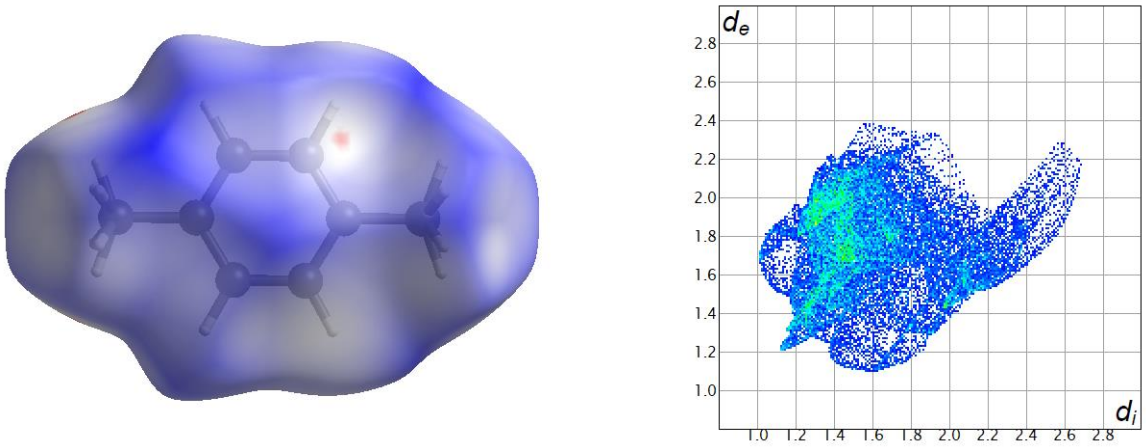

Figure 14: a) Hirshfeld surface generated around a *p*-xylene molecule and b) a two-dimensional fingerprint plot generated from the Hirshfeld surface.

2.5.2 Computational Studies

Calculations were performed using SPARTAN '10 for Windows [build 1.1.0 (March 20, 2011)] software, supplied by Wavefunction Inc.[150] Conformational searches were carried out using the Monte Carlo algorithm as implemented in the MMFF force field. The first one hundred lowest energy conformations were retained, and only the structures whose relative energies fell within the first 20 $kJ.mol^{-1}$ range were refined further. This was done at the DFT level using the B3LYP function, and progressively employing the 6-31G* and 6-311G* basis sets.

2.6.1 GC/MS Methods

A variety of columns and temperature programs were utilized during gas chromatography in order to separate guest peaks and quantify their relative peak areas. The methods used from each chapter is listed below. All columns used had a length of 30m, inner diameter of 250 µm, and a film thickness of 0.25 µm. An inlet temperature of 250 °C was employed in each experiment.

Chapter 3: An Agilent J&W DB-WAX column was used. From an initial temperature of 60 °C, a heating rate of 2.5 $°C.min^{-1}$ was employed up to 130 °C with a final hold time of 1 min.

Chapter 4: An Agilent J&W DB-WAX column was used. From an initial temperature of 50 °C, a heating rate of 1 $°C.min^{-1}$ was employed up to 160 °C with a final hold time of 10 min.

Chapter 5: An Agilent J&W Cyclosil-B column was used. From an initial temperature of 60 °C, a heating rate of 2.5 $°C.min^{-1}$ was employed up to 130 °C with a final hold time of 1 min.

Chapter 6: An Agilent J&W Cyclosil-B column was used. From an initial temperature of 50 °C, a heating rate of 2.5 $°C.min^{-1}$ was employed up to 90 °C with a final hold time of 1 min.

Chapter 7: An Agilent J&W Cyclodex-B column was used. From an initial temperature of 60 °C, a heating rate of 4 °C.min^{-1} was employed up to 145 °C with a final hold time of 1 min.

Chapter 8: An Agilent J&W DB-WAX column was used. From an initial temperature of 65 °C, a heating rate of 2 °C.min^{-1} was employed up to 105 °C with a final hold time of 1 min.

Chapter 9: An Agilent J&W Cyclosil-B column was used. From an initial temperature of 50 °C, a heating rate of 5 °C.min^{-1} was employed up to 160 °C with a final hold time of 5 min.

Chapter 3: Inclusion Compounds of DMT (73) with Aniline and the *N*-Alkylated Anilines

3.1 Introduction

Narayanan and Deshpande[151] reviewed the advances in *N*-alkylated aniline synthesis using solid acid catalysis in 2000. Industrially, aniline is mainly used for the production of methylene diphenylene isocyanate, a key intermediate in the synthesis of polyurethanes. Other applications of aniline are in the production of pigments and dyes, and as an antidegradant in rubbers. *N*-Methylaniline (NMA) is used as an antiknock agent in fuel, while *N*,*N*-dimethylaniline (DMA) finds routine application as an intermediate for pharmaceuticals, and also as a catalyst for polymerization reactions.[152–154] The synthesis of NMA is usually accomplished through methylation with methanol. While seemingly straightforward, this reaction experiences selectivity issues as a result of overalkylation to form DMA. Additionally, rearrangements of NMA and DMA may also occur, thus producing toluidines.[155] More recent advances in the selective synthesis of NMA and DMA were made by using a triphenylphospine/2,3-dichloro-5,6-dicyanobenzoquinone reagent system,[156] and *via* catalysis by means of dodecatungstophosphoric acid supported on K10 montmorilonite.[157] The manufacture of *N*-alkylated anilines continues to pose a challenge to chemists and, as such, the development of a simple and selective method for obtaining these anilines with high purity remains of great interest.

The separation of these anilines through fractional distillation is challenging due to the similarity in their boiling points (184.2, 196.2 and 194.2 °C, respectively). With this in mind, alternative separation technologies are attractive. Gaiker *et al*[158] used zeolites to separate these compounds, while Yebeutchou and Dalcanale[159] employed host-guest chemistry to sequester NMA from the reaction mixture thus disallowing overalkylation. It is thus prudent to investigate whether DMT has any affinity for aniline, NMA and DMA as a host compound and, if so, whether DMT shows selective inclusion towards any of these guests, and therefore whether this host may have successful future application in the separation of these guests.

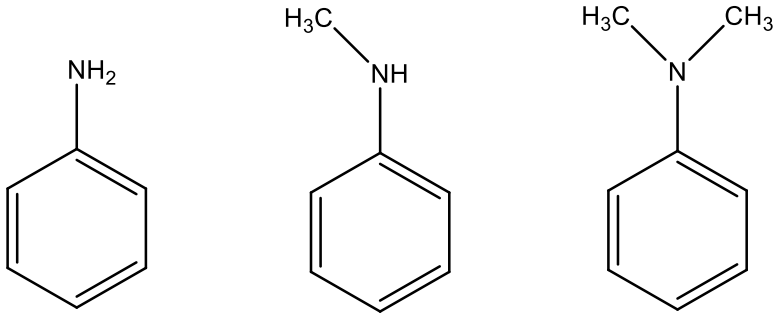

Aniline *N*-Methylaniline (NMA) *N,N*-Dimethylaniline (DMA)

3.2 Individual and Equimolar Binary and Ternary Inclusion Experiments

After recrystallizing DMT independently from aniline and the *N*-methyl-substituted anilines, the resultant solids were subjected to ^{1}H-NMR spectroscopy in order to determine whether inclusion had occurred. It was thus observed that DMT forms 2:1 host:guest complexes in each case (Table 5).

Table 5: Host:guest ratios of complexes formed with DMT during individual recrystallization experiments.

Guest	Host:guest
Aniline	2:1
NMA	2:1
DMA	2:1

*Determined using ^{1}H-NMR spectroscopy.

DMT was subjected to various competition experiments by recrystallizing it from equimolar binary and ternary mixtures of these anilines. Table 6 indicates the outcome of these experiments, where preferred guests are shown in bold italic font face. Analyses were carried out using GC-MS. In each case, the overall host:guest ratio remained 2:1. When DMT was recrystallized from a binary mixture of aniline and DMA, the latter was significantly preferred (85.3%), while an aniline/NMA experiment showed that the substituted aniline was, once more, preferably selected (85.1%). Aniline was therefore discriminated against in each of these experiments. An NMA/DMA experiment resulted in an inclusion complex comprising 40.8% NMA and 59.2% DMA. The ternary competition experiment afforded a selectivity order in accordance with that inferred from the binary competitions, namely that the host's selectivity increases in the order aniline << NMA < DMA.

Table 6: Competition experiments and H:G ratios obtained.*

Aniline	NMA	DMA	Guest ratios (% Standard deviation)$	Overall H:G ratio
x	***x***		14.9:***85.1*** (0.12)	2:1
x		***x***	14.7:***85.3*** (0.82)	2:1
	x	***x***	40.8:***59.2*** (0.32)	2:1
x	x	***x***	6.3:31.5:***62.2*** (0.21)(0.20)(0.03)	2:1

*Determined using GC-MS; $experiments were carried out in triplicate, and an average ratio is provided here with % e.s.d.'s in parentheses.

3.3 Host Selectivity Profiles with Changing Guest Concentrations in Binary and Ternary Guest Mixtures

This report investigated the host's selectivity behaviour during binary competition experiments where the guests were present in non-equimolar amounts. Three selectivity curves were thus obtained for the three combinations of guests.

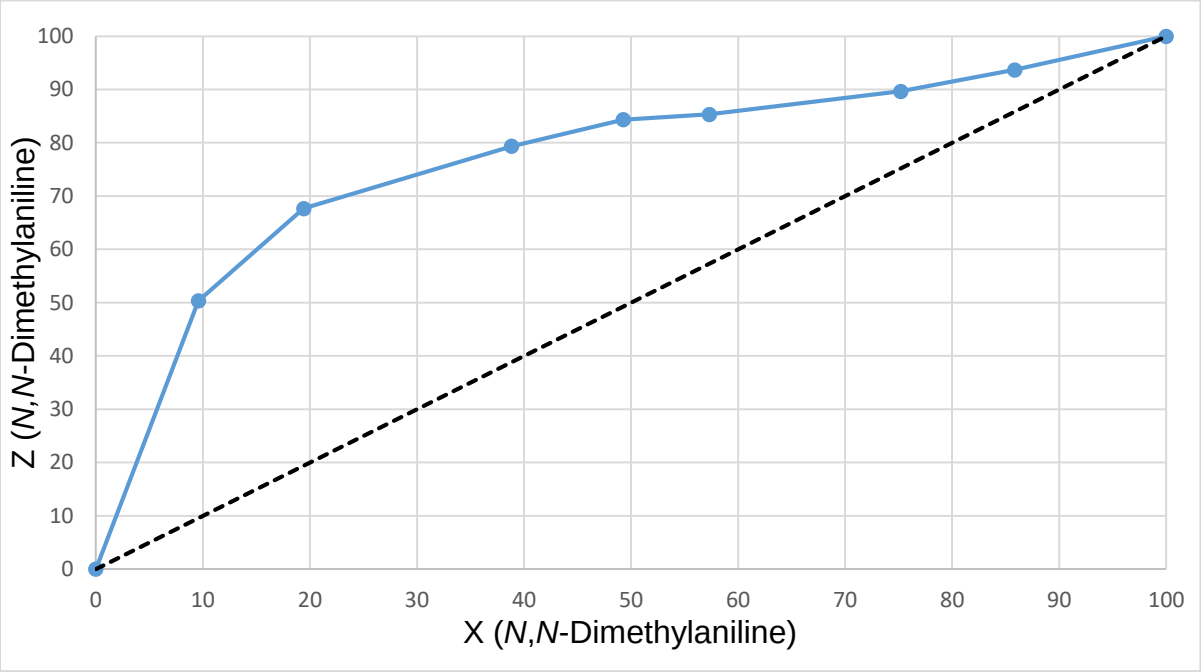

Figure 15: Selectivity curve obtained from the DMA/aniline experiments. Coloured blue is the molar fraction of DMA in the inclusion complex (Z) *vs* the molar fraction of DMA in the mother liquor (X). Black dashes indicate the theoretical line of no selectivity.

Figure 15 was obtained for the DMA/aniline experiment and indicates that even at low concentrations of DMA in the mother liquor, the fraction of DMA within the inclusion complex is significantly higher than that of aniline. At approximately 39% DMA, the amount of the guest in the complex is ~80% (and, therefore, aniline ~20%). A further increase in DMA in the mother liquor results in an inclusion complex even richer in DMA. However, aniline never becomes fully excluded – even at ~86% DMA, about 14% aniline was present in the crystalline complex. For DMA, the average selectivity coefficient, K, was found to be 5.64.

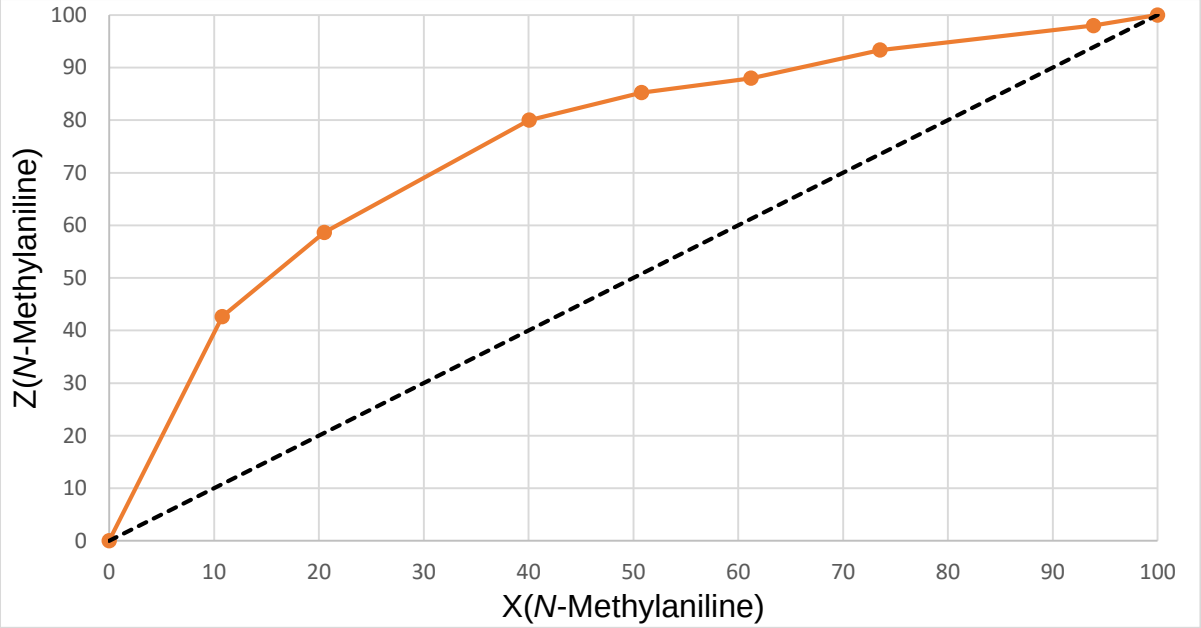

Figure 16: Selectivity curve for the NMA/aniline experiments. Coloured orange is the molar fraction of NMA in the inclusion complex (Z) *vs* the molar fraction of NMA in the mother liquor (X). Black dashes indicate the theoretical line of no selectivity.

The selectivity curve (Figure 16) obtained when aniline was made to compete against NMA produced a similar response to that in Figure 14. NMA was considerably preferred over the entire molar concentration range assessed. From a mother liquor composition of about 11% NMA and 89% aniline, crystals were harvested already containing as much as 43% NMA. Thereafter, as the NMA concentration in the mother liquor increased, so did the NMA concentration in the crystals. This trend was recorded up to a point reflecting an NMA mother liquor concentration of 94% resulting in crystals with an NMA content of 98%. K was found to be 5.16, slightly lower than that obtained for the DMA/aniline experiment. A comparison of the initial slopes of the curves in Figure 15 and Figure 16 indicates a marked preference for DMA over NMA as observed by the steeper curve in Figure 14 between 0–11% X.

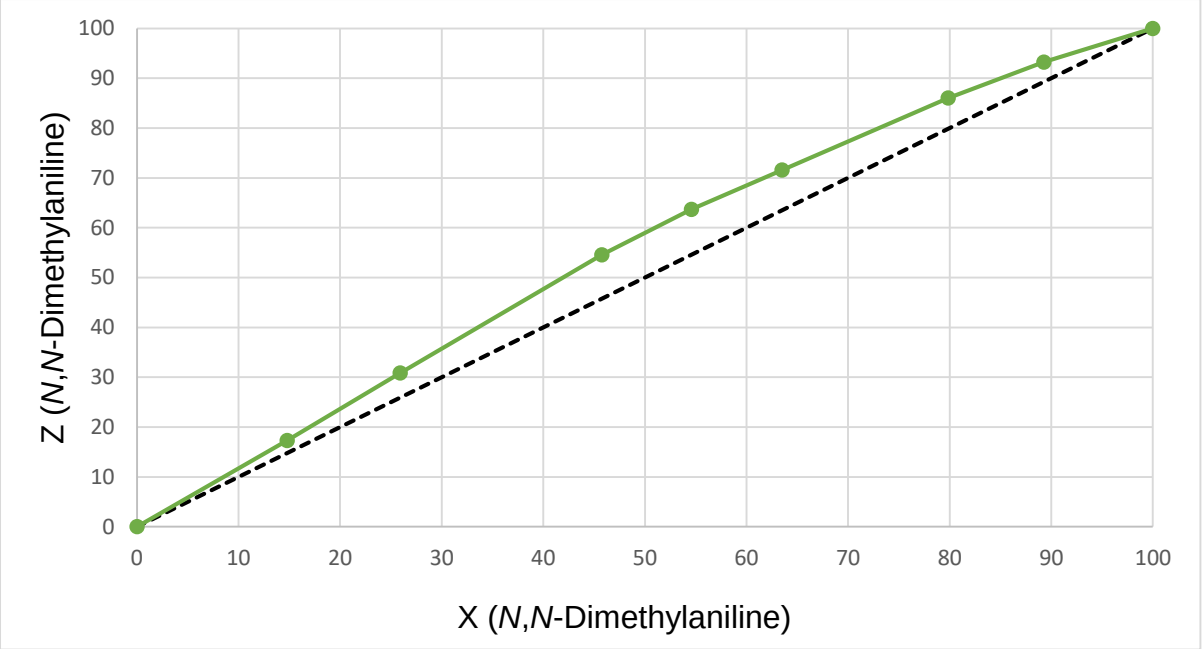

Figure 17: Selectivity curve from the DMA/NMA experiments. Coloured in green is the molar fraction of DMA in the inclusion complex (Z) *vs* the molar fraction of DMA in the mother liquor (X). Black dashes indicate the theoretical line of no selectivity.

When DMA and NMA competed, it became evident that the selectivity of the host for these two components was much lower compared with binary experiments involving aniline. The selectivity curve obtained from the DMA/NMA experiment has a flat trajectory, with all points relatively close to the theoretical line of no selectivity (Figure 17). However, regardless of the low selectivity exhibited, DMT still preferred DMA to NMA over the entire molar concentration range. The average selectivity coefficient for this competition curve was only 1.43 in favour of DMA.

Experiments were also carried out where DMT was recrystallized from mixtures containing all three of these guests with differing molar ratios, and so a ternary graph (Figure 18) was constructed. The aniline content of the inclusion complex obtained in each case decreased dramatically compared with the mother liquor from which the complex was harvested. In turn, the DMA content of the crystals increased, while the included NMA amount remained approximately comparable upon inclusion.

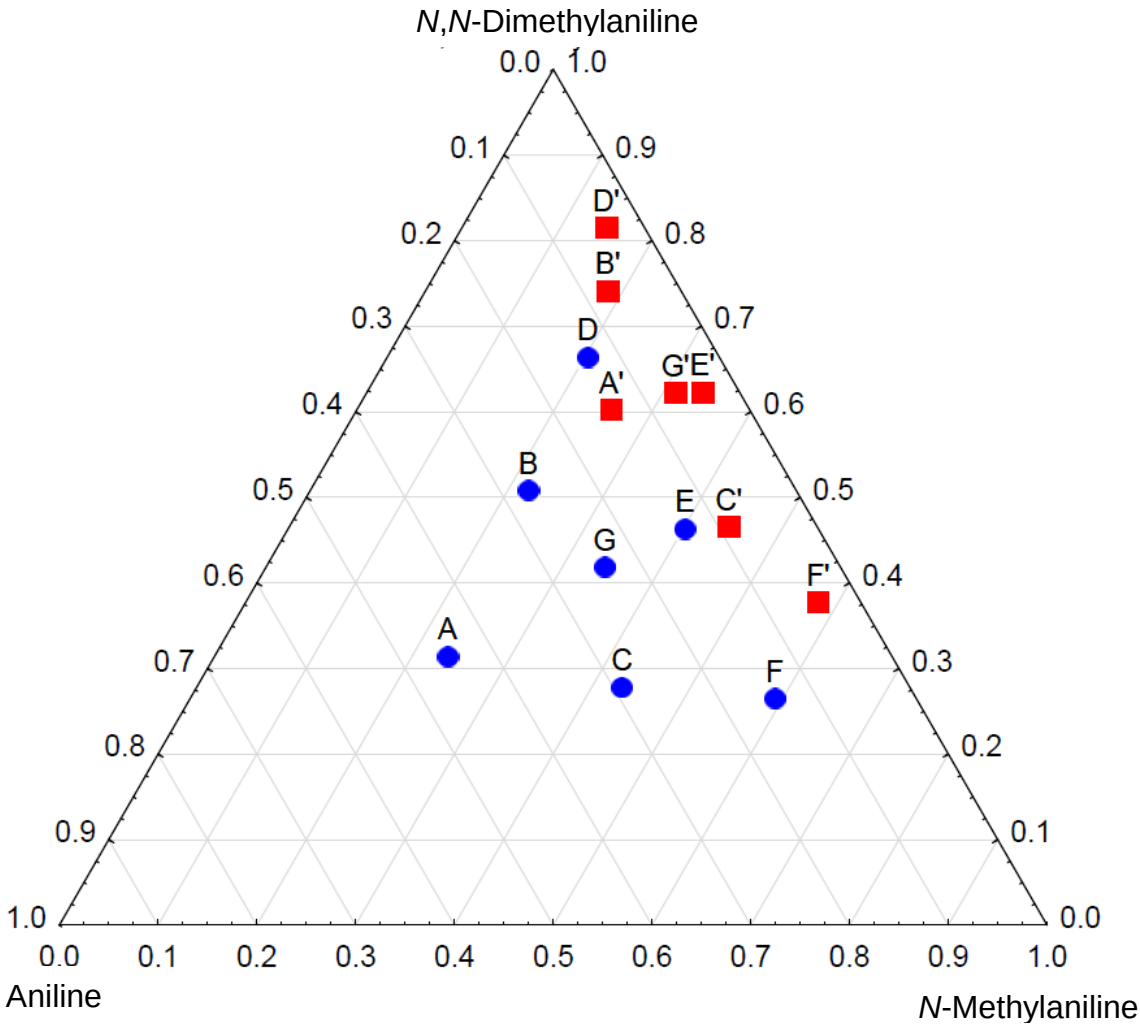

Figure 18: Ternary competition plot obtained from the aniline/NMA/DMA experiments. Blue circles indicate mother liquor compositions, while red squares indicate guest composition in the crystals.

3.4 Thermal analysis

The thermal stability of the three inclusion complexes was investigated by subjecting each complex to simultaneous thermogravimetric analysis and differential scanning calorimetry. The complexes were heated at 10 °C.min^{-1} under high purity nitrogen as a purge gas. The overlaid TG, derivative of the TG (DTG) and DSC traces thus obtained are provided in Figures 19–21. The onset temperatures for guest release were estimated from the TG and DTG traces, the guest release peak temperatures were obtained from the DTG trace, and the endotherm peak temperatures from the DSC trace.

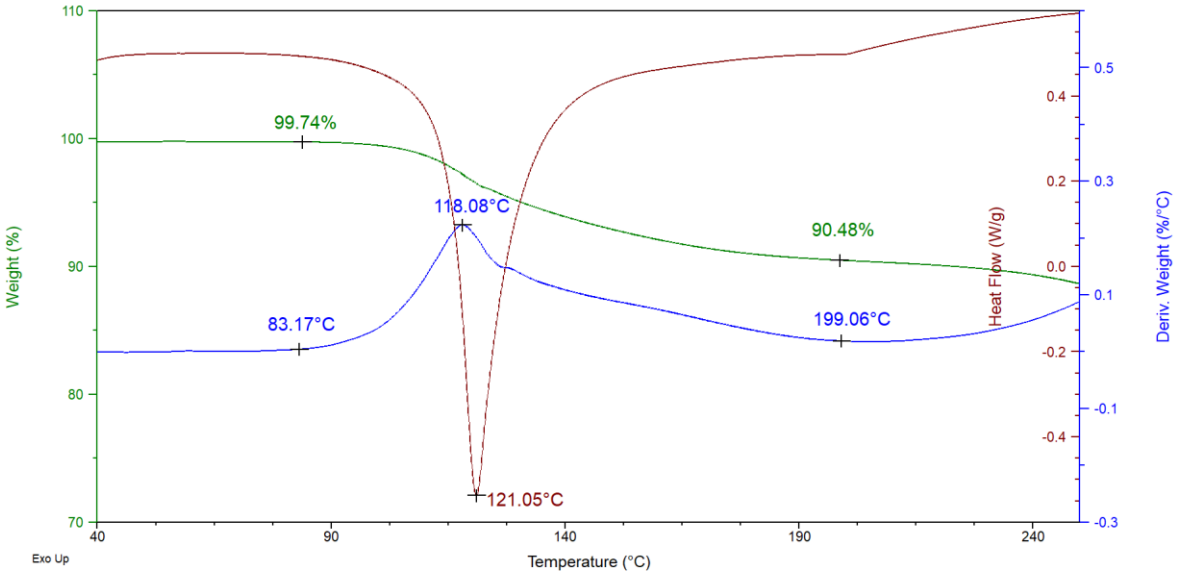

Figure 19: Overlaid TG (green), TG derivative (blue) and DSC (brown) traces for the 2DMT•aniline complex upon heating at 10 °C.min^{-1}.

The theoretical mass loss for a 2:1 DMT•aniline complex is 9.3% if all of the guest is driven off through heating. From the TG trace (Figure 19, green plot), a mass loss of ~9.3% was obtained after heating to ~199.1 °C, which thus correlates exactly with the theoretically-expected mass loss. Mass loss continued after 199 °C, and was due to decomposition of the host compound. The guest release event occurred over a single step over a temperature range of ~115.9 °C, with an onset temperature of 83.2 °C

(estimated from the DTG trace). The maximum rate of guest release was estimated at 118.1 °C (DTG), and the maximum heat flow at 121.1 °C (DSC). This endotherm is as a result of the host melt and guest release occurring concomitantly.

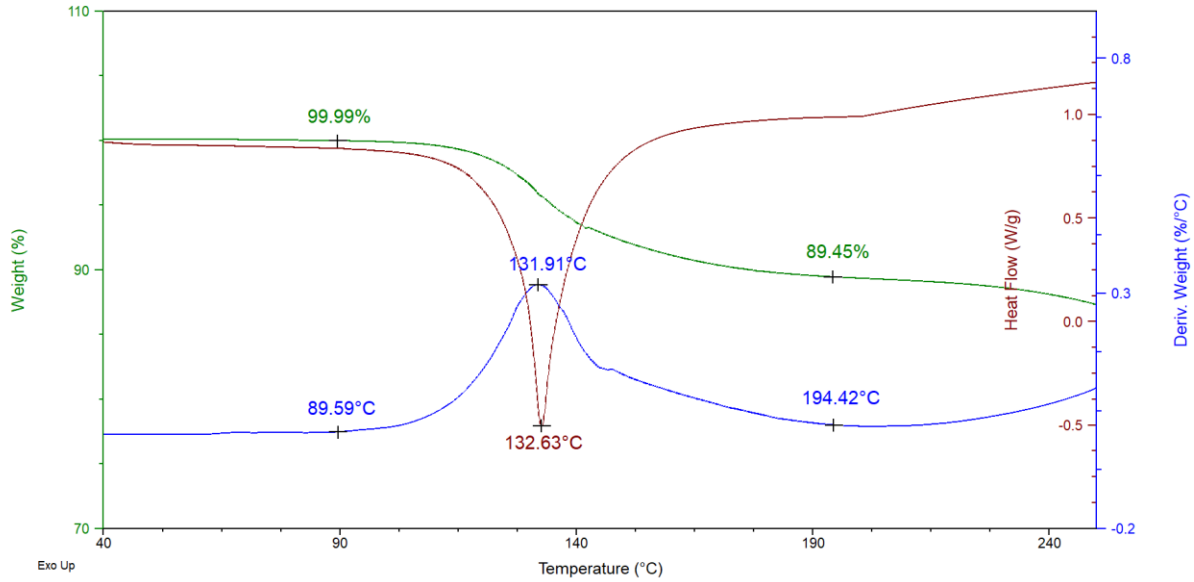

Figure 20: Overlaid TG (green), TG derivative (blue) and DSC (brown line) traces for the 2DMT•NMA complex upon heating at 10 °C.min^{-1}.

When subjecting the 2DMT•NMA complex to heating at 10 °C.min^{-1}, a TG trace was obtained (Figure 20, green plot) showing a mass loss of 10.5% which correlates, once more, exactly with the expected mass loss for a 2:1 complex (10.5%). All of the guest is released before ~195 °C. Mass loss again occurred in a single step spanning 104.8 °C. The onset temperature of mass loss was 89.6 °C, which is higher than observed for the aniline complex (83.2 °C). The temperature at which guest release was at a maximum rate was ~131.9 °C, while the endotherm peak temperature was ~132.6 °C. Both these values are significantly higher than that of the aniline complex (118.1 and 121.1 °C, respectively).

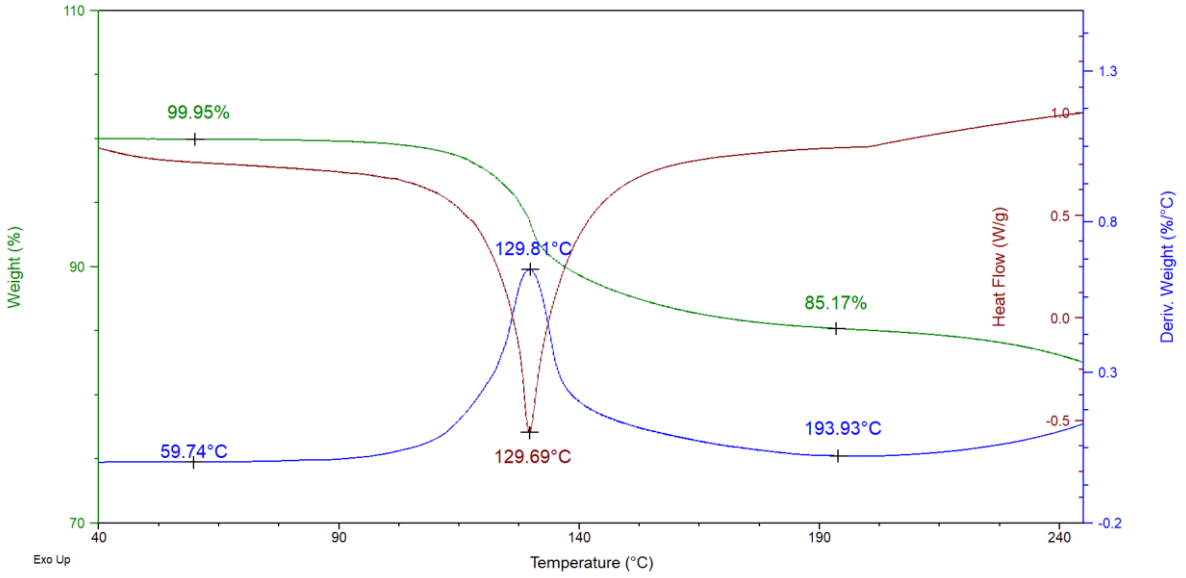

Figure 21: Overlaid TG (green), TG derivative (blue) and DSC (brown) traces for the 2DMT•DMA complex upon heating at 10 °C.min^{-1}.

The expected mass loss for a 2:1 DMT•DMA complex is 11.8%. From the green TG trace in Figure 21, however, a mass loss of 14.8% was observed. The TG/DSC experiment was repeated but with the same result. The onset temperature for the loss was estimated to be ~59.7 °C (blue curve), while the maximum rate of guest release occurred at ~129.8 °C and the endotherm peak temperature was 129.7 °C.

Table 7 summarises the temperatures at which the major thermal events occurred as obtained from these experiments. The term T_{on}–T_b has in the past been used as an indicator of the relative thermal stabilities of host-guest complexes, where T_{on} is the guest release onset temperature, and T_b the boiling point of pure guest.[160,161] More positive values are associated with more stable complexes. The term's validity relies on isostructural host packing (which is the case for these complexes, see later), as well as the accurate determination of the mass loss onset temperatures. In comparing T_{on}–T_b for the three aniline complexes, the stability order can be written as aniline (–101.0 °C) > NMA (–106.6 °C) > DMA (–134.5 °C). This is in direct contrast to the selectivity order determined from competition experiments and we cannot explain this result at this stage. However, T_p (blue DTG trace) is the temperature at which guest release is most rapid, and must thus also be related to the strength of enclathration: the higher T_p values are associated with complexes having higher thermal stabilities.

Here, T_p decreases in the order NMA (131.9 °C) ≈ DMA (129.8 °C) >> aniline (118.1 °C) (Table 7).

Table 7: Summary of the major thermal events observed in the aniline, NMA and DMA complexes with DMT.

Guest	T_b (°C)	T_{on}[a] (°C)	T_{on}–T_b (°C)	T_p[b] (°C)	T_{end}[c] (°C)	Mass loss % (Expected)
Aniline	184.2	83.2	-101.0	118.1	121.1	9.3 (9.3)
N-Methylaniline	196.2	89.6	-106.6	131.9	132.6	10.5 (10.5)
N,*N*-Dimethylaniline	194.2	59.7	-134.5	129.8	129.7	14.8(11.8)[d]

[a]T_{on} is the onset temperature for guest release estimated from the DTG; [b]T_p values were determined from the blue DTG traces; [c]T_{end} values were obtained from the brown DSC traces; [d]reasons for the much larger observed mass loss compared with that expected are not clear at this stage.

Considering the high selectivity for NMA and DMA displayed by DMT compared with aniline, as well as the very similar affinity of DMT for DMA and NMA in binary competition mixtures with aniline, it may be argued that the stability order based on T_p correlates better here with observations from competition experiments.

The use of T_{end}, the endotherm peak temperature, to predict relative complex stabilities could not be used here because these endotherms represent both host melt and guest release events, and not guest release alone.

3.5 Single Crystal X-Ray Analysis

To determine the factors influencing the selectivity and thermal stability order of the three aniline inclusion complexes, single crystal X-ray diffraction experiments were performed on crystals from each of these complexes. Table 8 lists crystal data and refinement parameters; it is clear from the data that the three complexes are isostructural, all crystallizing in the monoclinic crystal system with *C*2 symmetry.

Table 8: Crystallographic data for the complexes between DMT and the three aniline and methylaniline guests.

	2DMT•aniline	**2DMT•NMA**	**2DMT•DMA**
Chemical formula	$C_{30}H_{30}O_4$	$C_{30}H_{30}O_4$	$C_{30}H_{30}O_4$
	•0.5C_6H_7N*	•0.5C_7H_9N	•0.5$C_8H_{11}N$
Formula weight	1000.19	1016.23	1030.26
Crystal system	Monoclinic	Monoclinic	Monoclinic
Space group	*C*2	*C*2	*C*2
μ (Mo-Kα)/mm^{-1}	0.078	0.079	0.078
a/Å	17.3753(6)	17.4040(13)	17.2529(9)
b/Å	11.9583(4)	11.9799(8)	12.2593(6)
c/Å	14.1310(5)	14.0402(11)	14.1764(8)
alpha/°	90	90	90
beta/°	110.137(2)	109.729(3)	109.749(2)
gamma/°	90	90	90
V/Å ^{3}	2756.65(17)	2755.5(4)	2822.0(3)
Z	2	2	2
F(000)	1064	1084	1100
Temp./K	200	200	200
Restraints	1	1	6
Nref	6832	5988	6260
Npar	326	372	374
R	0.0442	0.0358	0.0333
wR2	0.1328	0.0913	0.0903

S	1.07	1.03	1.04
θ min-max/°	2.1, 28.4	1.5, 28.3	2.1, 28.3
Tot. data	48117	23996	27556
Unique data	6832	5988	6260
Observed data [I > 2.0 sigma(I)]	6293	5287	5728
R_{int}	0.021	0.025	0.017
Dffrn measured fraction θ full	0.999	1.00	0.999
Min. resd. dens. (e/ Å^3)	–0.55	–0.20	–0.18
Max. resd. dens. (e/ Å^3)	0.43	0.18	0.19

*The hydrogens on the amine nitrogen could not be located.

The 2DMT•aniline complex

Figure 22 shows the unit cell for the 2:1 DMT:aniline complex. The disorder present in the guest is due to a symmetry-generated guest molecule occupying the same position. It was not possible to locate or calculate the positions of the amine hydrogens of the guest in this case. Figure 23 shows a stereoview of the complex to better visualise the packing in three-dimensional space.

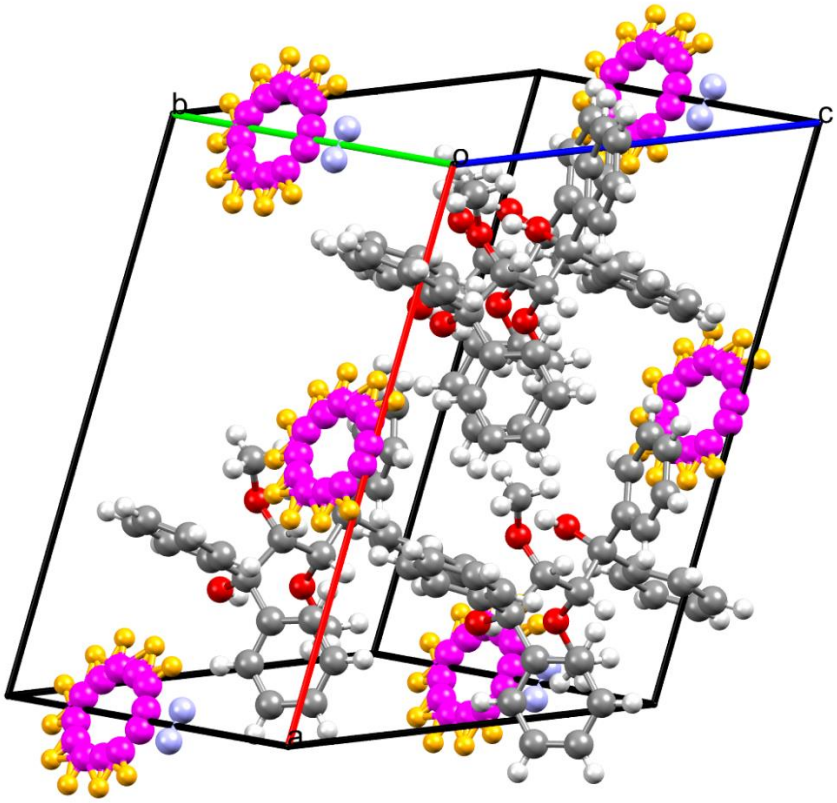

Figure 22: The unit cell for the 2DMT•aniline complex; the guest has the magenta carbon framework while the host has the grey carbon framework.

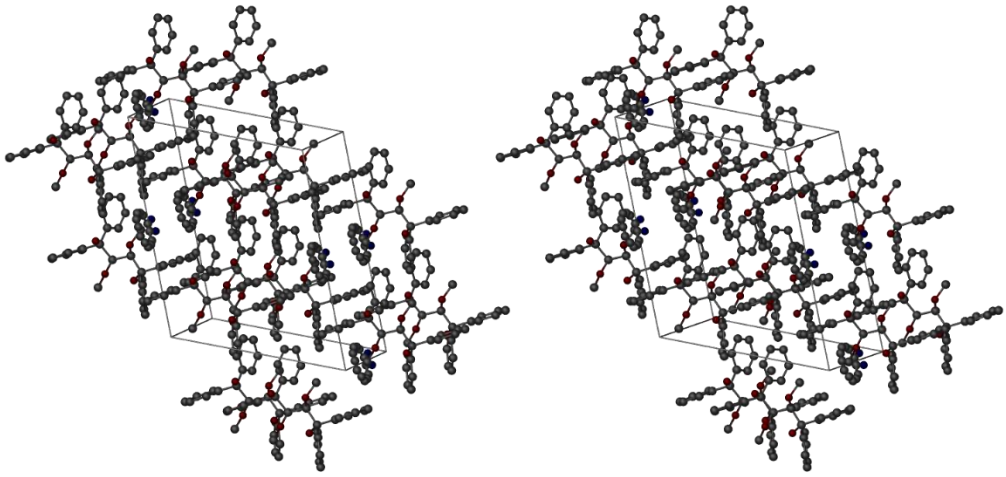

Figure 23: Stereoview of the 2DMT•aniline complex to show the packing in three dimensions.

The host geometry is maintained by a pair of intramolecular hydrogen bonds between the hydroxy and methoxy moieties on the butane backbone (Table 9 and Figure 24, blue lines). A variety of inter- and intra- molecular non-classical hydrogen bonding interactions ranging between 2.650(3) and 3.522(3) Å exist and these serve only to stabilize the host packing and geometry since none of these are between host and guest (Table 10).

Table 9: Classic intramolecular hydrogen bonding interactions in the 2DMT•aniline complex.

Non-covalent interaction	Distance (Å) D–A	Angle (°) D-H···A
(host)O-H···O(host methoxy)	2.675(2)	140
(host)O-H···O(host methoxy)	2.627(2)	140

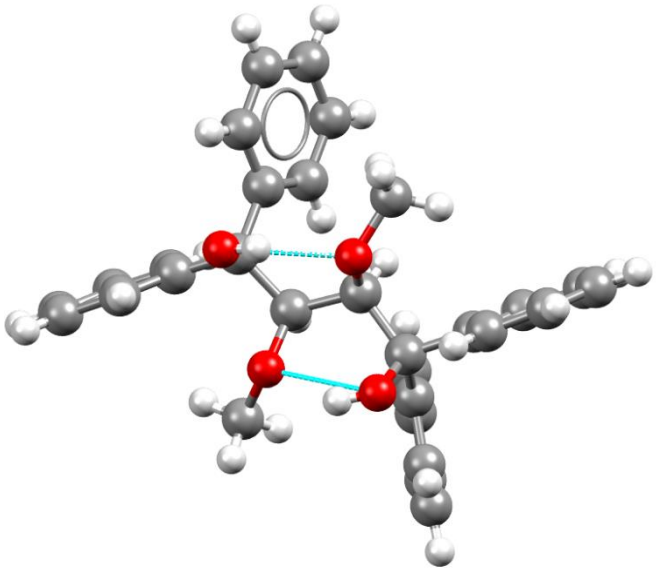

Figure 24: Host intramolecular hydrogen bonding, depicted with light-blue dashed lines.

Table 10: Non-classical hydrogen bonding interactions in the 2DMT•aniline complex.

Non-covalent interaction	Distance (Å) D–A	Angle (°) D-H···A
(host)*o*-ArH···O(host hydroxy)	2.650(3)	102
(host)*o*-ArH···O(host hydroxy)	2.756(3)	100
(host)*o*-ArH···O(host hydroxy)	2.766(3)	100
(host)*o*-ArH···O(host hydroxy)	2.653(3)	101
(host)*m*-ArH···O(host methoxy)[a]	3.522(3)	167
(host)*p*-ArH···O(host methoxy)[b]	3.293(4)	168

Symmetry operators: (a) 3/2–x, –1/2+y,1–z; (b) –1/2+x, –1/2+y, z.

As can be expected in systems containing aromatic moieties, the complex formed between DMT and aniline exhibits a multitude of host–host π–π stacking interactions. However, these interactions are weak and occur over relatively long distances, ranging between 4.72–5.97 Å. The shortest of these, 4.722(2) Å, is between the phenyl rings of adjacent host molecules (interaction 'a' in Figure 25), while a relatively short

intramolecular π–π stacking interaction [4.824(2) Å] occurs between two phenyl rings connected to the same carbon on the butane backbone of the host ('b' in Figure 25). A total of eight π–π stacking interactions are present between host and guest. These are all very weak, as observed by their bond lengths, with the shortest being 5.401(5) Å.

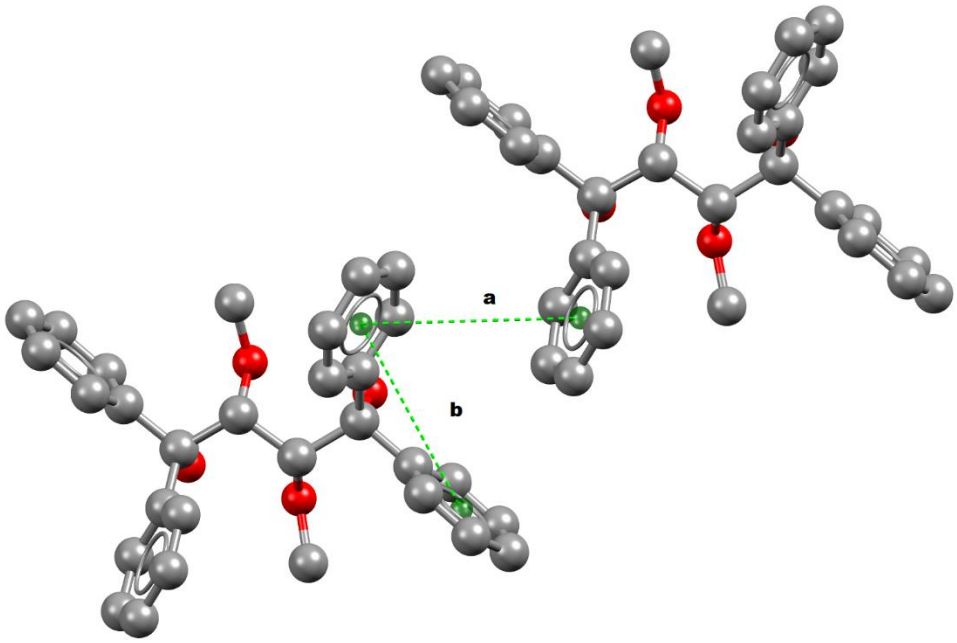

Figure 25: Prominent host–host π–π stacking interactions in the 2DMT•aniline complex. Interactions are shown by green dashed lines. Hydrogen atoms were omitted for clarity.

Table 11: C-H–π interactions in the 2DMT•aniline complex.

Non-covalent interaction	Distance (Å)	Angle(°)	Symmetry
(host methoxy)C-H···Cg(host)	2.92	148	x,y,z
(host methoxy)C-H···Cg(host)	2.85	146	x,y,z
(host methoxy)C-H···Cg(host)	2.84	149	x,y,z
(host methoxy)C-H···Cg(host)	2.83	145	x,y,z
(host)*p*-ArH···Cg(host)	2.99	169	1–x,y,1–z

Also present are five (host)C-H···π(host) interactions (Table 11). Four of these are intramolecular and occur between the methoxy methyl hydrogens and four adjacent phenyl rings. The fifth is intermolecular, between an aromatic hydrogen in the *para*-position of one host aromatic ring and a phenyl ring on an adjacent host (2.99 Å, 169°) (Figure 26).

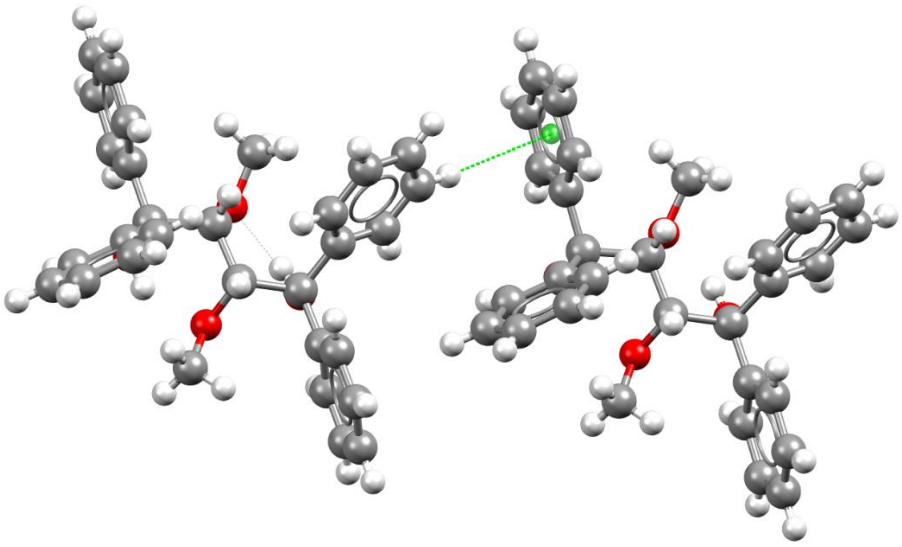

Figure 26: Intermolecular CH–π interaction between two host molecules. The interaction is shown by means of green dashed lines.

A variety of other short contacts exist, predominantly between host molecules. However, one involves an aromatic hydrogen in the *para*-position of the host aromatic ring and a carbon atom in the *ortho*-position of the guest molecule, with a distance of 2.86 Å and an angle of 148°. The interactions that are shorter than the sum of the van der Waals radii are summarised in Table 12.

Table 12: Short contact interactions in the 2DMT•aniline complex.

Non-covalent interaction	Distance (Å)	Angle(°)	Symmetry
(host)O-H···*p*-ArH(host)	2.32	104	–1/2+x,1/2+y,z
(host)*p*-ArH···H-O(host)	2.28	148	–1/2+x,–1/2+y,z
(host)*p*-ArH···*o*-ArC(guest)	2.86	148	1/2+x,1/2+y,1+z
(host)*p*-ArH···*m*-ArC(host)	2.86	146	1–x,y,–z

The nature of the guest packing was also assessed and is depicted in Figure 27. This is shown in spacefilling representation as this takes into account the more realistic van der Waals radii. It is interesting to note that the aniline molecules are packed such that the nitrogen atoms are alternated in their orientation between packing rows (Figure 27, left). The guest molecules were then removed from the packing calculation and the subsequent voids visualized in Mercury (Figure 27, right). It is clear that the aniline guest molecules occupy discrete cavities within the host crystal. These cavities comprised 16.1% of the unit cell volume.

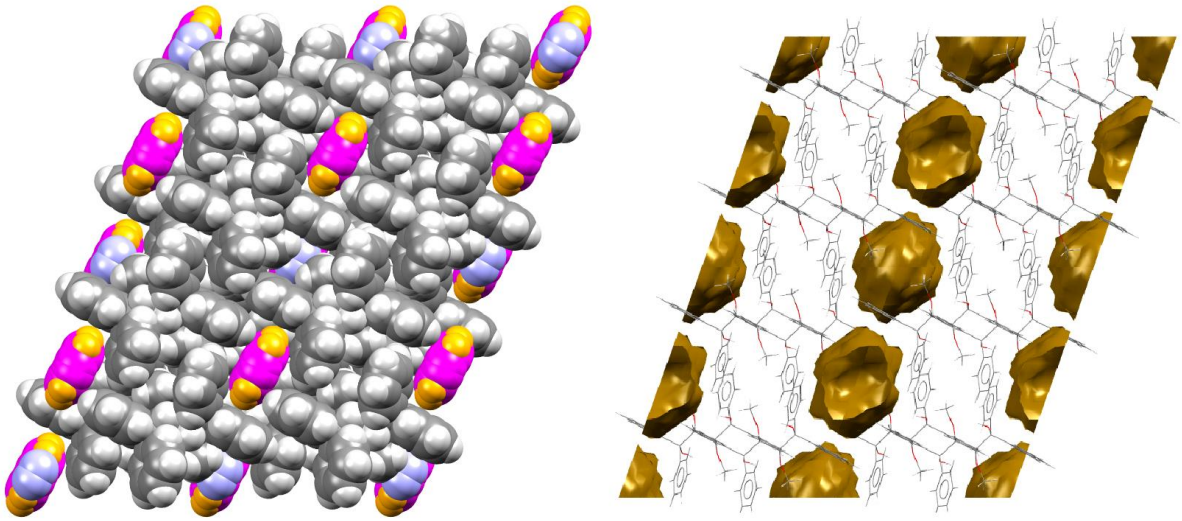

Figure 27: The host-guest packing using spacefilling representation (left) and the discrete cavity guest packing mode (right) of the 2DMT•aniline complex. The packing diagram uses the same colour scheme as in Figure 22. Both left and right images are several layers thick.

The 2DMT•NMA complex

Figure 28 shows the unit cell for the 2:1 DMT:NMA complex. The disorder in the guest is well-modelled and arises from the presence of a symmetry-generated guest molecule at the same site. Figure 29 depicts a stereoview of the complex.

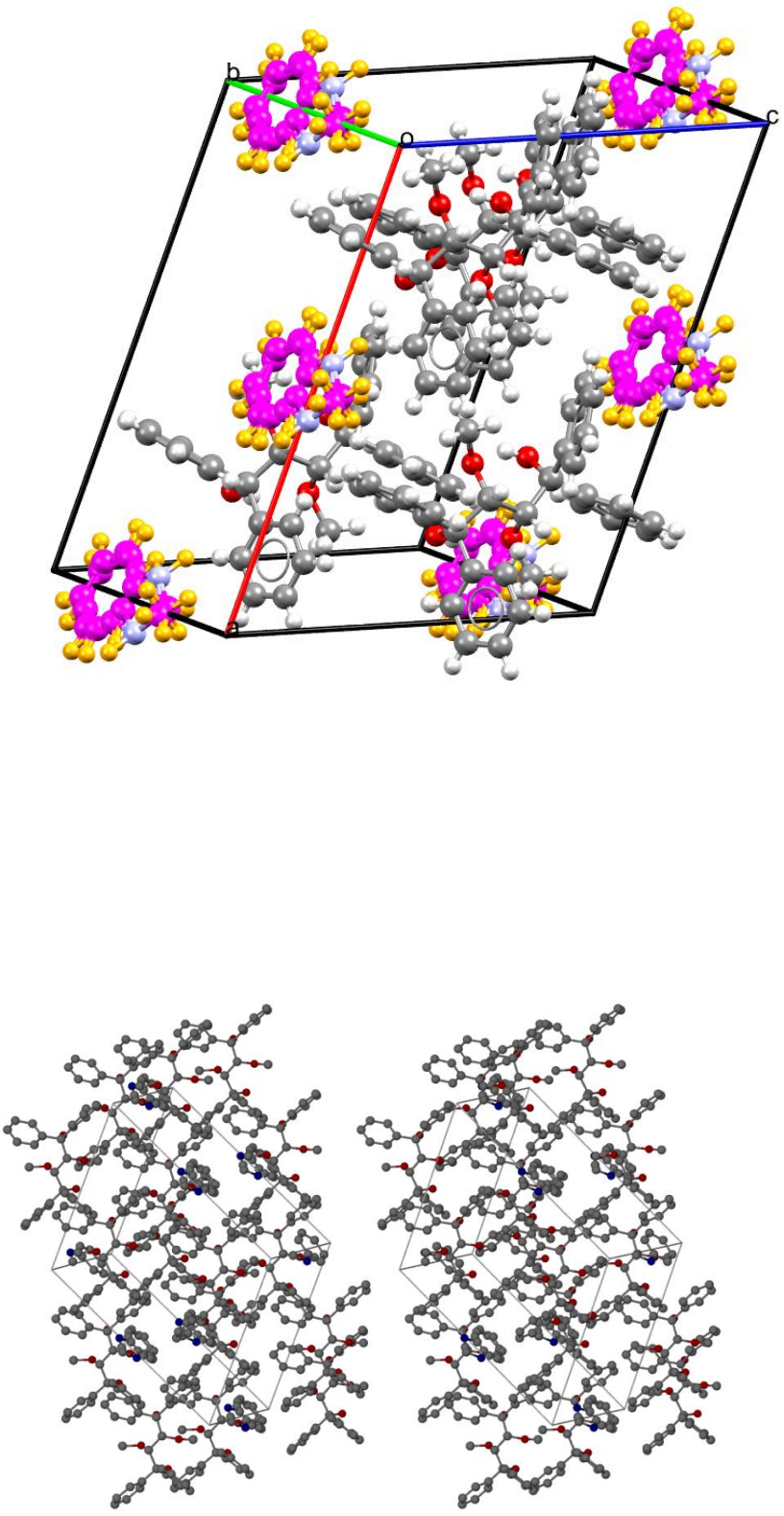

Figure 29: Stereoview of the 2DMT•NMA complex showing the three-dimensional packing of the structure.

The usual intramolecular 1,3- and 2,4- hydrogen bonds are present in the host, stabilizing the geometry of the butane backbone (Table 13, Figure 30a). Four prominent non-classical hydrogen bonding interactions further serve to stabilize the complex (Table 14). Three of these are C-H···O intramolecular host···host interactions [2.656(2)–2.758(3) Å, 100–102°], while the fourth is intermolecular [2.326(3) Å and 169°].

Table 13: Classic hydrogen bonds in the 2DMT•NMA complex.

Non-covalent interaction	Distance (Å) D–A	Angle (°) D-H···A
(host)O-H···O(host methoxy)	2.676(2)	140
(host)O-H···O(host methoxy)	2.621(2)	141

Table 14: Non-classic hydrogen bonding interactions in the 2DMT•NMA complex.

Non-covalent interaction	Distance (Å) D–A	Angle (°) D-H···A
(host)*o*-ArH···O(host hydroxy)	2.657(2)	102
(host)*o*-ArH···O(host hydroxy)	2.758(3)	100
(host)*o*-ArH···O(host hydroxy)	2.656(2)	101
(host)*p*-ArH···O(host hydroxy)[a]	2.326(3)	169

Symmetry operators: (a) –1/2+x,–1/2+y,z

The π–π stacking interactions in the complex range between 4.71 and 5.96 Å. The shorter of these is an intermolecular host···host interaction of 4.7120(1) Å, and an intramolecular host–host interaction of 4.836(1) Å (Figure 30b). A total of ten host···guest π–π stacking interactions range between 5.382(4) and 5.851(3) Å.

Furthermore, four intramolecular C-H–π interactions occur between the methoxy hydrogen atoms and adjacent phenyl rings of the host (Table 15).

Table 15: Intramolecular C-H–π interactions in the 2DMT•NMA complex.

Non-covalent interaction	Distance (Å)	Angle (°)	Symmetry
(host methoxy)C-H···Cg(host)	2.91	148	x,y,z
(host methoxy)C-H···Cg(host)	2.83	147	x,y,z
(host methoxy)C-H···Cg(host)	2.79	149	x,y,z
(host methoxy)C-H···Cg(host)	2.86	144	x,y,z

Numerous intermolecular short contacts are present between host molecules ranging between 2.31 and 2.87 Å, and 106–149°. These are all slightly smaller than the sum of the van der Waals radii of the interacting atoms and are therefore significant. Two intermolecular host···guest interactions of this type are present. One of these occurs between a carbon on a phenyl ring and the amine hydrogen [(host)*o*-ArC···H-N(guest), 2.63 Å, 140°], and the other between an aromatic hydrogen and the amine nitrogen [(host)*p*-ArH···N-C(guest), 2.65 Å, 162°] (Figure 30c).

Table 16: Short interactions in the 2DMT•NMA complex.

Non-covalent interaction	Distance (Å)	Angle (°)	Symmetry
(host)O-H···*p*-ArH(host)	2.32	106	–1/2+x,1/2+y,z
(host)*p*-ArH···H-O(host)	2.31	149	–1/2+x,1/2+y,z
(host)*p*-ArH···*m*-ArC(host)	2.87	145	1–x,y,–z
(host)*o*-ArC···H-N(guest)	2.63	140	2–x,y,–z
(host)*p*-ArH···N-C(guest)	2.65	162	2–x,y,–z

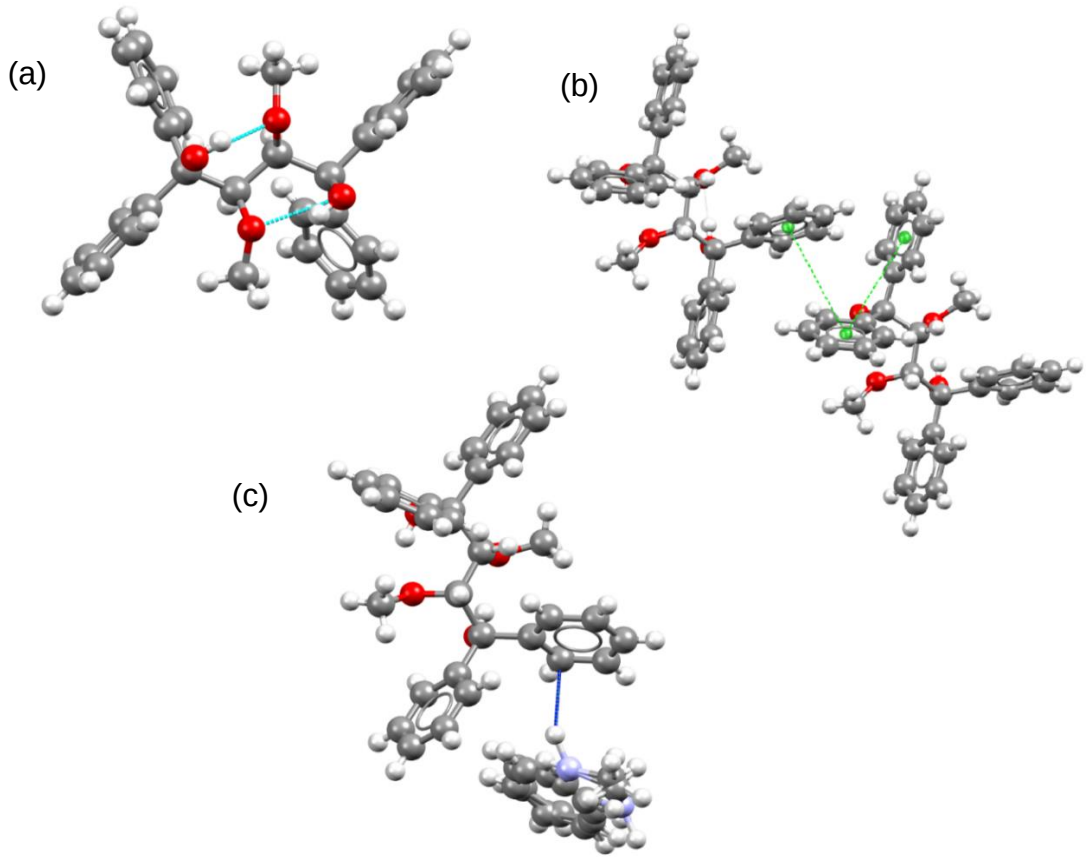

Figure 30: Various inter- and intra- molecular interactions between DMT and/or NMA; (a) intramolecular hydrogen bonding is shown in light blue; (b) shortest π–π stacking interactions in the host molecule (green); (c) intermolecular close contact between host and guest (dark blue).

Figure 31 represents the packing of the 2DMT•NMA complex. The molecules on the left are represented in spacefilling mode. The diagram on the right has the guest removed from the packing calculation and the resultant voids represented in brown. The NMA guests were seen to occupy discrete cavities much as in the case of aniline. These cavities occupy 16.3% of the unit cell volume.

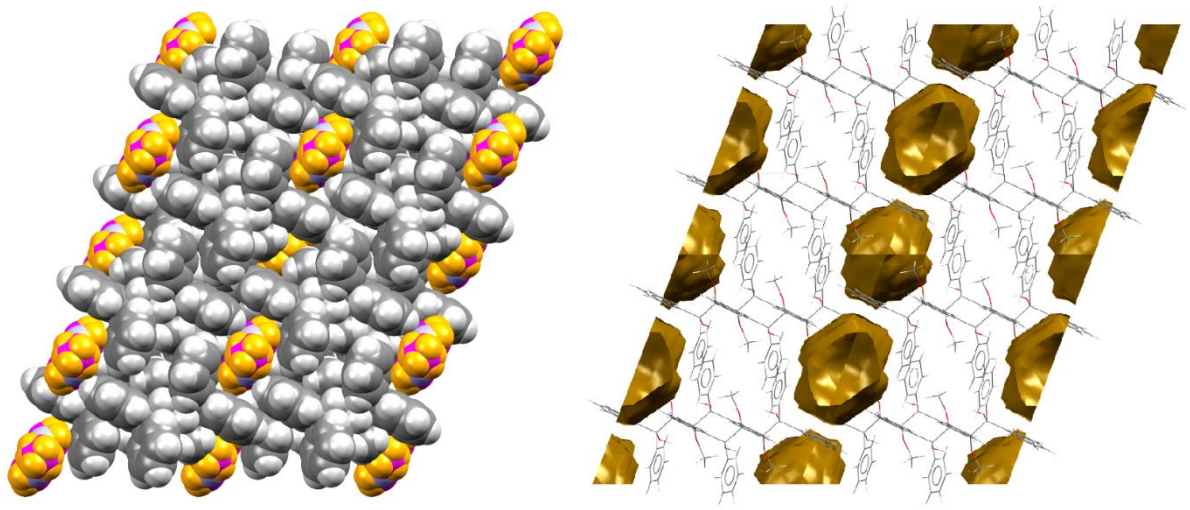

Figure 31: The host-guest packing using spacefilling representation (left) and the discrete cavity guest packing mode (right) of the 2DMT•NMA complex. The guest is represented in the same colour scheme as in Figure 27.

The 2DMT•DMA complex

The unit cell for the 2:1 H:G complex between DMT and DMA is provided in Figure 32. Disorder in the guest is symmetry-generated. Figure 33 shows the stereoview of the packing.

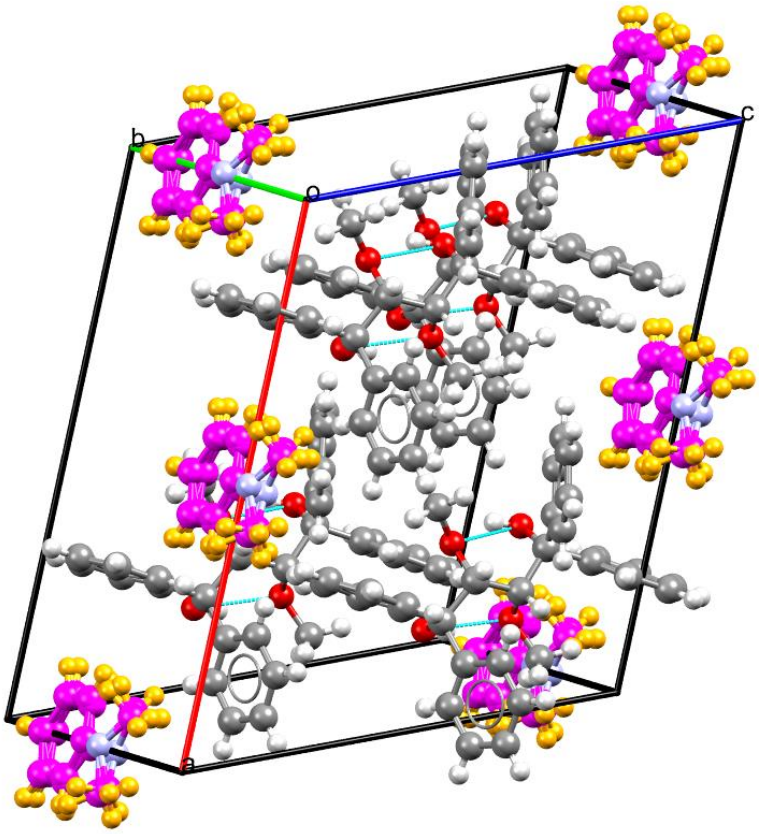

Figure 32: The unit cell for the 2DMT•DMA complex; the guest has the magenta carbon framework while the host has the grey carbon framework; hydrogen bonding is shown by means of light-blue dashed lines.

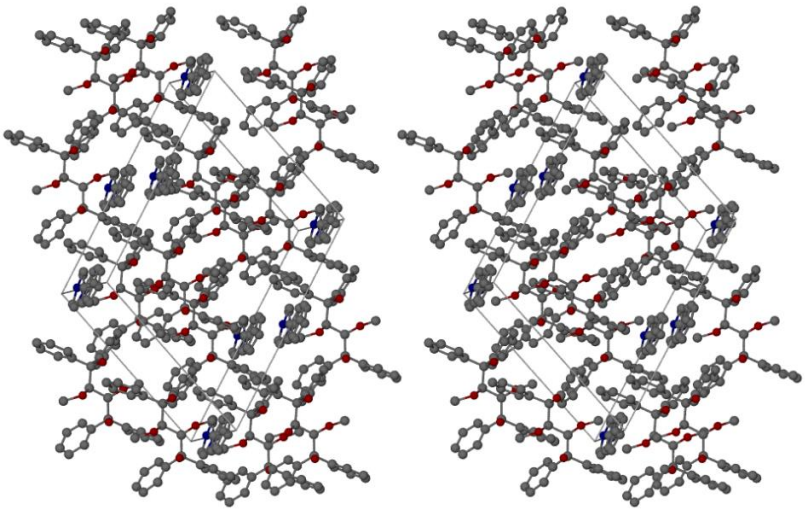

Figure 33: Stereoview of the 2DMT•DMA complex.

As with the preceding complexes, 1,3- and 2,4- intramolecular hydrogen bonds maintain the host geometry (Table 17, Figure 34a). A number of non-classical intramolecular hydrogen bonding interactions range between 2.640(2) and 2.759(2) Å, but their angles are relatively small (100–103°). One intermolecular non-classical hydrogen bond exists between two host molecules with an angle of 168°, albeit over a relatively long distance [3.316(3) Å] (Table 18).

Table 17: Classical intramolecular hydrogen bonding in the 2DMT•DMA complex.

Non-covalent interaction	Distance (Å) D–A	Angle (°) D-H···A
(host)O-H···O(host methoxy)	2.679(2)	141
(host)O-H···O(host methoxy)	2.629(2)	141

Table 18: Non-classical hydrogen bonding in the 2DMT•DMA complex.

Non-covalent interaction	Distance (Å) D–A	Angle (°) D-H···A
(host)*o*-ArH···O(host hydroxy)	2.662(2)	102
(host)*o*-ArH···O(host hydroxy)	2.755(2)	100
(host)*o*-ArH···O(host hydroxy)	2.759(2)	100
(host)*o*-ArH···O(host hydroxy)	2.640(2)	103
(host)*p*-ArH···O(host hydroxy)*	3.316(3)	168

*Symmetry operator: –1/2+x,–1/2+y,z.

A multitude of (host)···(host) π–π stacking interactions occur with the shortest being 4.836(1) Å (intramolecular) and 4.807(1) Å (intermolecular) (Figure 34b). A total of eight (host)···(guest) π–π stacking interactions range between 5.232(6) and 5.752(5) Å. Numerous C-H···π (Table 19) interactions also exist, and these are predominantly intramolecular in nature between methoxy hydrogens and adjacent phenyl rings. One intermolecular (host)C-H···π(host) interaction is also observed (2.97 Å, 173°) and, finally, a C-H···π interaction between a guest aromatic hydrogen and a host phenyl ring is also present (2.94 Å, 152°, Figure 34c).

Table 19: C-H–π interactions in the 2DMT•DMA complex.

Non-covalent interaction	Distance (Å)	Angle(°)	Symmetry
(host methoxy)C-H···Cg(host)	2.93	149	x,y,z
(host methoxy)C-H···Cg(host)	2.83	147	x,y,z
(host methoxy)C-H···Cg(host)	2.90	147	x,y,z
(host methoxy)C-H···Cg(host)	2.88	146	x,y,z
(host)*m*-ArH···Cg(host)	2.97	173	1–x,y,1–z
(guest methyl)C-H···Cg(host)	2.94	152	3/2–x,–1/2+y,–z

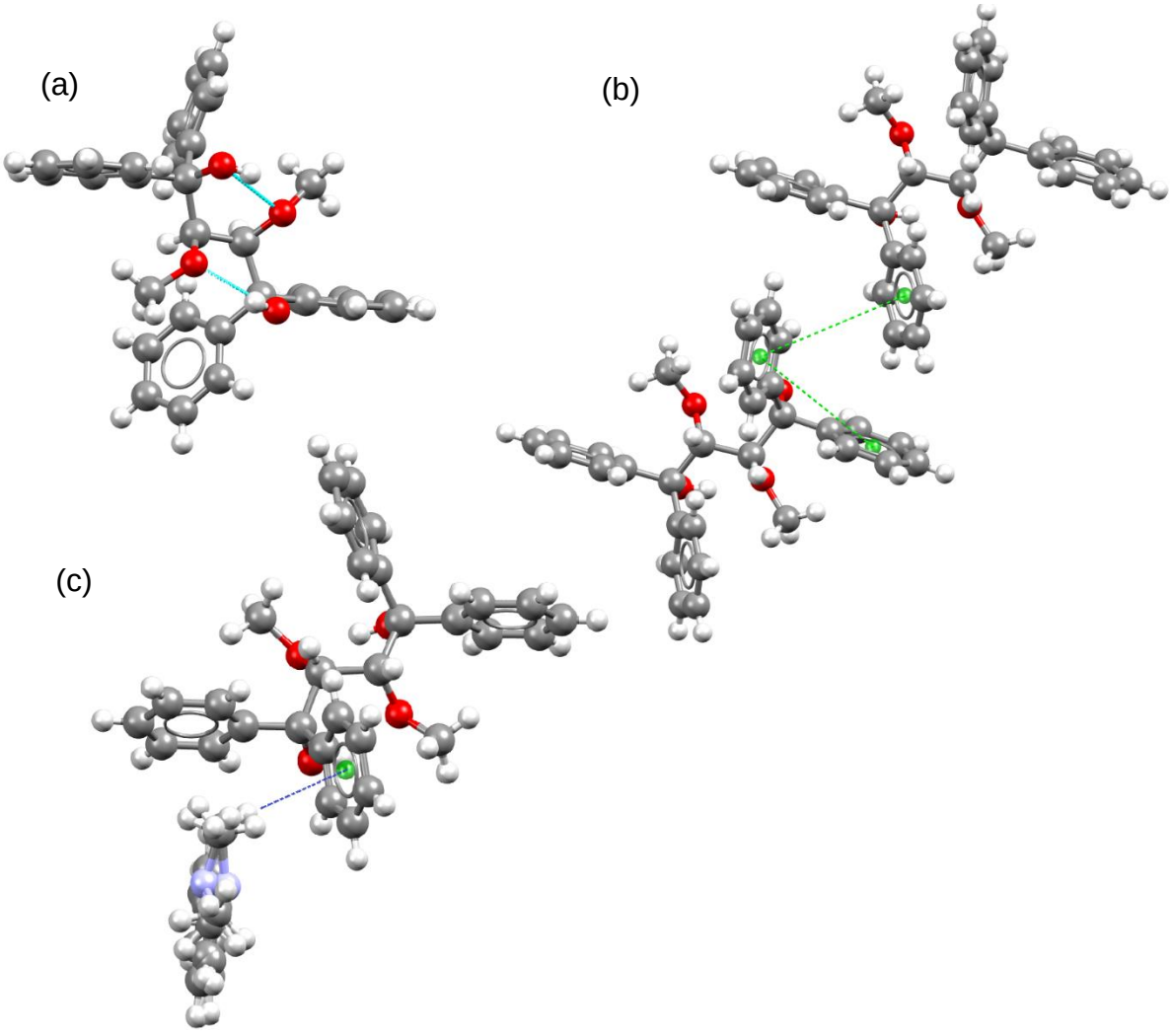

Figure 34: Various inter- and intra- molecular interactions in the 2DMT•DMA complex; (a) intramolecular hydrogen bonding (light blue); (b) π–π stacking interactions (green); (c) an intermolecular C–H–π interaction (dark blue).

The short contacts (Table 20) between host and guest in this complex are more numerous than in the preceding two complexes. Four intermolecular host–guest interactions exist, three of which range between 2.30 and 2.88 Å which is significant with respect to the sum of the van der Waals radii of the atoms involved. The fourth interaction is 2.14 Å (158°) and is much shorter (Figure 35). The remaining short contacts are summarised in Table 20.

Table 20: Short interactions in the 2DMT•DMA complex.

Non-covalent interaction	Distance (Å)	Angle (°)	Symmetry
(host)O-H···*p*-ArH(host)	2.31	102	–1/2+x,–1/2+y,z
(host)*p*-ArH···H-O(host)	2.31	149	–1/2+x,–1/2+y,z
(host)*p*-ArH···H-C(guest methyl)	2.14	158	3/2–x,1/2+y,1–z
(host)*p*-ArH···*m*-ArC(host)	2.88	146	1–x,y,–z
(guest methyl)C-H···*o*-ArC(host)	2.82	161	3/2–x,1/2+y,1–z
(host)*m*-ArC···H-C(guest methyl)	2.88	118	x,1+y,z
(host)*m*-ArH···*m*-ArH(guest)	2.30	126	1–x,y,–z

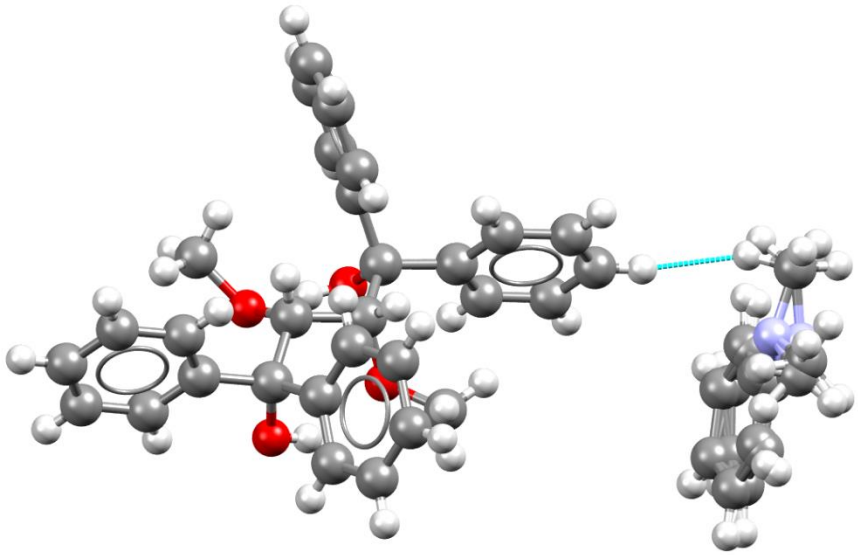

Figure 35: Intermolecular interaction between host and guest in the 2DMT•DMA complex. The interaction is depicted in light-blue.

The packing of the 2DMT•DMA complex is shown in Figure 36. Spacefilling representation was used in the diagram on the left, and the guest molecules were omitted from the packing calculation and the calculated voids indicated in brown on the right. The DMA guest molecules occupy discrete cavities.

Table 21 now presents a summary of the significant host–guest interactions as obtained from all of the diffraction data.

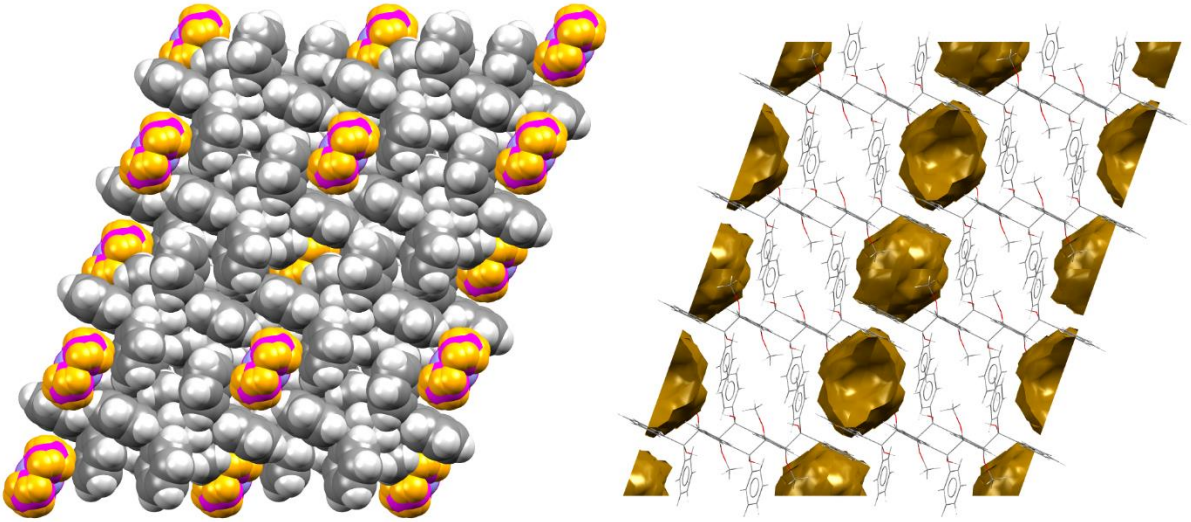

Figure 36: The host-guest packing using spacefilling representation (left) and the discrete cavity guest packing mode (right) in the 2DMT•DMA complex.

Table 21: Significant host–guest interactions for the complexes of DMT with aniline, NMA and DMA.*

Interaction	2DMT•Aniline	2DMT•NMA	2DMT•DMA
π–π	5.334(4)–5.834(4) Å (8 contacts)	5.382(4)–5.851(3) Å (10 contacts)	5.232(6)–5.752(5) Å (8 contacts)
CH–π	None	None	2.49 Å, 152° (guest methyl)CH···π(host)
Short contacts	2.86 Å, 148°, < (host)*p*-ArH···C–C(guest)	2.63 Å, 140°, << (guest)N–H···C–C(Host) 2.65 Å, 162°, < (host)*p*-ArH···N–C(guest)	2.14 Å, 158°, << (host)*p*-ArH···HC(guest methyl) 2.82 Å, 161°, < (guest methyl)CH···C–C(host) 2.88 Å, 123°, < (guest methyl)CH···C–C(host) 2.30 Å, 151°, < (guest)*m*-ArH···*m*-ArH(host)

*< denotes contacts less than the sum of the van der Waals Radii and << denotes contacts less than this sum minus 0.2 Å.

The reason for the behaviour of the host in competition experiments is immediately evident when considering the data in Table 21. Aniline is persistently discriminated against since NMA and DMA experience significantly more stabilizing host–guest interactions than aniline in the crystal. While a number of host–guest π–π interactions are evident in each of the three complexes, all of comparable strength [5.232(6)–5.851(3) Å], only one other host–guest short contact is observed in the 2DMT•aniline complex [2.86 Å, 148°, (host)*p*-ArH···C–C(guest)]. Furthermore, it is only the alkylated anilines that experience strong short interactions with the host molecule, measuring 2.63 Å (140°) [(guest)N–H···C–C(host)] in 2DMT•NMA, and 2.14 Å (158°) [(host)*p*-ArH···HC(guest methyl)] in 2DMT•DMA. These data also correlate with the observation that the host is more selective for DMA than NMA, as noted by the fact that only this guest (DMA) is involved in a (guest methyl)CH···π(host) interaction [2.94 Å, 152° (H···Cg, X-H···Cg)], the type of which is absent in the other two complexes; moreover, DMA also experiences an overall greater number of interactions than aniline and NMA.

3.6 Hirshfeld Surface Analysis

As it can be difficult to visualize the quantity and quality of contacts within the various X-ray structures, Hirshfeld surface analysis was used to better investigate the host–guest intermolecular interactions and draw further quantitative comparisons between the complexes being investigated.[149] The three-dimensional Hirshfeld surface topography for each guest was translated into two-dimensional fingerprint plots. The d_e and d_i axes represent the distances to the nearest atom outside and inside the surface, respectively (Figure 37).

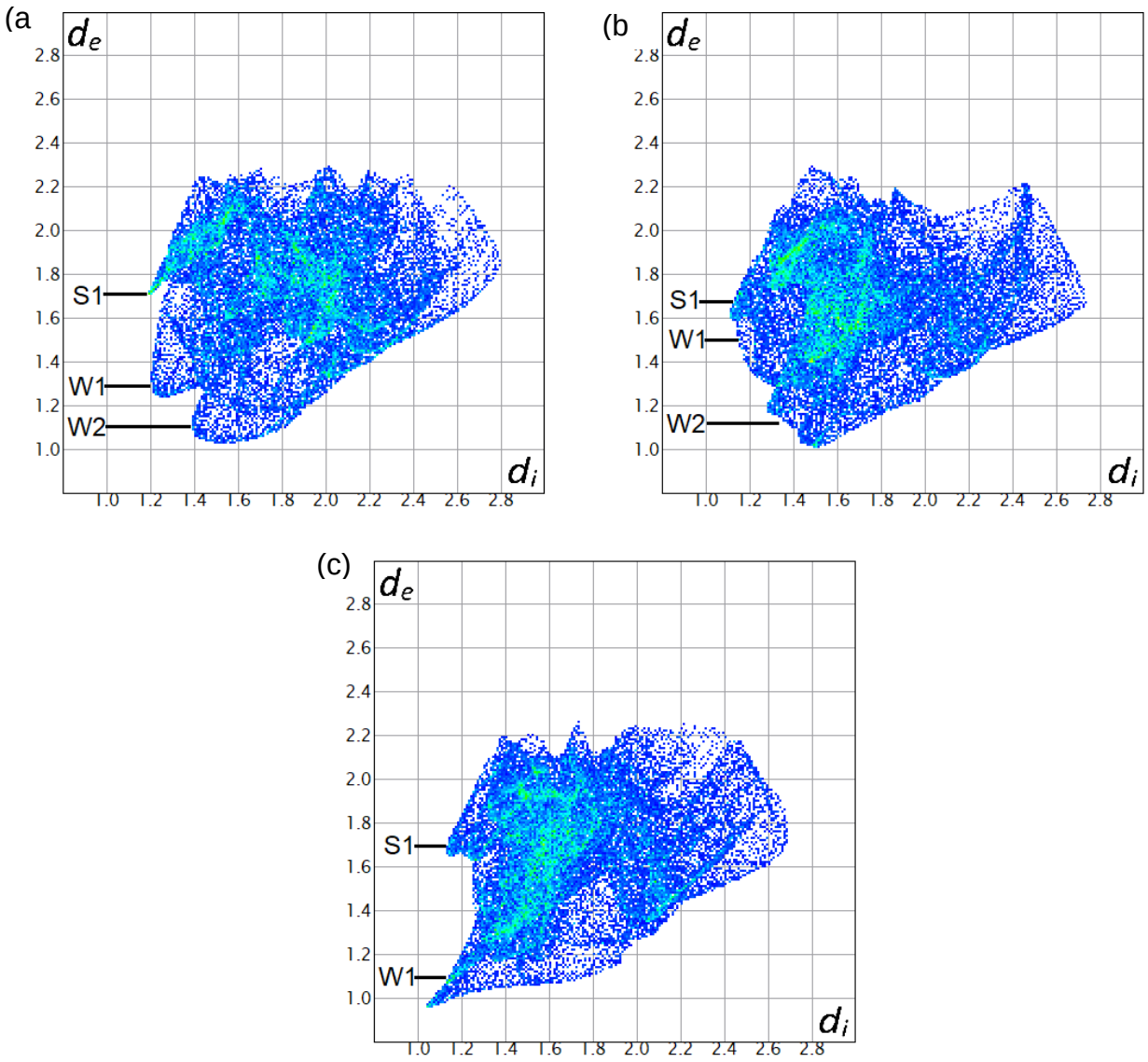

Figure 37: Two-dimensional fingerprint plots obtained from Hirshfeld surfaces for the complexes of a) 2DMT•aniline; b) 2DMT•NMA and c) 2DMT•DMA.

The 2D fingerprint plot for the 2DMT•aniline complex (Figure 37a) exhibits three distinct features, namely a spike labelled 'S1' and two wings labelled 'W1' and 'W2'. Spike S1 represents C···H interactions, while the wings W1 and W2 are indicative of H···H interactions. The plot generated from the 2DMT•NMA complex (Figure 37b) displays the same wing and spike features, but with considerable overlap of the regions, while that for the 2DMT•DMA complex (Figure 37c) also has the same spike, S1, for C···H interactions and one, very prominent wing, W1, indicative of H···H

interactions. Notably, W1 in Figure 37c extends much closer to the origin of the plot on both the d_e and d_i axes, indicating much closer interactions in this complex. Figure 38 is a graphical comparison of the percentages of intermolecular interactions between host and guest and *vice versa* in each complex.

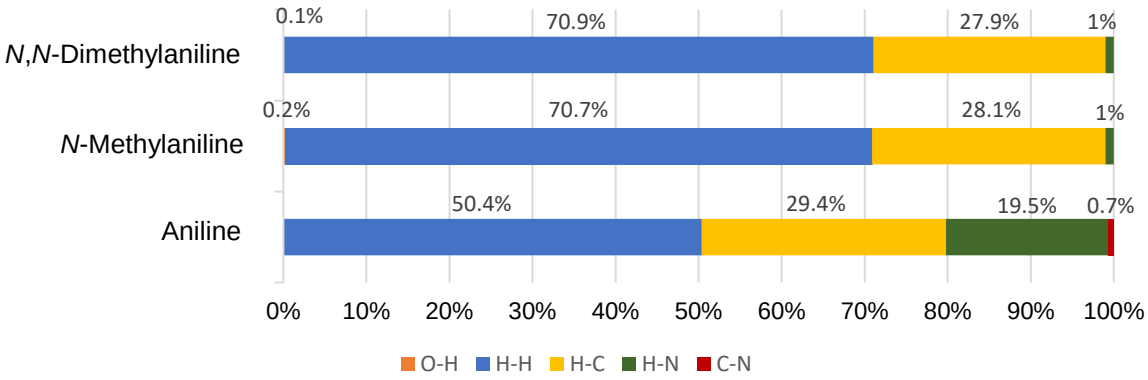

Figure 38: Graphical display showing the percentage intermolecular interactions in each complex.

From the intermolecular interaction percentages obtained from Hirshfeld surface analysis, one can see that, comparatively, the intermolecular interactions in the 2DMT•NMA and 2DMT•DMA complexes are strikingly similar. Both exhibit H···C and H···H interactions of approximately 28 and 71%, respectively. In the case of the 2DMT•aniline complex, however, the percentage of H···H interactions is much lower (50.4%). The percentage H···H interactions in the complexes are in the order aniline << NMA < DMA, which is in close agreement with the selectivity order observed for this host for these guests.

3.7 Conclusion

(−)-(*2R*,*3R*)-2,3-Dimethoxy-1,1,4,4-tetraphenylbutane-1,4-diol proved to be an efficient host compound for aniline, *N*-methylaniline and *N*,*N*-dimethylaniline, and showed high selectivity towards the alkylated anilines when recrystallized from mixtures of these guests. A host selectivity order of aniline << *N*-methylaniline < *N*,*N*-dimethylaniline was noted. SCXRD revealed that the alkylated anilines experience a greater number of stabilizing interactions in the host crystal than aniline, while the dialkylated aniline was the only guest to experience a (guest methyl)CH···π(host) interaction, in accordance with this host's selectivity order. Data from Hirschfeld surface analyses correlated exceedingly well with these observations when considering H···H interactions, and thermal analyses showed that aniline was not as tightly bound in the complex as the alkylated anilines. Host-guest chemistry using the title host compound, therefore, has the potential to separate alkylated anilines from unreacted aniline in methylation reactions of this substrate.

Chapter 4: Inclusion Compounds of DMT (73) with the Xylene Isomers and Ethylbenzene

4.1 Introduction

Ethylbenzene (EB), *p*-xylene (*p*X), *m*-xylene (*m*X) and *o*-xylene (*o*X) constitute the C8 aromatic fraction that is obtained from crude oil, and these compounds are useful starting materials for a variety of end-products. This includes the production of terephthalic acid, isophthalic acid, phthalic anhydride and styrene for application in the polymer industry. Furthermore, these aromatic compounds are frequently found in fuel as additives [up to 20% (w/w)].[162–167] The separation of the xylenes and ethylbenzene from one another as obtained from crude oil, however, is not trivial due to the similarities in their physical properties. The boiling points of *p*X, *m*X, *o*X and EB are 138.2, 139.1, 144.5 and 136.2 °C, respectively, which inherently means that techniques such as fractional distillations become tedious, time-consuming and are usually quite inefficient.[32] Much attention has therefore been dedicated to their separation involving techniques such as the aforementioned distillation, but also crystallization and absorption onto zeolites and into metal-organic crystals.[32, 168,169]

In this current investigation, we assessed the potential of using DMT as a host for the separation of these compounds from one another through selective crystallization, and report the findings here.

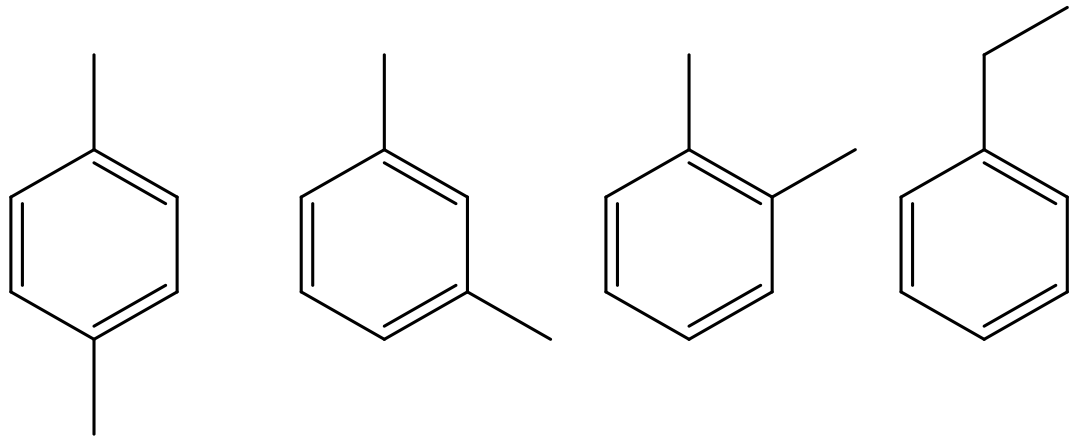

***p*X** ***m*X** ***o*X** **EB**

4.2 Individual and Equimolar Inclusion Experiments

After individual recrystallizations of DMT from *ortho*-, *meta*- and *para*-xylene, as well as ethylbenzene, ^{1}H-NMR spectra of the crystals isolated from each experiment showed that 2:1 host-guest complexes were formed in each case (Table 22).

Table 22: Host:guest ratios of complexes formed during individual recrystallization experiments.*

Guest	Host:guest
o-Xylene	2:1
m-Xylene	2:1
p-Xylene	2:1
Ethylbenzene	2:1

*Determined using ^{1}H-NMR spectroscopy with $CDCl_3$ as solvent.

A series of competition experiments were carried out in which DMT was recrystallized from various equimolar combinations of the xylene isomers and ethylbenzene. The crystals harvested from these vials were subjected to ^{1}H-NMR spectroscopy as well as GC-MS analysis, and the results are provided in Table 23 (where the preferred guest is displayed in bold italic font face). In each case, the total host:guest ratio remained 2:1 regardless of the number and type of guest species included. From these results, it is clear that DMT displays selectivity in the presence of mixtures of these guests. In particular, *p*X was preferentially included over *o*X in a 70.0:30.0 ratio, whereas *m*X was discriminated against, in favour of *p*X, in a 74.9:25.1 ratio. When *p*X was absent, the *ortho*-isomer was preferred over the *meta*-isomer (60.0:40.0). These binary competition experiments therefore indicated a selectivity order of *p*X >> *o*X > *m*X, and this was confirmed through a ternary competition experiment between all three isomers (54.0, 26.6 and 19.4% for *p*X, *o*X and *m*X, respectively).

Table 23: Competition experiments and H:G ratios obtained.*

***o*-Xylene**	***m*-Xylene**	***p*-Xylene**	**Ethylbenzene**	**Guest ratios (% Standard deviation)[$]**	**Overall H:G ratio**
X	X			***60.0***:40.0 (1.5)	2:1
X		***X***		30.0:***70.0*** (6.4)	2:1
	X	***X***		25.1:***74.9*** (2.1)	2:1
X	X	***X***		26.6:19.4:***54.0*** (0.5)(1.8)(1.9)	2:1
X			***X***	46.4:***53.6*** (2.1)	2:1
	X		***X***	38.0:***62.0*** (0.8)	2:1
		X	X	***60.7***:39.3 (1.5)	2:1
X	X	***X***	X	21.2:14.1:***40.6***:24.2 (3.0)(0.6)(4.5)(1.0)	2:1

*Determined using GC-MS; [$]experiments were carried out in triplicate; an average value is provided here with % estimated standard deviations in parentheses.

When ethylbenzene was used as a component in binary mixtures, it was favoured over *m*X (62.0:38.0) and *o*X (53.6:46.4). In an experiment comprising ethylbenzene and *p*X, the latter was, however, significantly preferred (60.7:39.3). The overall selectivity order of DMT for the four components was thus *p*X > EB > *o*X > *m*X, which correlated well with an equimolar competition experiment involving all four guests (40.6, 24.2, 21.2 and 14.1%, respectively).

4.3 Host Selectivity Profiles with Changing Guest Concentrations in Binary and Ternary Guest Mixtures

We subsequently investigated whether DMT was capable of discriminating between these C8 aromatic compounds when guest concentrations were varied. Hence DMT was recrystallized from mixtures containing differing molar amounts of the xylene isomers and ethylbenzene. Selectivity curves were thus constructed for the six combinations of guests.

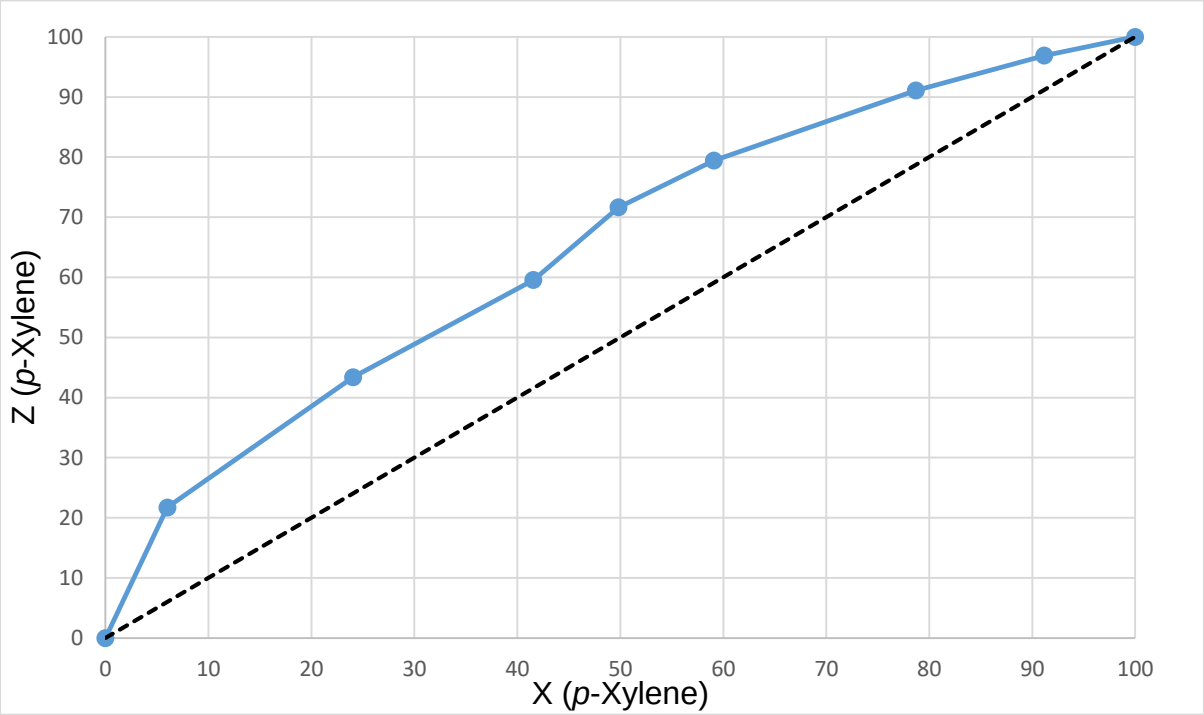

Figure 39: Selectivity curve of *p*-xylene *vs* *m*-xylene. Coloured blue is the molar fraction of *p*-xylene in the inclusion complex (Z) *vs* the molar fraction of *p*-xylene in the mother liquor (X). Black dashes indicate the theoretical line of no selectivity.

When *p*- and *m*- xylene competed, DMT preferentially included *p*X over the entire molar concentration range assessed (Figure 39). Initially, at a low concentration of *p*X in the mother liquor (~6%), crystals harvested contained approximately 21.7% *p*X. The percentage of included *p*X then increased as the mother liquor was further enriched with this guest. The crystals obtained from a mother liquor composition of ~91.2% *p*X

and 8.8% *m*X had a *p*X content of approximately 96.9%, indicating that the host still included *m*X even at low concentrations of this guest in the mother liquor. The selectivity coefficient, K, for *p*X in this experiment was determined to be 2.83.

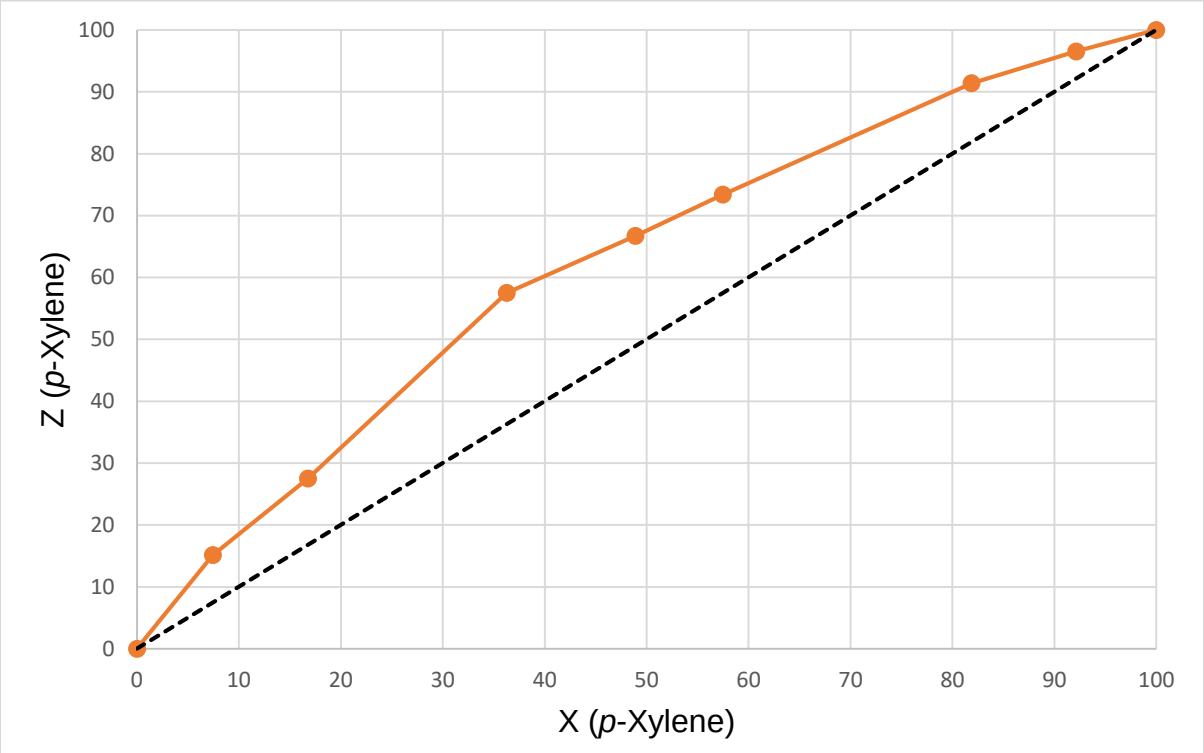

Figure 40: Selectivity curve of *p*-xylene *vs* *o*-xylene. Coloured orange is the molar fraction of *p*-xylene in the inclusion complex (Z) *vs* the molar fraction of *p*-xylene in the mother liquor (X). Black dashes indicate the theoretical line of no selectivity.

When competing with *o*X, *p*X behaved similarly as it did when in the presence of *m*X. DMT showed selectivity for *p*X over the entire molar range investigated (Figure 40). At an initial *p*X mother liquor concentration of 7.4%, the subsequent inclusion complex contained 15.1% *p*X, slightly less than in the *p*X/*m*X competition. This trend continued for each experiment, and is reflected by the selectivity constant, K, which was found to be slightly lower than before as well (K = 2.19).

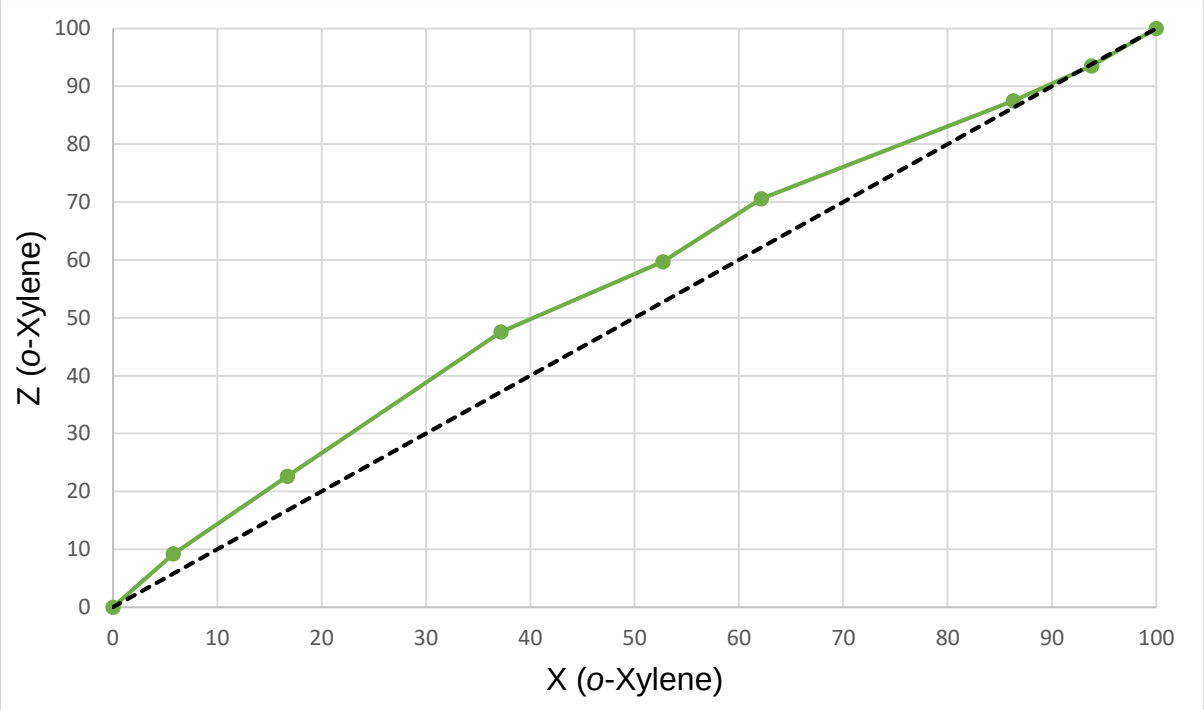

Figure 41: Selectivity curve of *o*-xylene *vs* *m*-xylene. Coloured green is the molar fraction of *o*-xylene in the inclusion complex (Z) *vs* the molar fraction of *o*-xylene in the mother liquor (X). Black dashes indicate the theoretical line of no selectivity.

The selectivity curve obtained for *o*X *vs* *m*X is characterized by a reasonably flat trajectory, with the data points relatively close to the theoretical line of no selectivity (Figure 41). This is indicative of a poor selectivity of DMT for *o*- and *m*- xylene when these guests are mixed. Initially, a mother liquor composition of 5.7% yielded crystals with 9.2% *o*X. Throughout the experiment, the percentage included *o*X remained slightly higher than in the mother liquor. However, at a mother liquor composition of ~86.3% *o*X, the crystals included only an additional 1.2% of this guest. The average selectivity coefficient, K, for this experiment was 1.36, significantly lower than in the previous two selectivity curves, as expected.

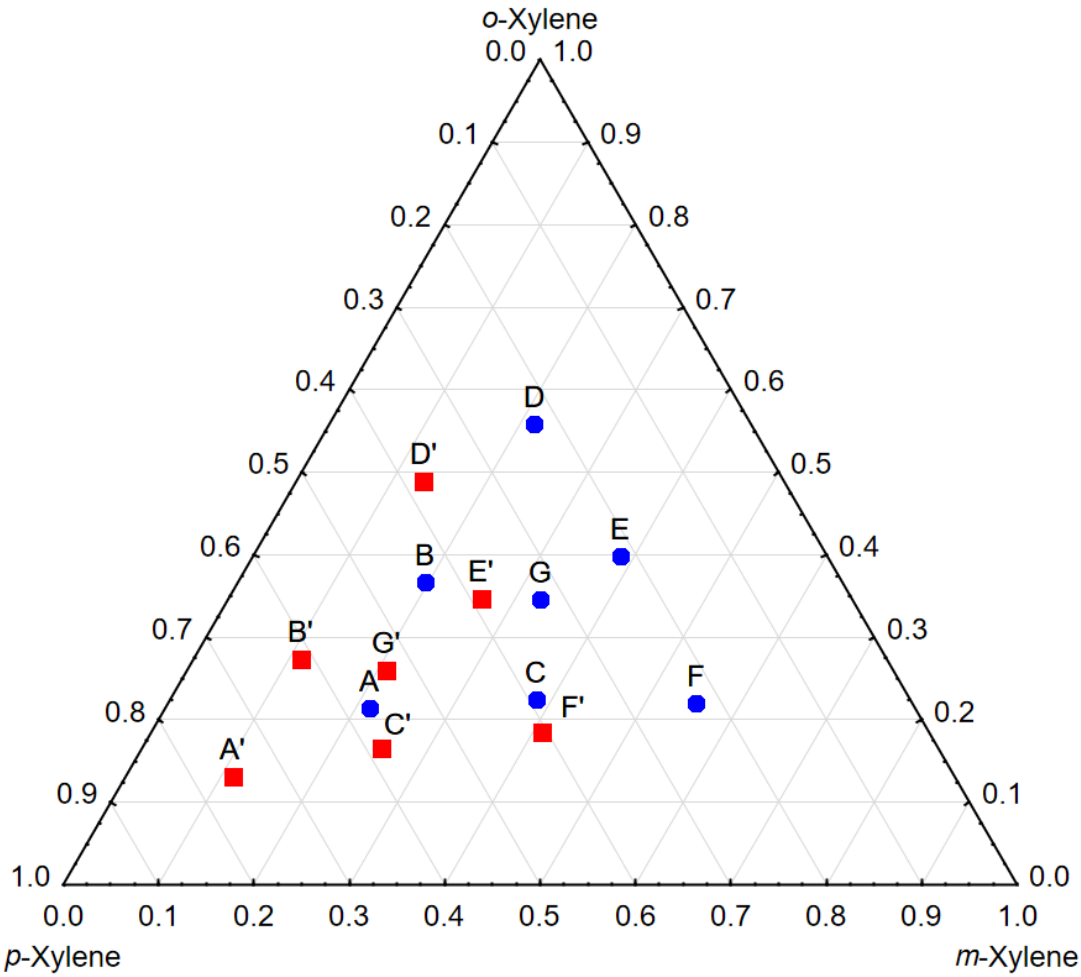

Figure 42: Ternary competition plot of *p*-xylene, *m*-xylene and *o*-xylene. Blue circles indicate mother liquor compositions, while red squares indicate guest composition of the crystals.

Experiments were carried out in which DMT was recrystallized from all three xylene isomers whilst differing their molar ratios. The mother liquor (blue circles) and inclusion complex (red squares) compositions were plotted, affording the ternary graph in Figure 42. The *p*X content of the inclusion complexes consistently increased relative to the mother liquor. Point G' experienced the largest increase (20.4%), whilst the *p*X content of point D' increased the least (15.0%). In contrast, the *m*X content decreased by between 8.3 (D') and 14.3% (F'). Similarly, *o*X in the inclusions was between 3.4 (B') and 9.4% (F') less than in the mother liquor. From these results, it can be concluded that the ternary selectivity order from these experiments, *p*X >> *o*X > *m*X, correlates exactly with the observations from the equimolar experiments.

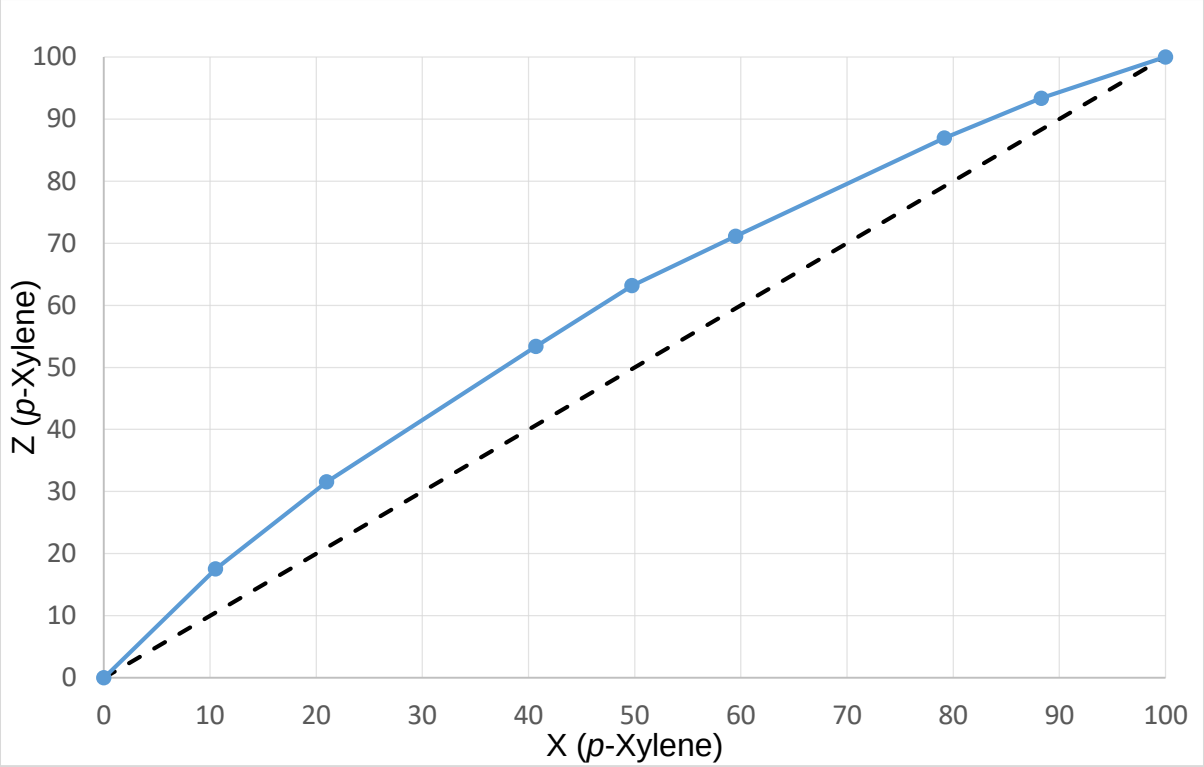

Figure 43: Selectivity curve of *p*-xylene *vs* ethylbenzene. Coloured blue is the molar fraction of *p*-xylene in the inclusion complex (Z) *vs* the molar fraction of *p*-xylene in the mother liquor (X). Black dashes indicate the theoretical line of no selectivity.

When *p*X and EB competed, *p*X was once more selected for over the entire course of the experiment (Figure 43). At a mother liquor composition of ~10.5% *p*X, the crystals contained ~17.5% *p*X (and 82.5% EB). At a higher concentration of *p*X (88.3%), the crystals were enriched up to ~93.4% with this guest. The average selectivity coefficient obtained for this competition curve was relatively low, at 1.75.

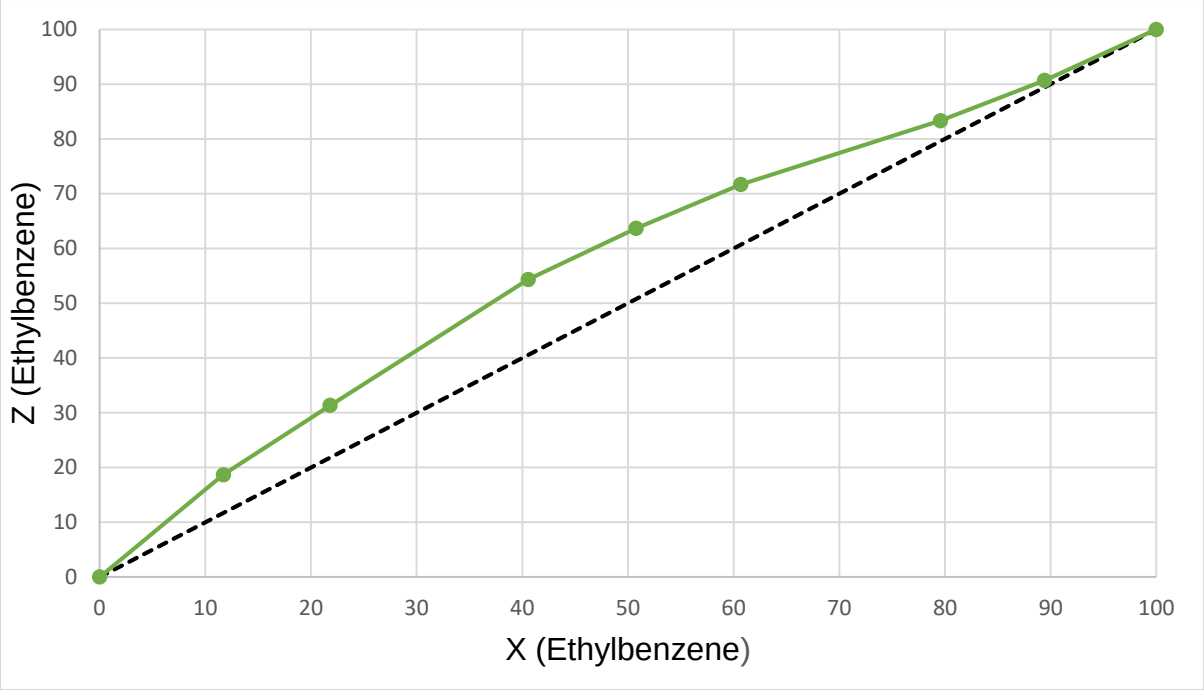

Figure 44: Selectivity curve of ethylbenzene *vs m*-xylene. Coloured green is the molar fraction of ethylbenzene in the inclusion complex (Z) *vs* the molar fraction of ethylbenzene in the mother liquor (X). Black dashes indicate the theoretical line of no selectivity.

In the case of EB *vs m*X (Figure 44), DMT now selected ethylbenzene rather than the xylene. The selectivity resembled that shown in Figure 43 but, at high EB concentrations, the selectivity for EB decreased significantly: a mother liquor concentration of 89.4% EB afforded crystals with only 90.7% EB. On average, the selectivity coefficient was 1.55 in favour of EB.

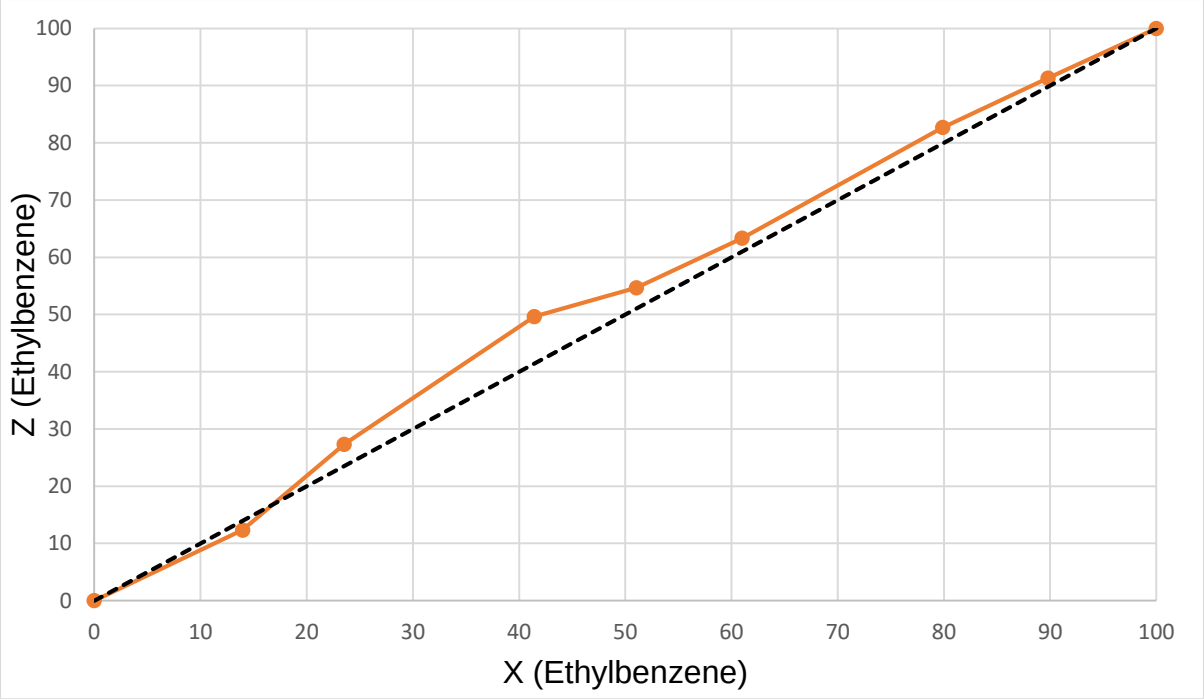

Figure 45: Selectivity curve of ethylbenzene *vs* *o*-xylene. Coloured orange is the molar fraction of ethylbenzene in the inclusion complex (Z) *vs* the molar fraction of ethylbenzene in the mother liquor (X). Black dashes indicate the theoretical line of no selectivity.

Lastly, DMT showed very little selectivity between EB and *o*X (Figure 45). Initially, EB was discriminated against to a small extent: when the mother liquor contained ~14% EB, the crystals harvested contained only 12.3% of this guest. Thereafter, an increase in selectivity towards EB was observed, and was relatively more significant at ~41.4% EB mother liquor composition at which point the crystals contained ~50% EB. At higher concentrations, the selectivity towards EB was very low, with points close to the theoretical line of no selectivity. In this case, K was only 1.16. The results obtained from the latter three selectivity curve experiments, therefore, also correlate with a host selectivity order of *p*X > EB > *o*X > *m*X as observed earlier.

4.4 Thermal Analysis

Thermal analyses were once more performed on all four inclusion complexes. Thermogravimetric analysis and differential scanning calorimetry were employed to determine the thermal events experienced by each complex during heating of the complexes at 10 °C.min^{-1} under high purity nitrogen purge gas. The TG, DTG and DSC traces thus obtained are provided in Figures 46–49, while Table 24 contains a summary of the significant thermal events occurring in each experiment.

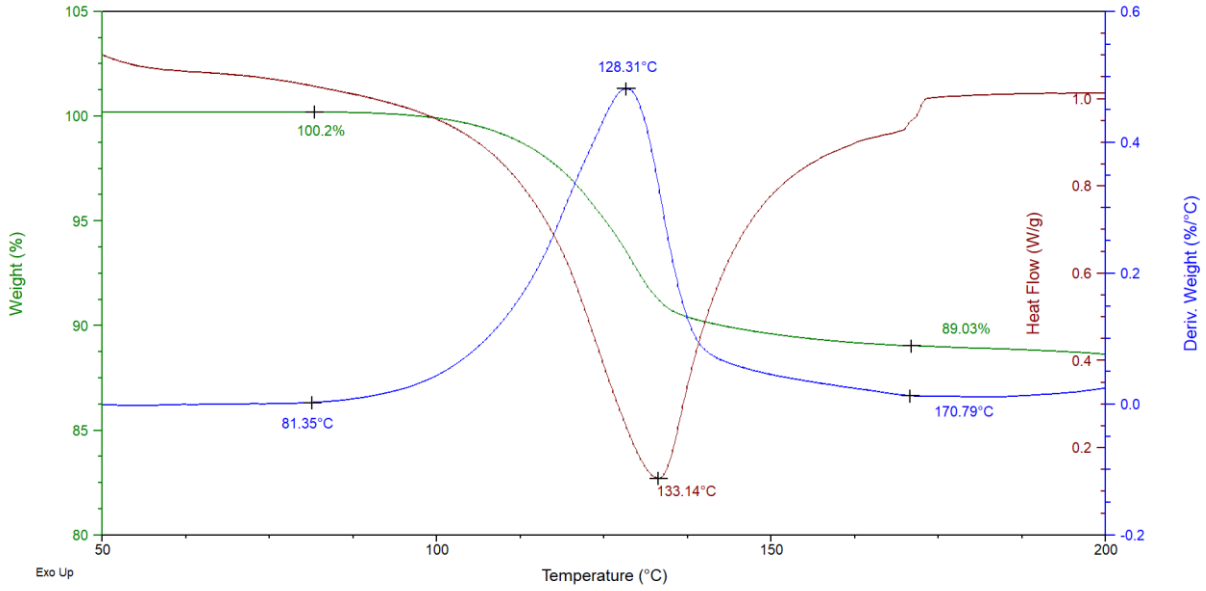

Figure 46: Overlaid TG (green), DTG (blue) and DSC (brown) traces for the 2DMT•*p*-xylene complex with heating at 10°.min^{-1}.

For a 2:1 DMT•*p*X complex, the expected mass loss upon removal of all the guest is 10.5%. The TG trace (Figure 46, green) indicated a mass loss of ~11.2% which correlates well with that expected. The onset temperature for the guest release process was approximately 81.4 °C, while cessation of mass loss occurred at ~170.8 °C. At higher temperatures, the host started decomposing, and mass loss was observed to occur once more. Only one endotherm resulted from this experiment with a peak maximum at approximately 133.1 °C (DSC), attributed to the concomitant host

melt and guest release events, while the maximum rate of guest release occurred at ~128.3 °C (DTG).

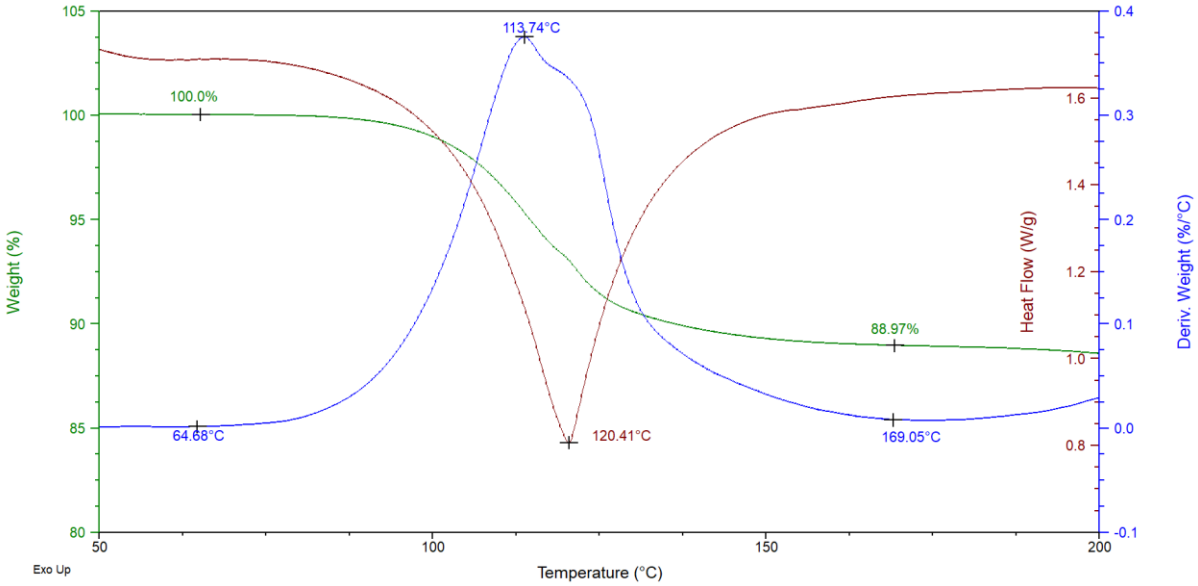

Figure 47: Overlaid TG (green), DTG (blue) and DSC (brown) traces for the 2DMT•*m*-xylene complex with heating at 10°.min^{-1}.

Mass loss for the 2DMT•*m*X inclusion complex proceeded over a single broad step (DSC) from ~64.7 °C to ~169.1 °C (DTG, Figure 47), although the DTG trace is somewhat unsymmetrical in this regard, and thus guest loss may be a little more convoluted than initially suspected from the DSC endotherm representing the mass loss. The mass loss percentage obtained (11.0%) is in good agreement with that expected (10.5%). The maximum rate of guest release occurred at ~113.7 °C (DTG) and the endotherm peak temperature was 120.4 °C (DSC). Both these values are significantly lower than for the 2DMT•*p*X complex.

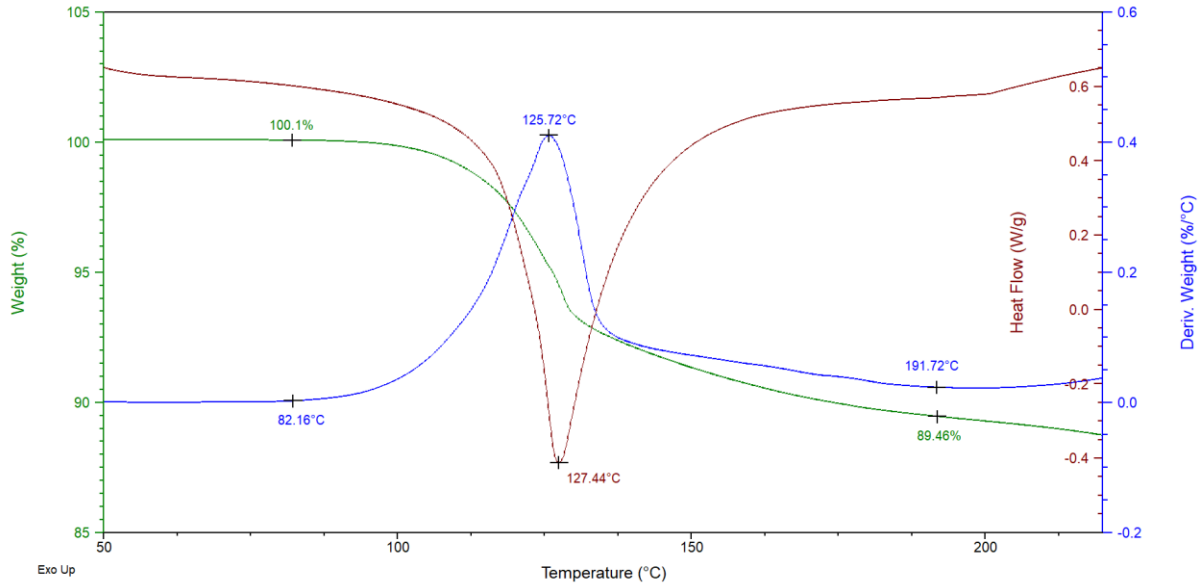

Figure 48: Overlaid TG (green), DTG (blue) and DSC (brown) traces for the 2DMT•*o*-xylene complex with heating at 10°.min^{-1}.

The thermal data for the 2DMT•*o*X complex was characterized by a mass loss onset temperature of ~82.2 °C (DTG), an endotherm peak temperature of 127.4 °C (DSC) and a mass loss peak temperature of 125.7 °C (DTG) (Figure 48). An observed mass loss of 10.6% is in excellent agreement with the theoretical mass loss of 10.5% expected for a 2:1 host:guest complex.

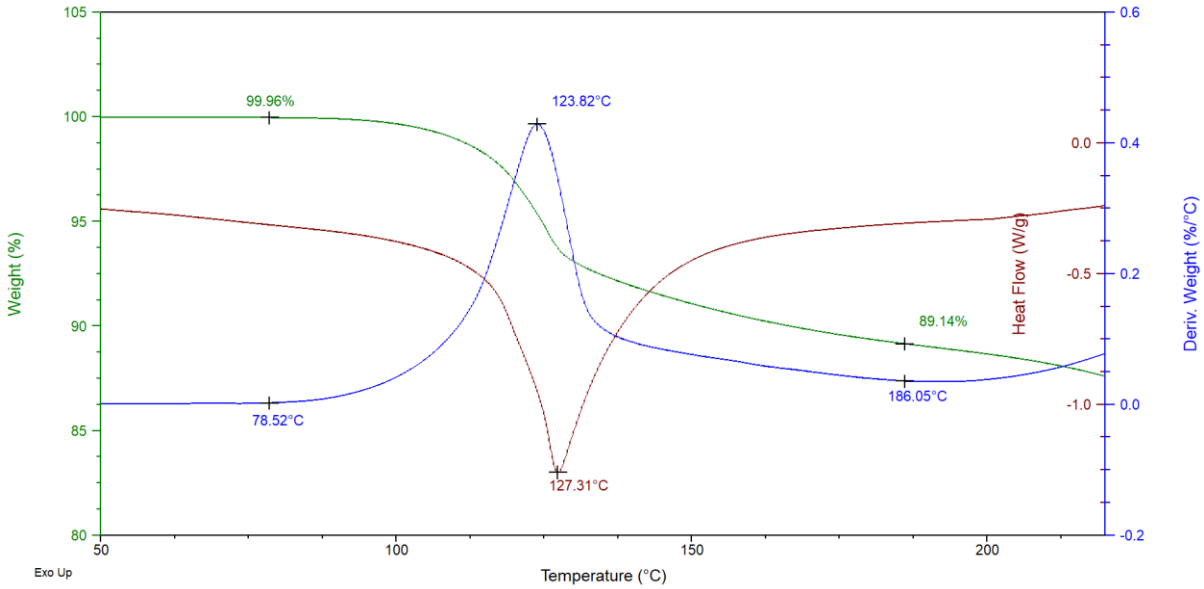

Figure 49: Overlaid TG (green), DTG (blue) and DSC (brown) traces for the 2DMT•ethylbenzene complex with heating at 10°.min^{-1}.

As with the C8 xylene isomers, mass loss for the 2DMT•EB complex also occurred over one step. The measured loss of 10.8% correlates well with the theoretical 10.5% requirement (Figure 49). The onset temperature for the guest release process was ~78.5 °C (DTG), and a single endotherm peak was observed at 127.3 °C (DSC), while the rate of mass loss reaches a maximum at approximately 123.8 °C (DTG).

Table 24: Summary of the major thermal events for the isomeric xylenes and ethylbenzene.

Guest	Guest boiling point, T_b (°C)	T_{on}[a] (°C)	$T_{on}-T_b$ (°C)	T_p[b] (°C)	T_{end}[c] (°C)	Mass loss % (Expected)
p-Xylene	138.4	81.3	–57.1	128.3	133.1	11.2 (10.5)
m-Xylene	139	64.7	–74.3	113.7	120.4	11.0 (10.5)
o-Xylene	144.4	82.2	–62.2	125.7	127.4	10.6 (10.5)
Ethylbenzene	136.2	78.5	–57.7	123.8	127.3	10.8 (10.5)

[a]T_{on} is the onset temperature for guest release estimated from the DTG; [b]T_p values were determined from the blue DTG traces, and are the temperatures at which the mass loss rate is the highest; [c]T_{end} values were obtained from the brown DSC traces, and are the peak endotherm temperatures.

From the summary provided in Table 24, the term T_{on}–T_b, permitted due to the isostructurality of the complexes in question,[160,161] gives rise to a stability order of *p*X (–57.1 °C) > EB (–57.7 °C) > *o*X (–62.2 °C) > *m*X (74.3 °C), and these data correlate exactly with observations made from competition experiments. Furthermore, values for T_p and T_{end} all agree with the findings that *p*X is the most preferred guest while the host is least selective for *m*X. Based on these results, it can be concluded that the thermal experiments here provided data which served as excellent predictors for the selectivity order displayed by DMT for these C8 aromatic compounds.

4.5 Single Crystal X-Ray Analysis

The four complexes were subjected to single crystal X-ray diffraction to ascertain reasons for the observed selectivity and relative thermal stability orders. Table 25 contains crystallographic data for the 2:1 host:guest complexes formed between DMT and *p*X, *m*X, *o*X and EB. These X-ray structures were submitted to the CCDC [reference numbers 1487158 (2DMT•*o*X), 1487159 (2DMT•*m*X), 1487160 (2DMT•*p*X) and 1487592 (2DMT•EB)].

Figure 50 shows the unit cells for these complexes. They all crystallize in the monoclinic *C*2 crystal system and have isostructural host frameworks. Within the 2DMT•*m*X complex, the guest is disordered around a two-fold rotational axis, whereas in the case of 2DMT•*p*X, a two-fold rotational axis passes through the benzene-methyl bond of the guest, resulting in each hydrogen having a symmetry-generated component and a site occupancy factor of 0.5. This results in the methyl group “appearing” to have six hydrogens. The guest in the 2DMT•EB complex has several layers of disorder, while *o*X within the 2DMT•*o*X complex displays no disorder.

Table 25: Crystallographic data for the complexes between DMT and the four C8 aromatic guests.

	2DMT•*o*X	**2DMT•*m*X**	**2DMT•*p*X**	**2DMT•EB**
Chemical formula	$C_{30}H_{30}O_4$	$C_{30}H_{30}O_4$	$C_{30}H_{30}O_4$	$C_{30}H_{30}O_4$
	$\bullet 0.5C_8H_{10}$	$\bullet 0.5C_8H_{10}$	$\bullet 0.5C_8H_{10}$	$\bullet 0.5C_8H_{10}$
Formula weight	507.62	507.62	507.62	507.62
Crystal system	Monoclinic	Monoclinic	Monoclinic	Monoclinic
Space group	*C*2	*C*2	*C*2	*C*2
μ (Mo-Kα)/mm^{-1}	0.078	0.078	0.078	0.078
a/Å	17.4473(10)	17.4861(6)	17.2780(9)	17.2668(8)
b/Å	11.9461(7)	12.0251(4)	12.2032(6)	12.0342(6)
c/Å	14.2501(8)	14.1656(5)	14.0896(6)	14.1665(7)
alpha/°	90	90	90	90
beta/°	109.916(2)	110.346(2)	110.135(2)	109.019(2)
gamma/°	90	90	90	90
V/$Å^3$	2792.5(3)	2792.79(17)	2789.2(2)	2783.0(2)
Z	4	4	4	4
F(000)	1084	1084	1084	1084
Temp./K	200	200	200	200
Restraints	1	1	2	1
Nref	6542	6788	6571	6923
Npar	348	373	349	371

R	0.0367	0.0356	0.0307	0.0412
wR2	0.1006	0.1003	0.0848	0.1185
S	1.04	1.04	1.03	1.04
θ min-max/°	2.3, 28.3	3.1, 28.3	2.1, 28.3	2.1, 28.4
Tot. data	25313	45279	46698	29307
Unique data	6542	6788	6571	6923
Observed data [I > 2.0 sigma(I)]	5980	6376	6296	6283
R_{int}	0.017	0.017	0.017	0.017
Dffrn measured fraction θ full	0.997	0.997	0.998	0.999
Min. resd. dens. (e/ Å^3)	–0.20	–0.22	–0.20	–0.31
Max. resd. dens. (e/ Å^3)	0.31	0.23	0.20	0.42

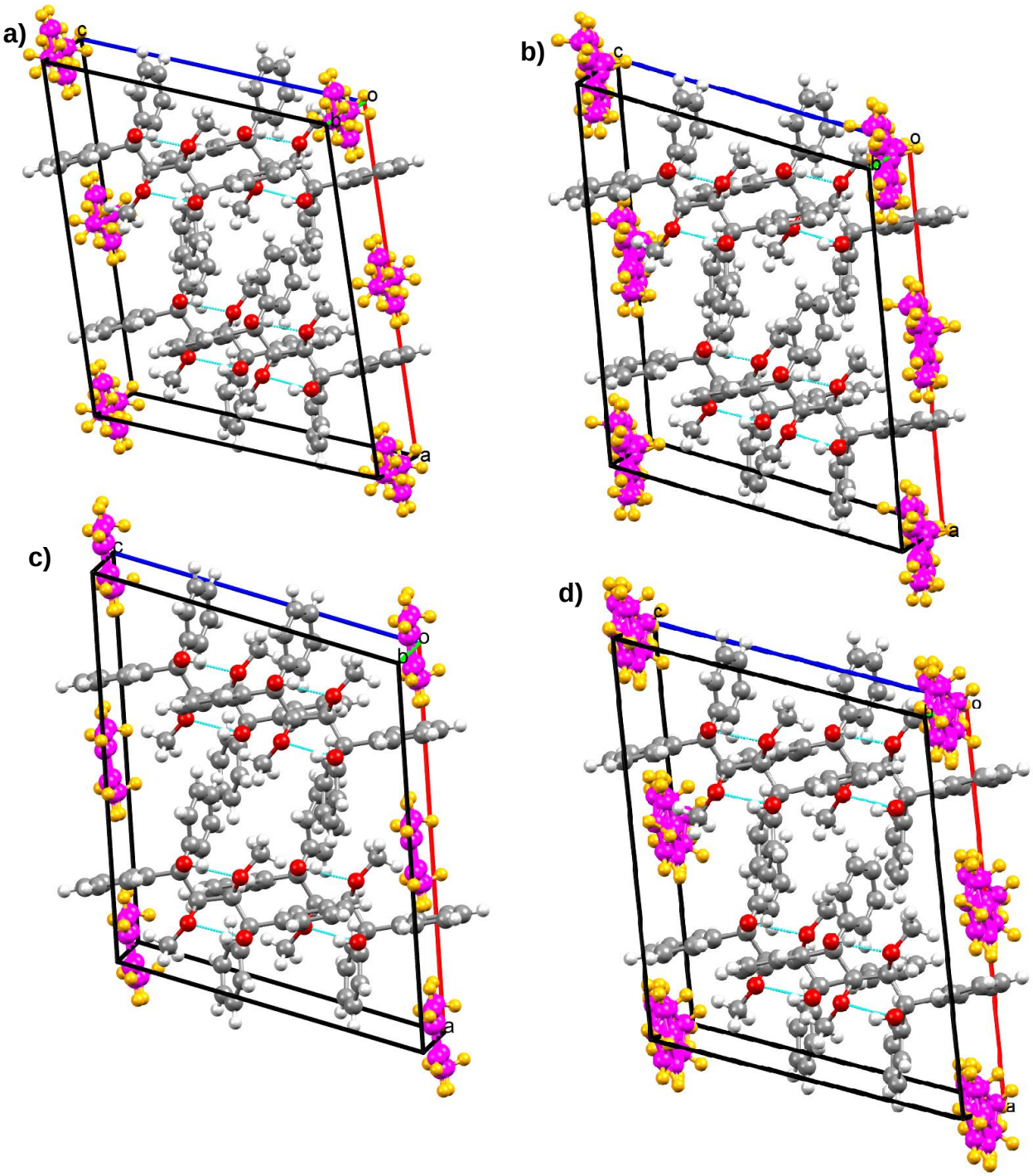

Figure 50: The unit cells for the DMT complexes with C8 aromatic guests; the guests have a magenta carbon framework, while the hosts have a grey carbon framework; hydrogen bonding is shown by means of light-blue dashed lines. a) 2DMT•*p*X; b) 2DMT•*m*X; c) 2DMT•*o*X; d) 2DMT•EB.

Hydrogen bonding

Classic hydrogen bonding interactions play an important role in maintaining the host geometry in all of the complexes. The hosts all experience similar 1,3- and 2,4-intramolecular hydrogen bonds between hydroxy and methoxy moieties on the butane backbone. These hydrogen bonds range in distance between 2.626(2) and 2.681(1) Å with angles of 139–142°. Figure 51 is a representative depiction of these intramolecular hydrogen bonds, while Table 26 lists these hydrogen bonding interactions in more detail.

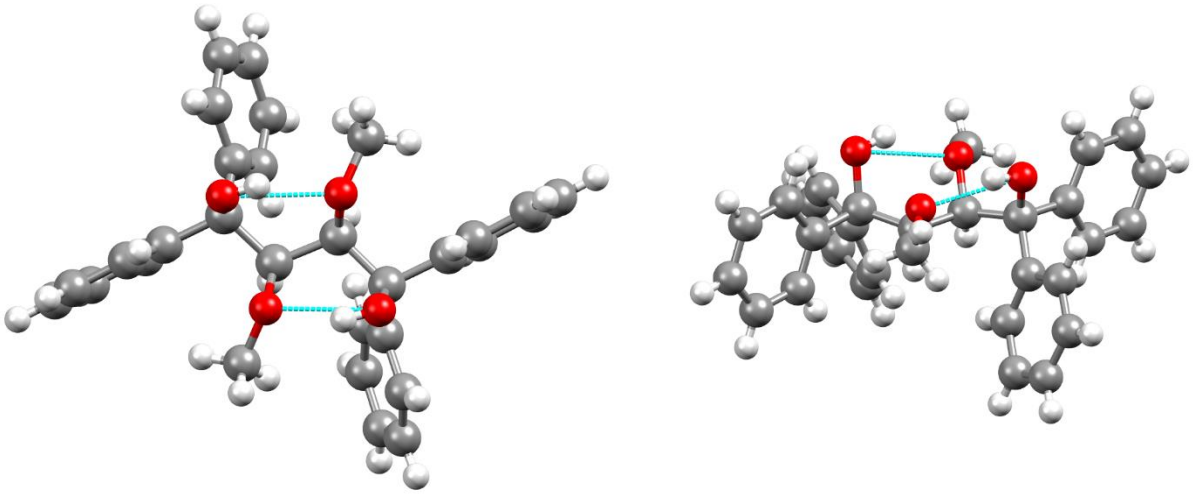

Figure 51: Two views of the host intramolecular hydrogen bonding, depicted with light-blue dashed lines.

Table 26: Classic intramolecular hydrogen bonding interactions in the DMT complexes with the xylene isomers and ethylbenzene.

Complex	Non-covalent interaction	Distance (Å) D–A	Angle (°) D-H···A
2DMT•*p*X	(host)O-H···O(host methoxy)	2.681(1)	140
	(host)O-H···O(host methoxy)	2.637(1)	142
2DMT•*m*X	(host)O-H···O(host methoxy)	2.675(2)	140
	(host)O-H···O(host methoxy)	2.626(2)	141
2DMT•*o*X	(host)O-H···O(host methoxy)	2.637(2)	142
	(host)O-H···O(host methoxy)	2.674(2)	140
2DMT•EB	(host)O-H···O(host methoxy)	2.672(2)	139
	(host)O-H···O(host methoxy)	2.627(2)	139

A variety of non-classic intramolecular hydrogen bonding interactions between host aromatic hydrogens in each complex with each of the hydroxyl oxygens are also present. However, they are all weak [2.648(2)–2.767(2) Å, 100–103°]. The complexes containing *o*X, *m*X and ethylbenzene also experience one non-classic intermolecular hydrogen bond, and these similarly involve interactions between aromatic hydrogen atoms and hydroxyl oxygen atoms [3.320(3)–3.357(3) Å, 169–174°]. The 2DMT•*p*X complex experiences two intermolecular interactions of this type [3.508(2) and 3.278(3) Å, with angles of 166 and 164° respectively (Figure 52)]. Table 27 lists these interactions in detail.

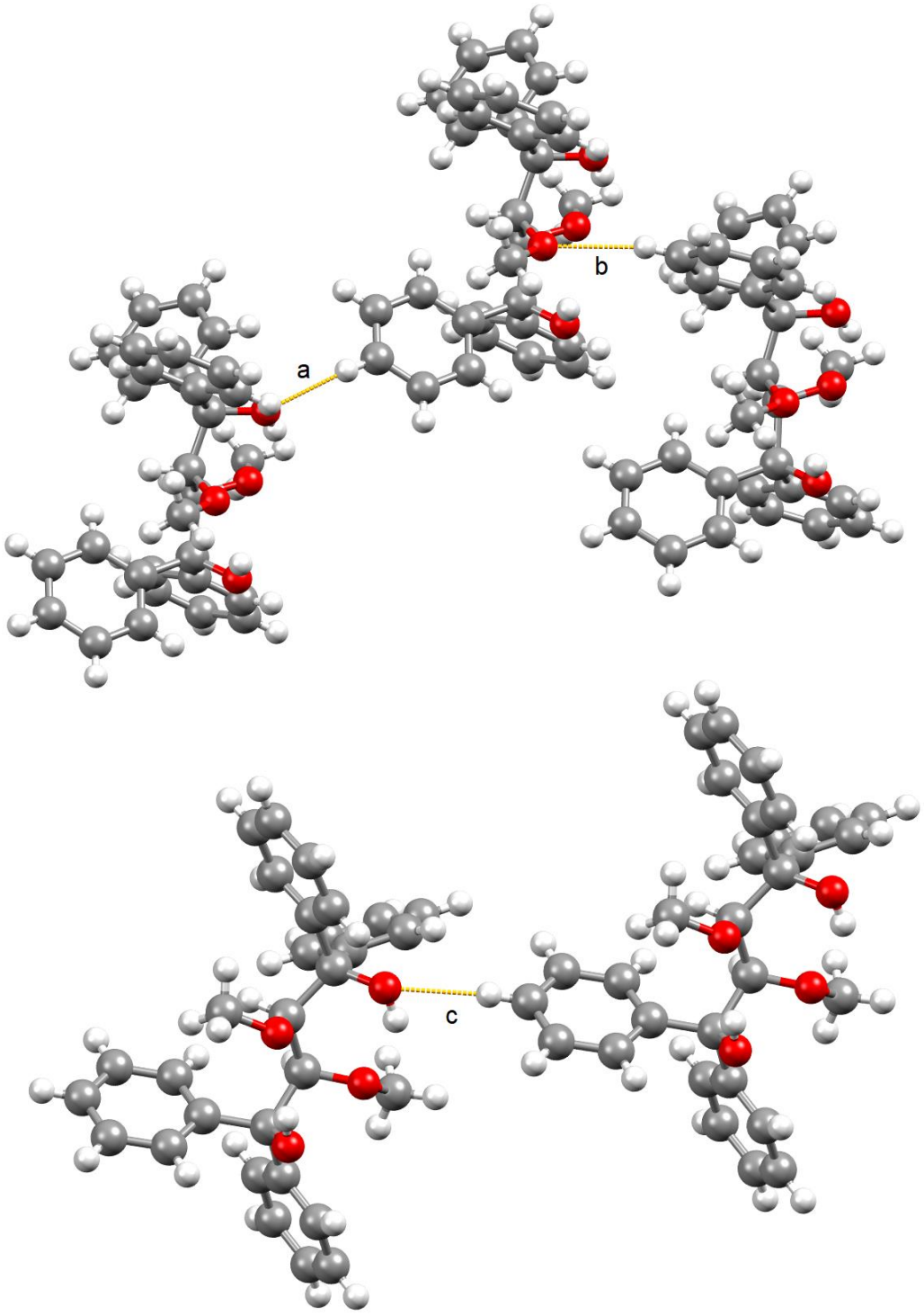

Figure 52: Various intermolecular non-classic hydrogen-bonding interactions depicted as orange dashes. Interactions 'a' and 'b' occur in the 2DMT•*p*X complex [(host)*p*-ArH···O(host hydroxy) and (host)*m*-ArH···O(host methoxy), respectively]. Interaction 'c' is representative of the remaining three complexes.

Table 27: Non-classic inter- and intra- molecular hydrogen bonding interactions in the DMT complexes with the xylene isomers and ethylbenzene.

Complex	Non-covalent interaction	Distance (Å) D–A	Angle (°) D-H···A
2DMT•*p*X	(host)*o*-ArH···O(host hydroxy)	2.656(2)	102
	(host)*o*-ArH···O(host hydroxy)	2.754(2)	100
	(host)*o*-ArH···O(host hydroxy)	2.767(2)	100
	(host)*o*-ArH···O(host hydroxy)	2.654(2)	101
	(host)*m*-ArH···O(host methoxy)[a]	3.508(2)	166
	(host)*p*-ArH···O(host hydroxy)[b]	3.278(3)	164
2DMT•*m*X	(host)*o*-ArH···O(host hydroxy)	2.660(2)	102
	(host)*o*-ArH···O(host hydroxy)	2.758(2)	100
	(host)*o*-ArH···O(host hydroxy)	2.660(2)	101
	(host)*p*-ArH···O(host hydroxy)[b]	3.320(3)	169
2DMT•*o*X	(host)*o*-ArH···O(host hydroxy)	2.648(2)	102
	(host)*o*-ArH···O(host hydroxy)	2.755(2)	100
	(host)*o*-ArH···O(host hydroxy)	2.760(3)	100
	(host)*o*-ArH···O(host hydroxy)	2.662(2)	103
	(host)*p*-ArH···O(host hydroxy)[b]	3.357(3)	174
2DMT•EB	(host)*o*-ArH···O(host hydroxy)	2.653(3)	102
	(host)*o*-ArH···O(host hydroxy)	2.752(3)	100
	(host)*o*-ArH···O(host hydroxy)	2.752(3)	100
	(host)*o*-ArH···O(host hydroxy)	2.650(3)	101
	(host)*p*-ArH···O(host hydroxy) [b]	3.333(4)	171

Symmetry operators: a) 3/2–x, –1/2+y, 1–z; b) –1/2+x, –1/2+y, z

π–π and CH–π interactions

A multitude of inter- and intra- molecular π–π stacking and C-H–π interactions exist within the four inclusion complexes, with the π–π stacking interactions being all relatively weak [4.702(2)–5.989(1) Å]. Each complex typically has two intramolecular π–π interactions of this type occurring between phenyl rings connected to the same carbon on the butane backbone [4.809(1)–4.812(2) Å]. Intermolecular host–host π–π

stacking interactions are equally weak, ranging between 4.702(2) and 4.819(2) Å (Figure 53). Lastly, the strongest π–π stacking interactions between host and guest range between 4.904(3) and 5.390(5) Å.

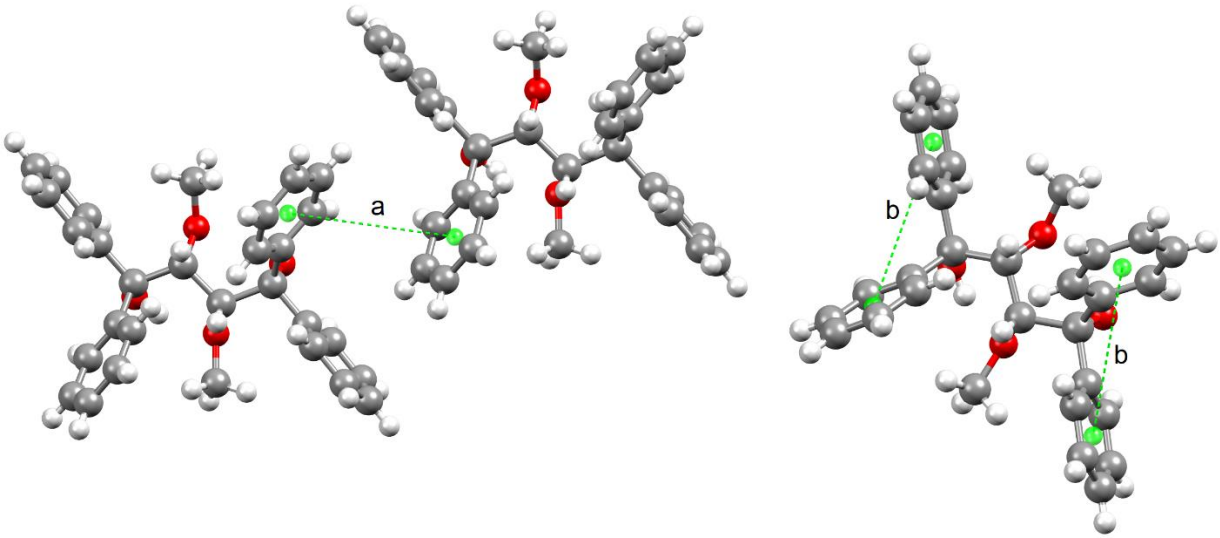

Figure 53: Representative π–π stacking interactions. Interaction 'a' indicates intermolecular host to host π–π stacking; 'b' shows intramolecular interactions of this type.

The C-H–π stabilizing interactions are evenly distributed over the four complexes. Intramolecular contacts of this type involve methoxy hydrogen atoms and phenyl rings within the same molecule (Figure 54). These vary from 2.82 to 2.97 Å (144–151°). Intermolecular C-H–π interactions (2.94–3.00 Å, 170–171°) occur between host aromatic hydrogen atoms and the aromatics of other host molecules (Figure 55, left). The latter is absent in the complex containing *m*-xylene, and in its stead is a host–guest C-H–π interaction involving a guest aromatic hydrogen and a phenyl ring centroid of the host molecule (2.93 Å,137°) (Figure 55, right). These interactions are summarized in Table 28.

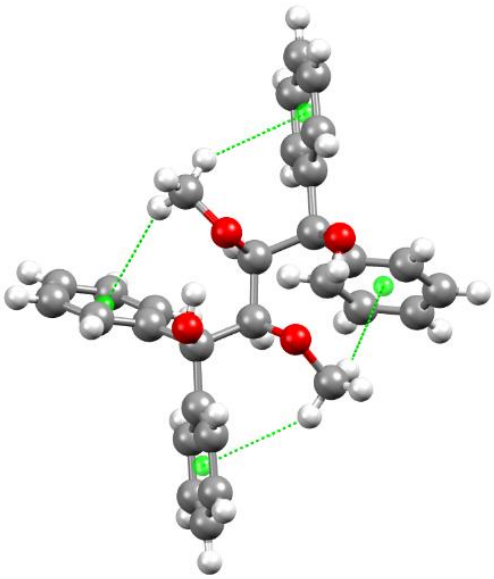

Figure 54: Representative intramolecular C-H–π stacking interactions of DMT.

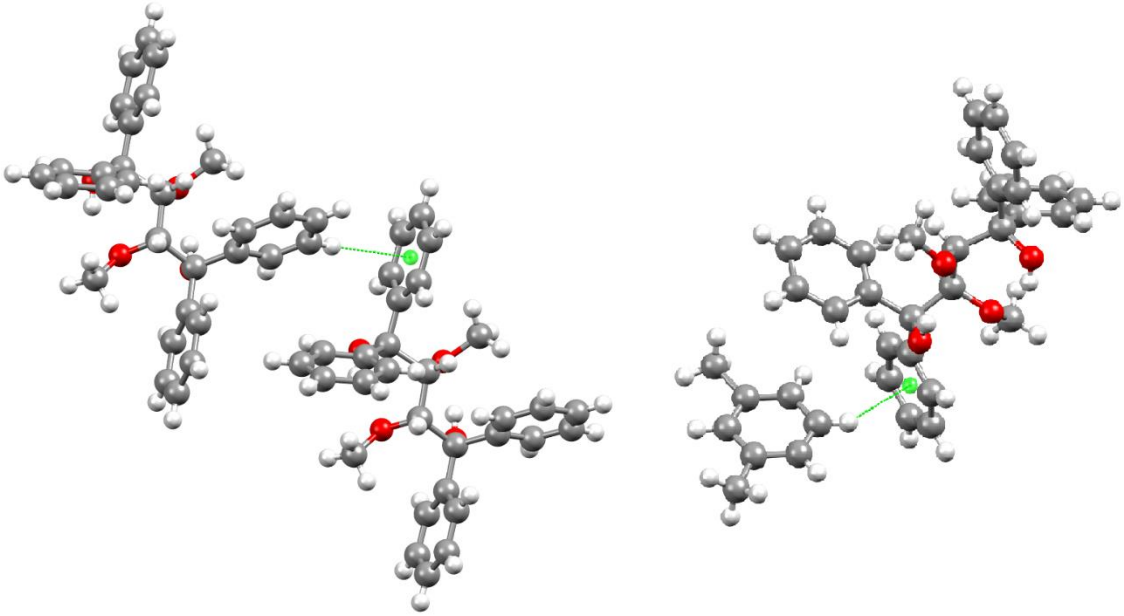

Figure 55: C-H–π stacking interactions in the DMT complexes with the C8 aromatic guests. On the left is intermolecular host–host interactions, and on the right the intermolecular host–guest interaction in the 2DMT•*m*X complex.

Table 28: C-H···π stabilizing interactions in the host-guest complexes of DMT and C8 aromatic guests.

Complex	Non-covalent interaction	Distance (Å)	Angle (°)	Symmetry operator
2DMT•*p*X	(host methoxy)C-H···Cg(host)	2.97	150	x,y,z
	(host methoxy)C-H···Cg(host)	2.85	147	x,y,z
	(host methoxy)C-H···Cg(host)	2.86	151	x,y,z
	(host methoxy)C-H···Cg(host)	2.86	145	x,y,z
	(host)*m*-ArH···Cg(host)	2.97	171	1–x, y, 1–z
2DMT•*m*X	(host methoxy)C-H···Cg(host)	2.91	148	x,y,z
	(host methoxy)C-H···Cg(host)	2.83	147	x,y,z
	(host methoxy)C-H···Cg(host)	2.82	150	x,y,z
	(host methoxy)C-H···Cg(host)	2.87	144	x,y,z
	(guest)*m*-ArH···Cg(host)	2.93	137	–1/2+x, –1/2+y, z
2DMT•*o*X	(host methoxy)C-H···Cg(host)	2.85	147	x,y,z
	(host methoxy)C-H···Cg(host)	2.88	148	x,y,z
	(host methoxy)C-H···Cg(host)	2.85	147	x,y,z
	(host methoxy)C-H···Cg(host)	2.90	147	x,y,z
	(host)*m*-ArH···Cg(host)	3.00	171	–x,y,1–z
2DMT•EB	(host methoxy)C-H···Cg(host)	2.88	148	x,y,z
	(host methoxy)C-H···Cg(host)	2.86	147	x,y,z
	(host methoxy)C-H···Cg(host)	2.85	145	x,y,z
	(host methoxy)C-H···Cg(host)	2.82	146	x,y,z
	(host)*m*-ArH···Cg(host)	2.94	170	1-x, y, 1–z

Short Contacts

A variety of other short contacts are also present throughout each complex. Those that are shorter than the sum of the van der Waals radii of the participating atoms comprise both host–host and host–guest interactions ranging between 2.11 and 2.89 Å (100–167°). Host–guest interactions typically occur between a host aromatic carbon or hydrogen atom and a guest hydrogen atom. The shortest of these are present in the 2DMT•EB complex (2.11 Å and 158°, Figure 56) and is between a host *para*-aromatic hydrogen and a CH_2 hydrogen of the guest ethyl group. No host–guest short contacts shorter than the van der Waals radii occur in the complex formed with *o*-xylene. A summary of these contacts is provided in Table 29.

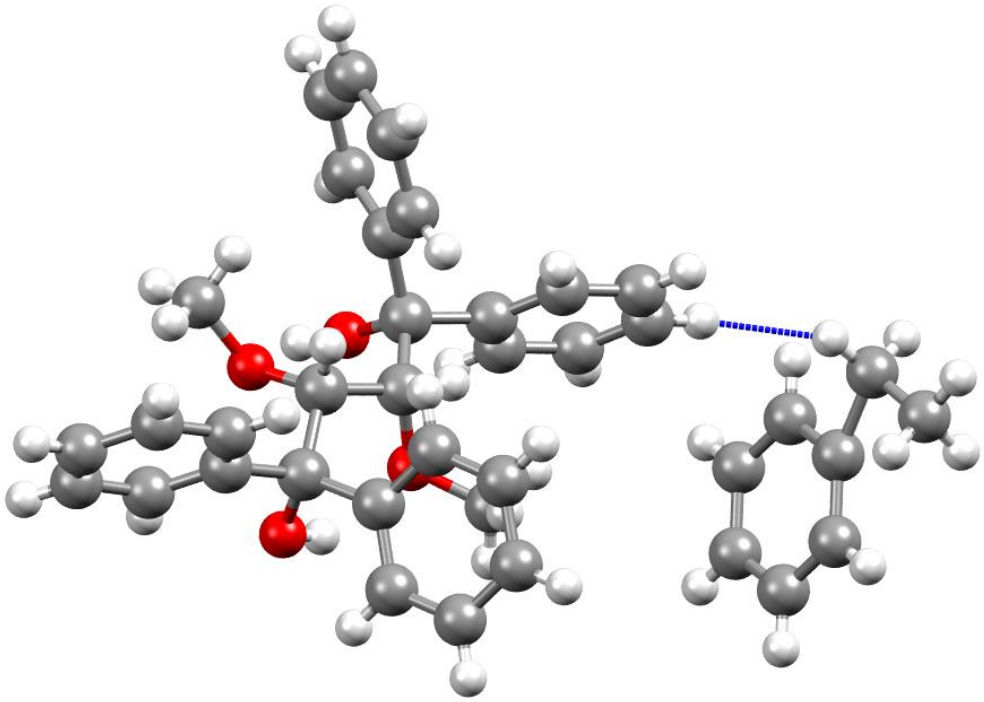

Figure 56: Short contact in the 2DMT•EB complex between host and guest (blue).

Table 29: Summary of the various contacts shorter than the van der Waals radii found in the DMT complexes with the xylene isomers and ethylbenzene.

Complex	Non-covalent interaction	Distance (Å)	Angle (°)	Symmetry operator
2DMT•*p*X	(host hydroxy)O-H···*p*-ArH(host)	2.29	107	–1/2+x,1/2+y,z
	(host hydroxy)O-H···*p*-ArH(host)	2.34	144	–1/2+x,1/2+y,z
	(host)*m*-ArC···H-C(guest methyl)	2.81	112	1–x,y,–z
	(host)*p*-ArH···*m*-ArC(guest)	2.85	147	3/2-x,1/2+y,1–z
2DMT•*m*X	(host hydroxy)O-H···*p*-ArH(host)	2.35	104	–1/2+x,–/2+y,z
	(host hydroxy)O-H···*p*-ArH(host)	2.34	149	1/2+x,1/2+y,z
	(host)*o*-ArC···*m*-ArH(guest)	2.79	161	1/2+x,1/2+y,z
	(host)*m*-ArH···H-C(guest methyl)	2.23	116	x,y,z
2DMT•*o*X	(host hydroxy)O-H···*p*-ArH(host)	2.32	154	1/2+x,1/2+y,z
	(host hydroxy)O-H···*p*-ArH(host)	2.30	167	–1/2+x,1/2+y,z
	(host)*p*-ArH···*m*-ArC(host)	2.82	152	–x,y,–z
2DMT•EB	(host hydroxy)O-H···*p*-ArH(host)	2.27	108	–1/2+x,1/2+y,z
	(host hydroxy)O-H···*p*-ArH(host)	2.25	151	1/2+x,1/2+y,z
	(host)*p*-ArH···*m*-ArC(host)	2.89	148	1–x,y,–z
	(host)*p*-ArH···H-C(guest CH_2)	2.11	158	x,y,z
	(host)*p*-ArH···H-C(guest CH_3)	2.23	135	2–x,y,2–z
	(host)*o*-ArC···H-C(guest CH_2)	2.75	100	x,y,–1+z

All the host–guest interactions obtained from these X-ray diffraction data are summarized in Table 30 in an attempt to more readily identify the significant interactions that assist in explaining the selectivity of DMT observed for these guests.

Table 30: Significant host–guest interactions for the complexes of DMT with the isomeric xylenes and ethylbenzene.

Interaction	2DMT•*p*X	2DMT•*m*X	2DMT•*o*X	2DMT•EB
π–π	5.246(1)–5.989(1)Å (5 contacts)	5.220(3)–5.905(3) Å (7 contacts)	5.341(2)–5.967(2) Å (6 contacts)	5.299(6)–5.960(4) Å (9 contacts)
CH–π	None	2.93 Å, 137° (guest)*m*-ArH···Cg(host)	None	None
Short contacts	2.81 Å, 112°, < (host)*m*-ArC···H-C(guest methyl) 2.85, 147°, < (host)*p*-ArH···*m*-ArC(guest)	2.79 Å, 161°, < (host)*o*-ArC···*m*-ArH(guest) 2.23 Å, 116°, < (host)*m*-ArH···H-C(guest methyl)	None	2.11 Å, 158°, << (host)*p*-ArH···H-C(guest CH_2) 2.23 Å, 135°, < (host)*p*-ArH···H-C(guest CH_3) 2.75 Å, 100°, < (host)*o*-ArC···H-C(guest CH_2)

*< denotes contacts less than the sum of the van der Waals radii and << denotes contacts less than this sum minus 0.2 Å

Unfortunately, a comparison of host–guest interactions in these complexes alone does not adequately explain the host's selectivity for these guests. A number of host–guest interactions exist in the complexes with *p*-xylene and ethylbenzene, as expected since these two guests were the most preferred. However, the lack of interactions in the *o*-xylene complex compared with the many interactions found in the least preferred *m*-xylene complex do not correlate with the observed selectivity order, and so X-ray data analyses alone, as it stands, cannot be used to explain this order.

For the sake of interest, the mode of packing in each complex was analysed by omitting the guests from the packing calculation and calculating the subsequent voids in the crystal (Figure 57, dark yellow). In each case, guests are accommodated in discrete cavities. Figure 58 provides a stereoview of the packing in the 2DMT•*p*X complex as representative example.

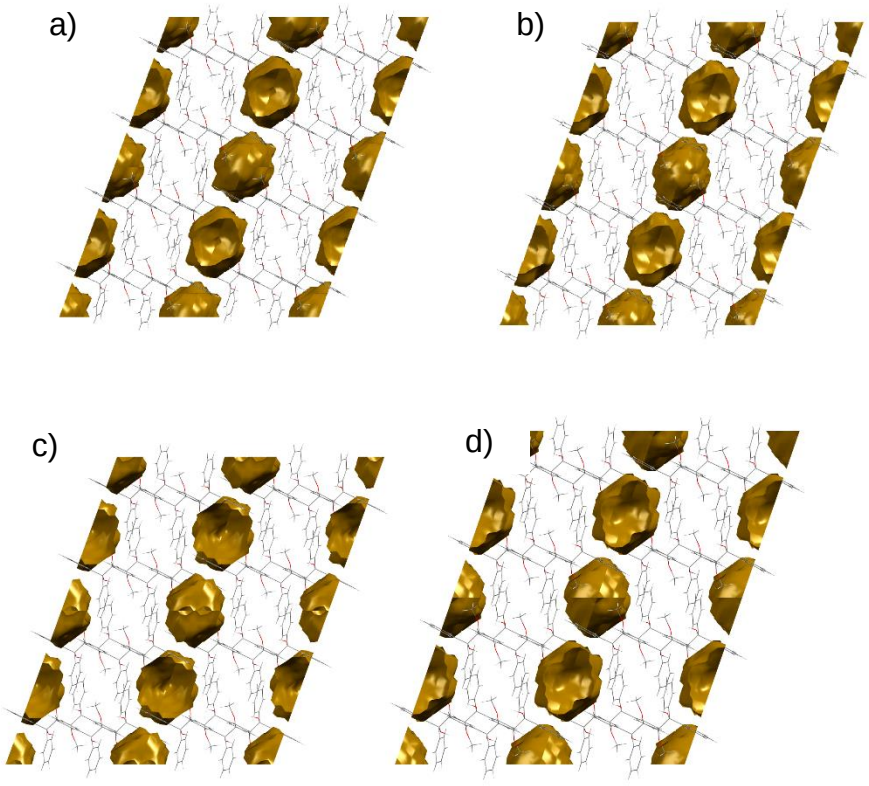

Figure 57: The discrete cavity guest packing mode in the complexes of DMT with C8 aromatic guests. a) 2DMT•*p*X; b) 2DMT•*m*X; c)2DMT•*o*X; d) 2DMT•EB.

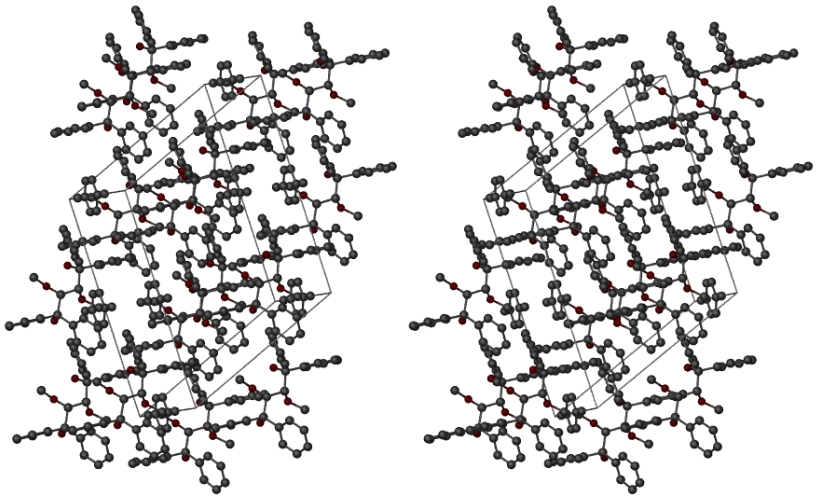

Figure 58: Stereoview of the 2DMT•*p*X complex to show the packing in three dimensions as representative sample.

4.6 Hirshfeld Surface Analysis

To better visualize and interpret the quantity and quality of contacts within these X-ray structures, Hirshfeld surface analysis was performed. Figure 59 shows the 2-dimensional fingerprint plots. All these plots share basic features. In the case of 2DMT•*p*X (Figure 59a), wings W1 and W2, as well as spike S2 are indicative of H···H interactions. W1 and W2 overlap with S1 and S3 respectively, areas representing C···H interactions. The fingerprint plot for the 2DMT•*m*X complex (Figure 59b) has one prominent wing area (W1) as well as S2, representative of H···H interactions, while S1 is typical of H···C interactions. Figure 59c depicts the fingerprint plot for the 2DMT•*o*X complex, and possesses the usual S1 spike for H···C interactions. Unlike the preceding two plots, the central S2 H···H spike is absent; in its stead are two broad wing areas (W1 and W2). The features for the 2DMT•EB plot (Figure 59d) include a thick S1 area (H···C interactions) and a singular large wing (W1, H···H) which extends much closer to the origin of the plot on both the d_e and d_i axes, indicating much closer interactions.

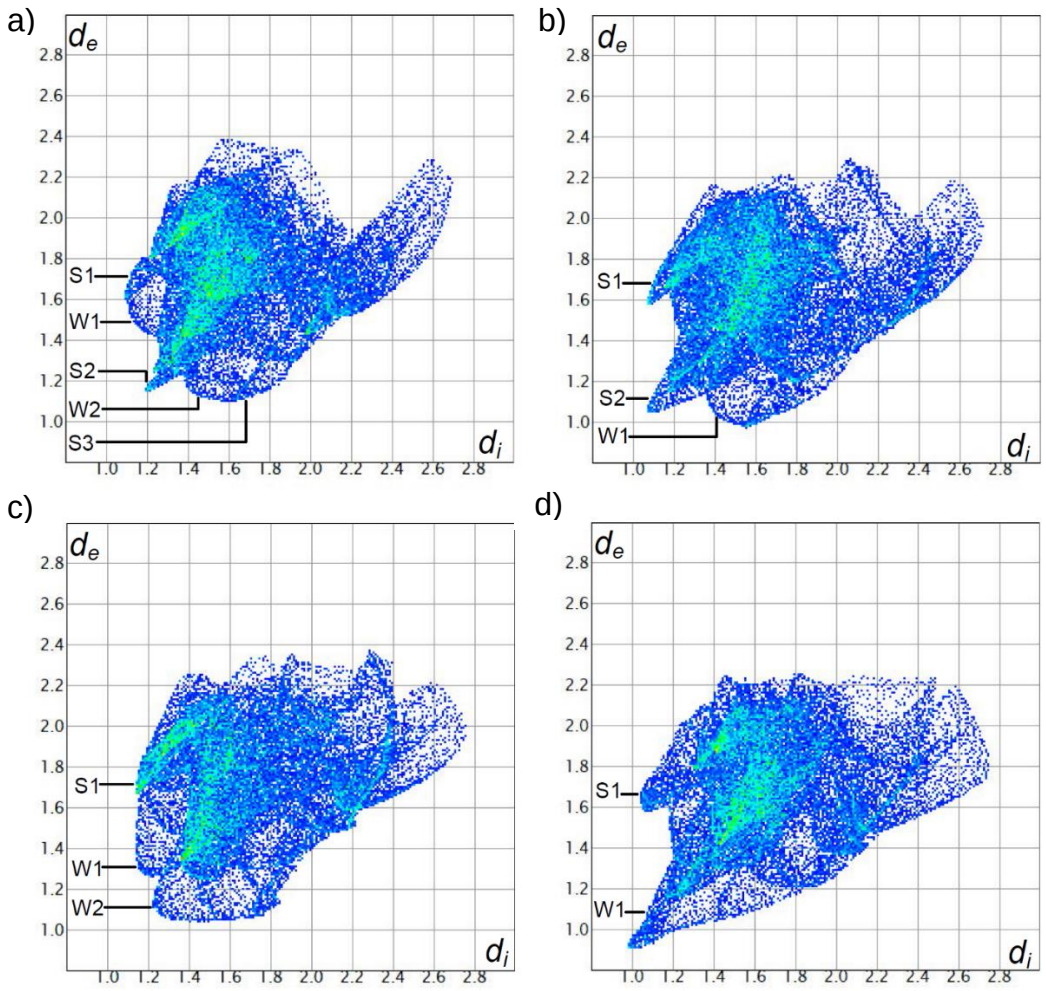

Figure 59: Two-dimensional fingerprint plots obtained from Hirshfeld surfaces for the inclusion complexes of a) 2DMT•*p*X, b) 2DMT•*m*X, c) 2DMT•*o*X, and d) 2DMT•EB.

Figure 60 graphically represents the percentage and type of the intermolecular interactions between different atoms. In all four complexes, H···H and H···C interactions dominate, with the 2DMT•*o*X complex having the lowest percentage of the former, and the highest percentage of the latter. O···H interactions are negligible, as only the complexes containing *m*-xylene and ethylbenzene experience these (0.2 and 0.1%, respectively). Furthermore, only the 2DMT•*m*X complex contains C···C interactions (0.2%). Comparatively, no definitive feature from Hirshfeld surface analysis can be singled out which may explain the selectivity order of DMT for the C8 aromatic compounds.

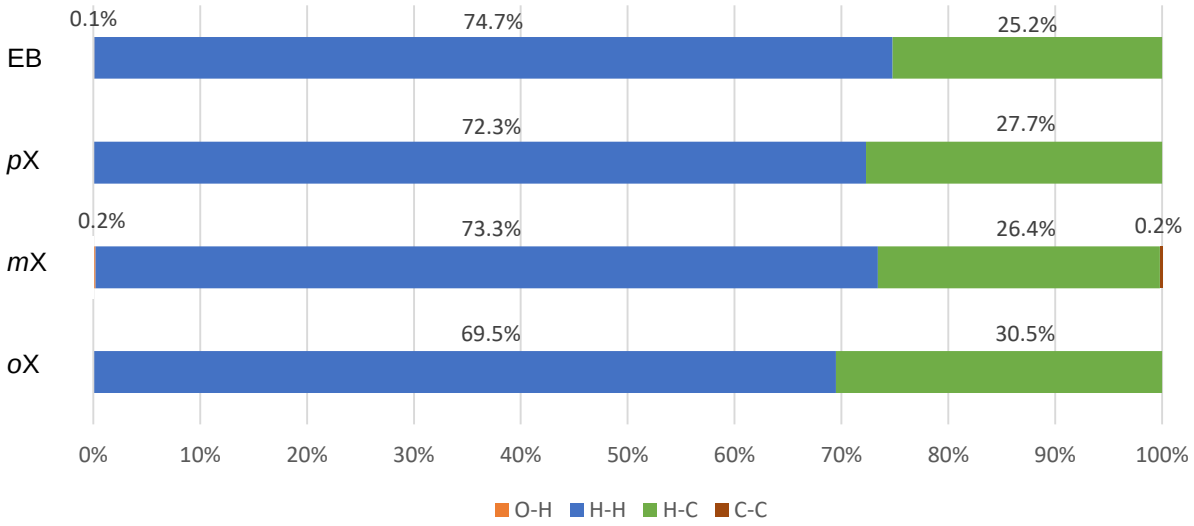

Figure 60: Graphical display showing the percentage and type of inter-molecular interactions in each complex.

4.7 Conclusion

DMT is a successful compound for complexing aromatic hydrocarbons such as the three isomeric xylenes and ethylbenzene. Competition experiments showed that DMT discriminated overwhelmingly in favour of *para*-xylene and consistently against *meta*-xylene. Ethylbenzene was the second preferred followed by *ortho*-xylene. Thermal experiments confirmed the selectivity order displayed by the host, and relative thermal stabilities (T_{on}–T_b) of these complexes correlated with the observed selectivity order. X-Ray data was not useful for determining the reasons for these observations: all host frameworks in the complexes are isostructural, all of the guests reside in very similar discrete cavities, and no distinctive intermolecular forces between host and guest could be singled out to explain these observations. Hirshfeld surface analyses, furthermore, were also not useful in this regard.

Chapter 5: Inclusion Compounds of DMT (73) with Aniline and the Toluidine Isomers

5.1 Introduction

The toluidines are methyl-substituted aniline isomers and comprise *p*-toluidine (*p*-TD), *m*-toluidine (*m*-TD) and *o*-toluidine (*o*-TD). These compounds have a variety of uses. They are routinely used as precursors to dyes and pigments, in the production of pesticides and herbicides, as hardeners for cyanoacrylate adhesives, and as surfactants.[170–173] They have similar boiling points (200.4, 203.3 and 200.3 °C, respectively). They are produced through the catalytic reduction of the corresponding nitrotoluene isomers. The methylation of aniline to yield the *N*-methyl- and *N*,*N*-dimethylaniline derivatives also results in the production of toluidine as a side product due to rearrangement.[155] It would therefore be advantageous to be able to sequester the toluidines formed in this fashion, or indeed to be able to separate the toluidine isomers from one another. As such, in this work, we endeavoured to determine whether DMT is capable of including the toluidines, to compare DMT's preference for the toluidines to that of the unsubstituted aniline, and finally to determine whether DMT shows discriminatory behaviour towards the toluidine isomers when these are present in mixtures.

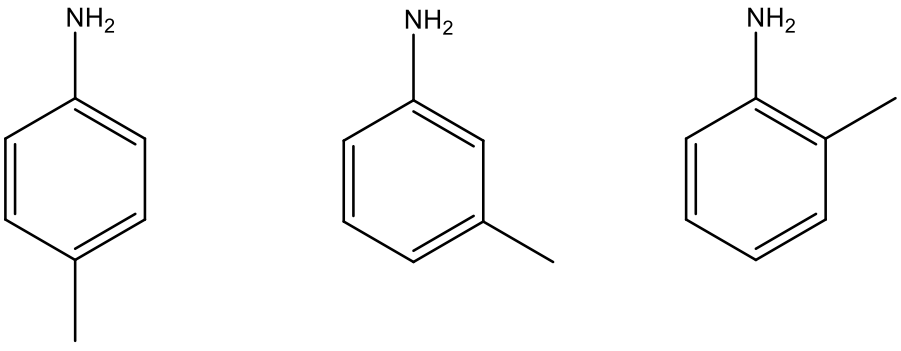

p-TD *m*-TD *o*-TD

5.2 Individual and Equimolar Inclusion Experiments

Following the recrystallization of DMT from individual mixtures of aniline and the toluidine isomers, the crystals thus obtained were subjected to ^{1}H-NMR spectroscopy. It was consequently determined that 2:1 host:guest complexes were formed in each case (Table 31).

Table 31: Host:guest ratios of complexes formed with DMT during individual recrystallization experiments.*

Guest	Host:guest
Aniline	2:1
o-TD	2:1
m-TD	2:1
p-TD	2:1

*Determined using ^{1}H-NMR spectroscopy.

A multitude of equimolar competition experiments were performed in which DMT was recrystallized from different combinations of aniline and the toluidine isomers. As with the complexes formed from individual guests, the overall host:guest ratios in these competition experiments remained 2:1 in each case (Table 32). A binary equimolar competition experiment between *o*-TD and *m*-TD indicated that DMT preferred the *ortho*-substituted guest by 72.5% in contrast to *m*-TD (27.5%). An experiment involving *o*-TD and *p*-TD resulted in DMT having a slight preference for *p*-TD (53.3%), while when *m*-TD and *p*-TD competed, *p*-TD was significantly preferred (71.3%). A ternary equimolar competition experiment involving all three toluidine isomers resulted in *p*-TD being included preferentially (44.2%) compared with 40.1% of *o*-TD and 15.7% of *m*-TD. Binary mixtures involving aniline and each of the toluidine isomers resulted in discrimination against aniline in each case. *p*-TD, *m*-TD and *o*-TD were significantly more preferred (83.8, 73.1 and 84.5%, respectively). Finally, a quaternary mixture incorporating all four guest solvents resulted in 40.0% *p*-TD being included, followed by *o*-TD, *m*-TD and aniline (35.7, 16.2 and 8.1%, respectively).

Table 32: Competition experiments and H:G ratios obtained.[#]

Aniline	*o*-TD	*m*-TD	*p*-TD	Guest ratios* (% e.s.d.)[$]	Overall H:G ratio
	x	x		**72.5**:27.5 (0.1)	2:1
	x		***x***	46.7:**53.3** (0.1)	2:1
		x	***x***	28.7:**71.3** (0.8)	2:1
	x	x	***x***	40.1:15.7: **44.2** (0.6)(1.1)(0.4)	2:1
x	***x***			15.5:**84.5** (1.4)	2:1
x		***x***		26.9:**73.1** (1.4)	2:1
x			***x***	16.2:**83.8** (1.2)	2:1
x	x	x	***x***	8.1:35.7:16.2:**40.0** (0.8)(1.1)(0.7)(0.7)	2:1

[#]Preferred guests are given in bold italic font face for ease of comparison; *determined using GC-MS; [$]experiments were carried out in triplicate, and an average ratio is provided here with % e.s.d.'s in parentheses.

5.3 Host Selectivity Profiles with Changing Guest Concentrations in Binary and Ternary Guest Mixtures

After being recrystallized from binary mixtures in which the guest molar concentrations were varied, selectivity curves of DMT towards aniline and the toluidine isomers were constructed. This was done after analysis (GC-MS) of both the crystals and the mother liquor from which the crystals had formed.

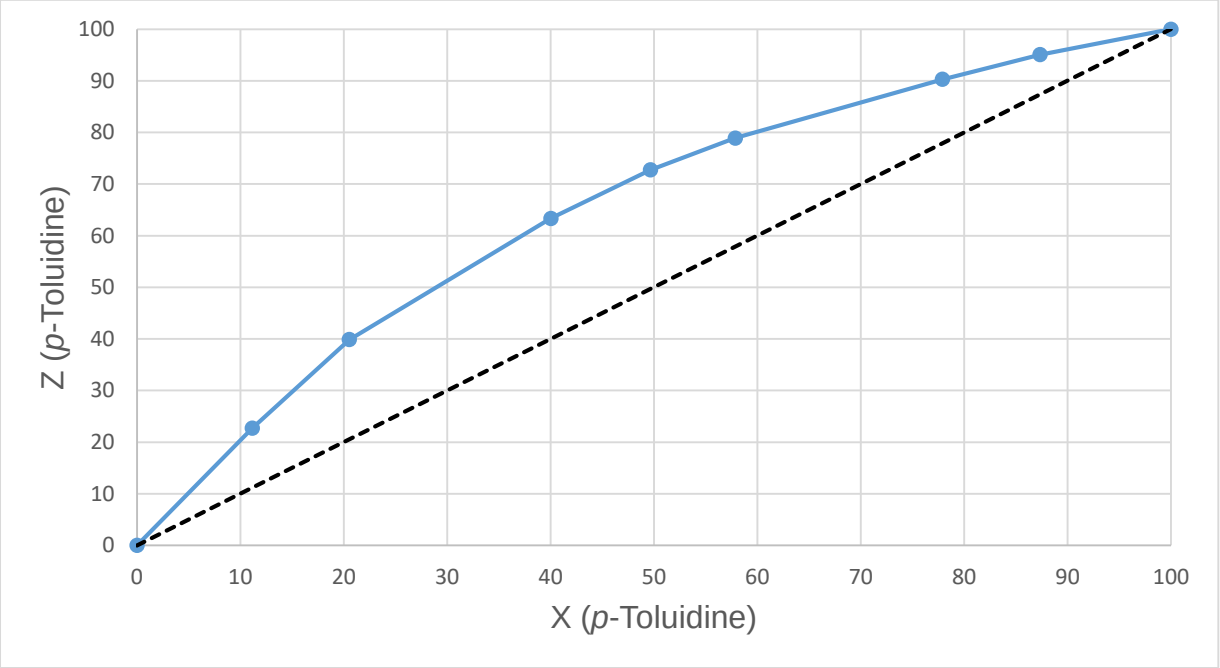

Figure 61: Selectivity curve obtained from the *p*-TD/*m*-TD experiments. Coloured blue is the molar fraction of *p*-TD in the inclusion complex (Z) *vs* the molar fraction of *p*-TD in the mother liquor (X). Black dashes indicate the theoretical line of no selectivity.

Figure 61 indicates the selectivity profile outcome of the competition experiment between *p*-TD and *m*-TD. From the plot, it can be seen that *p*-TD was preferred over *m*-TD at all guest compositions assessed. An experiment containing approximately 20.5% *p*-TD in the mother liquor furnished an inclusion complex containing ~40% *p*-TD. Similarly, when the mother liquor composition comprised ~78% *p*-TD, the crystals

contained 90% of this guest. K, the selectivity coefficient for these competition experiments, was calculated to be 2.62.

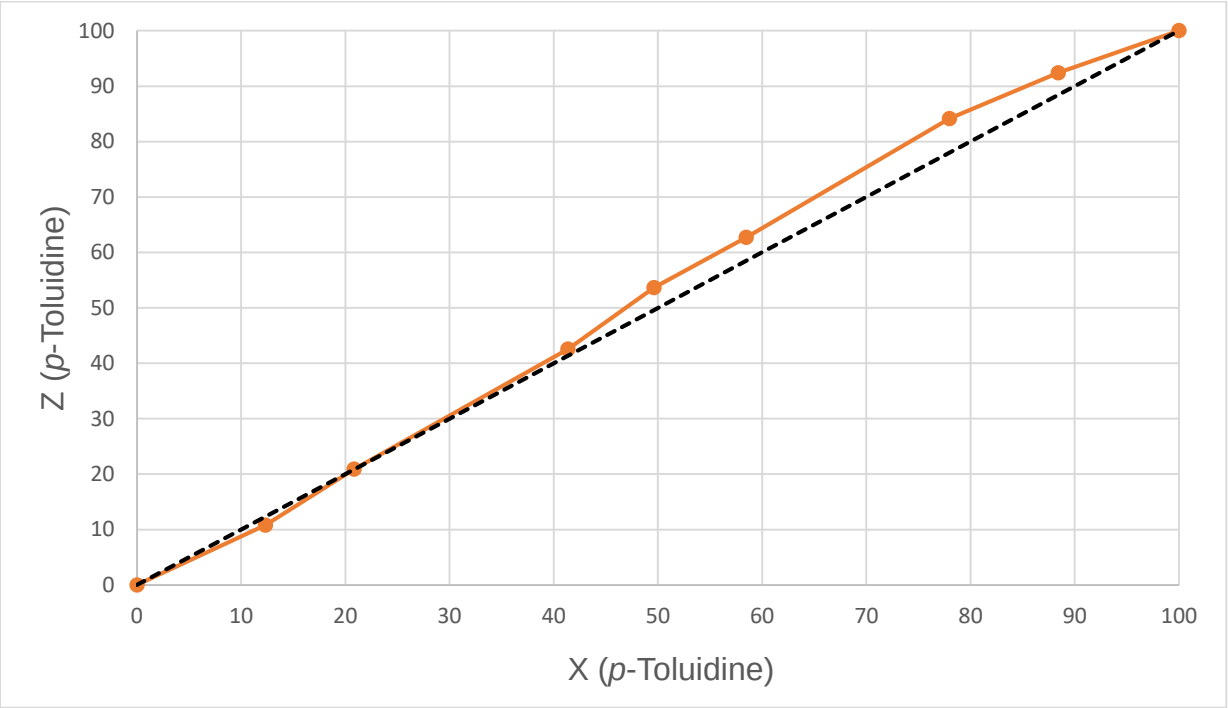

Figure 62: Selectivity curve obtained from the *p*-TD/*o*-TD experiments. Coloured orange is the molar fraction of *p*-TD in the inclusion complex (Z) *vs* the molar fraction of *p*-TD in the mother liquor (X). Black dashes indicate the theoretical line of no selectivity.

In contrast to Figure 61, the selectivity curve obtained for the competition experiments between *p*-TD and *o*-TD has a flat trajectory, closely matching that of the theoretical line of no selectivity (Figure 62). Initially, a mother liquor content of ~12% *p*-TD yielded crystals containing slightly less of this guest (11%), indicating a preference for *o*-TD. At a mother liquor content of 21% *p*-TD, the obtained inclusion complex also contained 21% of this guest indicating no selectivity at this point. Upon further increasing the amount of *p*-TD in the mother liquor to ~78%, crystals were obtained containing approximately 84% *p*-TD, indicating a shift in selectivity towards this guest. The average selectivity coefficient, K, for this curve was 1.19, significantly lower than in the previous result.

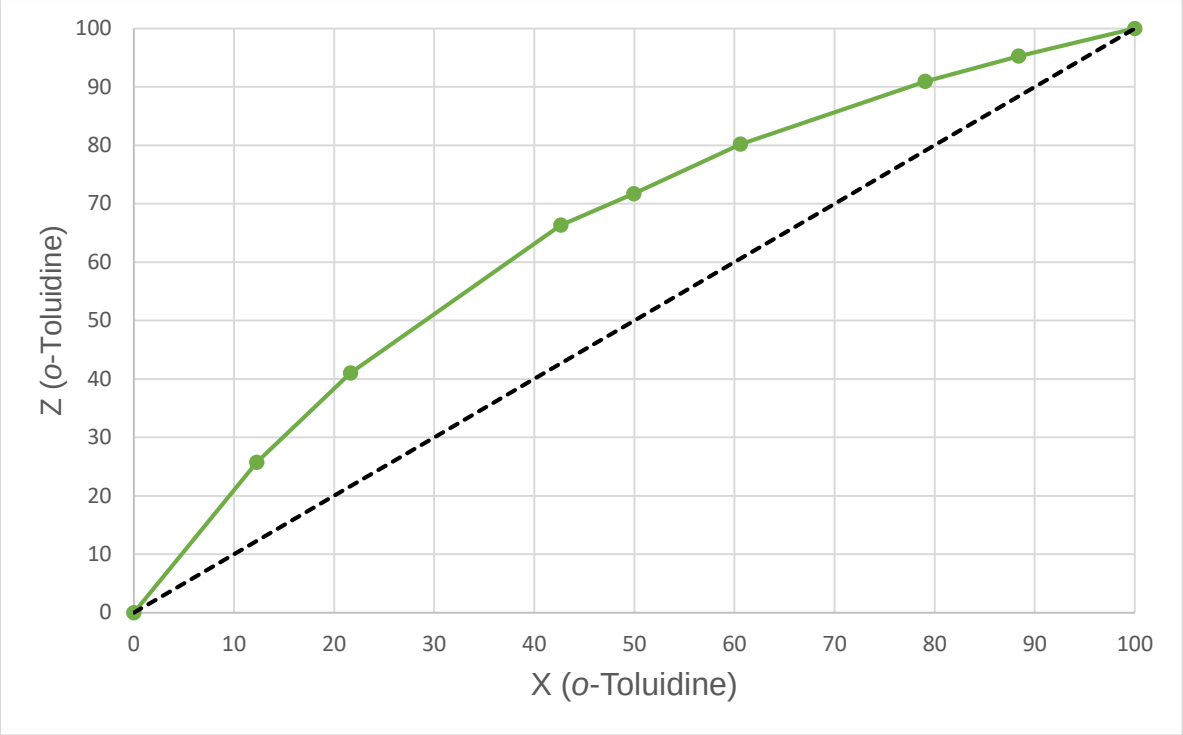

Figure 63: Selectivity curve obtained from the *o*-TD/*m*-TD experiments. Coloured green is the molar fraction of *o*-TD in the inclusion complex (Z) *vs* the molar fraction of *o*-TD in the mother liquor (X). Black dashes indicate the theoretical line of no selectivity.

Figure 63 shows the selectivity curve obtained when DMT was recrystallized from mixtures of *o*-TD and *m*-TD. DMT consistently discriminated in favour of *o*-TD throughout the experiment. A mother liquor comprised of 22% *o*-TD yielded crystals enriched with this guest up to 41%, whereas a mother liquor composition of ~61% *o*-TD allowed for the crystallization of an inclusion complex containing 80% of this guest. The average K for these experiments was determined to be 2.58.

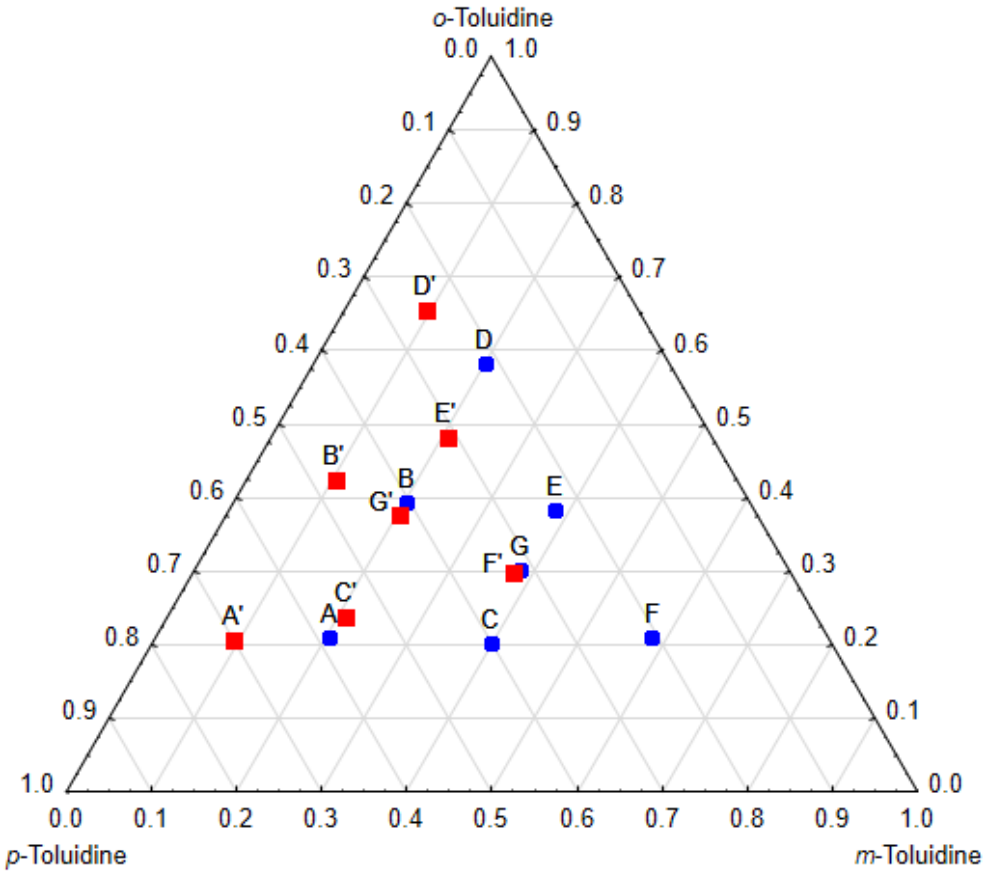

Figure 64: Ternary competition plot obtained from the *p*-TD/*m*-TD/*o*-TD experiments. Blue circles indicate mother liquor compositions, while red squares indicate guest compositions in the crystals.

Non-equimolar mixtures of *p*-TD, *m*-TD and *o*-TD were prepared from which DMT was recrystallized. The mother liquor compositions and guest composition of the inclusion complexes thus formed were analysed, and the ternary competition plot in Figure 64 constructed. These ternary competition mixtures resulted in an average increase in the *p*-TD content of the crystals of 9.5% when compared with the mother liquor. Likewise, the *o*-TD content increased by an average of 5.7%. The average *m*-TD content of the crystals decreased by 15.4% relative to the mother liquor.

We subsequently investigated whether any selectivity changes would occur when the toluidines were made to compete with unsubstituted aniline in binary mixtures. Figures 65–67 indicate the outcome of these experiments.

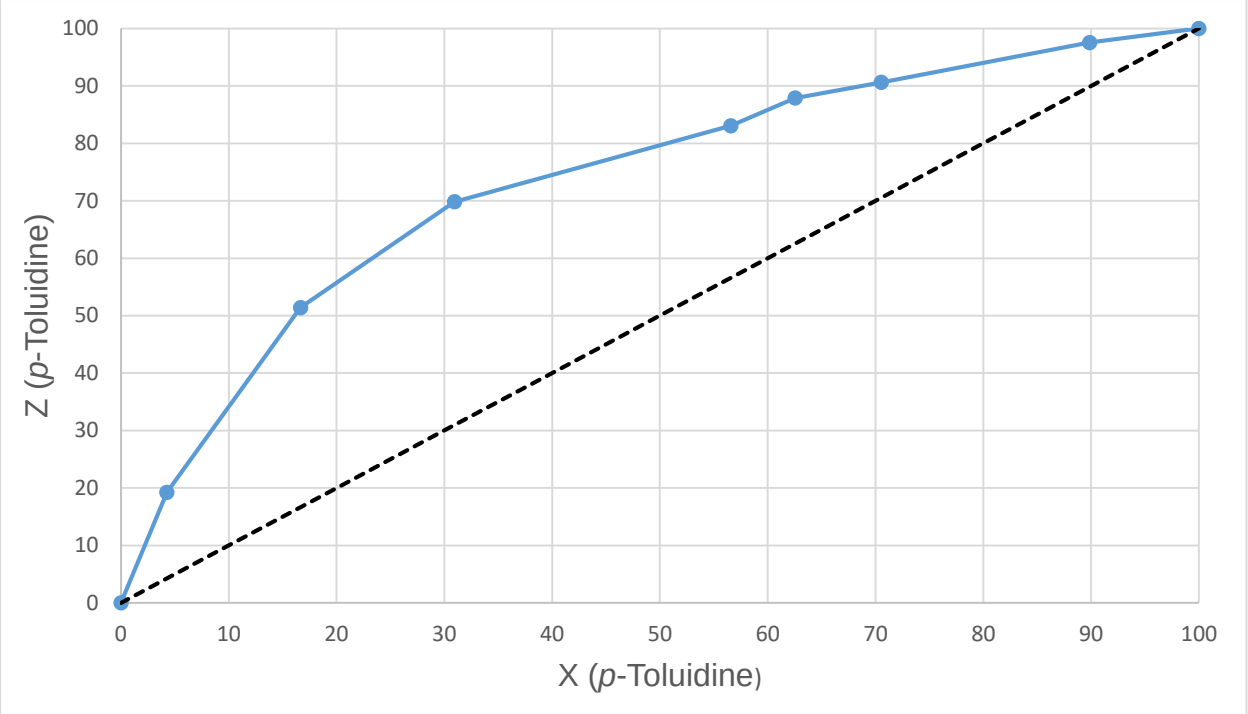

Figure 65: Selectivity curve obtained from the *p*-TD/aniline experiments. Coloured blue is the molar fraction of *p*-TD in the inclusion complex (Z) *vs* the molar fraction of *p*-TD in the mother liquor (X). Black dashes indicate the theoretical line of no selectivity.

When aniline was placed in competition with *p*-TD, the latter guest was strongly preferred throughout the concentration range (Figure 65). When crystallized from a mother liquor that contained approximately 4.2% *p*-TD, the inclusion complex already contained ~19.2% of this guest. At a point representing 62.5% *p*-TD, the crystals were determined to contain 87.9% of the preferred guest. The average K for this experiment was calculated to be 4.63, which is higher than in any of the preceding experiments involving the toluidine isomers.

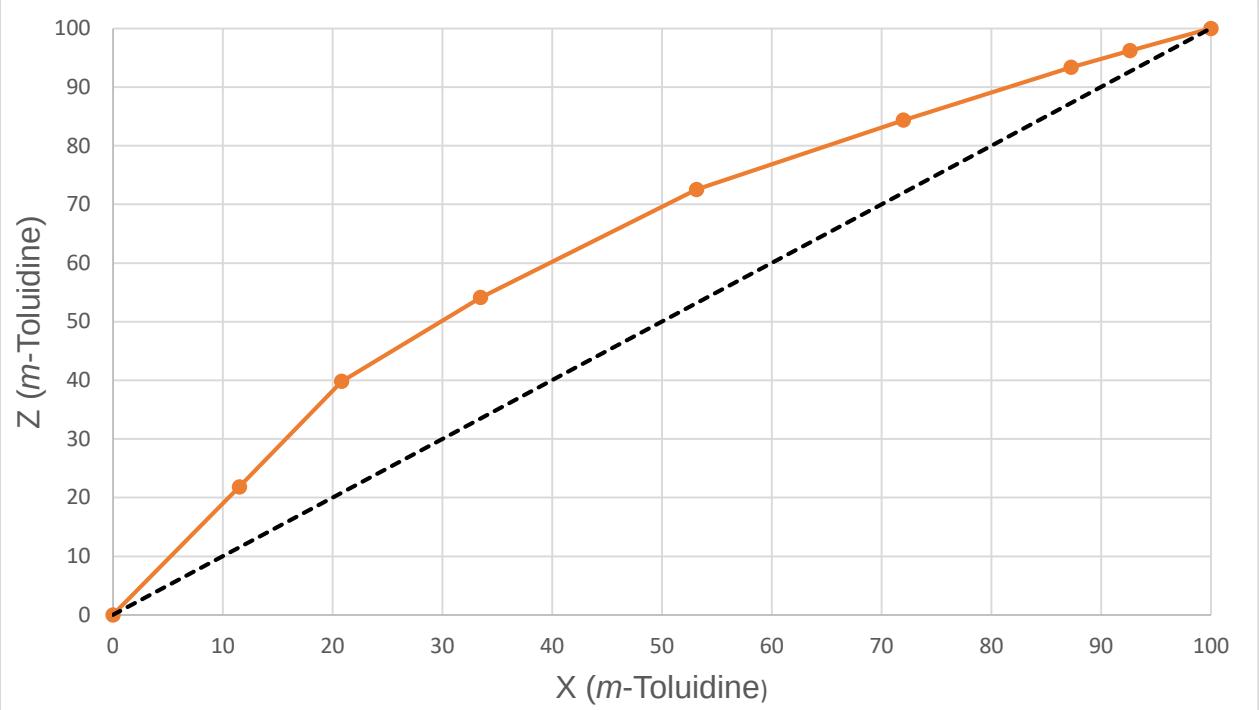

Figure 66: Selectivity curve obtained from the *m*-TD/aniline experiments. Coloured orange is the molar fraction of *m*-TD in the inclusion complex (Z) *vs* the molar fraction of *m*-TD in the mother liquor (X). Black dashes indicate the theoretical line of no selectivity.

Aniline was consistently discriminated against when in the presence of *m*-TD (Figure 66). This is exemplified by considering the experiment comprised of ~11.5% *m*-TD in the mother liquor, where resultant crystals contained approximately 21.8% of this guest. This trend continued over the entire molar concentration range assessed. Crystals containing 84.3% *m*-TD were obtained from a mother liquor composition of ~72.1% *m*-TD (and ~27.9% aniline). K in this case was determined to be 2.21.

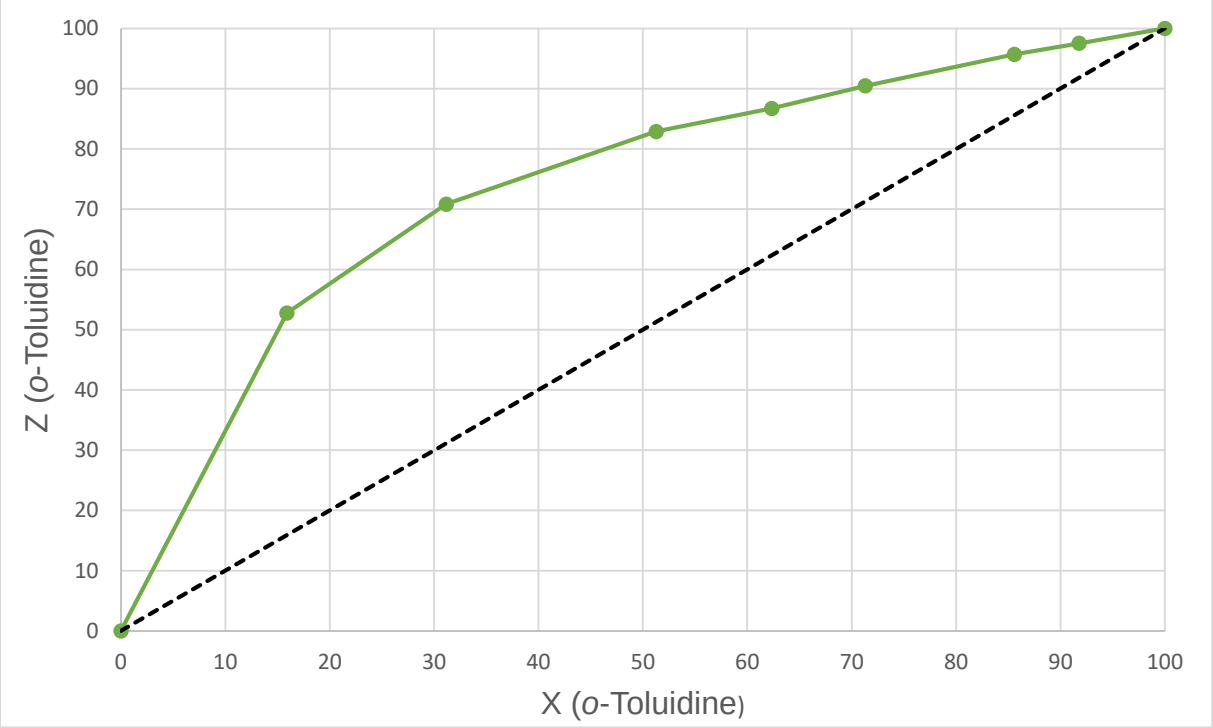

Figure 67: Selectivity curve obtained from the *o*-TD/aniline experiments. Coloured green is the molar fraction of *o*-TD in the inclusion complex (Z) *vs* the molar fraction of *o*-TD in the mother liquor (X). Black dashes indicate the theoretical line of no selectivity.

The selectivity curve generated from experiments between aniline and *o*-TD (Figure 67) resembles that of the *p*-TD/aniline curve. DMT clearly discriminated in favour of *o*-TD as crystals grown from a mother liquor containing ~15.9% *o*-TD contained ~52.7% of this guest, while an inclusion complex containing approximately 90.4% *o*-TD was isolated from a mother liquor enriched to 71.3% of this guest. The selectivity coefficient for this experiment is also comparable to that of the *p*-TD/aniline experiment (4.41).

Analysis of the binary equimolar and non-equimolar competition experiment results indicates an overall DMT selectivity order of *p*-TD > *o*-TD > *m*-TD when considering only the toluidine isomers. Upon adding aniline to the competition experiments, the selectivity order remained unchanged with respect to the toluidines, while aniline became the least preferred guest (*p*-TD > *o*-TD > *m*-TD > aniline).

5.4 Thermal Analysis

Thermal analysis was carried out on each complex to ascertain whether the thermal stability of these complexes are related to the selectivity order displayed by DMT. This was achieved by heating each complex at 10 °C.min^{-1} upon which the thermal events were monitored by means of thermogravimetric analysis and differential scanning calorimetry. Figures 68–70 show the TG, DTG and DSC traces obtained for each thermal experiment.

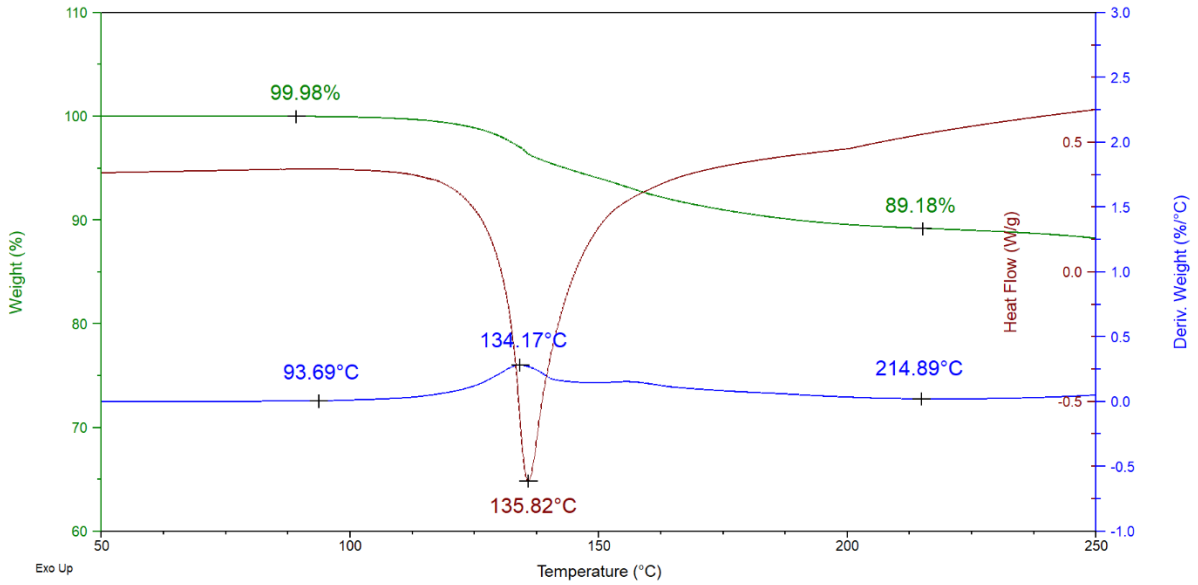

Figure 68: Overlaid TG (green), DTG (blue) and DSC (brown) traces for the 2DMT•*p*-TD complex upon heating at 10 °C.min^{-1}

A mass loss of 10.5% is expected upon removal of all the guest from a 2:1 DMT•*p*-TD complex. The TG trace (green) in Figure 68 indicates a mass loss of 10.8% which correlates well with that expected. The onset temperature of the mass loss process was ~93.7 °C and ceased at approximately 214.9 °C (DTG). The maximum rate of mass loss occurred at 134.2 °C, while a single endotherm peak, representing the simultaneous guest release and host melt processes, was observed at ~135.8 °C (DSC).

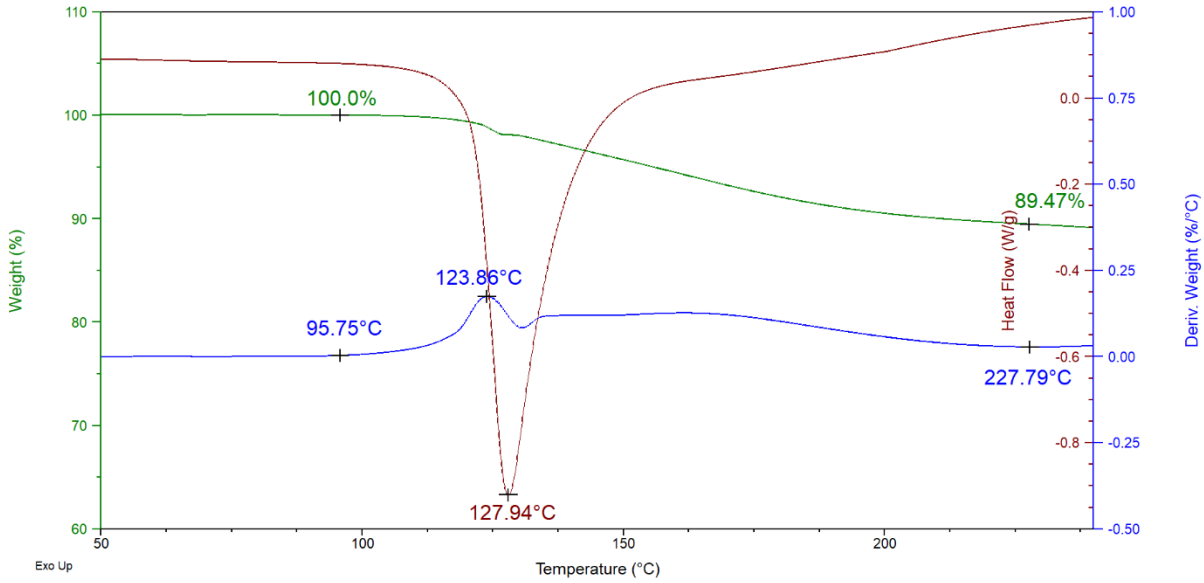

Figure 69: Overlaid TG (green), DTG (blue) and DSC (brown) traces for the 2DMT•*m*-TD complex upon heating at 10 °C.min^{-1}

The mass loss experienced by the 2DMT•*m*-TD complex was determined to be ~10.5% which is in excellent agreement with the expected amount for a 2:1 complex (Figure 69, TG, also 10.5%). Mass loss due to guest release commenced from approximately 95.8 °C and continued until ~227.8 °C (DTG). Again, a single endotherm peak (DSC), as a result of guest release and the melting of the host, was found at 127.9 °C, while the maximum rate of mass loss was determined to occur at ~123.9 °C (DTG).

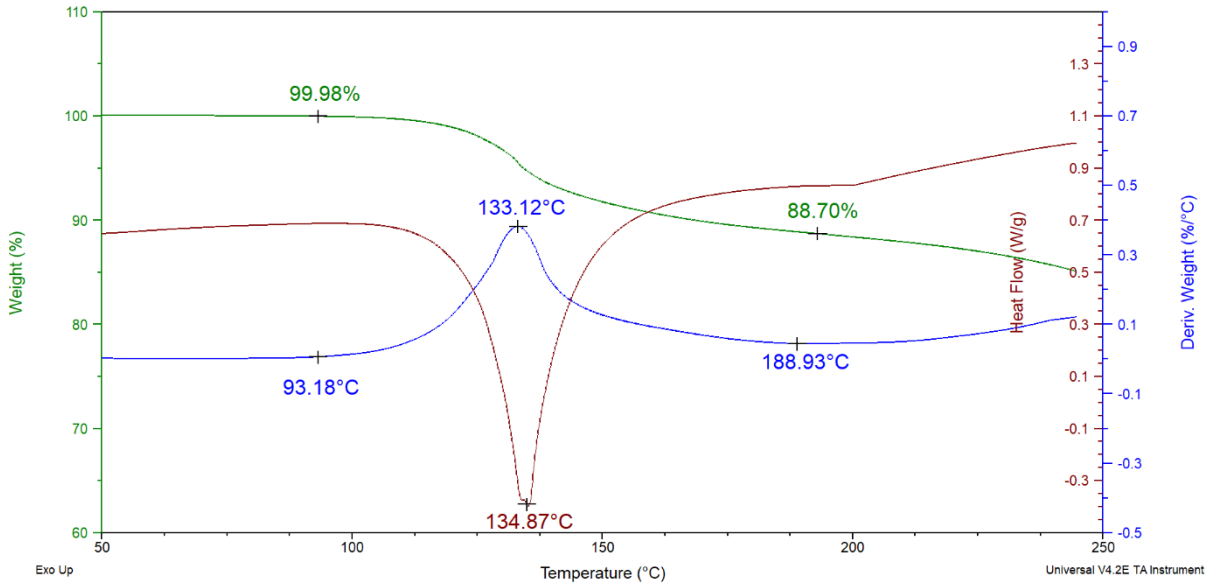

Figure 70: Overlaid TG (green), DTG (blue) and DSC (brown) traces for the 2DMT•*o*-TD complex upon heating at 10 °C.min^{-1}

The mass loss obtained upon heating a 2:1 DMT•*o*-TD was determined to be 11.3% which is, once more, in reasonable agreement with the expected amount of 10.5% (Figure 70, TG). The mass loss process occurred within a range of 93.2 and 188.9°C (DTG). Once more, the highest rate of mass loss was observed at ~133.1°C, while the endotherm peak associated with this mass loss and the melting of the host occurred at approximately 134.9 °C.

The major thermal events for these inclusion complexes are summarized in Table 33, together with that of aniline for ease of comparison (see Section 3.4). The term T_{on}–T_b, when used as a predictor of the relative thermal stability of complexes,[160,161] indicated a stability order of aniline > *p*-TD > *o*-TD > *m*-TD. While this thermal stability order correlates with the selectivity order for the toluidine isomers, it is uncertain why the thermal stability of aniline is so large when it was the least preferred guest. Consideration of the peak endotherm temperature (T_{end}) of these complexes indicates a thermal stability order of *p*-TD (135.8 °C) > *o*-TD (134.9 °C) > *m*-TD (127.9 °C) > aniline (121.1 °C) which is in direct agreement with the aforementioned selectivity order DMT exhibits towards these guests. Furthermore, T_p values estimated from the DTG curves and whose values represent the temperature at which guest loss is most rapid, also correlates exactly with the observed selectivity order [*p*-TD (134.2 °C) > *o*-

TD (133.1 °C) > *m*-TD (123.9 °C) > aniline (118.1 °C)]. In the present instance, therefore, T_{on}–T_b was unreliable when predicting the host's selectivity for various guests, while both T_p and T_{end} were dependable here.

Table 33: Summary of the major thermal events observed in the aniline and toluidine complexes with DMT.

Guest	T_b (°C)	T_{on} (°C)[a]	T_{on}–T_b (°C)	T_p (°C)[b]	T_{end} (°C)[c]	Mass loss % (Expected)
Aniline[d]	184.2	83.2	–101.0	118.1	121.1	9.3 (9.3)
p-Toluidine	200.4	93.7	–106.7	134.2	135.8	10.8 (10.5)
m-Toluidine	203.3	95.8	–107.5	123.9	127.9	10.5 (10.5)
o-Toluidine	200.3	93.2	–107.1	133.1	134.9	11.3 (10.5)

[a]T_{on} is the onset temperature for guest release estimated from the DTG; [b]T_p values were determined from the blue DTG traces; [c]T_{end} values are obtained from the brown DSC traces; [d]the thermal data for the 2DMT•aniline complex is added here for ease of comparison (see Section 3.4).

5.5 Single Crystal X-Ray Analysis

The individual inclusions of DMT with the toluidine isomers were further analysed by means of single crystal X-ray diffraction. Analysis of the crystallographic data for these complexes indicated that the host framework of each complex is isostructural and that the complexes crystallized in the monoclinic *C*2 crystal system in each case. Figure 71 is a stereoview for the 2DMT•*p*-TD complex as representative example to show the host–guest packing. Table 34 lists the crystallographic data for the complexes with the toluidine isomers, while Figure 72 shows the unit cells of each. The guest in each complex displays symmetry-generated disorder, but this disorder is well modelled.

Table 34: Crystallographic data for the complexes of DMT with the isomeric toluidine guests.

	2DMT•*p*-TD	**2DMT•*m*-TD**	**2DMT•*o*-TD**
Chemical formula	$C_{30}H_{30}O_4$ •$0.5C_7H_9N$	$C_{30}H_{30}O_4$ •$0.5C_7H_7N$	$C_{30}H_{30}O_4$ •$0.5C_7H_7N$
Formula weight	1016.23	1014.22	1014.22
Crystal system	Monoclinic	Monoclinic	Monoclinic
Space group	*C*2	*C*2	*C*2
μ (Mo-Kα)/mm^{-1}	0.079	0.079	0.079
a/Å	17.2804(19)	17.4485(15)	17.3965(11)
b/Å	12.0944(14)	12.0156(8)	11.9219(7)
c/Å	14.0931(16)	14.1121(10)	14.2165(9)
alpha/°	90	90	90
beta/°	110.363(4)	110.179(2)	109.803(3)
gamma/°	90	90	90
V/$Å^3$	2761.3(5)	2777.1(3)	2774.1(3)
Z	2	2	2
F(000)	1084	1080	1080
Temp./K	200	200	200
Restraints	1	1	1

Nref	6617	6833	5477
Npar	351	372	372
R	0.0366	0.0339	0.0318
wR2	0.0946	0.0929	0.0893
S	1.05	1.04	1.04
θ min-max/°	2.1, 28.3	2.1, 28.3	2.1, 28.3
Tot. data	22149	54025	30507
Unique data	6617	6833	5477
Observed data [I > 2.0 sigma(I)]	5913	6525	5040
R_{int}	0.021	0.016	0.020
Dffrn measured fraction θ full	0.998	0.999	1.000
Min. resd. dens. (e/ Å^3)	–0.21	–0.23	–0.15
Max. resd. dens. (e/ Å^3)	0.27	0.21	0.19

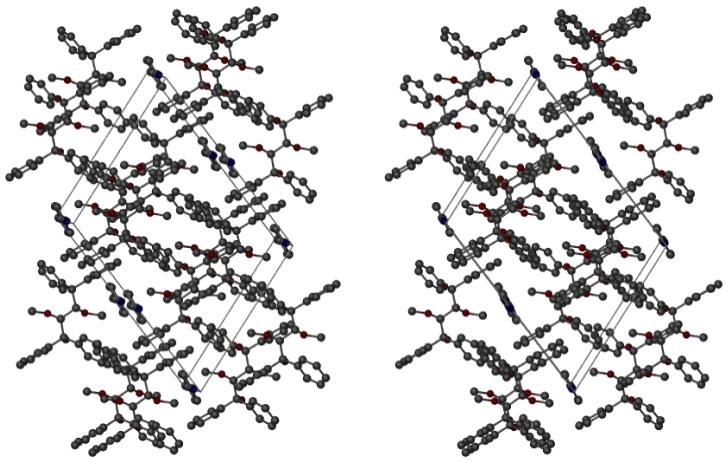

Figure 71: Stereoview of the 2DMT•*p*-TD complex to show the packing in three dimensions, as representative sample.

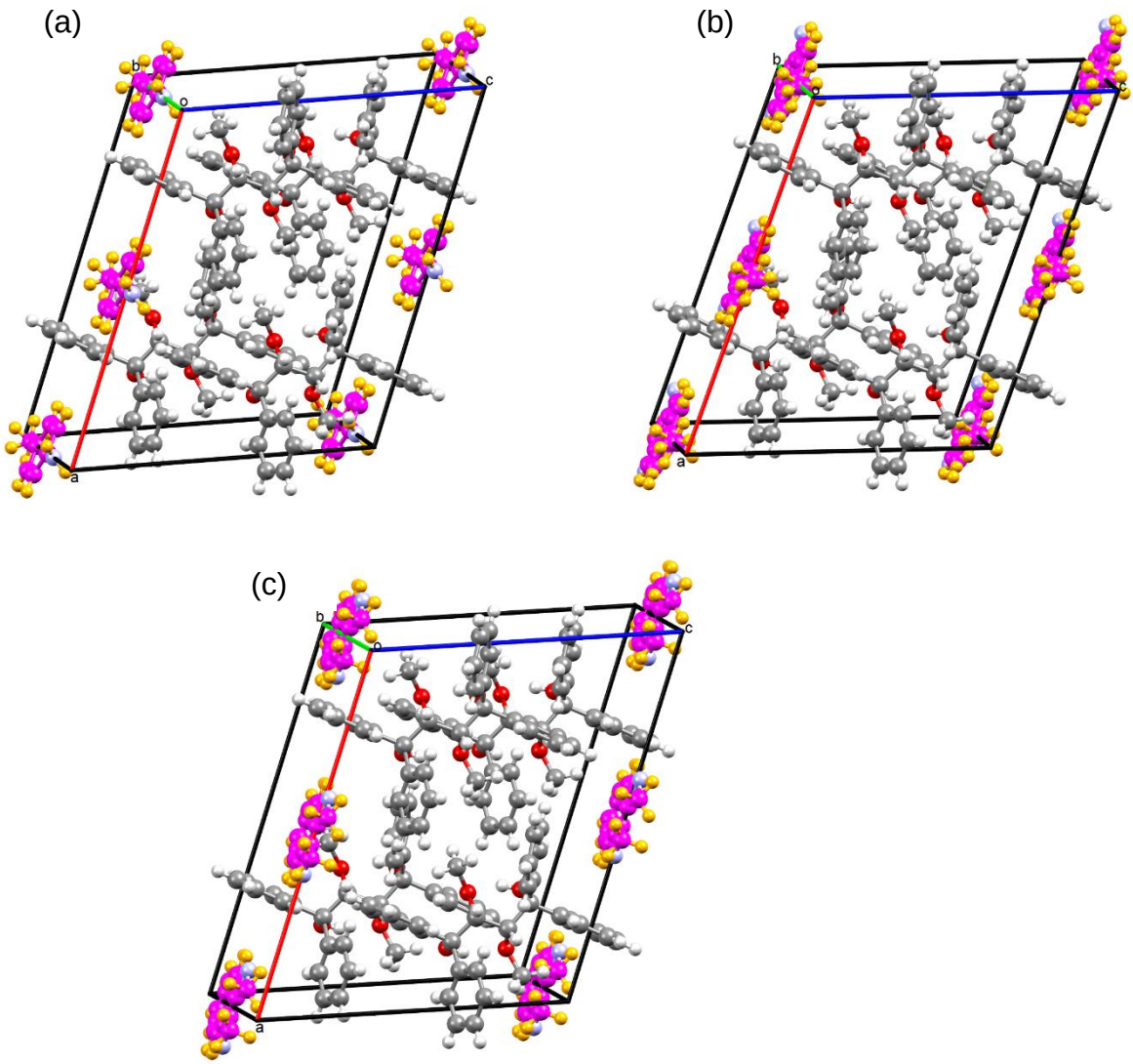

Figure 72: The unit cells for the DMT complexes with the toluidine isomers; the guests have a magenta carbon framework, while the hosts have a grey carbon framework; a) 2DMT•*p*-TD, b) 2DMT•*m*-TD, c) 2DMT•*o*-TD; the isostructural nature of all the host frameworks are clearly evident from these figures.

Hydrogen Bonding

Classic hydrogen bonding interactions are seen only within the host framework of these complexes. These manifest as 1,3- and 2,4- intramolecular hydrogen bonds between host hydroxy and methoxy moieties on the butane backbone. These hydrogen bonds range in distance between 2.627(2) and 2.680(2) Å, with angles between 139 and 142° (Table 35). Figure 73 is a typical illustration of these hydrogen bonds.

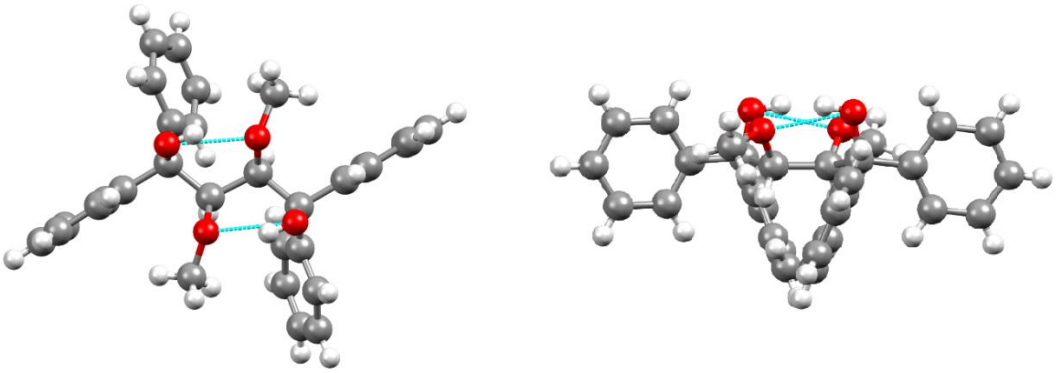

Figure 73: Two views of the host intramolecular hydrogen bonding, depicted with light-blue dashed lines.

Table 35: Classic intramolecular hydrogen bonding interactions in the DMT complexes with aniline and the toluidine guests.

Complex	Non-covalent interaction	Distance (Å) D–A	Angle (°) D-H···A
2DMT•aniline	(host)O-H···O(host methoxy)	2.675(2)	140
	(host)O-H···O(host methoxy)	2.627(2)	140
2DMT•*p*-TD	(host)O-H···O(host methoxy)	2.680(2)	140
	(host)O-H···O(host methoxy)	2.637(2)	141
2DMT•*m*-TD	(host)O-H···O(host methoxy)	2.679(2)	139
	(host)O-H···O(host methoxy)	2.629(2)	142
2DMT•*o*-TD	(host)O-H···O(host methoxy)	2.674(2)	139
	(host)O-H···O(host methoxy)	2.631(2)	141

Numerous non-classic intramolecular hydrogen bonding interactions are also present within the host structure of each complex. These typically occur between an *ortho*-aromatic hydrogen and a methoxy oxygen. These interactions range between 2.650(3) and 2.766(3) Å (100–102°). Furthermore, each complex exhibits intermolecular non-classic hydrogen bonds between a host *meta*- or *para*- aromatic hydrogen and a host methoxy or hydroxy oxygen atom of another molecule [3.277(3)–3.522(3) Å and 165–172°]. The 2DMT•*m*-TD and 2DMT•*o*-TD complexes have only one such interaction each. In addition, the 2DMT•*o*-TD complex also experiences an interaction between a host *para*-aromatic hydrogen and a guest amine nitrogen atom [3.466(6) Å, 177°]. Figure 74 shows representative examples of the intermolecular non-classic hydrogen bonding in these complexes, while Table 36 lists these interactions in detail.

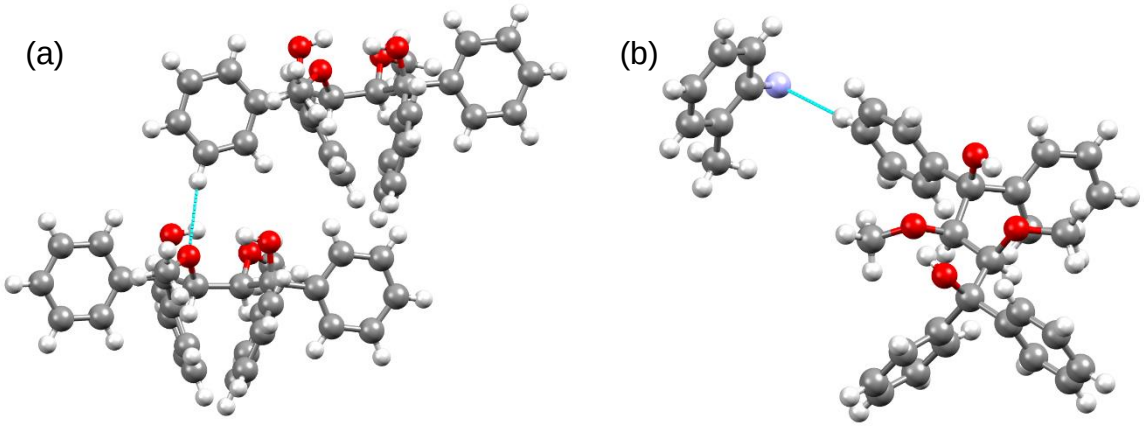

Figure 74: Intermolecular non-classic hydrogen bonding interactions depicted as blue dashes; a) a (host)*m*-ArH···O(host methoxy) interaction occurring in the 2DMT•*p*-TD complex, and b) a (host)*p*-ArH···N(guest amine) interaction occurring in the 2DMT•*o*-TD complex.

Table 36: Non-classic inter- and intra- molecular hydrogen bonding interactions in the DMT complexes with aniline and the toluidine guests.

Complex	Non-covalent interaction	Distance (Å) D–A	Angle (°) D-H···A
2DMT•aniline	(host)*o*-ArH···O(host hydroxy)	2.650(3)	102
	(host)*o*-ArH···O(host hydroxy)	2.756(3)	100
	(host)*o*-ArH···O(host hydroxy)	2.766(3)	100
	(host)*p*-ArH···O(host hydroxy)	2.653(3)	101
	(host)*m*-ArH···O(host methoxy)[a]	3.522(3)	167
	(host)p-ArH···O(host hydroxy)[b]	3.293(4)	168
2DMT•*p*-TD	(host)*o*-ArH···O(host hydroxy)	2.655(2)	102
	(host)*o*-ArH···O(host hydroxy)	2.756(3)	100
	(host)*o*-ArH···O(host hydroxy)	2.762(3)	100
	(host)*o*-ArH···O(host hydroxy)	2.654(3)	101
	(host)*m*-ArH···O(host methoxy)[a]	3.487(3)	166
	(host)*p*-ArH···O(host hydroxy)[b]	3.277(3)	165
2DMT•*m*-TD	(host)*o*-ArH···O(host hydroxy)	2.661(2)	102
	(host)*o*-ArH···O(host hydroxy)	2.762(2)	100
	(host)*o*-ArH···O(host hydroxy)	2.656(2)	101
	(host)*p*-ArH···O(host hydroxy)[b]	3.309(3)	169
2DMT•*o*-TD	(host)*o*-ArH···O(host hydroxy)	2.656(2)	102
	(host)*o*-ArH···O(host hydroxy)	2.757(2)	100
	(host)*o*-ArH···O(host hydroxy)	2.647(2)	102
	(host)p-ArH···N(guest amine)[c]	3.466(6)	177
	(host)*p*-ArH···O(host hydroxy) [b]	3.328(3)	172

Symmetry operators: a) 3/2–x,–1/2+y,1–z; b) –1/2+x,–1/2+y,z; c) x,y,1+z

π–π and CH–π Interactions

A number of inter- and intra- molecular π–π stacking interactions are present throughout these host-guest complexes with aniline and the toluidine guests. These interactions are all relatively weak, and span over a distance of 4.743(2)–5.974(2) Å. Each host molecule has two intramolecular stacking interactions of this type between two phenyl rings connected to the same carbon on the butane backbone [4.748(2)–4.857(2) Å], while intermolecular host–host interactions range between 4.748(2) and 5.939(2) Å. A comparable number of host–guest π–π stacking interactions exist in each complex with lengths of 5.033(3)–5.974(2) Å.

Furthermore, CH–π interactions are consistently present in these complexes, both intramolecular between phenyl rings of a host molecule and methoxy hydrogen atoms of the same host (2.82–2.95 Å, 145–150°), as well as intermolecular between a phenyl ring of one host and a *meta*-aromatic hydrogen of another host (2.97–2.99 Å, 169–170°). It is interesting to note that the 2DMT•*m*-TD complex lacks this intermolecular interaction type. Figure 75 shows some of these interactions for a better understanding, while Table 37 lists the CH–π interactions in more detail.

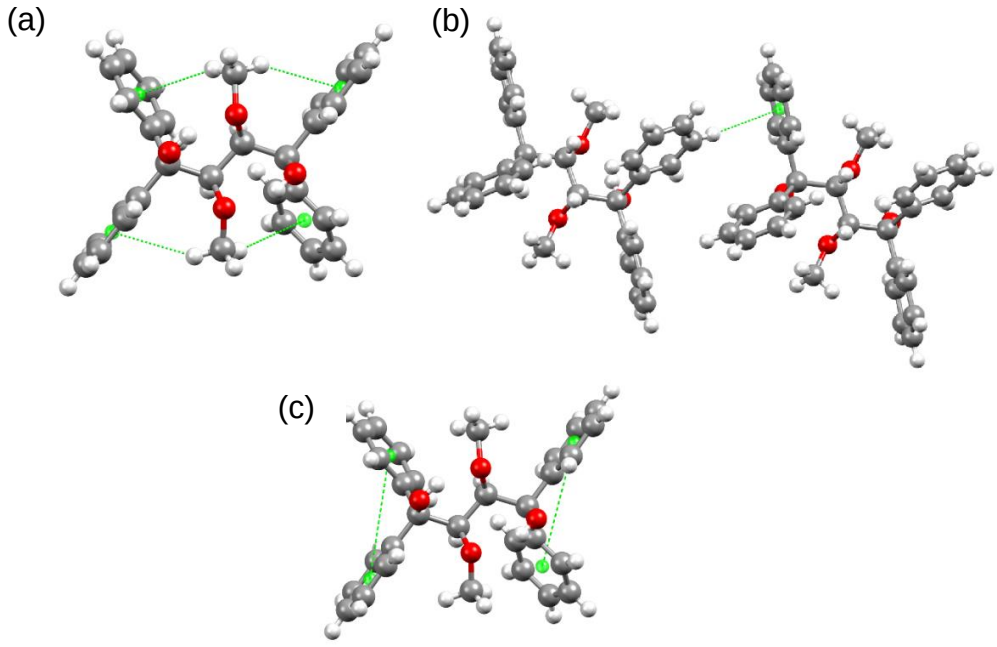

Figure 75: Representative CH–π and π–π interactions shown as green dashed lines for a) host–host intramolecular CH–π interactions, b) a host–host intermolecular CH–π interaction and c) a host–host intramolecular π–π stacking interaction.

Table 37: CH–π stabilizing interactions in the host-guest complexes of DMT with aniline and the toluidine guests.

Complex	Non-covalent interaction	Distance (Å)	Angle (°)	Symmetry operator
2DMT•aniline	(host methoxy)C-H···Cg(host)	2.92	148	x,y,z
	(host methoxy)C-H···Cg(host)	2.85	146	x,y,z
	(host methoxy)C-H···Cg(host)	2.84	149	x,y,z
	(host methoxy)C-H···Cg(host)	2.83	145	x,y,z
	(host)*m*-ArH···Cg(host)	2.99	169	1–x, y, 1–z
2DMT•*p*-TD	(host methoxy)C-H···Cg(host)	2.95	150	x,y,z
	(host methoxy)C-H···Cg(host)	2.86	147	x,y,z
	(host methoxy)C-H···Cg(host)	2.87	148	x,y,z
	(host methoxy)C-H···Cg(host)	2.76	145	x,y,z
	(host)*m*-ArH···Cg(host)	2.97	170	1–x, y, 1–z
2DMT•*m*-TD	(host methoxy)C-H···Cg(host)	2.92	147	x,y,z
	(host methoxy)C-H···Cg(host)	2.84	146	x,y,z
	(host methoxy)C-H···Cg(host)	2.82	150	x,y,z
	(host methoxy)C-H···Cg(host)	2.85	144	x,y,z
2DMT•*o*-TD	(host methoxy)C-H···Cg(host)	2.90	148	x,y,z
	(host methoxy)C-H···Cg(host)	2.85	147	x,y,z
	(host methoxy)C-H···Cg(host)	2.84	148	x,y,z
	(host methoxy)C-H···Cg(host)	2.84	146	x,y,z
	(host)*m*-ArH···Cg(host)	2.97	170	1–x, y, 1–z

Short Contacts

Many other contacts shorter than the van der Waals radii of the participating atoms may be observed within these complexes. These are intermolecular in nature, comprising both host–guest and host–host interactions and range between 2.27 and 2.89 Å (104–177°). The shortest interaction occurs between two host molecules in the 2DMT•*o*-TD complex [(host hydroxy)O-H···*p*-ArH(host), 2.27 Å, 107°]. This complex also has the shortest host–guest interaction [(host)*p*-ArH···N-C(guest amine), 2.52 Å, 177°]. Table 38 lists these contacts in detail, while Figure 76 displays two of these interaction types.

Table 38: Summary of the various contacts shorter than the van der Waals radii in the DMT complexes with aniline and the toluidine isomers.

Complex	Non-covalent interaction	Distance (Å)	Angle (°)	Symmetry operator
2DMT•aniline	(host hydroxy)O-H···*p*-ArH(host)	2.32	104	–1/2+x,1/2+y,z
	(host hydroxy)O-H···*p*-ArH(host)	2.28	148	–1/2+x,–1/2+y,z
	(host)*p*-ArH··· *m*-ArC(host)	2.86	146	1–x,y,–z
	(host)*p*-ArH···*o*-ArC(guest)	2.86	148	1/2+x,1/2+y,1+z
2DMT•*p*-TD	(host hydroxy)O-H···*p*-ArH(host)	2.28	106	–1/2+x,1/2+y,z
	(host hydroxy)O-H···*p*-ArH(host)	2.31	145	1/2+x,1/2+y,z
	(host)*p*-ArH···*m*-ArC(host)	2.86	144	1–x,y,–z
	(host)*p*-ArH···*o*-ArC(guest)	2.89	144	1/2+x,1/2+y,z
2DMT•*m*-TD	(host hydroxy)O-H···*p*-ArH(host)	2.31	106	–1/2+x,1/2+y,z
	(host hydroxy)O-H···*p*-ArH(host)	2.34	149	1/2+x,1/2+y,z
	(host)*p*-ArH···*m*-ArC(host)	2.88	143	1–x,y,–z
	(host)*o*-ArC···*p*-ArH(guest)	2.88	156	x,y,z
2DMT•*o*-TD	(host hydroxy)O-H···*p*-ArH(host)	2.27	107	–1/2+x,1/2+y,z
	(host hydroxy)O-H···*p*-ArH(host)	2.30	152	1/2+x,1/2+y,z
	(host)*p*-ArH···*m*-ArC(host)	2.84	149	1–x,y,–z
	(host)*p*-ArH···N-C(guest amine)	2.52	177	x,y,1+z

(a) (b)

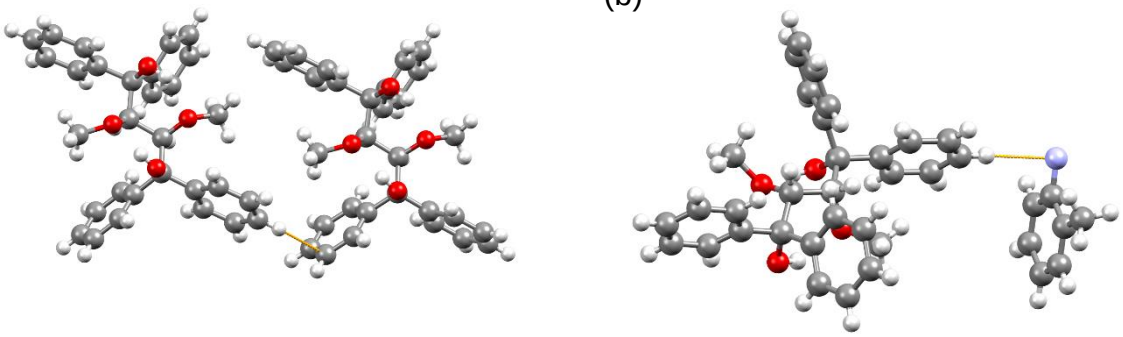

Figure 76: Short contacts in a) the 2DMT•*m*-TD complex [(host)*p*-ArH···*m*-ArC(host)] and b) 2DMT•*o*-TD complex [(host)*p*-ArH···N-C(guest amine)].

The host–guest interactions obtained from all the X-ray diffraction experiments for each complex is summarised in Table 39 for ease of comparison, and thus to facilely extract from it any meaningful interactions that may further the explanation for the selectivity order of DMT observed for these guests. From this table, it is clear that host-guest interactions are evenly distributed in these complexes with aniline and the toluidine isomers. Each experience eight π–π stacking interactions of comparable strength, and no CH–π stabilizing interactions. All four also experience a single host–guest short contact less than the van der Waals radii of the participating atoms. The short contact in the 2DMT•*o*-TD complex is much shorter than in the other complexes and involves the guest nitrogen. In summary then, a comparison of these host–guest interactions unfortunately does not explain DMT's selectivity order for these guests.

The mode of packing in all these complexes were also investigated and, in each case, guests were accommodated in discrete cavities (Figure 77).

Table 39: Significant host–guest interactions for the complexes of DMT with aniline and the isomeric toluidine guests.

Interaction	2DMT•aniline	2DMT•*p*-TD	2DMT•*m*-TD	2DMT•*o*-TD
π–π	5.33(4)–5.834(4) Å (8 contacts)	5.316(2)–5.862(2) Å (8 contacts)	5.033(3)–5.971(2) Å (8 contacts)	5.359(4)–5.891(4) Å (8 contacts)
CH–π	None	None	None	None
Short contacts	2.86 Å, 148°, < (host)*p*-ArH···*o*-ArC(guest)	2.89 Å, 144°, < (host)*p*-ArH···o-ArC(guest)	2.88 Å, 156°, < (host)*o*-ArC···*p*-ArH(guest)	2.52 Å, 177°, << (host)*p*-ArH···N-C(guest amine)

*< denotes contacts less than the sum of the van der Waals radii and << denotes contacts less than this sum minus 0.2 Å.

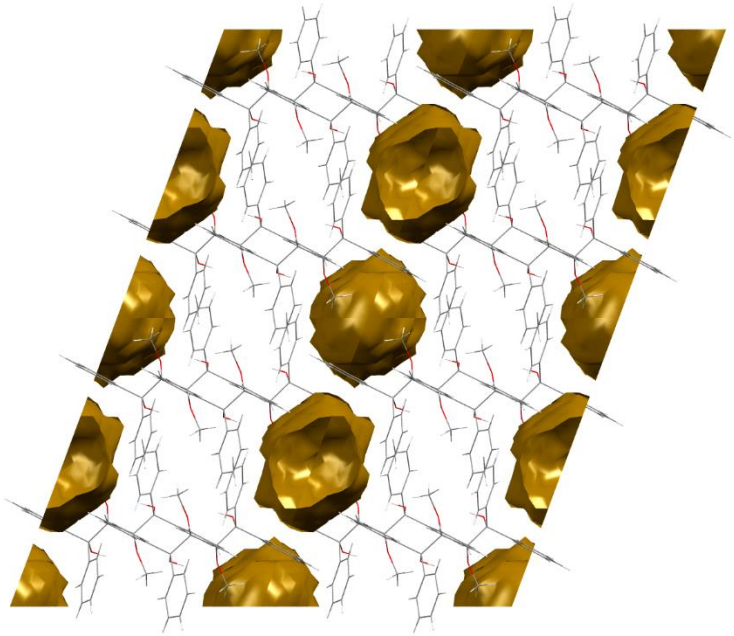

Figure 77: The discrete cavity guest packing mode in the 2DMT•*p*-TD complex as a representative example of the guest packing in all the complexes with the toluidines and aniline.

5.6 Hirshfeld Surface Analysis

Hirshfeld surface analysis was, once more, used to visualize and interpret the quantity of contacts in these complexes between host and guest. Figure 78a shows the fingerprint plot obtained for the 2DMT•*p*-TD complex. Wing W1 is indicative of C···H interactions, while W2 and W3 represent H···H interactions. Similar features are present in the 2DMT•*m*-TD and 2DMT•*o*-TD complexes (Figure 78b and Figure 78c), where the features denoted as W1 or W2 are indicative of H···H interactions. However, in the latter two complexes, the C···H interactions are now visualized as spikes (S1). Figure 79 quantifies the types of interactions in each complex in a graphic manner. In all four complexes, H···H and C···H interactions dominate whereas C···N and O···H interactions are negligible. The percentage H···H interactions decrease in the order *p*-TD (70.9%) > *o*-TD (68.3%) > *m*-TD (58.7%) > aniline (50.4%) which

correlates exactly with the selectivity order observed for DMT towards these guests. Furthermore, the opposite trend is observed when considering the percentage H···N interactions. The most preferred guest exhibits the lowest amount of this interaction type (*p*-TD, 0.5%), which sequentially increases up to the least preferred guest (aniline, 19.5%).

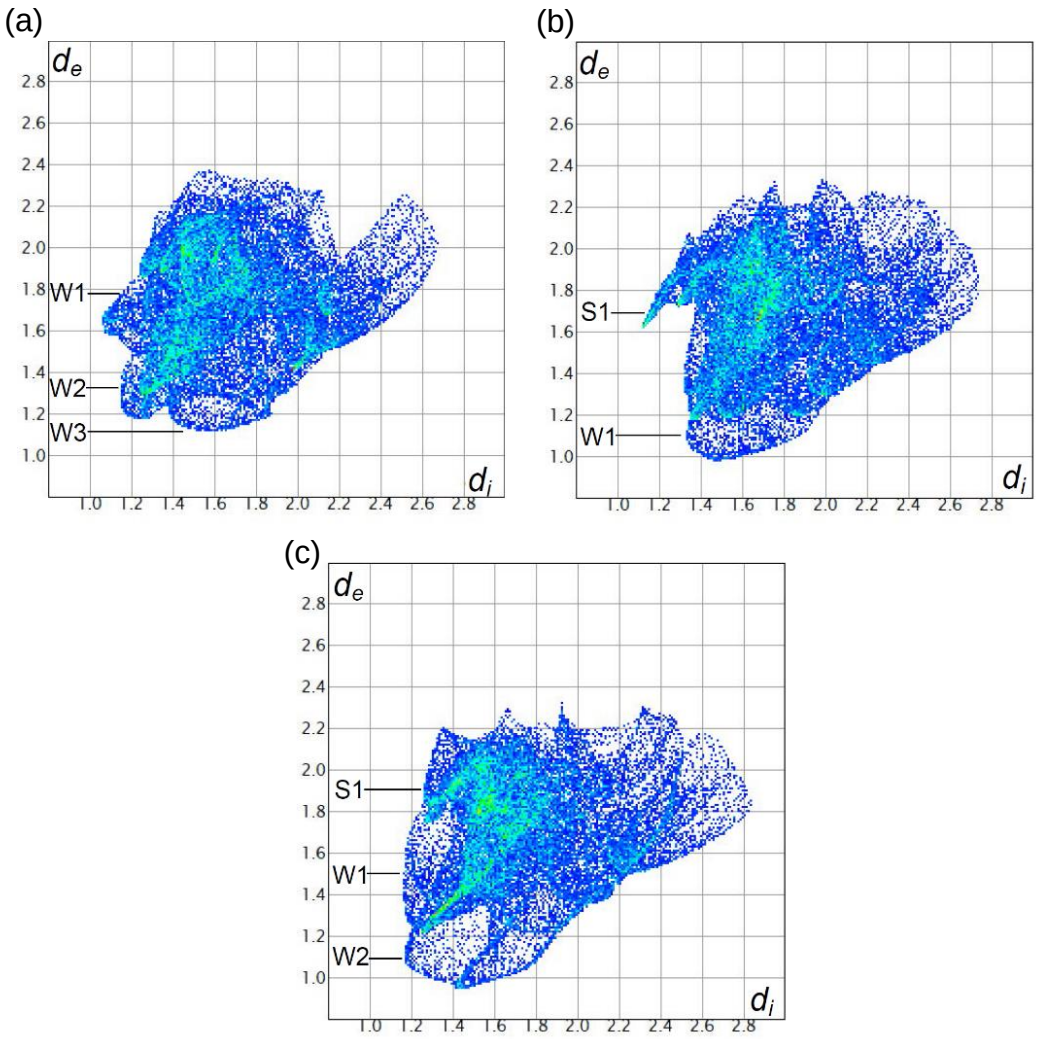

Figure 78: Two-dimensional fingerprint plots obtained from Hirshfeld surfaces for the inclusion complexes of a) 2DMT•*p*-TD; b) 2DMT•*m*-TD and c) 2DMT•*o*-TD.

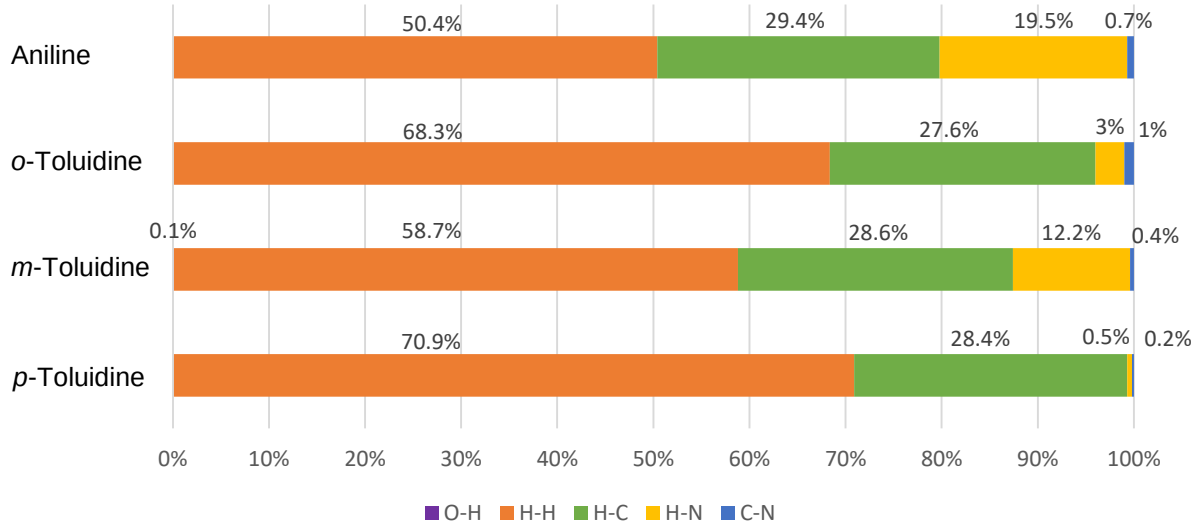

Figure 79: Graphical display showing the percentage and type of intermolecular interactions in each complex.

5.7 Conclusion

DMT was found to be a successful host for the inclusion of the toluidine isomers, having formed 2:1 host:guest complexes with each. Competition experiments were performed which showed that DMT has a near-equal preference for *p*-TD and *o*-TD, whereas it discriminated against *m*-TD, and more so against unsubstituted aniline. Thermal analyses confirmed this selectivity order as demonstrated by ever-increasing T_{end} and T_p values with increasing DMT selectivity. Single crystal X-ray analysis did not reveal any specific host–guest interactions which would provide reasons for DMT's selectivity order for these guests since all of these interactions were evenly distributed throughout each complex and usually with comparable strength. Hirshfeld surface analysis, however, indicated a correlation between the relative amount of H···H interactions between host and guest and the selectivity order shown by the host: the higher the percentage H···H interactions, the more preferred the guest was.

Chapter 6: Inclusion Compounds of DMT (73) with Toluene, Ethylbenzene and Cumene

6.1 Introduction

The aromatic compounds toluene, ethylbenzene (EB) and cumene represent a series of potential guest molecules with increasing molecular weight and varying molecular shapes. Toluene, or methylbenzene, is a common solvent which finds application in paints and fullerene chemistry, whilst EB finds use in the production of styrene, amongst many others.[174–177] Cumene, or isopropylbenzene, may be converted to cumene hydroperoxide which is used in the production of acetone and phenol, or as an oxidizing agent.[178,179] We reported earlier (Chapter 3) that DMT showed selective behaviour when recrystallized from mixtures containing aniline, *N*-methylaniline (NMA) and *N,N*-dimethylaniline (DMA). In that work, the host selectivity was in the order aniline << NMA < DMA. This result was initially surprising especially considering that the H-bond donating ability of these guests also decreases in the same order. However, upon closer inspection of the host–guest interactions, it was revealed that none of these guests behave as H-bond donors in the solid-state complexes, and other interactions were responsible for their enclathration. Toluene, EB and cumene have molecular shapes that broadly approximate that of aniline, NMA and DMT respectively, although subtle shape differences between these groups exist. The molecular geometry of the methylene carbon of toluene, EB and cumene is tetrahedral. On the other hand, the geometry of the nitrogen atom of aniline, NMA and DMA approximates to pyramidal as the resonance interaction between the aromatic ring and the nitrogen lone pair of electrons contribute to flattening of the nitrogen.[180] We thus decided to compare DMT's selectivity for toluene, EB and cumene with that demonstrated in the presence of the anilines in an effort to establish whether molecular shape plays a significant role in the selectivity of the host.

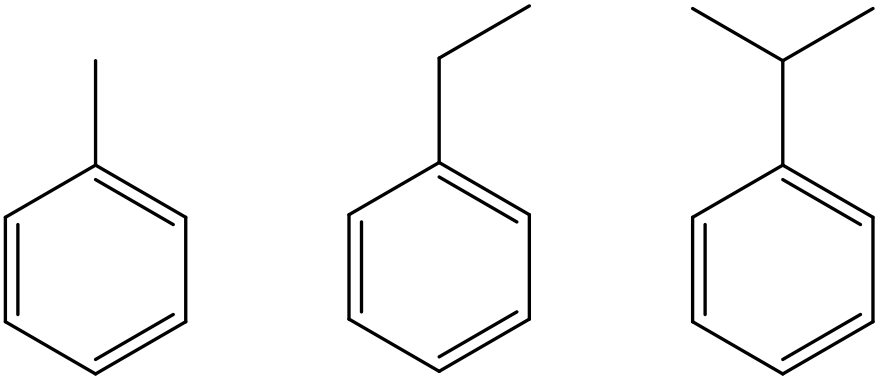

Toluene Ethylbenzene Cumene

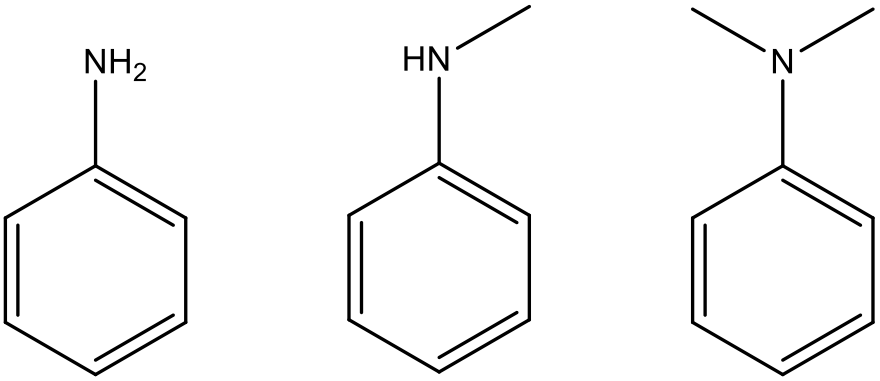

Aniline NMA DMA

6.2 Individual and Equimolar Inclusion Experiments

^{1}H-NMR spectra obtained for the inclusion complexes of DMT with toluene and cumene showed that, as with EB, 2:1 host:guest complexes were formed in each case (Table 40).

Table 40: Host:guest ratios of complexes formed during individual recrystallization experiments.

Guest	Host:guest*
Toluene	2:1
Ethylbenzene	2:1
Cumene	2:1

*Determined using ^{1}H-NMR spectroscopy with $CDCl_3$ as solvent.

A series of four equimolar binary and one equimolar ternary competition experiments were carried out in which DMT was recrystallized from combinations of toluene, EB and cumene. The crystals produced in these experiments were analysed using proton NMR spectroscopy and GC-MS analysis. The proportion of each guest included and the overall host:guest ratio are presented in Table 41. In an experiment between toluene and EB, toluene was only slightly more preferred, as 51.2% of this guest was included by the host. When toluene and cumene competed, toluene was again preferred (66.6%), and when the host was recrystallized from EB/cumene, EB was preferentially selected (63.1%). From these binary equimolar competition experiments, a selectivity order of toluene > EB > cumene may be inferred. However, in an equimolar ternary competition experiment, EB was found to be the more preferred component (39.3%), followed by toluene (34.7%) and cumene (26.0%).

Table 41: Competition experiments and H:G ratios obtained.*

Toluene	Ethylbenzene	Cumene	Guest ratios (% Standard deviation)[$]	Overall H:G ratio
X	X		***51.2***:48.8 (0.4)	2:1
X		X	***66.6***:33.4 (0.9)	2:1
	X	X	***63.1***:36.9 (1.0)	2:1
X	***X***	X	34.7:***39.3***:26.0 (0.4)(0.1)(1.0)	2:1

*Determined using GC-MS; [$]experiments were carried out in triplicate; an average value is provided here with % estimated standard deviation in parentheses.

These selectivity results differ from those with the anilines when considering molecular shape and therefore, perhaps, molecular shape is not an important consideration in the selective behaviour of the host, or perhaps the subtle changes in molecular shape, when comparing toluene with aniline, EB with NMA, and cumene with DMA, affect the selectivity of the host.

6.3 Host Selectivity Profiles with Changing Guest Concentrations in Binary and Ternary Guest Mixtures

In order to determine whether DMT maintained its selective behaviour towards these substituted benzene guests at different molar concentrations, this host was recrystallized from binary mixtures containing different molar amounts of toluene, EB and cumene. This allowed for the construction of selectivity curves representative of the three combinations of guests.

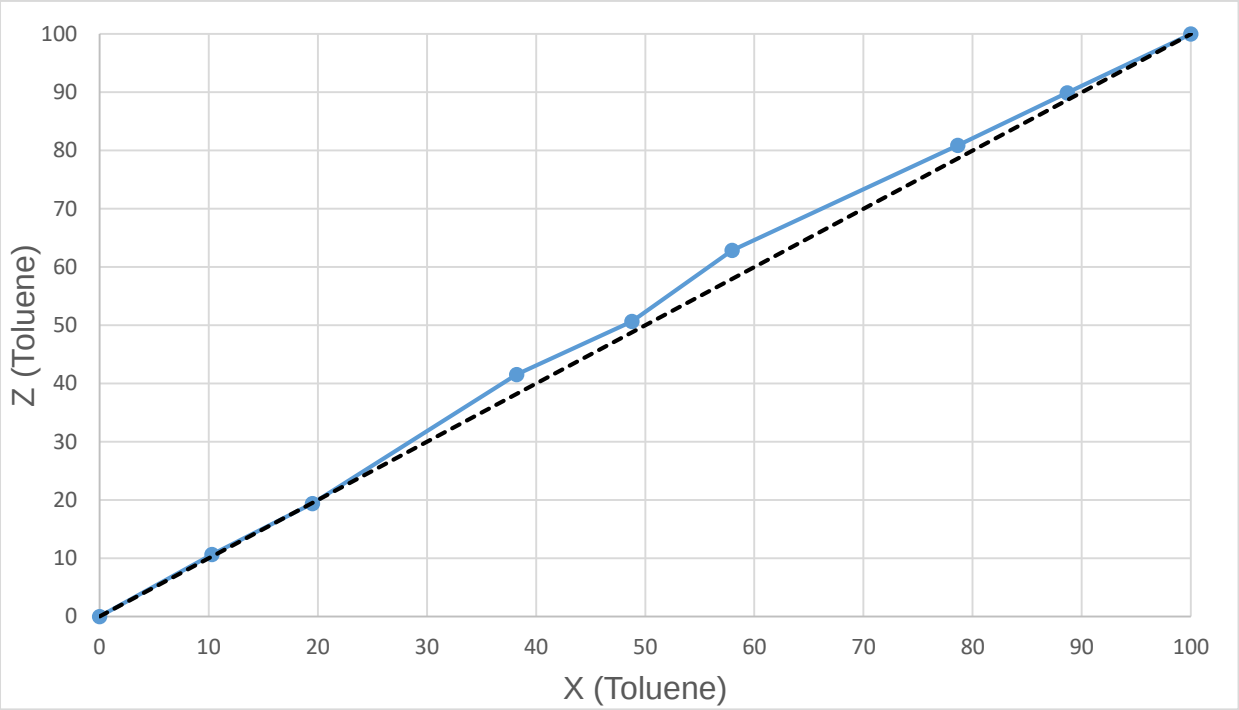

Figure 80: Selectivity curve of toluene *vs* EB. Coloured blue is the molar fraction of toluene in the inclusion complex (Z) *vs* the molar fraction of toluene in the mother liquor (X). Black dashes indicate the theoretical line of no selectivity.

Figure 80 indicates the selectivity curve for toluene *vs* EB, from which it can easily be seen that DMT shows very little selectivity between these two guests. At low concentrations of toluene, DMT has no selectivity towards either guest as represented by the fact that experimental data points are located on the theoretical line of no

selectivity. A slight increase in selectivity towards toluene is demonstrated by a point corresponding to ~38% of this guest in the mother liquor. Crystals obtained from this experiment were found to contain ~41.5% toluene. An experiment showing a relatively high selectivity towards toluene was obtained at a mother liquor concentration of ~58%, which produced an inclusion complex containing ~63% of this guest. The average selectivity coefficient, K, for toluene in this experiment was determined to be 1.11, which is very close to unity.

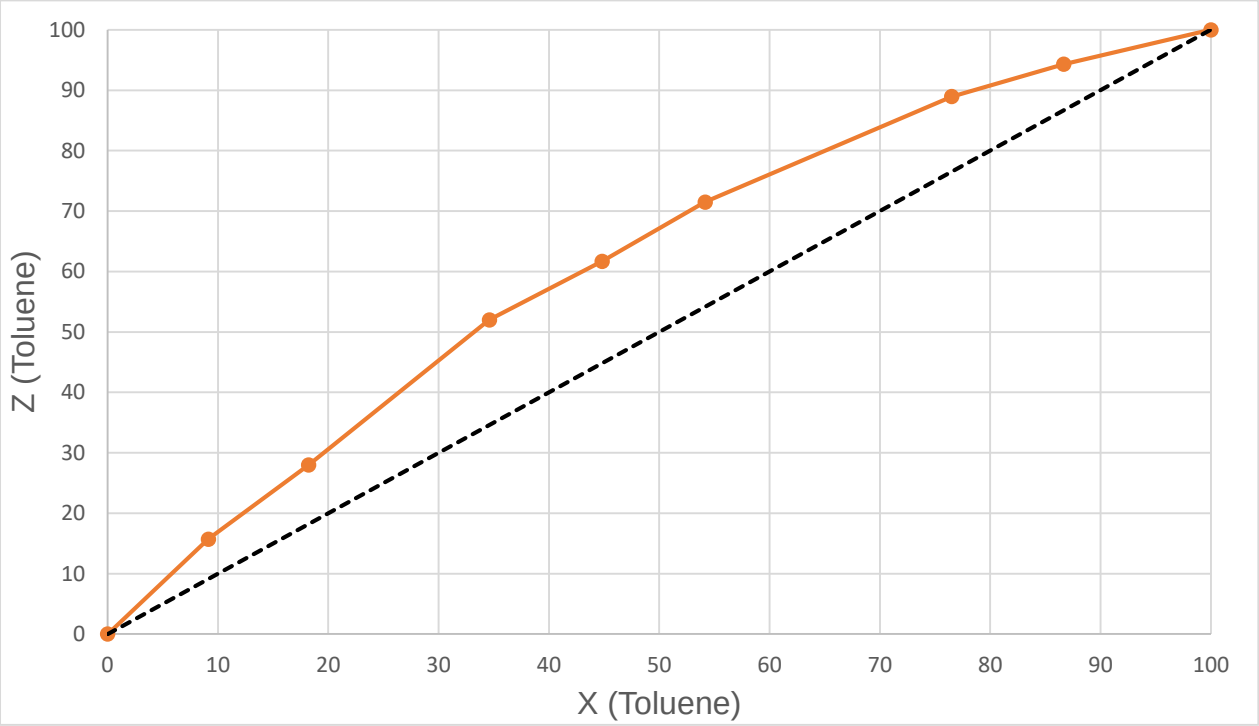

Figure 81: Selectivity curve of toluene *vs* cumene. Coloured orange is the molar fraction of toluene in the inclusion complex (Z) *vs* the molar fraction of toluene in the mother liquor (X). Black dashes indicate the theoretical line of no selectivity.

Unlike the experiment between toluene and EB, Figure 81 indicates a marked increase in selectivity by DMT in favour of toluene over cumene. A toluene concentration of ~18% in the mother liquor produced a solid containing ~28% toluene, while crystals containing approximately 89% toluene were recovered when DMT was recrystallized from a mother liquor containing ~76.5% of this guest. The selectivity coefficient for

this experiment was determined to be 2.11, substantially higher than for the toluene/EB curve (1.11), as expected.

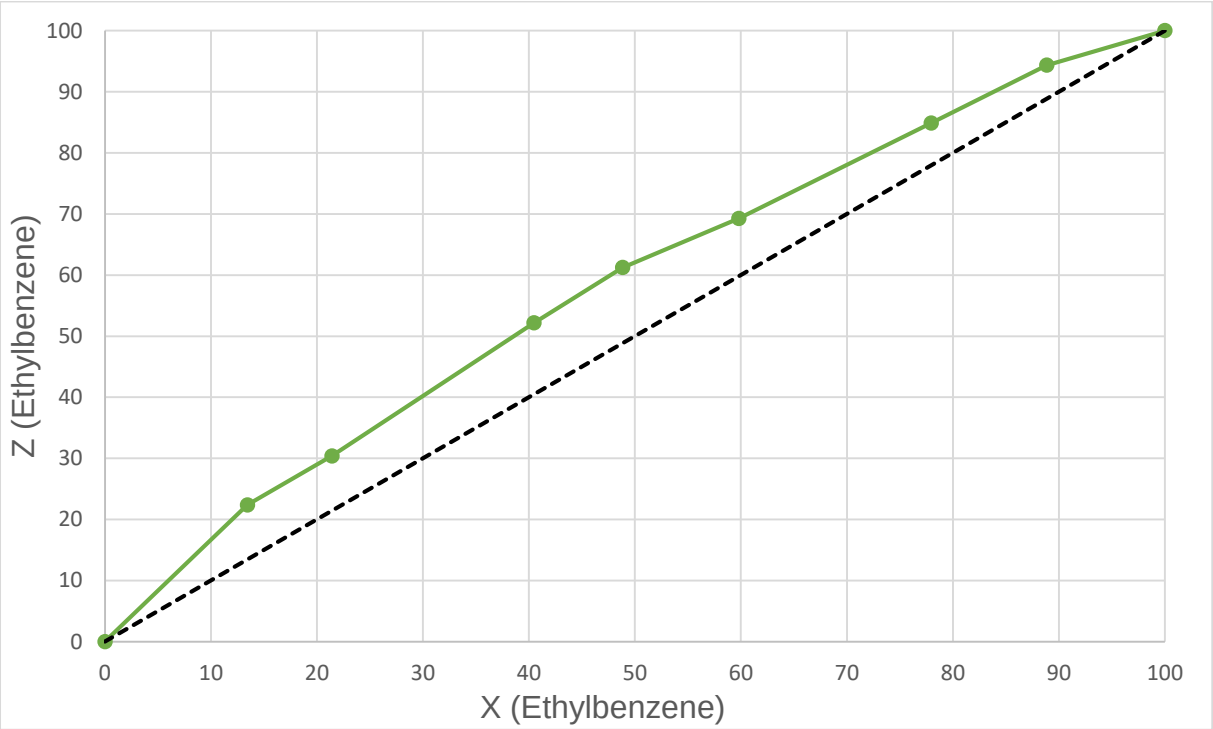

Figure 82: Selectivity curve of EB *vs* cumene. Coloured green is the molar fraction of EB in the inclusion complex (Z) *vs* the molar fraction of EB in the mother liquor (X). Black dashes indicate the theoretical line of no selectivity.

Cumene was discriminated against when in the presence of EB (Figure 82), in a similar fashion as when in the presence of toluene. An initial mother liquor concentration of approximately 13% EB produced an inclusion complex containing ~22% EB, while at higher EB concentrations, a mother liquor concentration of ~78% resulted in crystals containing ~85% EB. The selectivity coefficient for this experiment was intermediate between the preceding two experiments (K = 1.70). A comparison of the three selectivity coefficients generated from these experiments therefore confirm the selectivity order determined from equimolar binary competition experiments, namely, toluene > EB > cumene.

DMT was subsequently recrystallized from mixtures containing all three substituted benzene guests in various ratios. The blue circles, representing mother liquor composition, was plotted against the inclusion complex composition (red squares) to generate the ternary plot in Figure 83. The general trend displayed in this plot was a consistent decrease in cumene composition while toluene and EB experienced an increase on average over all data points relative to the mother liquor. The average decrease over all data points for cumene was approximately 8.9%, and the largest decrease was experienced at point B (~11.2%). The average increase of EB over all the data points was slightly higher (~4.8%) than that for toluene (~4.1%), even though the host was selective for toluene in binary competition mixtures. Point A represents the experiment with the highest increase in toluene content (8.7%), while point E shows that for the largest EB increase (7.8%) relative to the mother liquor.

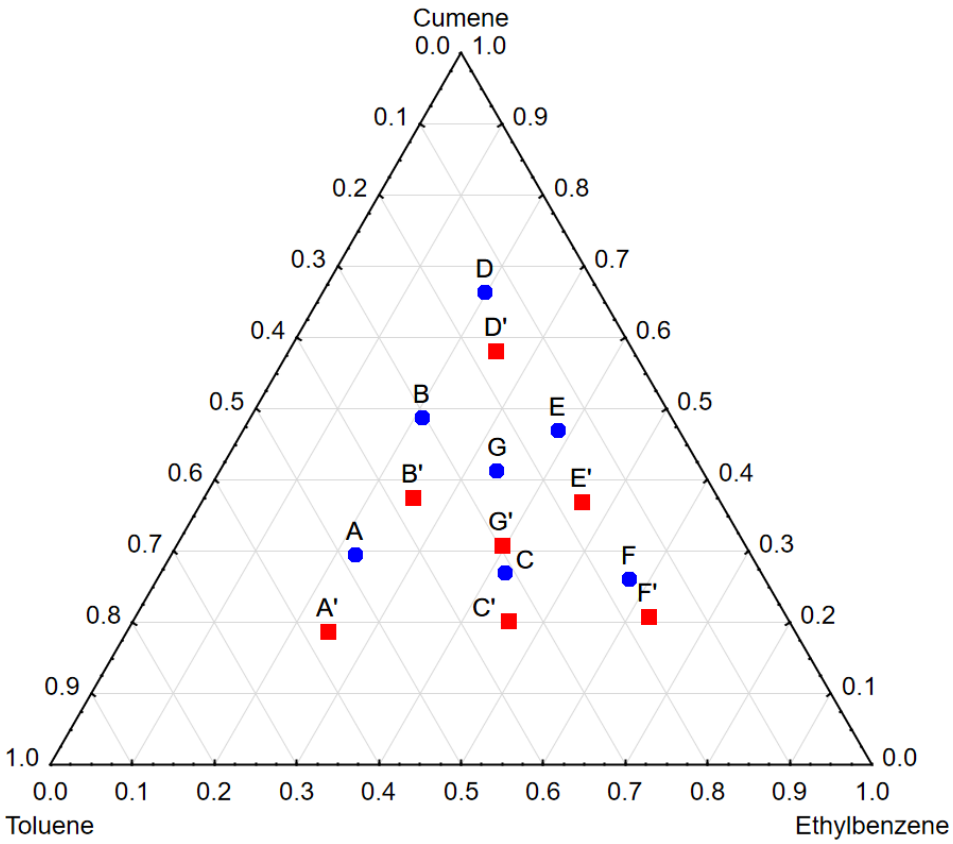

Figure 83: Ternary competition plot obtained when DMT was recrystallized from mixtures containing toluene, EB and cumene in varying amounts. Blue circles indicate mother liquor compositions and red squares guest compositions of complexes formed after crystallization.

6.4 Thermal Analysis

Thermal analyses were performed on the complexes of DMT with toluene and cumene, and compared with the thermal data obtained for the complex with EB (Section 4.4). Differential scanning calorimetry (DSC) and thermogravimetric analyses (TG) were conducted at a heating rate of 10 °C.min^{-1} under high purity nitrogen as a purge gas. Figure 84 and Figure 85 provide the TG, DTG and DSC traces obtained while Table 42 compares the temperatures of the significant thermal events occurring in each experiment.

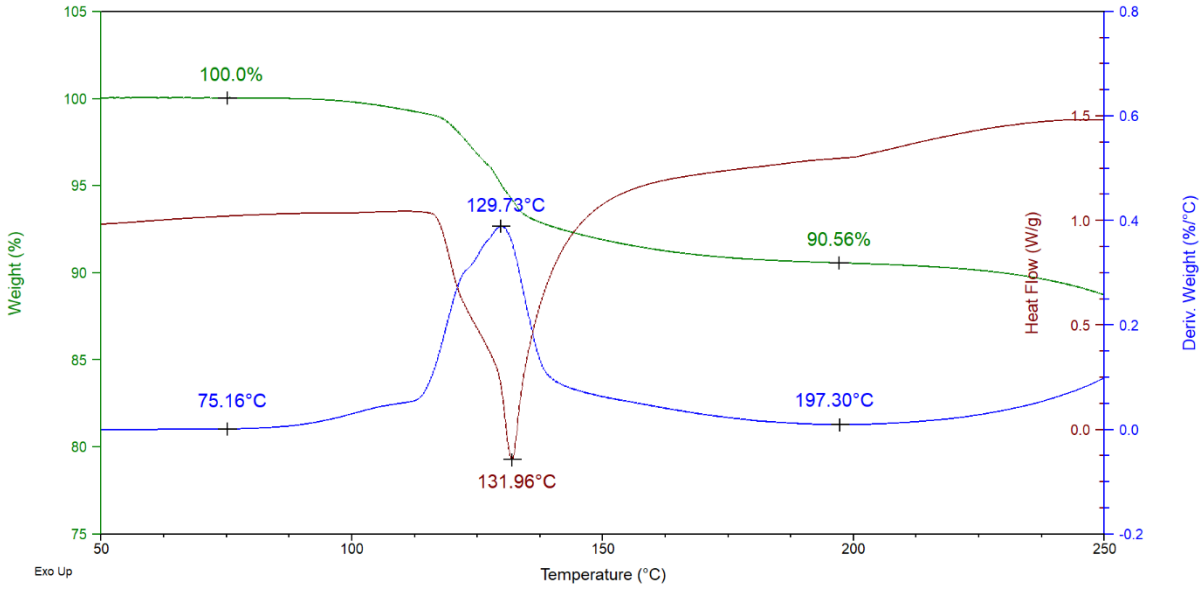

Figure 84: Overlaid TG (green), DTG (blue) and DSC (brown) traces for the 2DMT•toluene complex with heating at 10°.min^{-1}.

For the 2:1 DMT•toluene complex, the mass loss expected upon removal of the guest is 9.2%. A mass loss of 9.4% was obtained from the TG trace in Figure 84 (green), which is in excellent agreement with that expected. The onset temperature for the guest release process was at ~75.2 °C (DTG), and mass loss was determined to cease at approximately 197.3 °C, after which the mass decreased again due to decomposition of the host. A single unsymmetrical endotherm was observed which represents both the melting of the host and the guest release events, with a peak

endotherm temperature of ~132.0 °C (DSC). The maximum rate of guest release occurred at approximately 129.7 °C (DTG).

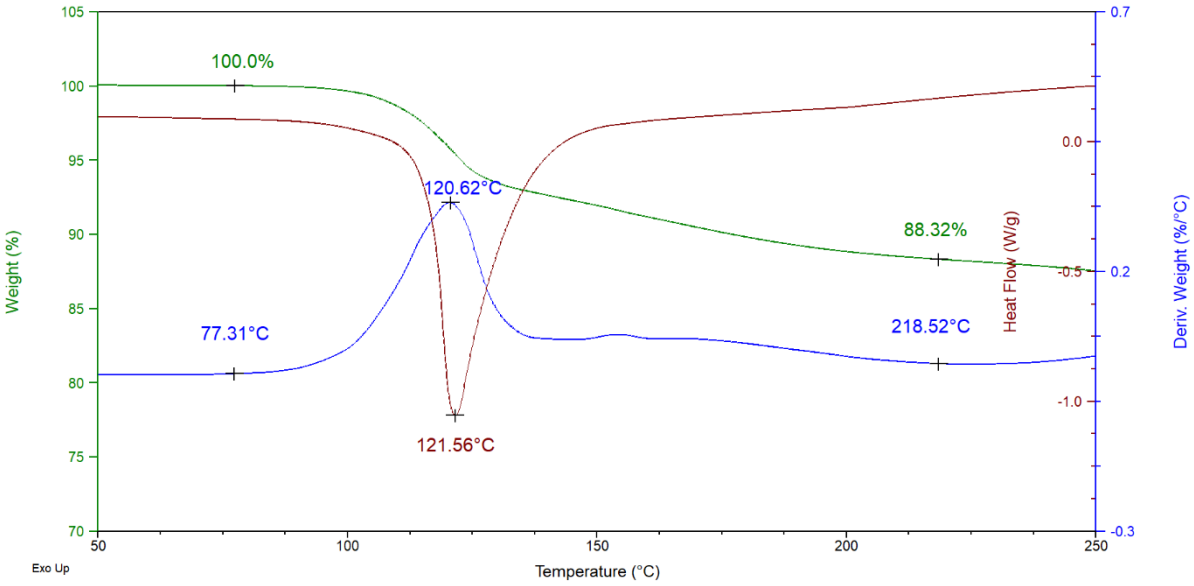

Figure 85: Overlaid TG (green), DTG (blue) and DSC (brown) traces for the 2DMT•cumene complex with heating at 10°.min^{-1}.

The mass loss percentage for the 2DMT•cumene complex was determined to be ~11.7% (TG, Figure 85) which is in excellent agreement with the expected amount (11.7%). The mass loss event due to guest loss commenced at approximately 77.3 °C and ceased at ~218.5 °C (DTG). The single endotherm, due to concomitant guest release and host melt, has a peak temperature of ~121.6 °C (DSC), while the maximum rate of guest release occurred at ~120.6 °C (DTG).

Table 42: Summary of the major thermal events for the complexes of DMT with the alkyl-substituted benzenes.

Guest	Guest boiling point, T_b (°C)	T_{on}[a] (°C)	$T_{on}-T_b$ (°C)	T_p[b] (°C)	T_{end}[c] (°C)	Mass loss % (Expected)
Toluene	110.6	75.2	–35.4	129.7	131.9	9.4 (9.2)
Ethylbenzene[d]	136.2	78.5	–57.7	123.8	127.3	10.8 (10.5)
Cumene	152.4	77.3	–75.1	120.6	121.6	11.7 (11.7)

[a]T_{on} is the onset temperature for guest release estimated from the DTG; [b]T_p values were determined from the blue DTG traces, and are the temperatures at which the mass loss rate is the highest; [c]T_{end} values were obtained from the brown DSC traces, and are the peak endotherm temperatures; [d]repeated from Chapter 4 for ease of comparison.

An evaluation of the thermal events presented in Table 42 indicates a correlation between the selectivity order of DMT towards the substituted aromatics in equimolar binary competition experiments described earlier and each of the three major thermal parameters evaluated. The peak mass loss temperature (T_p) correlates well with this selectivity order, that is, toluene (129.7 °C) > EB (127.3 °C) > cumene (121.6 °C). The peak endotherm temperatures (T_{end}) follow a similar trend [toluene (131.9 °C) > EB (127.3 °C) > cumene (121.6 °C)]. In addition, the evaluation of the term T_{on}–T_b[160,161] unambiguously yields the same result: an order of toluene (–35.4 °C) > EB (–57.7 °C) > cumene (–75.1 °C) was obtained. Thermal experiments, therefore, served as a good predictor of the overall selectivity that DMT displayed for these alkyl-substituted benzene guests in the equimolar binary competition experiments.

6.5 Single Crystal X-Ray Analysis

The complexes of DMT with toluene and cumene were subjected to single crystal X-ray diffraction in order to determine supporting reasons for the selectivity order displayed by DMT for the substituted benzene guests. Table 43 contains crystallographic data for these 2:1 complexes (the data for the 2DMT•EB complex were obtained from Chapter 4, and repeated here for ease of comparison).

Figure 86 shows the unit cells for the two new complexes. Both of these crystallized in the monoclinic *C*2 crystal system, and all three host frameworks are therefore isostructural (see Chapter 4 for these data for the EB complex). The guest in the complex with cumene is disordered around a special point. Figure 87 demonstrates the host-gust packing by means of a stereoview, using 2DMT•toluene as representative example.

Table 43: Crystallographic data for the complexes between DMT and the three substituted benzene guests.

	2DMT•toluene	**2DMT•EB**	**2DMT•cumene**
Chemical formula	$C_{30}H_{30}O_4$ •$0.5C_7H_8$	$C_{30}H_{30}O_4$ •$0.5C_8H_{10}$	$C_{30}H_{30}O_4$ •$0.5C_9H_{12}$
Formula weight	500.63	507.62	514.66
Crystal system	Monoclinic	Monoclinic	Monoclinic
Space group	*C*2	*C*2	*C*2
μ (Mo-Kα)/mm^{-1}	0.078	0.078	0.078
a/Å	17.3412(6)	17.2668(8)	17.1139(6)
b/Å	11.9827(4)	12.0342(6)	12.0772(5)
c/Å	14.0871(5)	14.1665(7)	14.3270(5)
alpha/°	90	90	90
beta/°	109.892(2)	109.019(2)	107.460(2)
gamma/°	90	90	90
V/$Å^3$	2752.57(17)	2783.0(2)	2824.79(18)
Z	2	4	2
F(000)	1068	1084	1100
Temp./K	200	200	200
Restraints	5	1	1
Nref	6037	6923	6398
Npar	326	371	380
R	0.0377	0.0412	0.0351
wR2	0.1008	0.1185	0.0899
S	1.03	1.04	1.03
θ min-max/°	2.1, 28.3	2.1, 28.4	2.1, 28.3
Tot. data	19477	29307	26304
Unique data	6037	6923	6398
Observed data [I > 2.0 sigma(I)]	5479	6283	5519
R_{int}	0.017	0.017	0.020
Dffrn measured fraction θ full	0.999	0.999	1.000

Min. resd. dens. (e/ Å^3)	–0.33	–0.31	–0.17
Max. resd. dens. (e/ Å^3)	0.31	0.42	0.20

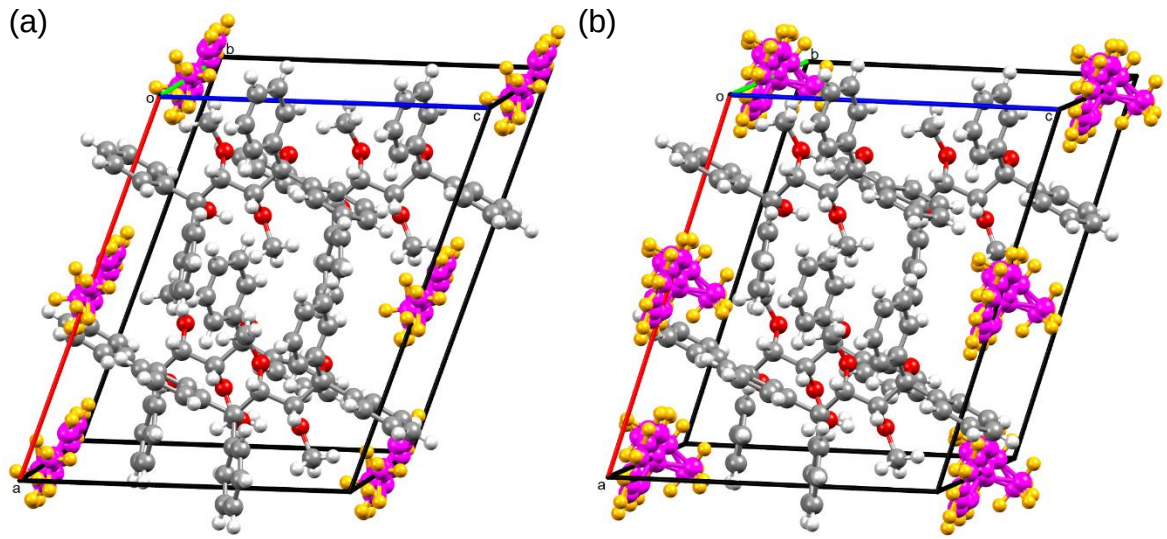

Figure 86: The unit cells for the DMT complexes with a) toluene and b) cumene. The guests have a magenta carbon framework, while the hosts have a grey carbon framework. Host frameworks are isostructural.

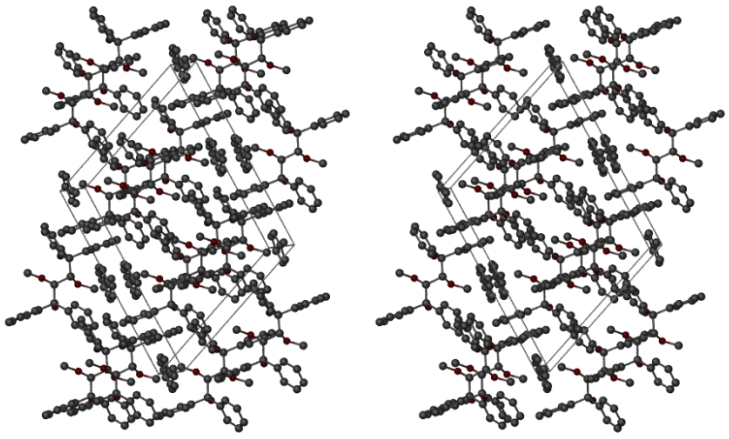

Figure 87: Stereoview of the 2DMT•toluene complex to show the packing in three dimensions, as representative sample.

Hydrogen bonding

Classic hydrogen bonding interactions are observed in these complexes. They present as 1,3- and 2,4- intramolecular interactions between hydroxy and methoxy moieties on the butane backbone. These interactions range between 2.627(2) and 2.673(2) Å, with angles of 139–140°. Figure 88 is a representation of these intramolecular hydrogen bonds in the 2DMT•toluene complex, and Table 44 lists these interactions in detail.

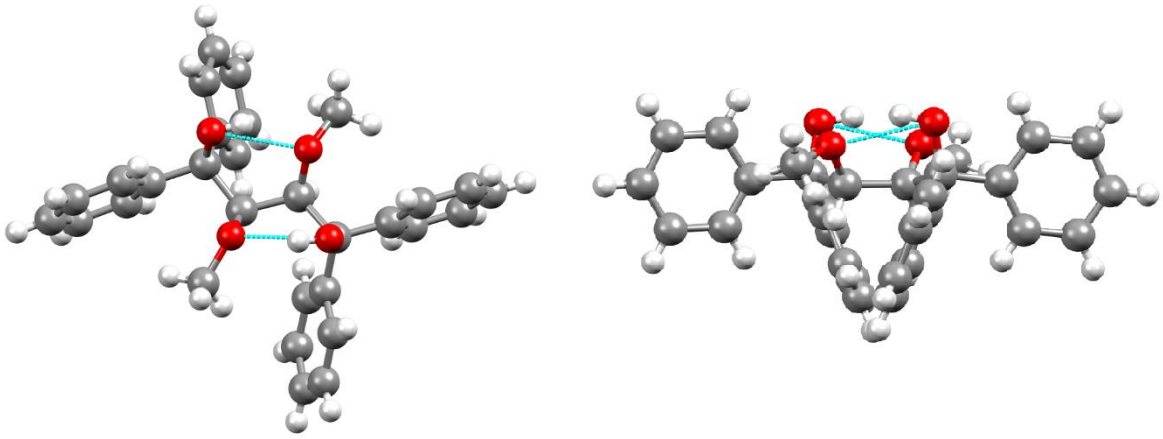

Figure 88: Two views of the host intramolecular hydrogen bonding, depicted with light-blue dashed lines.

Table 44: Classic intramolecular hydrogen bonding interactions in the DMT complexes with the substituted benzenes.

Complex	Non-covalent interaction	Distance (Å) D–A	Angle (°) D-H···A
2DMT•toluene	(host)O-H···O(host methoxy)	2.673(2)	140
	(host)O-H···O(host methoxy)	2.629(2)	140
2DMT•EB	(host)O-H···O(host methoxy)	2.672(2)	139
	(host)O-H···O(host methoxy)	2.627(2)	139
2DMT•cumene	(host)O-H···O(host methoxy)	2.671(2)	139
	(host)O-H···O(host methoxy)	2.646(2)	140

Non-classic hydrogen bond interactions are present both intra- and inter- molecularly. The majority of these interactions are intramolecular in nature between an *ortho*-aromatic hydrogen of the host and an hydroxy oxygen of the same molecule. These are all relatively weak [2.647(2)–2.759(2) Å, 100–103°]. Each complex also experiences one intermolecular host–host interaction involving a *para*-aromatic hydrogen and a host hydroxy atom [3.291–3.434 Å, 168–175 °]. Figure 89 depicts these intra- and inter- molecular interactions in the 2DMT•cumene complex, while Table 45 further lists all of these interactions.

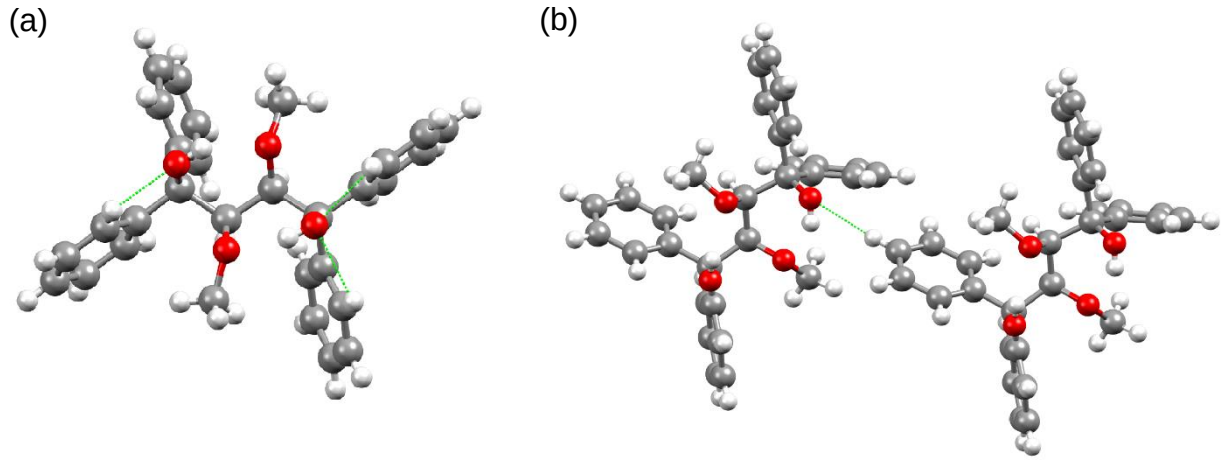

Figure 89: Non-classic hydrogen bonding interactions depicted by means of green dashed lines; a) an intramolecular interaction; b) an intermolecular interaction.

Table 45: Non-classic inter- and intra- molecular hydrogen bonding interactions in the DMT complexes with the substituted benzene guests.

Complex	Non-covalent interaction	Distance (Å) D–A	Angle (°) D-H···A
2DMT•toluene	(host)*o*-ArH···O(host hydroxy)	2.651(3)	102
	(host)*o*-ArH···O(host hydroxy)	2.759(3)	100
	(host)*o*-ArH···O(host hydroxy)	2.653(3)	101
	(host)*p*-ArH···O(host hydroxy)[a]	3.291(4)	168
2DMT•EB	(host)*o*-ArH···O(host hydroxy)	2.653(3)	102
	(host)*o*-ArH···O(host hydroxy)	2.752(3)	100
	(host)*o*-ArH···O(host hydroxy)	2.752(3)	100
	(host)*o*-ArH···O(host hydroxy)	2.650(3)	101
	(host)*p*-ArH···O(host hydroxy)[a]	3.333(4)	171
2DMT•cumene	(host)*o*-ArH···O(host hydroxy)	2.647(2)	103
	(host)*o*-ArH···O(host hydroxy)	2.747(2)	101
	(host)*o*-ArH···O(host hydroxy)	2.752(2)	100
	(host)*o*-ArH···O(host hydroxy)	2.650(2)	102
	(host)*p*-ArH···O(host hydroxy)[a]	3.434(3)	175

Symmetry operators: a) –1/2+x,–1/2+y,z

π–π and CH–π interactions

All three complexes display π–π stacking interactions that are weak in nature. Host–host intermolecular interactions range between 4.570(6) and 5.996(3) Å. The shortest host–guest π–π interactions of this type are found to be between 4.570(6) and 5.299(6) Å. Intramolecular stacking interactions between phenyl rings of the same host molecule occur in the range 4.788(1)–4.872(2) Å. Each complex has two of the latter interactions, and Figure 90 shows representative examples of these interactions in the 2DMT•cumene complex.

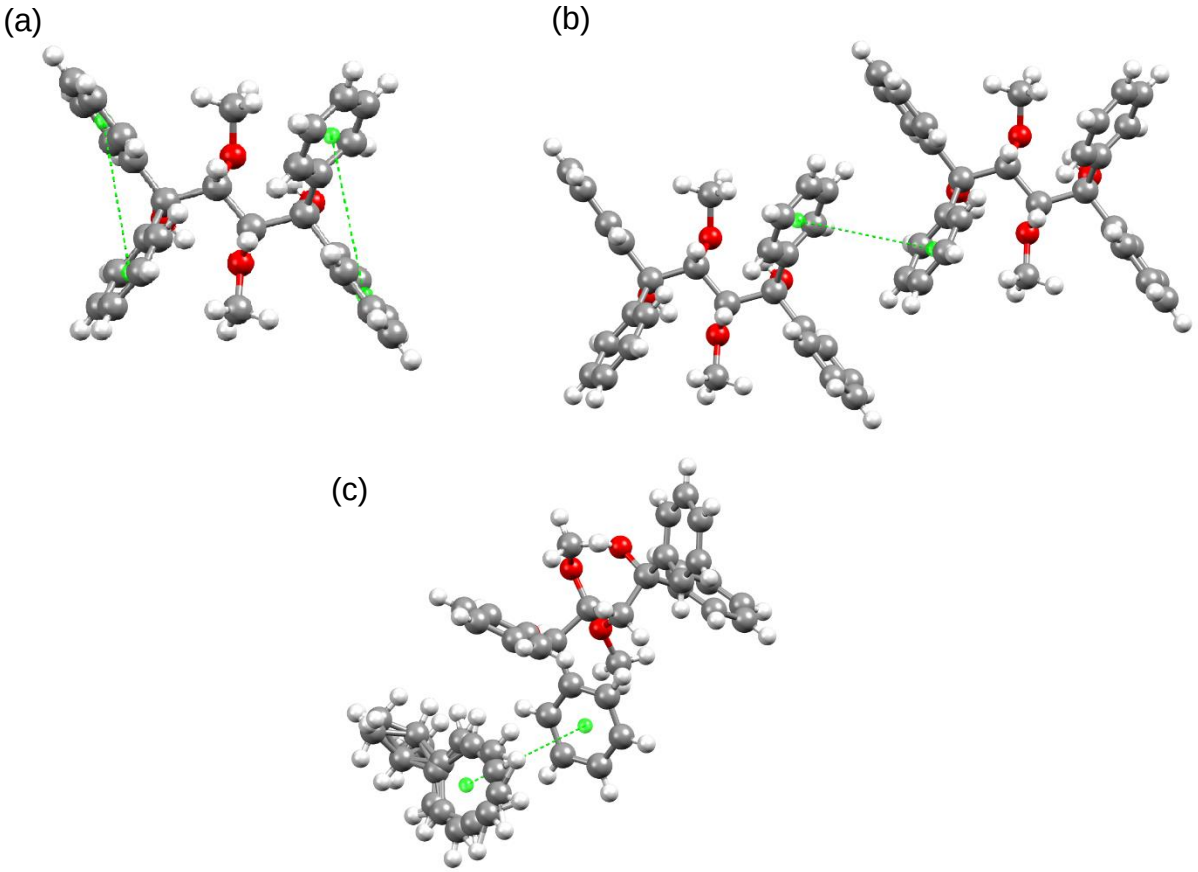

Figure 90: Representative π–π stacking interactions. Interaction 'a' indicates intramolecular stacking interactions; 'b' shows intermolecular host–host interactions of this type; 'c' shows a host–guest stacking interaction.

C-H–π stabilizing interactions in these complexes predominantly involve interactions between a methoxy hydrogen of the host and a phenyl ring on the same molecule (2.80–2.92 Å, 145–149°) (Table 46). Four of these interactions are present in each complex, while one intermolecular host–host C-H–π interaction is observed in each. The intermolecular interactions range between 2.83–2.97 Å and 166–170° (Figure 91).

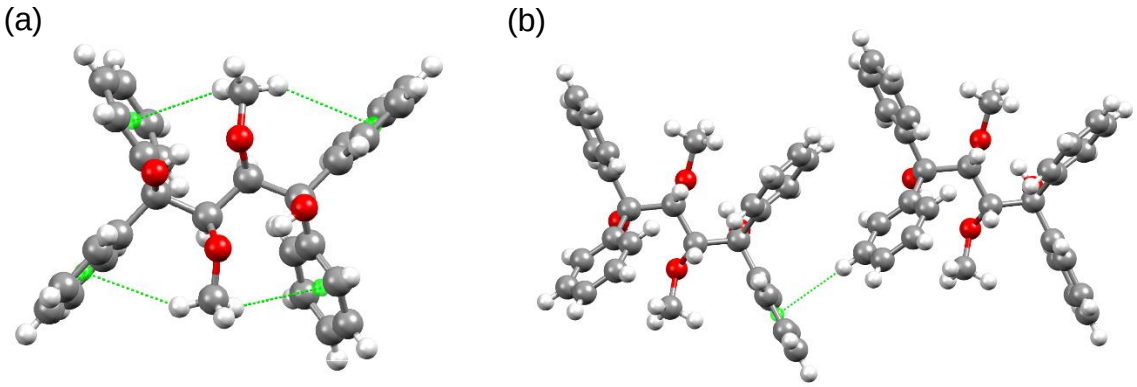

Figure 91: Representative intra- and inter- molecular C-H–π stabilizing interactions; 'a' depicts the intramolecular interactions of this type; 'b' shows a host–host intermolecular C-H–π interaction.

Table 46: C-H–π stabilizing interactions in the host-guest complexes of DMT and the substituted benzenes.

Complex	Non-covalent interaction	Distance (Å)	Angle (°)	Symmetry operator
2DMT•toluene	(host methoxy)C-H···Cg(host)	2.92	149	x,y,z
	(host methoxy)C-H···Cg(host)	2.86	147	x,y,z
	(host methoxy)C-H···Cg(host)	2.82	149	x,y,z
	(host methoxy)C-H···Cg(host)	2.80	146	x,y,z
	(host)*m*-ArH···Cg(host)	2.97	170	1–x, y, 1–z
2DMT•EB	(host methoxy)C-H···Cg(host)	2.88	148	x,y,z
	(host methoxy)C-H···Cg(host)	2.86	147	x,y,z
	(host methoxy)C-H···Cg(host)	2.85	145	x,y,z
	(host methoxy)C-H···Cg(host)	2.82	146	x,y,z
	(host)*m*-ArH···Cg(host)	2.94	170	1–x, y, 1–z
2DMT•cumene	(host methoxy)C-H···Cg(host)	2.88	145	x,y,z
	(host methoxy)C-H···Cg(host)	2.89	148	x,y,z
	(host methoxy)C-H···Cg(host)	2.87	145	x,y,z
	(host methoxy)C-H···Cg(host)	2.85	148	x,y,z
	(host)*m*-ArH···Cg(host)	2.83	166	1–x, y, 1–z

Short Contacts

Contacts shorter than the van der Waals radii of the participating atoms are predominantly present between host molecules. Host–host interactions range between 2.22–2.89 Å with angles of 107–162°. They typically occur between a host hydroxy hydrogen atom of one host and an aromatic hydrogen of another. Furthermore, the 2DMT•toluene complex has a short contact between a hydrogen atom in the *para*-position of the host and a carbon in the *meta*-position of another host (2.86 Å, 145°), while the 2DMT•cumene complex has a similar contact but between a host and guest molecule (2.89 Å, 168°). Table 47 lists these contacts in detail while Figure 92 depicts representative examples of these interactions.

Table 47: Summary of the various contacts shorter than the van der Waals radii found in the DMT complexes with the substituted aromatic guests.

Complex	Non-covalent interaction	Distance (Å)	Angle (°)	Symmetry operator
2DMT•toluene	(host hydroxy)O-H···*p*-ArH(host)	2.28	107	–1/2+x,1/2+y,z
	(host hydroxy)O-H···*p*-ArH(host)	2.28	144	1/2+x,1/2+y,z
	(host)*p*-ArH···*m*-ArC(host)	2.86	145	1–x,y,–z
2DMT•EB	(host hydroxy)O-H···*p*-ArH(host)	2.27	108	–1/2+x,1/2+y,z
	(host hydroxy)O-H···*p*-ArH(host)	2.25	151	1/2+x,1/2+y,z
	(host)*p*-ArH···*m*-ArC(host)	2.89	148	1–x,y,–z
	(host)*p*-ArH···H-C(guest CH_2)	2.11	158	x,y,z
	(host)*p*-ArH···H-C(guest CH_3)	2.23	135	2–x,y,2–z
	(host)*o*-ArC···H-C(guest CH_2)	2.75	100	x,y,–1+z
2DMT•cumene	(host hydroxy)O-H···*p*-ArH(host)	2.28	114	–1/2+x,1/2+y,z
	(host hydroxy)O-H···*p*-ArH(host)	2.22	162	1/2+x,1/2+y,z
	(host)*p*-ArH···*m*-ArC(guest)	2.89	168	1/2+x,–1/2+y,1+z

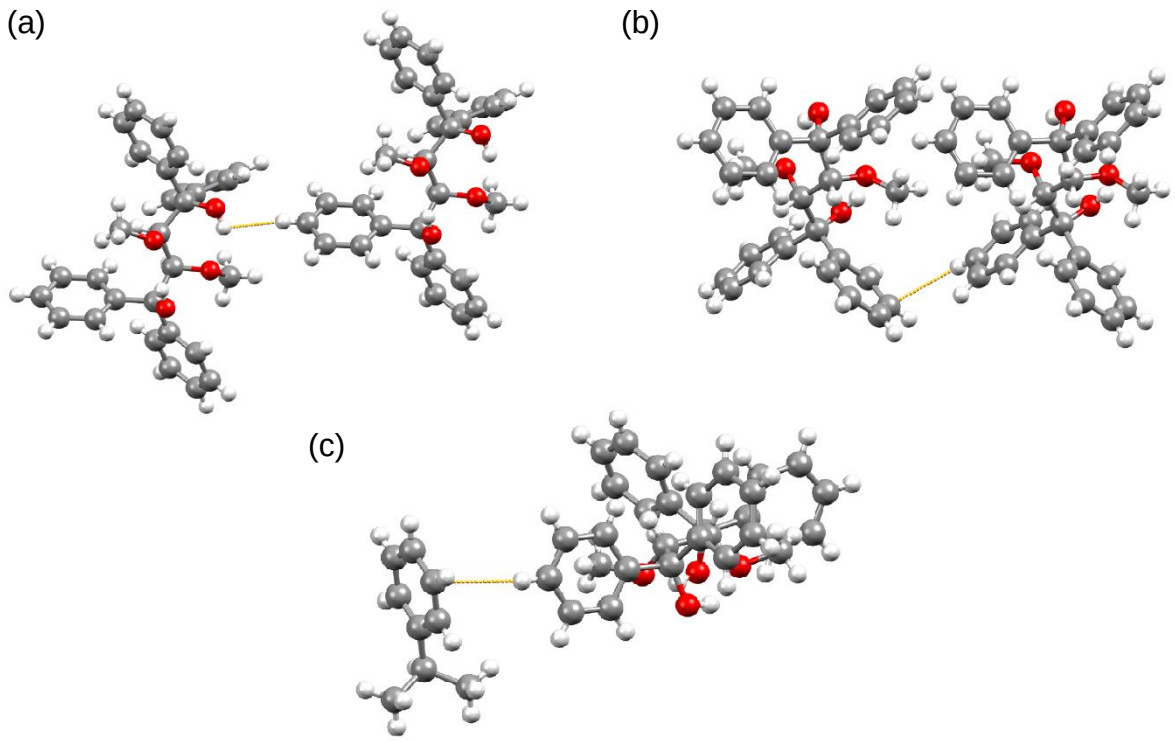

Figure 92: Short contacts in the DMT complexes with toluene and cumene; 'a' and 'b' show intermolecular host–host interactions in the complex with toluene, while 'c' depicts a host–guest interaction in the cumene complex. Interactions are shown by means of orange dashed lines.

Table 48 contains a comparison of all the host–guest interactions in each complex in order to more readily identify significant interactions that may contribute to DMT's selectivity towards these guests.

Table 48: Significant host–guest interactions for the complexes of DMT with the substituted aromatic guests.

Interaction	2DMT•toluene	2DMT•EB[a]	2DMT•cumene
π–π	5.281(3)–5.805(3) Å (8 contacts)	5.299(6)–5.960(4) Å (9 contacts)	4.570(6)–5.996(3) Å (7 contacts)
CH–π	None	None	None
Short contacts	None	2.11 Å, 158°, << (host)*p*-ArH···H-C(guest CH_2) 2.23 Å, 135°, < (host)*p*-ArH···H-C(guest CH_3) 2.75 Å, 100°, < (host)*o*-ArC···H-C(guest CH_2)	2.89 Å, 168°, < (host)*p*-ArH···*m*-ArC(guest)

*< denotes contacts less than the sum of the van der Waals radii and << denotes contacts less than this sum minus 0.2 Å; [a]repeated from Chapter 4 for ease of comparison.

A comparison of host–guest interactions does not adequately explain the selectivity order that DMT displays for these guests. A comparatively high number of host–guest interactions exist in the 2DMT•EB complex, but this guest is still discriminated against by DMT in binary competition experiments in favour of toluene, which displayed no significant host–guest short contacts. In contrast, cumene, which was consistently disfavoured, has a comparable number of π–π stacking interactions and a short contact which the toluene complex lacks.

For further interest, the mode of packing of each complex was again analysed by omitting the guest from the packing calculation. Guests were accommodated in discrete cavities in each case. A representative slice from the 2DMT•cumene complex illustrates these cavities in Figure 93 (dark yellow).

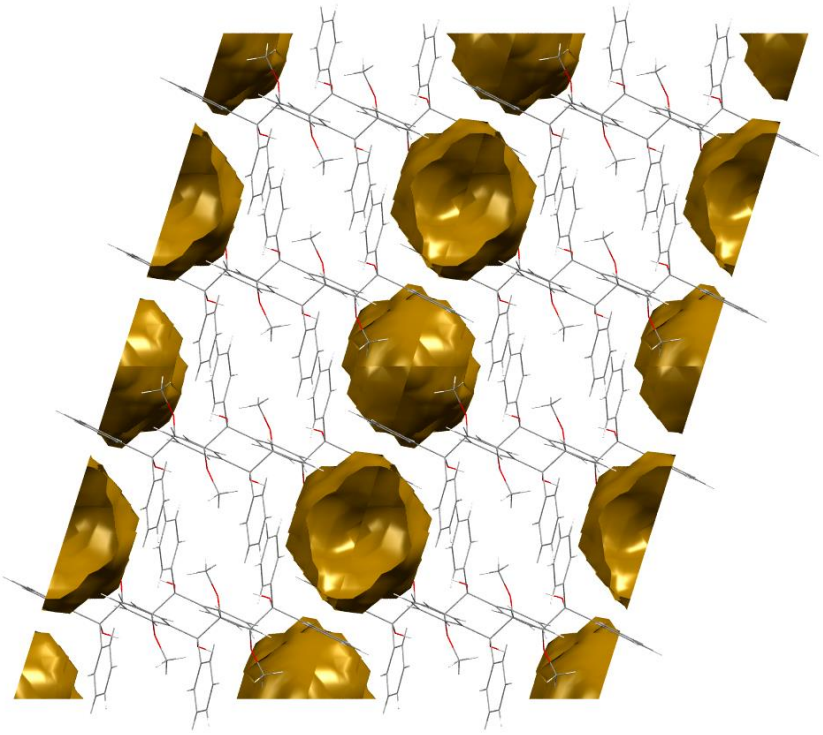

Figure 93: The discrete cavity guest packing in the 2DMT•cumene complex.

6.6 Hirshfeld Surface Analysis

An analysis of the two-dimensional Hirshfeld surfaces of the guests in these complexes may assist in elucidating reasons for DMT's selective behaviour in the presence of mixtures containing toluene, EB and cumene by allowing easier visualization of the distribution of all host–guest interactions in each complex. Figure 94a shows the fingerprint plot from the 2DMT•toluene complex. This plot is characterised by a spike, S1, indicative of H···C interactions. It is slightly overlapped by the much larger wing, W1, representative of H···H interactions. The 2DMT•cumene complex (Figure 94b) shares the same S1 spike (H···C interactions), whereas two distinct wings (W1 and W2) represent H···H interactions. The fingerprint plot for the 2DMT•EB complex (Figure 94c) is shown here for ease of comparison (see Chapter 4.6).

Figure 95 graphically represents the percentage and type of intermolecular interactions experienced by the different atoms present in each complex. The amount of H···H and H···C interactions are relatively evenly distributed through each complex. The complexes of toluene and EB have very similar H···H percentages (72.8 and 72.3%, respectively). This fact is mirrored with respect to their H···C percentages (27.2 and 27.7%). The 2DMT•cumene complex, on the other hand, experiences slightly more H···H interactions, but fewer H···C interactions (75.5 and 22.4%, respectively). This complex also has a significant percentage of C···C interactions (2.1%). The percentage H···C interactions present in the three complexes correlates closely with the host selectivity order, and it is therefore perhaps these interaction types that drive the host to behave in the manner that it does when in the presence of these mixed guests. However, Hirshfeld surface analysis, in this instance, is not a convincing tool to use to predict the selectivity behaviour of DMT for these three alkylated aromatic guests.

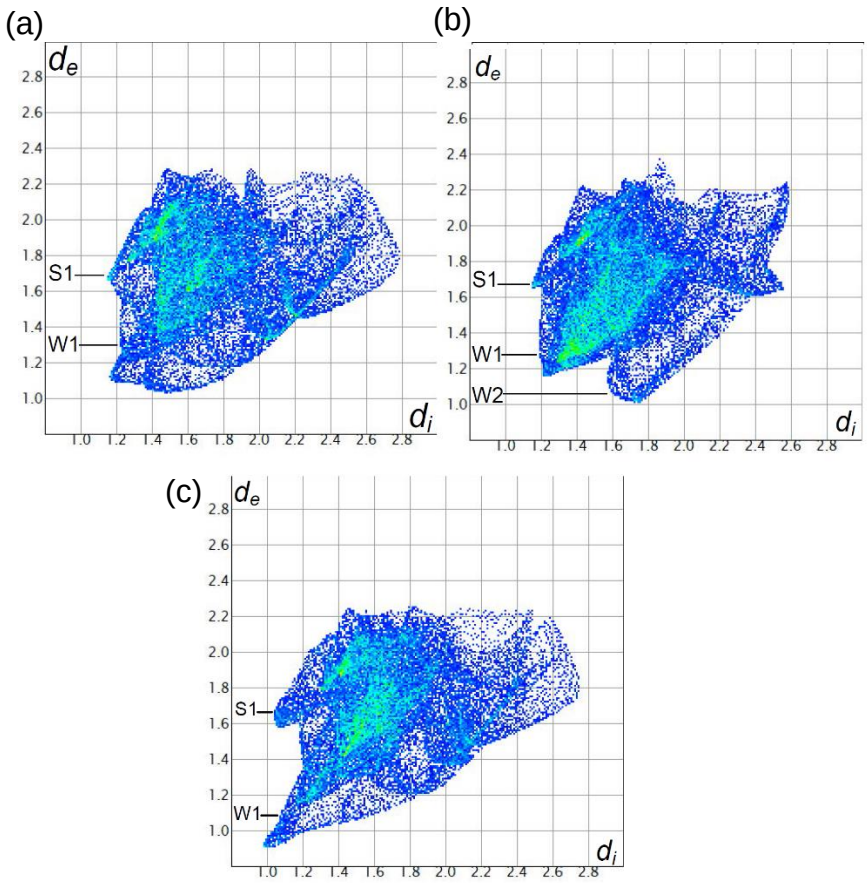

Figure 94: Two-dimensional fingerprint plots obtained from Hirshfeld surfaces for the guests in inclusion complexes of a) 2DMT•toluene, b) 2DMT•cumene and c) 2DMT•EB.

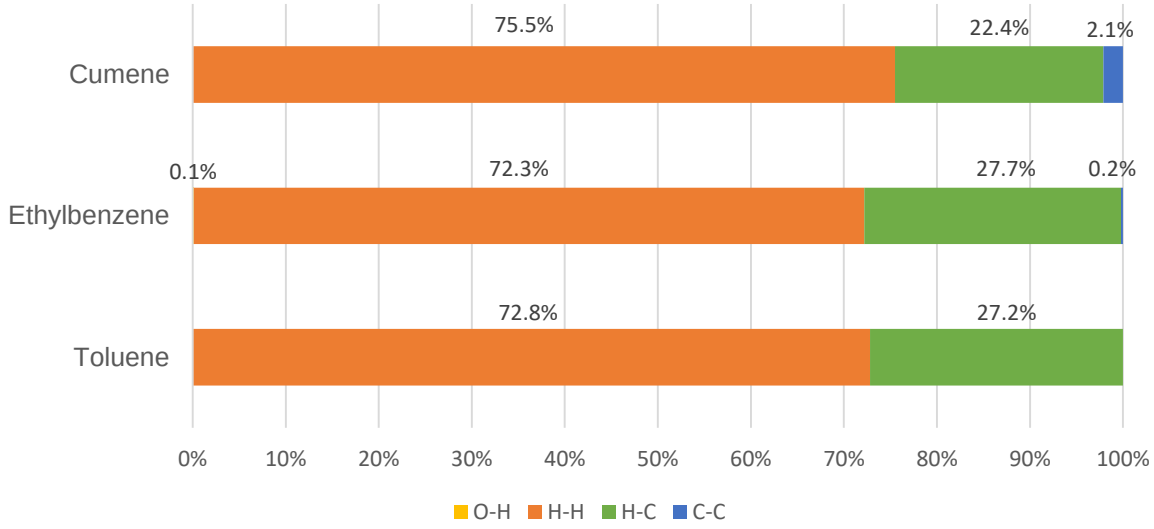

Figure 95: Graphical display showing the percentage and type of intermolecular interactions in each complex.

6.7 Conclusion

DMT proved successful in forming inclusion complexes with both toluene and cumene in addition to the previously-discussed ethylbenzene (Chapter 4). The inclusion complexes, in each case, had a 2:1 host:guest ratio. Competition experiments indicated that DMT discriminated against cumene in binary and ternary competitions for all guest compositions assessed. Toluene was slightly preferred over ethylbenzene when considering only the binary mixture experiments, but when cumene was present, as in the case of the ternary competition mixture, EB was slightly preferred over toluene. Thermal experiments confirmed the selectivity order of the host obtained from the binary competitions, since the relative thermal stabilities of these complexes correlated well with the selectivity order of the host. Single crystal X-ray analysis did not prove useful in the determination of factors that promote the observed selectivity order. The isostructurality of all the complexes in question, as well as the contradictory amount of short contacts between host and guest, did not lend itself to further explain the host behaviour. Finally, Hirshfeld analysis, which provide an average representation of the host–guest interactions, suggests some correlation between the relative amounts the H···C interactions and the selectivity order displayed by DMT, but was not convincing. Interestingly, there was no correlation in the selectivity of DMT towards the broad molecular shape of these guest molecules: the more branched *N,N*-dimethylaniline was selected over *N*-methylaniline and aniline (see Chapter 3), whereas the more branched host, cumene, was discriminated against in these current experiments.

Chapter 7: Inclusion Compounds of DMT (73) with Nitrobenzene and the Nitrotoluene Isomers

7.1 Introduction

Nitrobenzene, *p*-nitrotoluene (*p*-NT), *m*-nitrotoluene (*m*-NT) and *o*-nitrotoluene (*o*-NT) are derivatives of benzene and toluene with an electron-withdrawing nitro (-NO_2) group. The nitrotoluene isomers see routine use as building blocks in the production of agricultural chemicals, explosives and dyes (commonly *via* reduction to their corresponding toluidines).[181,182] Specifically, *p*-NT is often sulfonated to yield 4-nitrotoluene-2-sulphonic acid which may be further utilized as a synthetic intermediate, or crystals thereof may be used in optical applications.[183] Most of the nitrobenzene in production is converted to aniline which has a variety of applications, but nitrobenzene is also sometimes used as a solvent for certain reactions.[184,185] Industrially, it is produced through the mixed acid nitration of benzene. Similarly, the nitrotoluenes are synthesized through nitration of toluene. This process affords a mixture of the nitrotoluene isomers with an *o*-NT:*p*-NT ratio of ~1.6 (with *m*-NT a minor product). The boiling points of *o*-NT (222.0 °C) and *m*-NT (232.0 °C) are sufficiently different to allow their separation through fractional distillation, after which *p*-NT may be isolated through crystallization as it has a relatively high melting point (51.6 °C).[173] Even though the separation of these nitroaromatic compounds is well established, it is still of academic interest to study DMT's ability to include, or indeed discriminate, between these compounds in order to further elucidate the mechanisms by which any selective inclusion occurs.

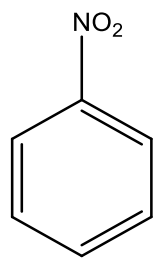

Nitrobenzene

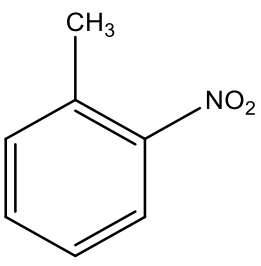

o-NT

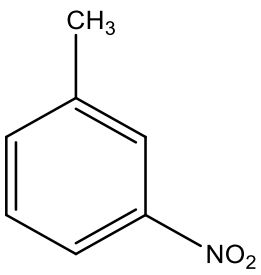

m-NT

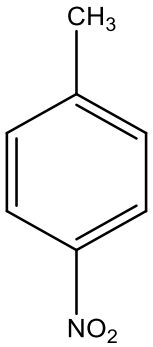

p-NT

7.2 Individual and Equimolar Inclusion Experiments

Recrystallizations of DMT from each guest afforded inclusion complexes with nitrobenzene, *p*-, *m*- and *o*- nitrotoluene. ^{1}H-NMR spectroscopy of these solids indicated that 2:1 host:guest complexes were formed in each case (Table 49).

Table 49: Host:guest ratios of complexes formed during individual recrystallization experiments.*

Guest	Host:guest
Nitrobenzene	2:1
p-Nitrotoluene	2:1
m-Nitrotoluene	2:1
o-Nitrotoluene	2:1

*Determined using ^{1}H-NMR spectroscopy with $CDCl_3$ as solvent.

Competition experiments were subsequently carried out during which DMT was allowed to crystallize from different combinations of equimolar mixtures of nitrobenzene and the nitrotoluene isomers. The solids thus obtained were subjected to both ^{1}H-NMR spectroscopy and GC-MS analysis, the results of which are provided in Table 50. In each experiment, the overall host:guest ratio remained 2:1, and the preferred guest is indicated in bold italic font face. A binary competition experiment between *o*-NT and *m*-NT resulted in DMT preferentially including *o*-NT (66.4%). When *o*-NT and *p*-NT competed, the latter experienced favourable discrimination (83.2%), while when this guest and *m*-NT were in competition, *p*-NT was again preferred (77.7%). Nitrobenzene was selected for when competing against *o*-NT (71.9%) and *m*-NT (79.7%). However, very little selectivity could be discerned in a competition between nitrobenzene and *p*-NT, where *p*-NT was included to an amount of only 50.4%. These binary experiments therefore afforded a host selectivity order of nitrobenzene ≈ *p*-NT > *o*-NT > *m*-NT. In a ternary competition experiment comprising the nitrotoluenes, *p*-NT (66.2%) was preferred over *m*-NT (20.6%) which was, now, selected over *o*-NT (13.2%). Similarly, a quaternary competition experiment resulted

in *p*-NT (39.9%) being preferred over nitrobenzene (30.2%) followed by *m*-NT (17.1%) and *o*-NT (12.8%). Clearly the host selectivity order is not always consistent and depends on the competing guests present.

Table 50: Competition experiments and H:G ratios obtained.*

Nitrobenzene	*o*-NT	*m*-NT	*p*-NT	Guest ratios (% e.s.d.)[$]	Overall H:G ratio
	x	x		**66.4**:33.6 (2.3)	2:1
	x		***x***	16.8:**83.2** (1.0)	2:1
		x	***x***	22.3:**77.7** (1.1)	2:1
	x	x	***x***	13.2:20.6:**66.2** (0.3)(0.5)(0.7)	2:1
x	x			**71.9**:28.1 (1.2)	2:1
x		x		**79.7**:20.3 (2.6)	2:1
x			***x***	49.6:**50.4** (1.2)	2:1
x	x	x	***x***	30.2:12.8:17.1:**39.9** (0.8)(1.2)(0.7)(1.0)	2:1

*Determined using GC-MS; [$]experiments were carried out in triplicate; an average value is provided here with % estimated standard deviation in parentheses.

7.3 Host Selectivity Profiles with Changing Guest Concentrations in Binary and Ternary Guest Mixtures

The ability of the host molecule, DMT, to include nitrobenzene and the nitrotoluene isomers in a discriminatory fashion through a varied concentration range of guests was subsequently investigated. DMT was recrystallized from non-equimolar binary mixtures of nitrobenzene and the nitrotoluene isomers. Analysis of the composition of the mother liquor and the included guests upon crystallization allowed for the construction of selectivity curves depicted in Figures 96–102.

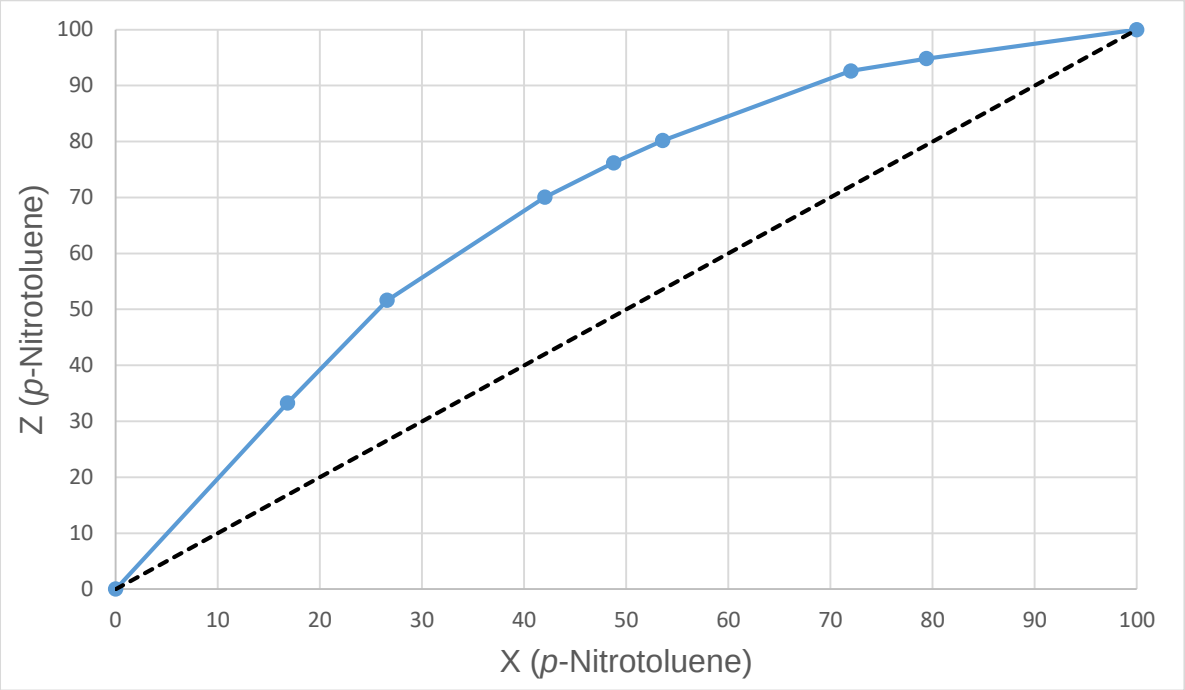

Figure 96: Selectivity curve of *p*-NT *vs* *m*-NT. Coloured blue is the molar fraction of *p*-NT in the inclusion complex (Z) *vs* the molar fraction of *p*-NT in the mother liquor (X). Black dashes indicate the theoretical line of no selectivity.

Figure 96 indicates the selectivity curve obtained when DMT was recrystallized from various non-equimolar binary mixtures of *p*-NT and *m*-NT. The general shape of the curve indicates that DMT's selectivity towards *p*-NT is not exclusively dependent on

the concentration of either guest present, as *p*-NT was preferentially included throughout the experiment. An experiment in which the mother liquor composition of *p*-NT was approximately 26.6% afforded crystals which already contained ~51.6% of this guest, while crystals obtained from a vial comprised of 72.0% *p*-NT (and 28.0% *m*-NT) had included 92.6% *p*-NT. The average selectivity coefficient, K, for this curve was calculated to be 3.59.

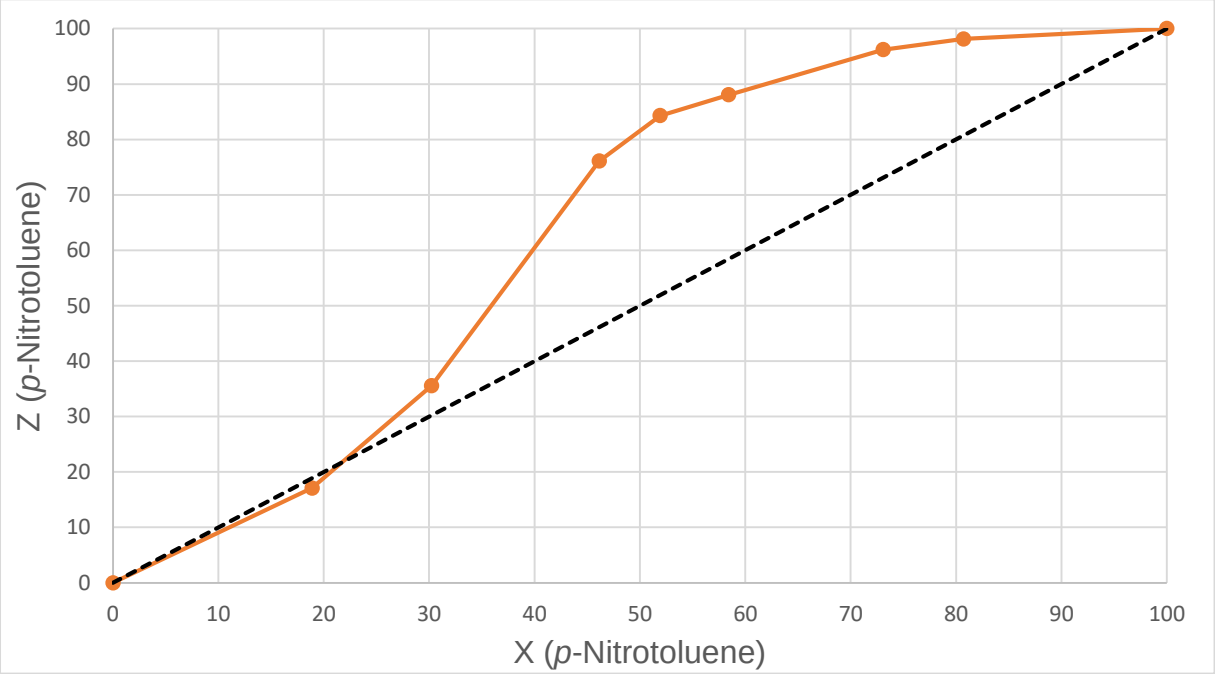

Figure 97: Selectivity curve of *p*-NT *vs* *o*-NT. Coloured orange is the molar fraction of *p*-NT in the inclusion complex (Z) *vs* the molar fraction of *p*-NT in the mother liquor (X). Black dashes indicate the theoretical line of no selectivity.

Initially, at low molar concentrations of *p*-NT, DMT does not display significant selectivity for either *p*-NT or *o*-NT, as demonstrated by an experiment consisting of ~18.8% *p*-NT resulting in crystals containing only 17.1% *p*-NT (Figure 97). However, at higher *p*-NT concentrations, this guest becomes significantly more preferred. When the mother liquor was comprised of ~46.1% *p*-NT, DMT crystals contained ~76.1% of this guest. This trend continued as demonstrated by a mother liquor composition of

approximately 73.1% *p*-NT resulting in an inclusion complex containing ~96.2% of this guest. The average selectivity coefficient for this curve was 5.42.

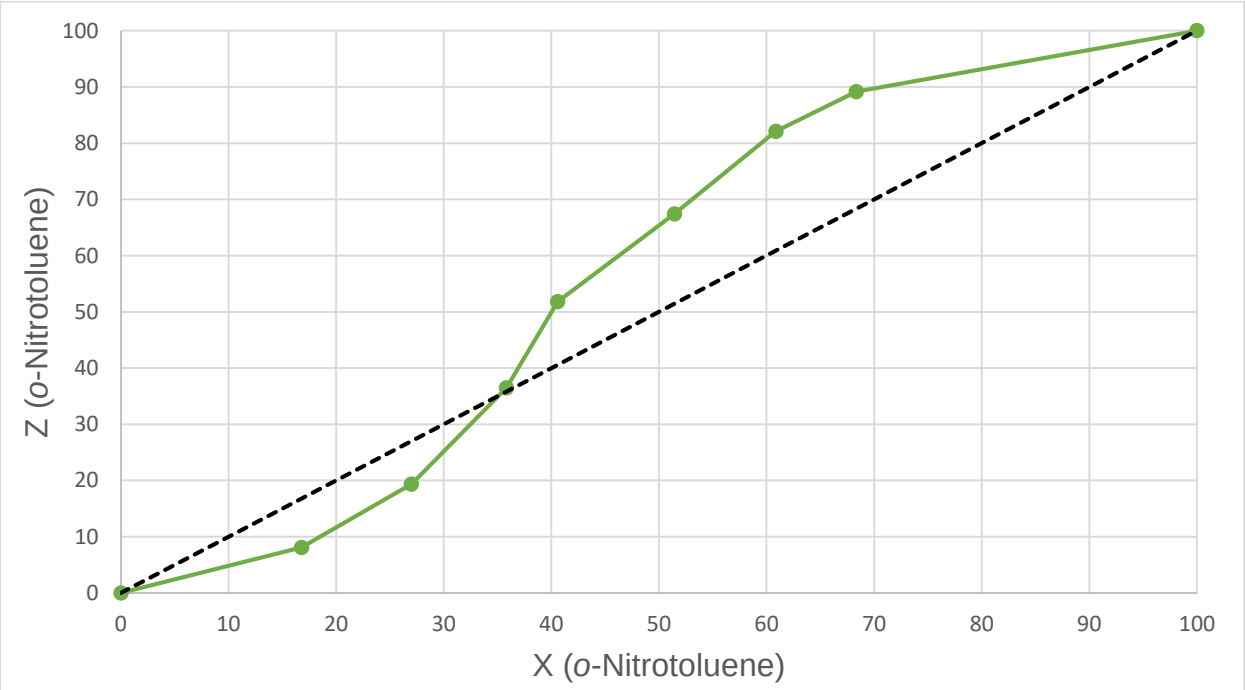

Figure 98: Selectivity curve of *o*-NT *vs* *m*-NT. Coloured green is the molar fraction of *o*-NT in the inclusion complex (Z) *vs* the molar fraction of *o*-NT in the mother liquor (X). Black dashes indicate the theoretical line of no selectivity.

Figure 98 shows the selectivity curve of DMT obtained when this host was recrystallized from various binary mixtures of *m*-NT and o-NT. Initially, DMT shows a clear preference for *m*-NT as indicated by the data points, at low *o*-NT concentrations, below the theoretical line of no selectivity. For example, an experiment comprising 26.9% *o*-NT in the mother liquor produced crystals containing only ~19.4% *o*-NT. A point of inflexion occurs at a mother liquor content of ~35.8% *o*-NT which yielded crystals containing approximately 36.4% of this guest. From this point onwards, higher mother liquor concentrations of *o*-NT resulted in DMT discriminating in favour of *o*-NT. When the mother liquor composition was 60.9% *o*-NT, DMT included this guest to an amount of 82.1%. Due to the change in guest selectivity with a change in guest concentration, the K value has been omitted here.

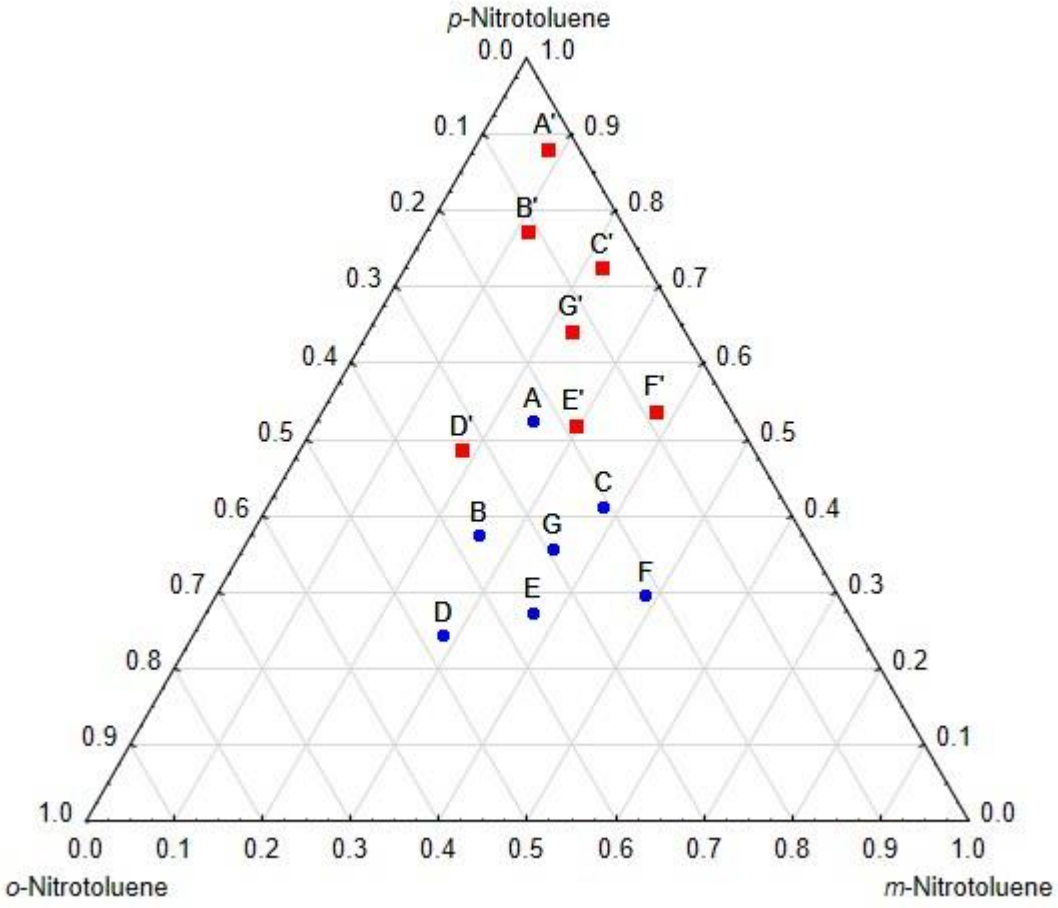

Figure 99: Ternary competition plot obtained when DMT was recrystallized from mixtures containing the nitrotoluene isomers in varying amounts. Blue circles indicate the mother liquor compositions and red squares guest compositions of complexes formed.

DMT was subsequently recrystallized from various non-equimolar ternary mixtures of all three nitrotoluene isomers. Analysis of mother liquor compositions (blue circles) and inclusion complex compositions (red squares) allowed for the construction of the ternary plot in Figure 99. The general trend observed from this plot indicates a large shift towards higher *p*-NT compositions in the complexes as compared to the mother liquor. The average increase of *p*-NT over all the data points in the inclusion complex compared to the mother liquor was determined to be ~29.9%. Consequently, the included amount of *m*-NT decreased on average by 12.6% compared to the mother liquor, and *o*-NT by 17.3%.

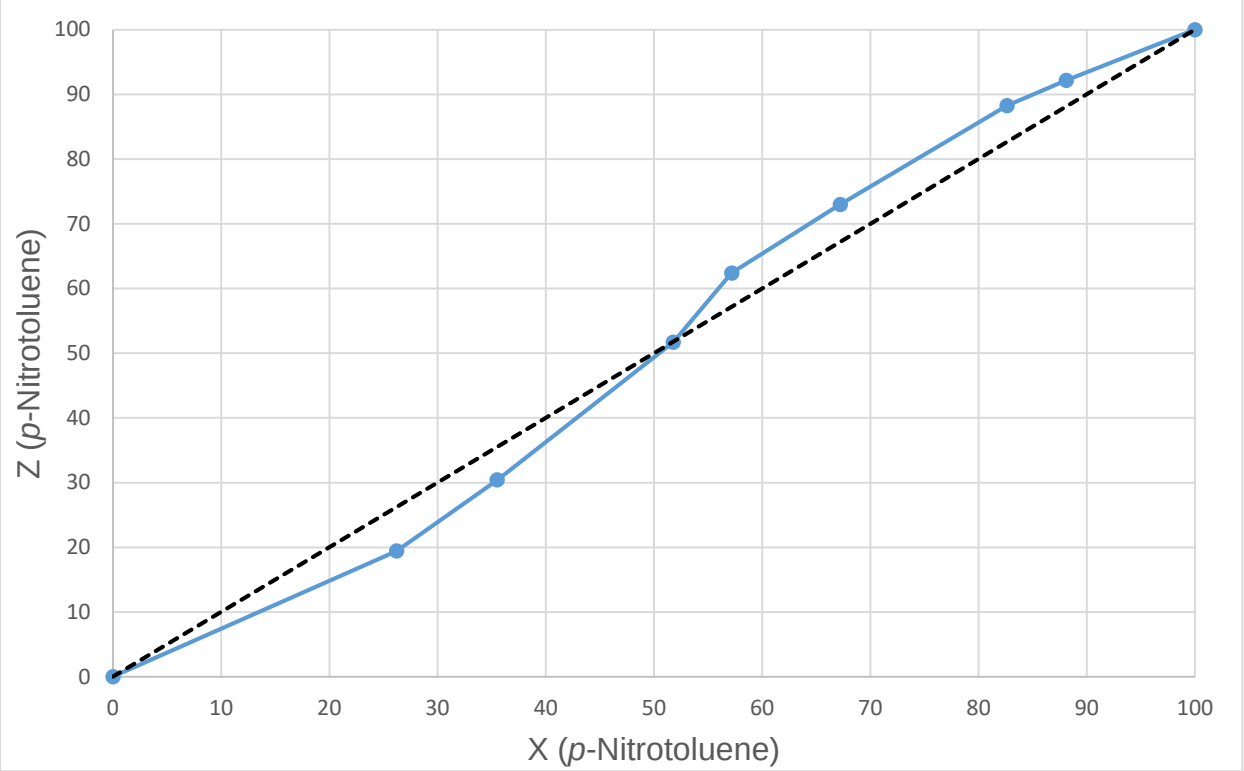

Figure 100: Selectivity curve of *p*-NT *vs* nitrobenzene. Coloured blue is the molar fraction of *p*-NT in the inclusion complex (Z) *vs* the molar fraction of *p*-NT in the mother liquor (X). Black dashes indicate the theoretical line of no selectivity.

A selectivity experiment wherein DMT was recrystallized from mixtures of *p*-NT and nitrobenzene was performed and the resultant curve shown in Figure 100. As in the case of Figure 98 (*o*-NT *vs* *m*-NT), DMT displays concentration-dependent selectivity towards *p*-NT and nitrobenzene, and this selectivity was very low throughout. At low *p*-NT concentrations in the mother liquor, nitrobenzene was preferentially included. When crystals were grown from a mixture of these two guests with a mother liquor composition of 26.2% *p*-NT, they contained only 19.4% *p*-NT. DMT was unable to discriminate between the two guests when the mother liquor contained ~51.8% *p*-NT and 48.2% nitrobenzene. At higher *p*-NT mother liquor concentrations, DMT discriminated somewhat in favour of the methyl-substituted guest. As the guest selectivity is concentration dependent, the average selectivity coefficient has been omitted.

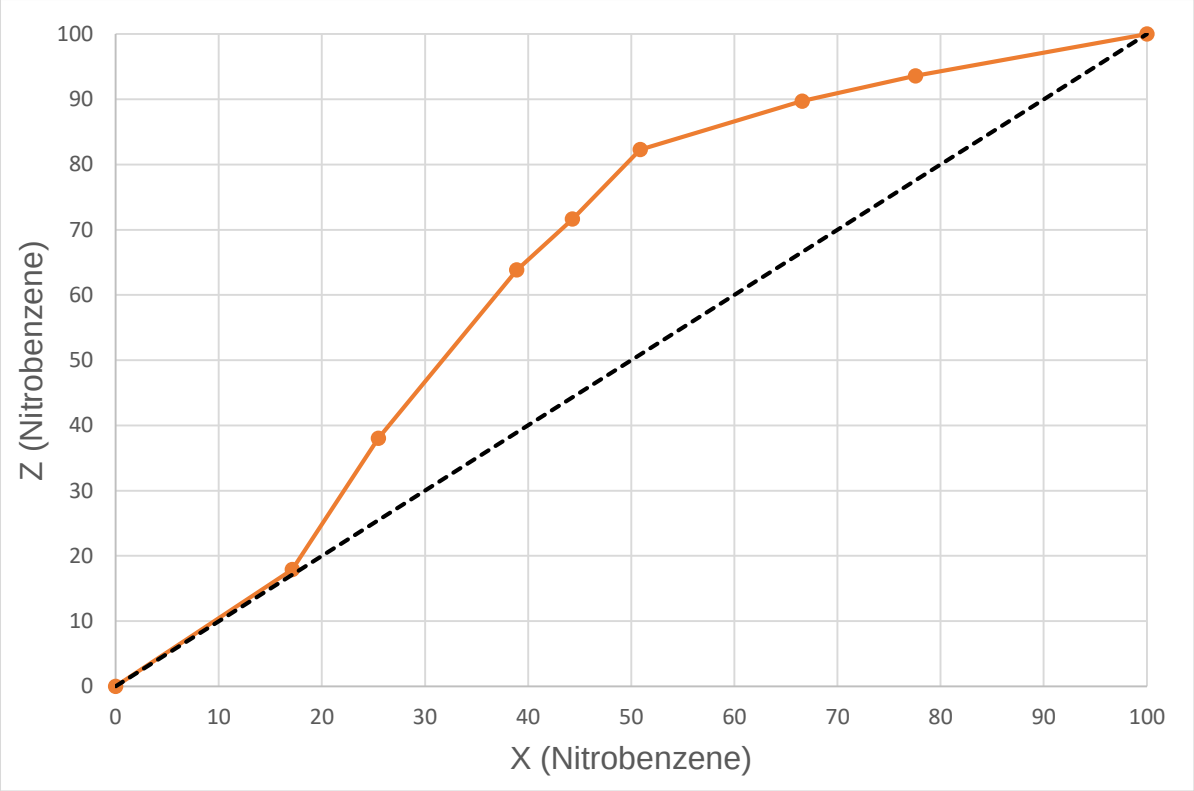

Figure 101: Selectivity curve of nitrobenzene *vs* *m*-NT. Coloured orange is the molar fraction of nitrobenzene in the inclusion complex (Z) *vs* the molar fraction of nitrobenzene in the mother liquor (X). Black dashes indicate the theoretical line of no selectivity.

Similar to Figure 97 (*p*-NT *vs* *o*-NT), the curve obtained for the selectivity experiments between *m*-NT and nitrobenzene shows an initial period of no selectivity by DMT between these two guests, as demonstrated by a point at which the mother liquor content of nitrobenzene was ~17.1% (Figure 101). This experiment gave rise to crystals containing ~17.8% nitrobenzene. At higher nitrobenzene mother liquor concentrations, DMT discriminated significantly in favour of this guest. Crystals grown from a nitrobenzene-rich mother liquor (77.5%) contained 93.6% of this guest. K for this curve was determined to be 3.13.

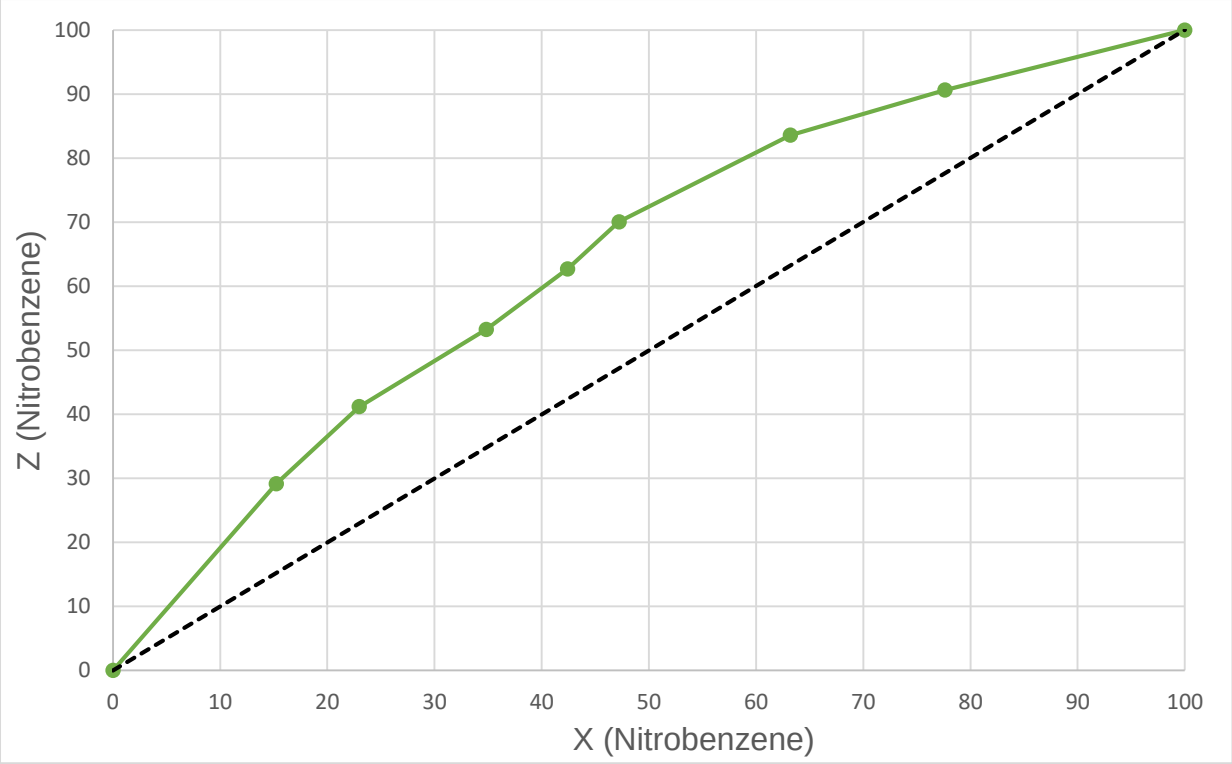

Figure 102: Selectivity curve of nitrobenzene *vs* *o*-NT. Coloured green is the molar fraction of nitrobenzene in the inclusion complex (Z) *vs* the molar fraction of nitrobenzene in the mother liquor (X). Black dashes indicate the theoretical line of no selectivity.

The selectivity curve constructed from the experiments between *o*-NT and nitrobenzene (Figure 102) shows that nitrobenzene was preferentially included by DMT across the entire molar range of these guests that was assessed. A nitrobenzene concentration of ~22.9% in the mother liquor produced a solid containing approximately 41.2% nitrobenzene, while crystals containing ~83.6% nitrobenzene were produced when DMT was recrystallized from a mother liquor containing 63.2% of this guest. The selectivity coefficient for this experiment was determined to be 2.49.

A comparison of these selectivity curves, as well as the results obtained from the equimolar binary, ternary and quaternary competition experiments indicate that, in general nitrobenzene and *p*-NT are favoured by DMT, while *o*-NT and *m*-NT are disfavoured. Selectivity between the preferred guests (nitrobenzene and *p*-NT) is more concentration-dependent. Similarly, DMT discriminates between *o*-NT and *m*-NT based on the concentration of the guests present.

7.4 Thermal Analysis

Simultaneous thermogravimetric analysis and differential scanning calorimetry experiments were carried out on each of the complexes of DMT with the nitro-substituted aromatic guests. Figures 103–106 show the resultant TG, DTG and DSC traces obtained upon heating the solids at 10 °C.min^{-1} under high purity nitrogen as purge gas.

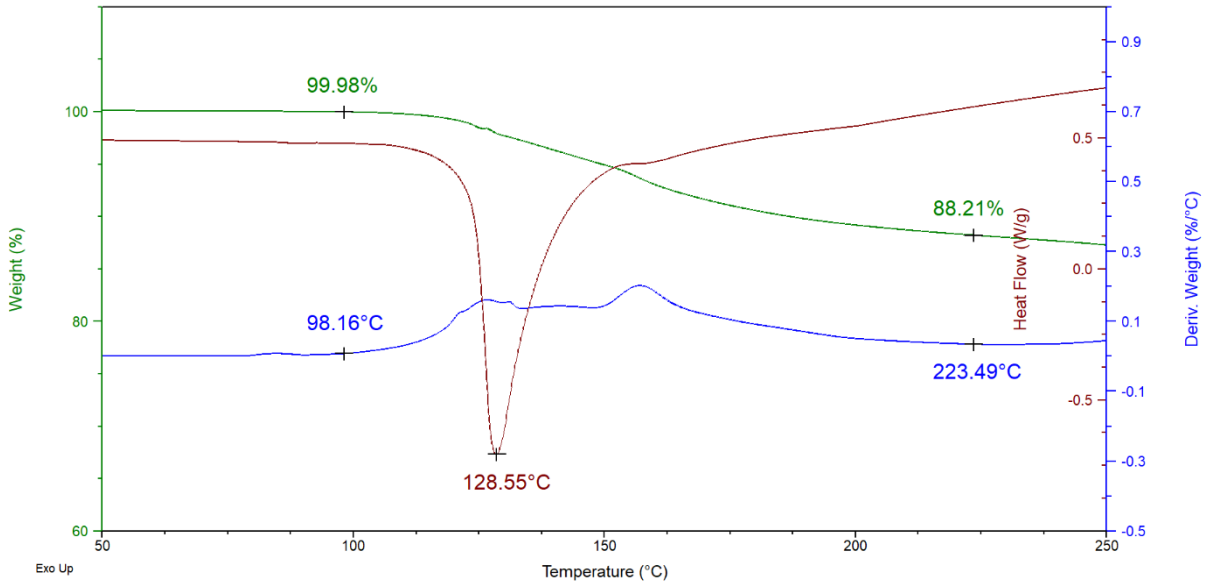

Figure 103: Overlaid TG (green), DTG (blue) and DSC (brown) traces for the 2DMT•nitrobenzene complex upon heating at 10 °C.min^{-1}.

The expected mass loss for a 2:1 2DMT•nitrobenzene complex was calculated to be 11.9%. The DTG trace (Figure 103, blue) experienced a plateaux at ~223.5 °C which corresponds to a mass loss of ~11.8%, which is in excellent agreement with that expected. The onset of the mass loss process was estimated to occur at 98.2 °C (DTG). Lastly, the endotherm peak temperature, which represents the guest release and the host melt, occurred at ~128.6 °C (DSC).

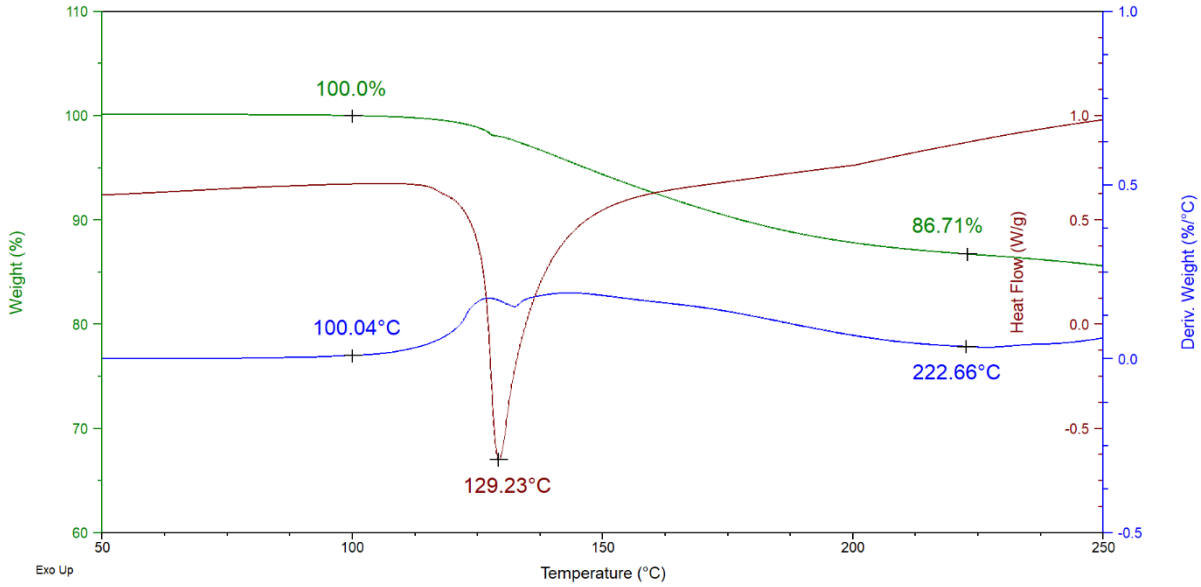

Figure 104: Overlaid TG (green), DTG (blue) and DSC (brown) traces for the 2DMT•*p-NT* complex upon heating at 10 °C.min^{-1}.

Upon heating, the 2DMT•*p*-NT complex experienced a mass loss of ~13.3% (Figure 104, green TG) which correlates well with that expected for a 2:1 host:guest complex (13.1%). The guest release onset temperature was approximately 100.0 °C (DTG) and loss continued until ~222.7 °C. Finally, the peak temperature of the single endotherm was measured to be ~129.2 °C, and represents both host melt and guest release.

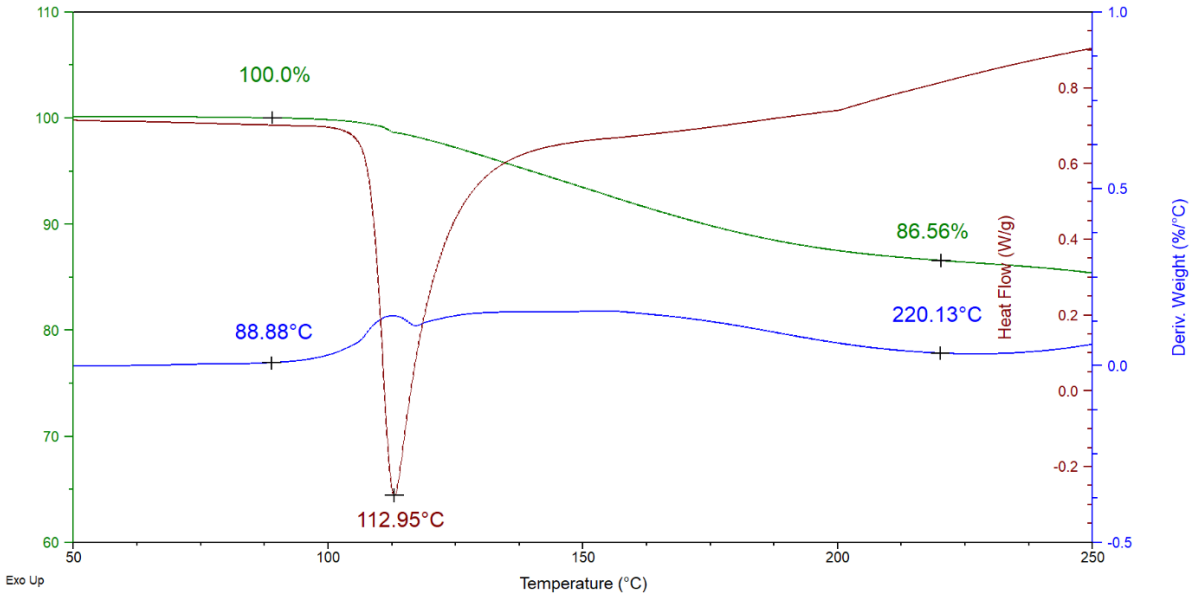

Figure 105: Overlaid TG (green), DTG (blue) and DSC (brown) traces for the 2DMT•*m*-NT complex upon heating at 10 °C.min^{-1}.

The DTG trace (Figure 105, blue) for the 2DMT•*m*-NT complex indicates a cessation of mass loss at ~220.1 °C. This corresponds to a mass loss of 13.4% (TG) which is again a positive indication of a 2:1 host:guest complex (13.1%). The guest release process was estimated to initiate at ~88.9 °C (DTG) while the peak endotherm for both guest release and host melt was significantly lower than in the preceding complexes (~113.0 °C).

Finally, when subjected to heating, the 2DMT•*o*-NT complex experienced a mass loss of ~13.5%, again correlating well with the expected 13.1% (Figure 106, TG). The onset temperature of mass loss was estimated at ~79.8 °C (DTG), while the endotherm peak temperature was determined to be ~116.5 °C.

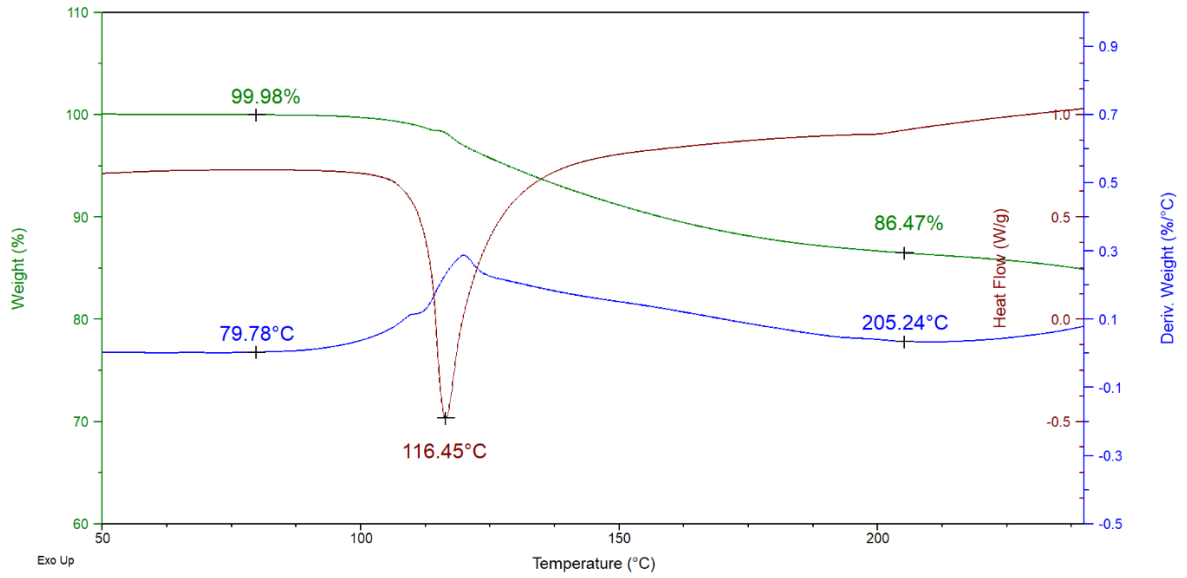

Figure 106: Overlaid TG (green), DTG (blue) and DSC (brown) traces for the 2DMT•*o*-NT complex upon heating at 10 °C.min^{-1}.

Table 51 summarises the relevant thermal data. The onset temperature (T_{on}) of the guest release process, as well as the endotherm peak temperature (T_{end}), for the 2DMT•nitrobenzene and 2DMT•*p*-NT are very similar for both complexes (98.2, 100.0 °C and 128.6, 129.2 ° C), alluding to these guests experiencing similar binding strengths in the complexes (Table 51). From competition experiments (equimolar and non-equimolar), the host displayed somewhat ambivalent selectivity towards nitrobenzene and *p*-NT, and this is therefore evident in these thermal experiments as well. T_{on} and T_{end} values for these two complexes are also significantly higher than for the 2DMT•*m*-NT and 2DMT•*o*-NT complexes, as expected when considering that DMT's selectivity for *m*-NT and *o*-NT was low.

The crystals of all four complexes have isostructural host packing (see Section 7.5), and therefore T_{on}–T_b is a valid consideration. The 2DMT•nitrobenzene and 2DMT•*p*-NT complexes have less negative T_{on}–T_b values (–112.6 and –138.3 °C, respectively) than the 2DMT•*o*-NT (–142.2 °C) and 2DMT•*m*-NT (–143.1 °C) complexes. This is in accordance with the observation that nitrobenzene and *p*-NT guests are more preferred than *o*-NT and *m*-NT.

Table 51: Summary of the major thermal events observed in the nitrobenzene and nitrotoluene complexes with DMT.

Guest	T_b (°C)	T_{on} (°C)[a]	T_{on}–T_b (°C)	T_{end} (°C)[b]	Mass loss % (Expected)
Nitrobenzene	210.8	98.2	–112.6	128.6	11.8 (11.9)
p-Nitrotoluene	238.3	100.0	–138.3	129.2	13.3 (13.1)
m-Nitrotoluene	232.0	88.9	–143.1	113.0	13.4 (13.1)
o-Nitrotoluene	222.0	79.8	–142.2	116.5	13.5 (13.1)

[a]T_{on} is the onset temperature for guest release estimated from the DTG; [b]T_{end} values were obtained from the brown DSC traces.

7.5 Single Crystal X-Ray Analysis

Crystals of the individual inclusions of DMT with nitrobenzene and the nitrotoluene isomers were subjected to single crystal X-ray diffraction studies. Table 52 contains crystallographic data for the 2:1 complexes thus obtained. Figure 107 shows the unit cells for these four complexes. They all crystallized in the monoclinic *C*2 crystal system and all four host frameworks are isostructural owing to similar unit cell dimensions. The guests in all these complexes exhibit symmetry-generated disorder. Figure 108 demonstrates the host-guest packing by means of a stereoview, using 2DMT•*p*-NT as a representative example.

Table 52: Crystallographic data for the complexes between DMT and the nitro-substituted aromatic guests.

	2DMT•*p*-NT	**2DMT•*m*-NT**	**2DMT•*o*-NT**	**2DMT•nitro-benzene**
Chemical formula	$2C_{30}H_{30}O_4 \bullet C_6H_5NO_2$	$2C_{30}H_{30}O_4 \bullet C_7H_7NO_2$	$2C_{30}H_{30}O_4 \bullet C_7H_7NO_2$	$2C_{30}H_{30}O_4 \bullet C_6H_5NO_2$
Formula weight	1046.22	1046.22	1046.22	1032.19
Crystal system	Monoclinic	Monoclinic	Monoclinic	Monoclinic
Space group	*C*2	*C*2	*C*2	*C*2
μ (Mo-Kα)/mm^{-1}	0.084	0.083	0.082	0.083
a/Å	17.155(2)	17.4167(10)	17.4337(9)	17.2792(9)
b/Å	12.2752(17)	12.1276(7)	12.0313(7)	12.0018(7)
c/Å	13.9597(19)	14.0545(9)	14.3683(8)	13.9820(8)
alpha/°	90	90	90	90
beta/°	109.557(6)	109.768(3)	110.512(2)	108.757(2)
gamma/°	90	90	90	90
V/$Å^3$	2770.1(6)	2793.7(3)	2822.7(3)	2745.6(3)
Z	2	2	2	2
F(000)	1112	1112	1112	1096
Temp./K	200	200	200	200

Restraints	1	2	5	2
Nref	6853	6824	6814	6787
Npar	359	389	353	380
R	0.0338	0.0366	0.0466	0.0340
wR2	0.0886	0.0980	0.1355	0.0895
S	1.03	1.04	1.04	1.02
θ min-max/°	2.1, 28.4	1.5, 28.3	2.1, 28.3	2.1, 28.3
Tot. data	27460	29120	28821	26189
Unique data	6853	6824	6814	6787
Observed data [I > 2.0 sigma(I)]	6447	6040	0.017	6177
R_{int}	0.017	0.019	0.017	0.018
Dffrn measured fraction θ full	0.999	0.999	1.000	0.999
Min. resd. dens. (e/ Å^3)	–0.23	–0.16	–0.32	–0.17
Max. resd. dens. (e/ Å^3)	0.20	0.20	0.48	0.18

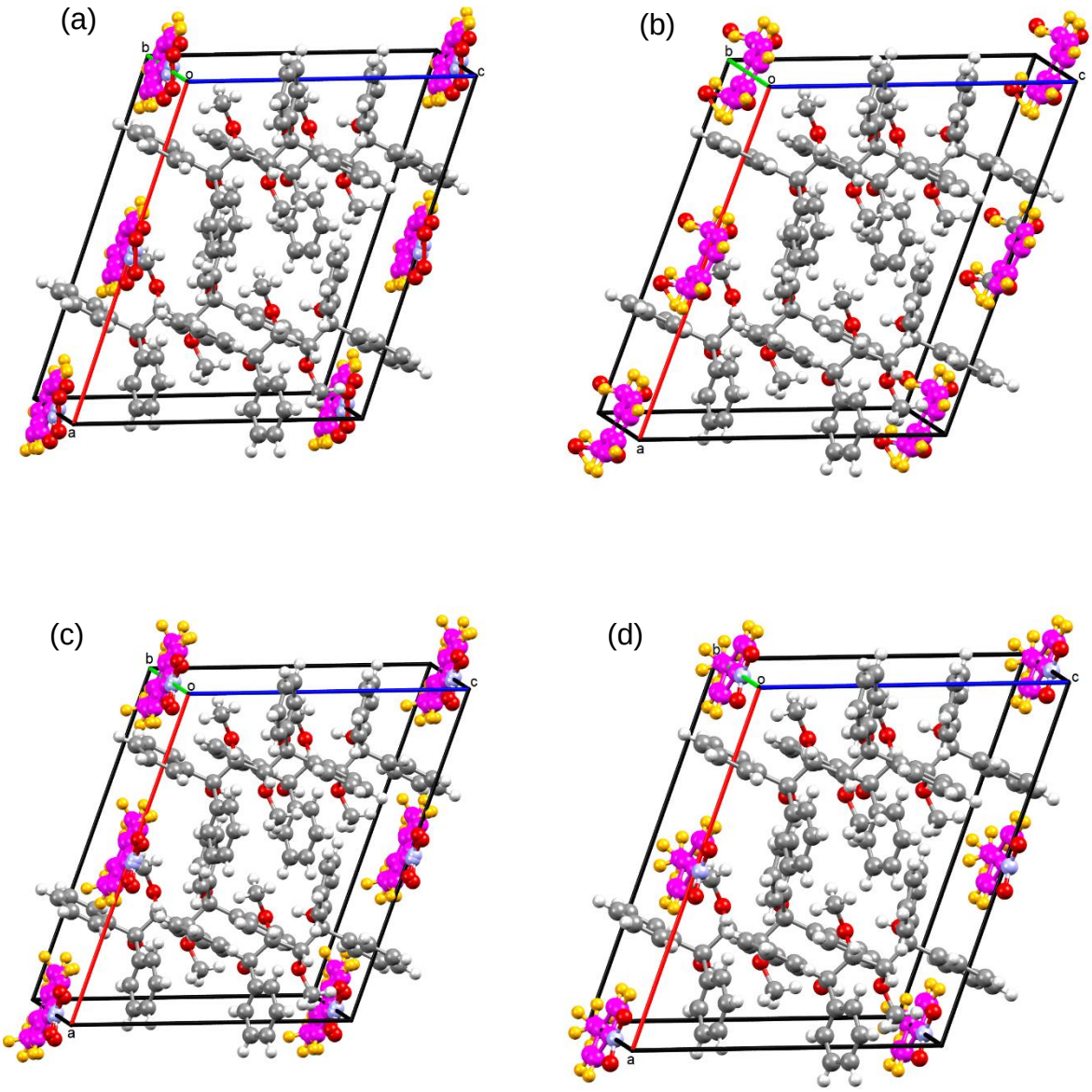

Figure 107: The unit cells for the DMT complexes with a) nitrobenzene, b) *o*-NT, c) *m*-NT and d) *p*-NT. Isostructural host frameworks are clearly evident here.

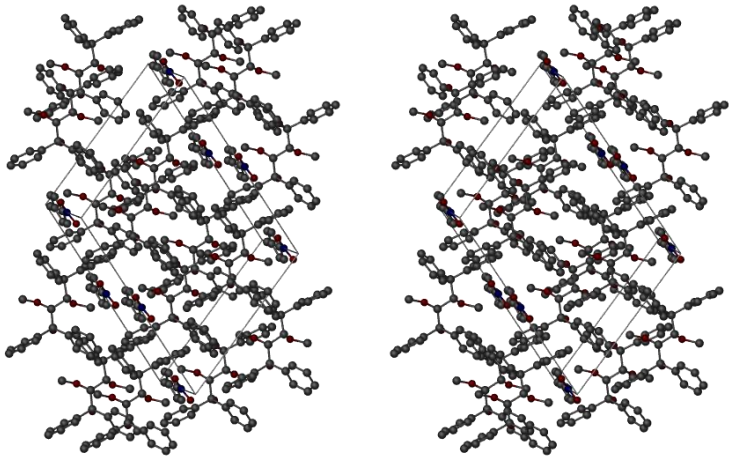

Figure 108: Stereoview of the 2DMT•*p*-NT complex to show packing in three dimensions, as a representative example.

Hydrogen Bonding

Classic hydrogen bonding interactions in these complexes present only as a pair of 1,3- and 2,4- intramolecular interactions between hydroxy and methoxy groups on the butane backbone of the host. They range in distance between 2.624(2) and 2.679(2) Å and 140–142° (Table 53). Figure 109 is a visual representation of these interactions in the 2DMT•*m*-NT complex.

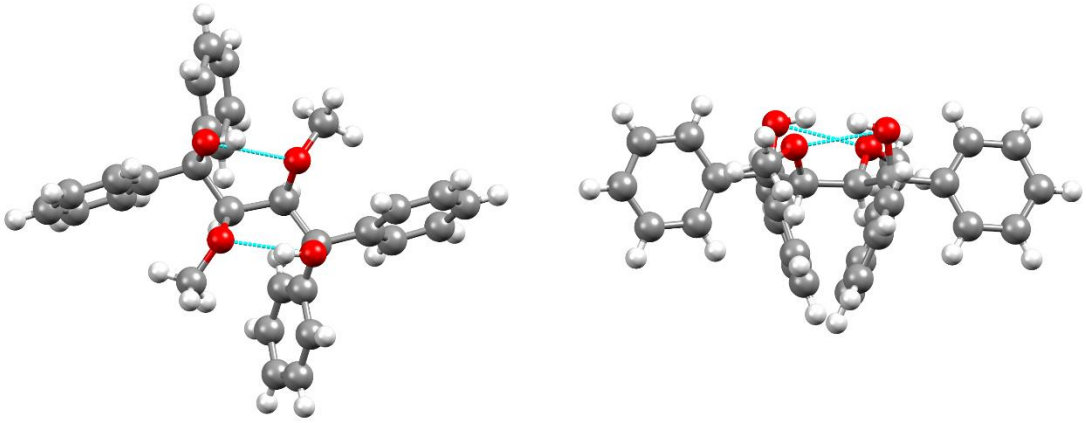

Figure 109: Two views of the host intramolecular hydrogen bonding, depicted with light-blue dashed lines (as in the 2DMT•*m*-NT complex).

Table 53: Classic intramolecular hydrogen bonding interactions in the DMT complexes with the nitro-substituted aromatic guests.

Complex	Non-covalent interaction	Distance (Å) D–A	Angle (°) D-H···A
2DMT•nitrobenzene	(host)O-H···O(host methoxy)	2.673(2)	140
	(host)O-H···O(host methoxy)	2.636(2)	141
2DMT•*p*-NT	(host)O-H···O(host methoxy)	2.679(2)	141
	(host)O-H···O(host methoxy)	2.648(3)	141
2DMT•*m*-NT	(host)O-H···O(host methoxy)	2.679(2)	140
	(host)O-H···O(host methoxy)	2.636(2)	142
2DMT•*o*-NT	(host)O-H···O(host methoxy)	2.667(3)	141
	(host)O-H···O(host methoxy)	2.624(2)	142

Intra- and inter- molecular non-classic hydrogen bonding interactions are found in all four complexes. The majority of these are intramolecular in nature and occur between a host *ortho*-hydrogen and a hydroxy oxygen atom of the same host [2.653(3)–2.761(4) Å, 100–102°]. Each of the four complexes has a single intermolecular interaction of this type between a host *para*-hydrogen and a hydroxy oxygen of another host molecule, the shortest of which occurs in the 2DMT•*p*-NT complex [3.268(3) Å, 166°]. This complex has an additional intermolecular non-classic hydrogen bond interaction between a host *meta*-hydrogen and a methoxy oxygen of another host [3.455(2) Å, 168°]. Finally, the 2DMT•*o*-NT complex also exhibits such an intermolecular interaction between a host *meta*-hydrogen and a nitro-oxygen of a guest molecule [3.332(2) Å, 136°]. Figure 110 depicts some of these interactions and Table 54 lists them in more detail.

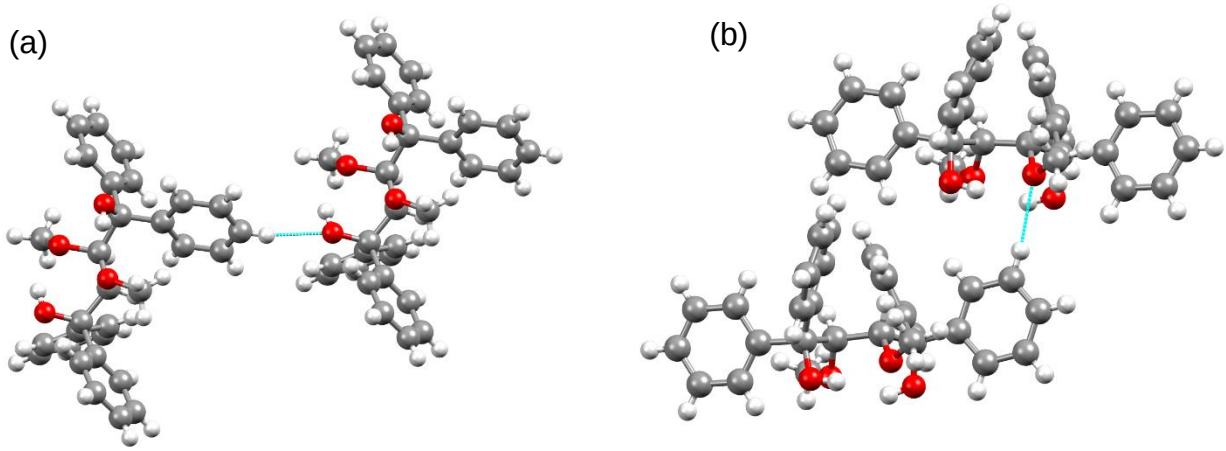

Figure 110: Two intermolecular non-classic host–host hydrogen bonding interactions in the 2DMT•*p*-NT complex depicted as light-blue dashes; a) (host)*p*-ArH···O(host hydroxy); b) (host)*m*-ArH···O(host methoxy).

Table 54: Non-classic inter- and intra- molecular hydrogen bonding interactions in the DMT complexes with the nitro-substituted aromatic guests.

Complex	Non-covalent interaction	Distance (Å) D–A	Angle (°) D-H···A
2DMT•nitrobenzene	(host)*o*-ArH···O(host hydroxy)	2.653(3)	102
	(host)*o*-ArH···O(host hydroxy)	2.759(2)	100
	(host)*o*-ArH···O(host hydroxy)	2.761(2)	100
	(host)*o*-ArH···O(host hydroxy)	2.669(2)	101
	(host)*p*-ArH···O(host hydroxy)[a]	3.309(3)	171
2DMT•*p*-NT	(host)*o*-ArH···O(host hydroxy)	2.653(2)	102
	(host)*o*-ArH···O(host hydroxy)	2.748(2)	100
	(host)*o*-ArH···O(host hydroxy)	2.751(2)	100
	(host)*o*-ArH···O(host hydroxy)	2.665(2)	100
	(host)*m*-ArH···O(host methoxy)[b]	3.455(2)	168
	(host)*p*-ArH···O(host hydroxy)[a]	3.268(3)	166
2DMT•*m*-NT	(host)*o*-ArH···O(host hydroxy)	2.661(3)	102
	(host)*o*-ArH···O(host hydroxy)	2.761(3)	100
	(host)*o*-ArH···O(host hydroxy)	2.767(3)	100
	(host)*p*-ArH···O(host hydroxy)[a]	3.325(3)	171
2DMT•*o*-NT	(host)*o*-ArH···O(host hydroxy)	2.654(3)	102
	(host)*o*-ArH···O(host hydroxy)	2.760(4)	100
	(host)*o*-ArH···O(host hydroxy)	2.761(4)	100
	(host)*o*-ArH···O(host hydroxy)	2.654(3)	102
	(host)*p*-ArH···O(host hydroxy) [c]	3.324(4)	170
	(host)*m*-ArH···O(guest nitro)[d]	3.332(2)	136

Symmetry operators: a) –1/2+x,–1/2+y,z; b) 3/2–x,–1/2+y,1–z; c) 1/2+x,–1/2+y,z; d) 1–x,y,2–z

π–π and CH–π interactions

Weak π–π stacking interactions are widespread throughout these complexes. Intermolecular interactions between two host molecules range between 4.712(1)–5.996(1) Å. Similarly, host–guest interactions of this type measure between 4.842(2)–5.883(3) Å. In addition, each complex exhibits two intramolecular π–π stacking interactions between phenyl rings connected to the same carbon on the butane backbone and these are understandably shorter [4.802(2)–4.880(1)]. Figure 111 shows representative examples of these interactions.

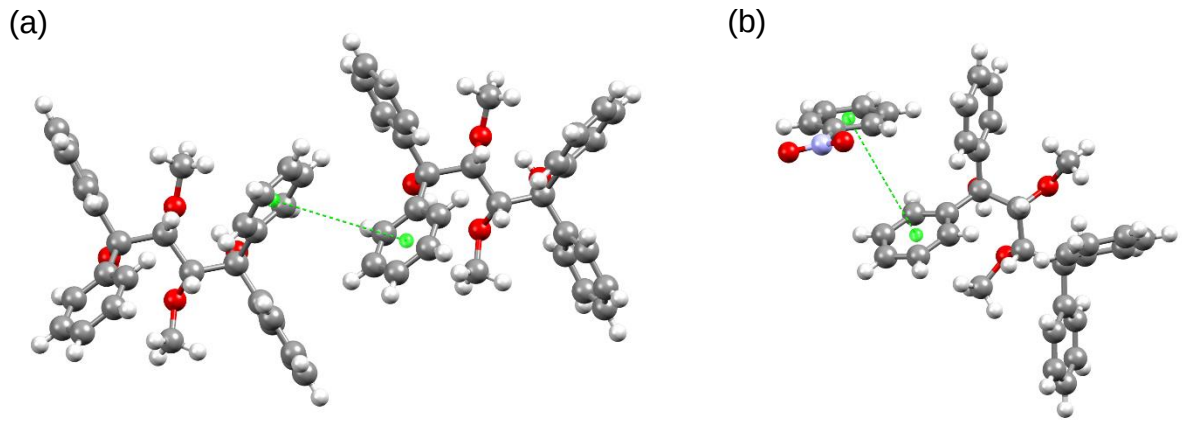

Figure 111: Two π–π stacking interactions from the 2DMT•nitrobenzene complex; a) an intermolecular host–host interaction; b) an intermolecular host–guest interaction.

Inter- and intra- molecular CH–π interactions are observed throughout these complexes. These all involve only host molecules. The majority are intramolecular between a host methoxy hydrogen and an adjacent phenyl ring [2.81–2.96 Å, 142–153°]. With the exception of 2DMT•*m*-NT, each complex also has an intermolecular CH–π interaction between a host *meta*-hydrogen and a phenyl ring of another host. These interactions all have a length of 2.97 Å (170–174°), and are listed in Table 55, while Figure 112 displays some of these interactions for better clarity.

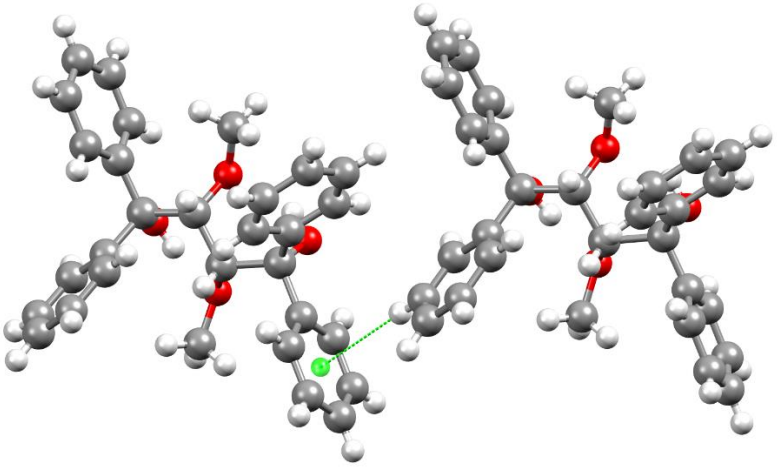

Figure 112: CH–π stabilizing interaction between two hosts in the 2DMT•nitrobenzene complex. The interaction is depicted as a green dashed line.

Table 55: CH–π stabilizing interactions in the host–guest complexes of DMT with the nitro-substituted aromatic guests.

Complex	Non-covalent interaction	Distance (Å)	Angle (°)	Symmetry operator
2DMT•nitrobenzene	(host methoxy)C-H···Cg(host)	2.91	149	x,y,z
	(host methoxy)C-H···Cg(host)	2.87	147	x,y,z
	(host methoxy)C-H···Cg(host)	2.81	152	x,y,z
	(host methoxy)C-H···Cg(host)	2.81	144	x,y,z
	(host)*m*-ArH···Cg(host)	2.97	171	1–x, y, 1–z
2DMT•*p*-NT	(host methoxy)C-H···Cg(host)	2.96	152	x,y,z
	(host methoxy)C-H···Cg(host)	2.87	147	x,y,z
	(host methoxy)C-H···Cg(host)	2.92	153	x,y,z
	(host methoxy)C-H···Cg(host)	2.88	144	x,y,z
	(host)*m*-ArH···Cg(host)	2.97	174	1–x, y, 1–z
2DMT•*m*-NT	(host methoxy)C-H···Cg(host)	2.91	150	x,y,z
	(host methoxy)C-H···Cg(host)	2.84	147	x,y,z
	(host methoxy)C-H···Cg(host)	2.84	153	x,y,z
	(host methoxy)C-H···Cg(host)	2.90	142	x,y,z
2DMT•*o*-NT	(host methoxy)C-H···Cg(host)	2.92	149	x,y,z
	(host methoxy)C-H···Cg(host)	2.84	147	x,y,z
	(host methoxy)C-H···Cg(host)	2.87	150	x,y,z
	(host methoxy)C-H···Cg(host)	2.88	145	x,y,z
	(host)*m*-ArH···Cg(host)	2.97	170	1–x, y, 1–z

Short contacts

A multitude of other short contacts is also present in each complex. The contacts that are shorter than the sum of the van der Waals radii of the participating atoms are listed in Table 56. Host–host short contacts are comprised mainly of interactions between a host hydroxy hydrogen and a *para*-aromatic hydrogen of another host, the shortest of which occurs in the 2DMT•nitrobenzene complex (2.26 Å, 151°). Notable host–guest short contacts include a (host)*p*-ArH···O-N(guest nitro) interaction in the 2DMT•nitrobenzene complex (2.66 Å, 160°), a (host)*o*-ArC···*o*-ArH(guest) interaction in the 2DMT•*m*-NT complex (2.69 Å, 150°), and (host)*m*-ArH···O-N(guest nitro) in the 2DMT•*o*-NT complex (2.59 Å, 136°) (Figure 113). Table 56 lists these short contacts in more detail.

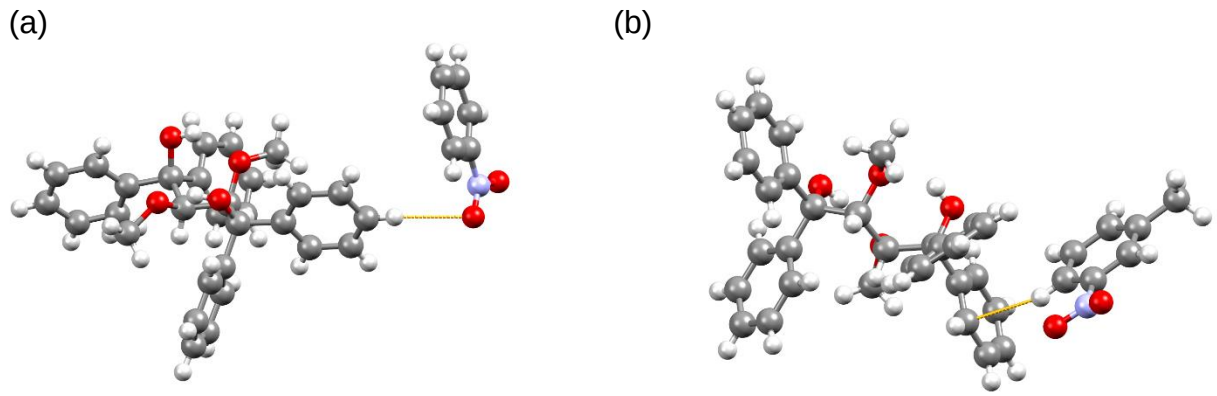

Figure 113: Short contacts in the complexes of a) 2DMT•nitrobenzene [(host)*p*-ArH···O-N(guest nitro)] and b) 2DMT•*m*-NT [(host)*o*-ArC···*o*-ArH(guest)].

Table 56: Summary of the various contacts shorter than the van der Waals radii found in the DMT complexes with the nitro-substituted aromatic guests.

Complex	Non-covalent interaction	Distance (Å)	Angle (°)	Symmetry operator
2DMT•nitro-benzene	(host hydroxy)O-H···*p*-ArH(host)	2.29	108	–1/2+x,1/2+y,z
	(host hydroxy)O-H···*p*-ArH(host)	2.26	151	1/2+x,1/2+y,z
	(host)*p*-ArH··· *m*-ArC(host)	2.84	147	1–x,y,–z
	(host)*p*-ArH···O-N(guest nitro)	2.66	160	3/2–x,1/2+y,1–z
2DMT•*p*-NT	(host hydroxy)O-H···*p*-ArH(host)	2.30	104	–1/2+x,1/2+y,z
	(host methoxy)C-O···*m*-ArH(host)	2.52	118	3/2–x,1/2+y,1–z
	(host hydroxy)O-H···*p*-ArH(host)	2.28	146	1/2+x,1/2+y,z
2DMT•*m*-NT	(host hydroxy)O-H···*p*-ArH(host)	2.36	104	–1/2+x,1/2+y,z
	(host hydroxy)O-H···*p*-ArH(host)	2.33	150	1/2+x,1/2+y,z
	(host)*o*-ArC···*o*-ArH(guest)	2.69	150	1/2+x,1/2+y,z
	(host)*m*-ArH···H-C(guest methyl)	2.25	113	x,y,z
2DMT•*o*-NT	(host hydroxy)O-H···*p*-ArH(host)	2.38	101	1/2+x,–1/2+y,z
	(host hydroxy)O-H···*p*-ArH(host)	2.35	151	–1/2+x,1/2+y,z
	(host)*m*-ArH···O-N(guest nitro)	2.59	136	1–x,y,2–z

All the notable host–guest interactions obtained from these X-ray diffraction data are now summarized in Table 57 for ease of comparison and to extract any further explanation for the selectivity behaviour of DMT observed for these guests. Host–guest π–π stacking interactions are the most numerous throughout these complexes, with the largest number occurring in the preferred 2DMT•nitrobenzene complex (9) and the lower number in the less preferred 2DMT•*o*-NT complex (6). None of the complexes showed any CH–π stacking interactions. Further consideration of the interactions listed in this table does not expand on the understanding of DMT's preference for these guests as the complex formed with the more preferred p-NT guest experienced no short contacts. In contrast, the lesser preferred 2DMT•o-NT complex had one short contact while the 2DMT•*m*-NT complex had two short contacts of which one is significantly shorter than the sum of the van der Waals radii of the participating atoms.

Table 57: Significant host–guest interactions for the complexes of DMT with the nitro-substituted aromatic guests.

Interaction	2DMT•nitrobenzene	2DMT•*p*-NT	2DMT•*m*-NT	2DMT•*o*-NT
π–π	5.217(4)–5.845(3)Å (9 contacts)	5.191(1)–5.788(1) Å (8 contacts)	4.842(2)–5.883(3) Å (8 contacts)	4.901(2)–5.434(3) Å (6 contacts)
CH–π	None	None	None	None
Short contacts	2.66 Å, 160°, < (host)*p*-ArH···O-N(guest nitro)	None	2.69 Å, 150°, << (host)*o*-ArC···*o*-ArH(guest) 2.25 Å, 113°, < (host)*m*-ArH···H-C(guest methyl)	2.59 Å, 136°, < (host)*m*-ArH···O-N(guest nitro)

*< denotes contacts less than the sum of the van der Waals radii and << denotes contacts less than this sum minus 0.2 Å.

The mode of guest packing was also investigated but did not advance the argument further since all the guests are held in discrete cavities in each complex; this is unsurprising as the host packing is isostructural (Figure 114).

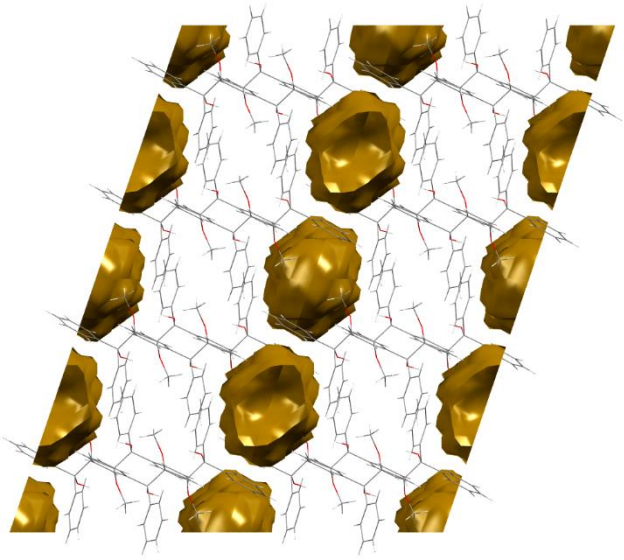

Figure 114: The discrete cavity guest packing mode in the 2DMT•nitrobenzene complex as representative example of the guest packing in all the complexes with the nitro-substituted aromatic guests.

7.6 Hirshfeld Surface Analysis

Hirshfeld surface analysis was, once more, employed in order to visualise the quantity of contacts in these host-guest complexes. The fingerprint plot for the 2DMT•nitrobenzene complex (Figure 115a) is characterised by a spike, S1, indicative of C···H interactions. It is overlapped, however, by the wing W1 and, together with W2, these represent H···H interactions. Finally, W2 overlaps with W3 which is the result of O···H interactions between host and guest. In contrast, the fingerprint plot of the 2DMT•*p*-NT complex (Figure 115b) is more simplified, with C···H interactions being visualized by W1, and W2 being representative of H···H interactions. O···H interactions are found spread out further away from the origin of the plot. The 2DMT•*m*-NT fingerprint (Figure 115c) exhibits two prominent spikes. S1 is indicative

of C···H interactions while S2 and W1 arise due to H···H interactions. Finally, the 2DMT•*o*-NT complex (Figure 115d) has an area, W1, telling of C···H interactions being overlapped by W2 for H···H interactions. The prominent spike S1 is as a result of O···H interactions, while S2 is again due to C···H contacts.

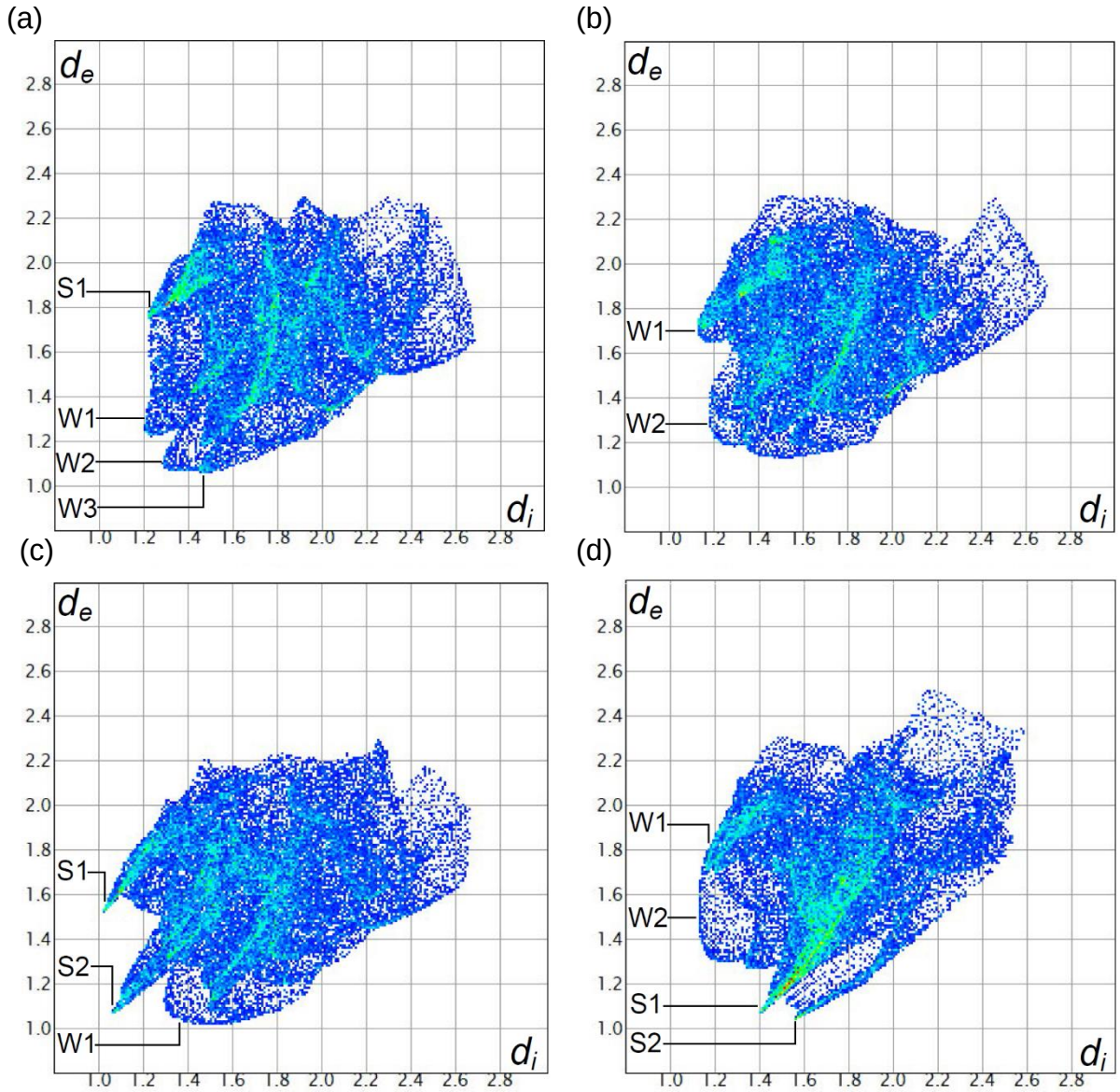

Figure 115: Two-dimensional fingerprint plots obtained from Hirshfeld surfaces for the inclusion complexes of a) 2DMT•nitrobenzene, b) 2DMT•*p*-NT, c) 2DMT•*m*-NT and d) 2DMT•*o*-NT.

The quantity and type of each interaction are shown in Figure 116 in a graphic manner. While the amount of H···H interactions is relatively evenly distributed across these complexes (42–48%), it would appear as though the lesser preferred *m*-NT guest has the highest percentage of these interactions (48%), as well as the lowest amount of C···H interactions (15%). Furthermore, the more preferred guests, nitrobenzene and *p*-NT, are the only guests to experience N···H interactions (1.5% and 2.5%, respectively). That no definite trends can be identified from Figure 116 for the 2DMT•nitrobenzene and 2DMT•*p*-NT complexes may be symptomatic of the more concentration-dependent behaviour DMT exhibits towards these guests.

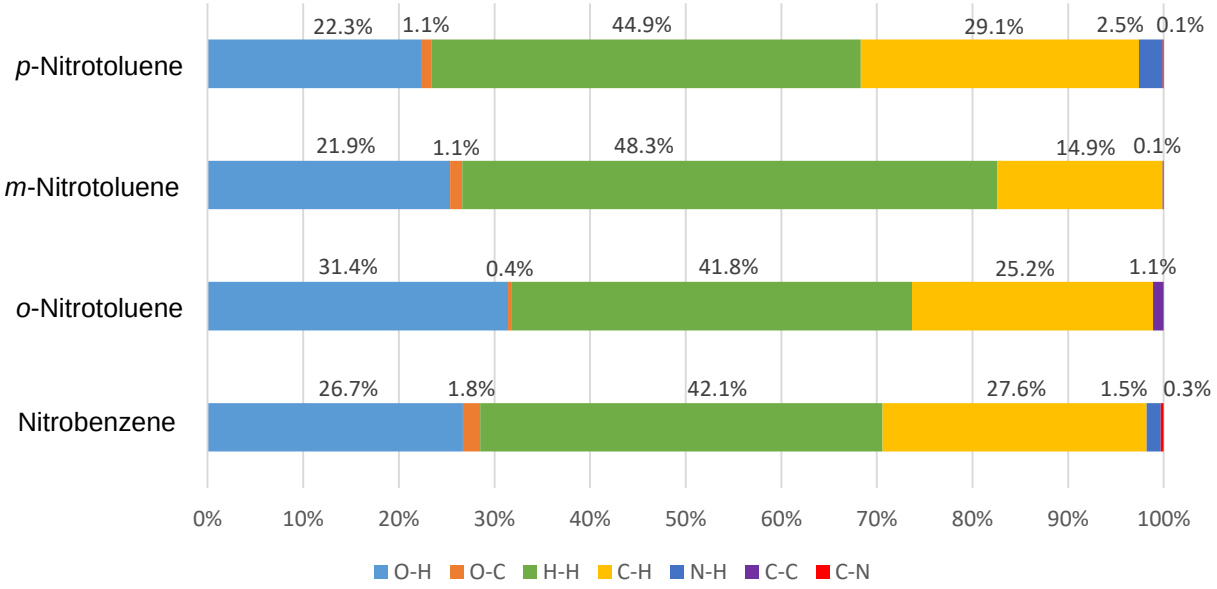

Figure 116: Graphical display showing the percentage and type of intermolecular interactions in each complex.

7.7 Conclusion

DMT was successful in forming 2:1 host:guest inclusion compounds with nitrobenzene and the nitrotoluene isomers. An equimolar binary competition experiment demonstrated that DMT has a near-equal preference for *p*-NT and nitrobenzene, whereas p-NT (39.9%) is preferred over nitrobenzene (30.2%) in a quaternary mixture. Non-equimolar binary competition experiments between these two guests indicated that DMT's preference toward them changed based on the concentration of the guests, and therefore host selectivity remained low for these guests when they competed. Significantly, nitrobenzene and *p*-NT were both preferred over *o*-NT and *m*-NT. Selectivity between *o*-NT and *m*-NT was also based on their concentrations when mixed. Thermal analyses correlated well with the observation that nitrobenzene and *p*-NT were more preferred to *o*-NT and *m*-NT as determined by the decreasing values of T_{on}–T_b. Single crystal X-ray analysis did not reveal any significant insights into the reasons for the selectivity displayed by DMT, but Hirshfeld surface analysis did show that only *p*-NT and nitrobenzene, the preferred guests, experience any N···H interactions.

Chapter 8: Inclusion Compounds of DMT (73) with Anisole and the Methylanisole Isomers

8.1 Introduction

Anisole, *p*-methylanisole (*p*-MA), *m*-methylanisole (*m*-MA) and *o*-methylanisole (*o*-MA) are aromatic compounds obtained from the methylation of phenol or the appropriate cresol. The methylation proceeds in high yield under basic conditions with dimethyl sulfate as methylating agent. These anisoles are all routinely used in fragrances and perfumes, and are also starting materials in the synthesis of natural products.[173] *p*-MA is a precursor to *p*-anisaldehyde, which has application in the fragrance industry and as a drug precursor.[186] *p*-MA serves as a starting material in the synthesis of (±)-cacalol, while *m*-MA has been employed in the preparation of calyciphylline A-type alkaloids; *o*-MA is a building block in the synthesis of (±)-mutisianthol.[187-189] While not usually present in mixtures, it is still interesting from an academic point of view to determine whether or not DMT will selectively include these compounds and, if so, to investigate the driving force behind any selective behaviour displayed by the host.

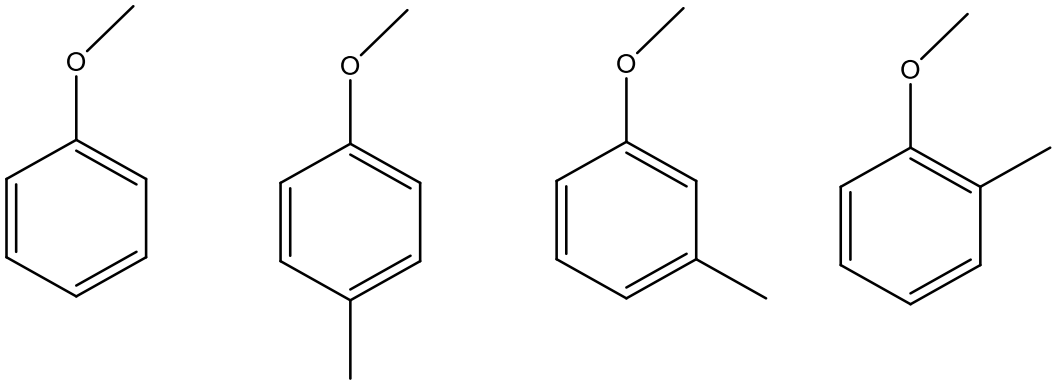

Anisole *p*-MA *m*-MA *o*-MA

8.2 Individual and Equimolar Inclusion Experiments

After independent recrystallizations of DMT from anisole and the isomeric methylanisoles, the resultant solids were subjected to ^{1}H-NMR spectroscopy. Consequently, it was found that DMT included each of these guests in a 2:1 host:guest ratio (Table 58).

Table 58: Host:guest ratios of complexes formed with DMT during individual recrystallization experiments.*

Guest	Host:guest
Anisole	2:1
o-MA	2:1
m-MA	2:1
p-MA	2:1

*Determined using ^{1}H-NMR spectroscopy

Various binary and ternary competition experiments were carried out by recrystallizing DMT from equimolar mixtures of these anisole guests. In each competition experiment, the overall host:guest ratio remained 2:1 (Table 59). A binary experiment involving *o*-MA and *m*-MA showed that DMT preferred the latter guest (71.6%), while that comprising *o*-MA and *p*-MA showed a DMT preference for *p*-MA (88.8%). This guest was also preferred when competing with *m*-MA (*p*-MA, 73.5%). When unsubstituted anisole was made to compete with the methylanisole guests, anisole was now consistently preferred. In a binary experiment between anisole and *p*-MA, 66.9% of anisole was extracted from the mixture. Similarly, anisole was preferred when competing against *m*-MA (86.7%) and *o*-MA (92.6%). In a ternary competition experiment between only the methylanisole guests, *p*-MA (58.5%) was preferred over *m*-MA (29.1%) and *o*-MA (12.4%). As with the binary experiments, ternary competitions in which anisole was used as a component resulted in DMT preferentially including anisole once more. Using an anisole/*p*-MA/*m*-MA mixture, 46.0% of anisole was included, while the anisole/*p*-MA/*o*-MA and anisole/*m*-MA/*o*-MA experiments

resulted in anisole inclusions of 51.1 and 68.0%, respectively. A quaternary competition mixture incorporating all four guest solvents resulted in 44.0% of anisole being included followed by *p*-MA, *m*-MA and *o*-MA (35.9, 14.6 and 5.5%, respectively).

Table 59: Competition experiments and H:G ratios obtained.*

Anisole	*o*-MA	*m*-MA	*p*-MA	Guest ratios (% e.s.d.)[$]	Overall H:G ratio
	x	***x***		28.4:**71.6** (1.14)	2:1
	x		***x***	11.2:**88.8** (0.98)	2:1
		x	***x***	26.5:**73.5** (0.07)	2:1
	x	x	***x***	12.4:29.1:**58.5** (4.13)(1.91)(2.92)	2:1
x	x			**92.6**:7.4 (0.47)	2:1
x		x		**86.7**:13.3 (0.49)	2:1
x			x	**66.9**:33.1 (0.49)	2:1
x	x	x		**68.0**:9.5:22.5 (1.40)(1.39)(1.35)	2:1
x	x		x	**51.1**:6.3:42.6 (1.27)(1.10)(0.99)	2:1
x		x	x	**46.0**:14.9:39.1 (1.35)(1.15)(1.02)	2:1
x	x	x	x	**44.0**:5.5:14.6:35.9 (1.22)(1.02)(0.97)(1.13)	2:1

*Determined using GC-MS; [$]experiments were carried out in triplicate, and an average ratio is provided here with % e.s.d.'s in parentheses

8.3 Host Selectivity Profiles with Changing Guest Concentrations in Binary and Ternary Guest Mixtures

DMT was subsequently recrystallized from binary solutions in which the guests were present in non-equimolar amounts, and selectivity curves were constructed from the data obtained after the analysis (GC-MS) of both resultant crystals and the mother liquors.

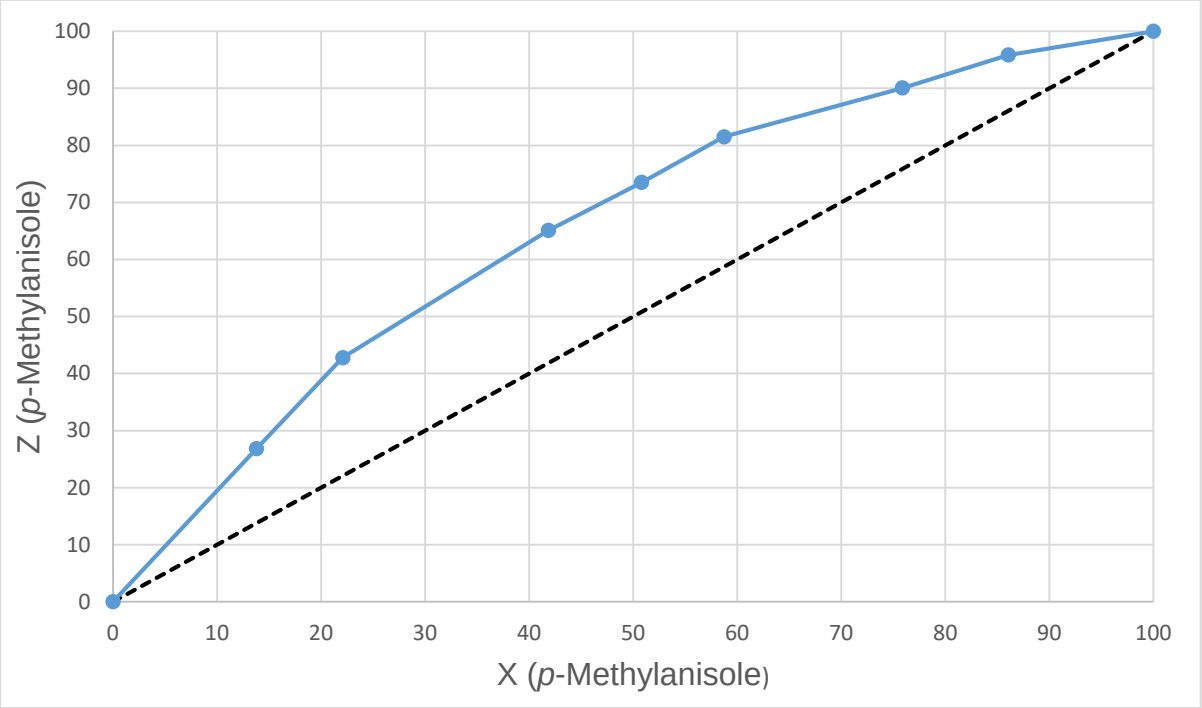

Figure 117: Selectivity curve obtained from the *p*-MA/*m*-MA experiments. Coloured blue is the molar fraction of *p*-MA in the inclusion complex (Z) *vs* the molar fraction of *p*-MA in the mother liquor (X). Black dashes indicate the theoretical line of no selectivity.

Figure 117 was obtained from the *p*-MA/*m*-MA experiment and indicated that *p*-MA was preferred over *m*-MA over all the guest composition ratios assessed. With a mother liquor composition of approximately 22% *p*-MA, the crystals contained ~43% *p*-MA. Increasing the *p*-MA content in the mother liquor (~76%) further decreased the

m-MA content in the inclusion complex (~10%). The selectivity coefficient, K, for this competition mixture, was found to be 2.84.

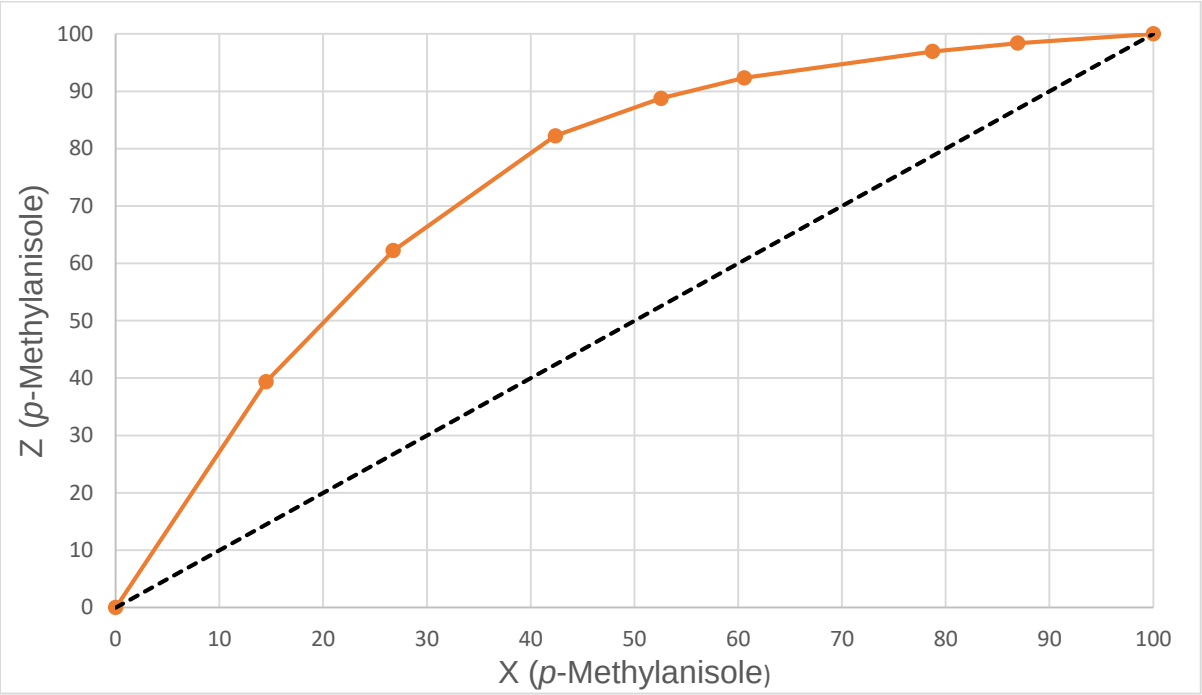

Figure 118: Selectivity curve obtained from the *p*-MA/*o*-MA experiments. Coloured orange is the molar fraction of *p*-MA in the inclusion complex (Z) *vs* the molar fraction of *p*-MA in the mother liquor (X). Black dashes indicate the theoretical line of no selectivity.

When *p*-MA was made to compete against *o*-MA in unequal amounts, the selectivity curve in Figure 118 resulted. *p*-MA was considerably preferred over *o*-MA over the entire molar concentration range. At low *p*-MA concentrations (~14.5%), the crystals already contained ~39% *p*-MA, and at a mother liquor composition of ~61% *p*-MA, the inclusion complex contained ~92% *p*-MA. From this point onwards, the included *p*-MA content approached 100%: at a mother liquor composition of ~87% *p*-MA the inclusion complex contained ~98% of this guest. In comparison to Figure 117, it is clear that DMT is more selective towards *p*-MA when in competition with *o*-MA than it is when *p*-MA and *m*-MA competed, and the selectivity coefficient for this experiment, 6.77, confirmed this observation since it is significantly higher than in the *p*-MA/*m*-MA experiments (2.84).

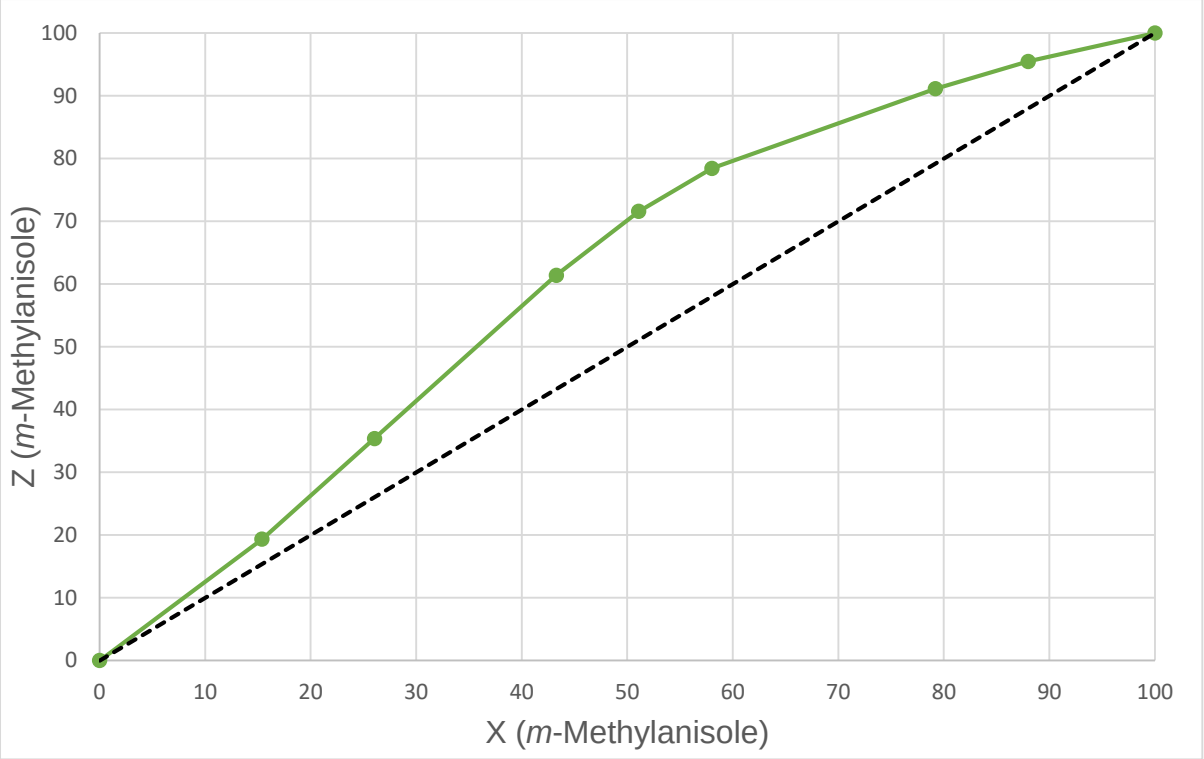

Figure 119: Selectivity curve obtained from the *m*-MA/*o*-MA experiments. Coloured green is the molar fraction of *m*-MA in the inclusion complex (Z) *vs* the molar fraction of *m*-MA in the mother liquor (X). Black dashes indicate the theoretical line of no selectivity.

In contrast to Figure 118, the selectivity curve for the *m*-MA/*o*-MA experiment has a much flatter trajectory (Figure 119). Initially, there existed a lower DMT selectivity for these two guests: at a mother liquor composition of ~15% *m*-MA, the inclusion complex contained only ~19% of this guest. At higher *m*-MA concentrations, the selectivity increased for *m*-MA, as demonstrated by the point corresponding to a mother liquor content of ~79%, where an inclusion content of ~91% of *m*-MA was obtained. The average selectivity coefficient for this experiment was 2.22, the lowest of the three calculated thus far.

A further selectivity experiment was carried out during which DMT was recrystallized from mixtures containing all three methylanisole guests in differing molar amounts. In all seven recrystallizations performed, the percentage *m*-MA in the inclusion complex decreased by ~1.3–11.7% relative to the mother liquor. The *o*-MA content decreased also, but to a larger extent (12.0–20.8%), while the amount of *p*-MA in the inclusion

complexes increased substantially in each case (15.4–26.3%). Figure 120 shows the ternary selectivity plot for these experiments, with the red squares indicating that the guest content of the inclusion complexes drifted noticeably towards higher *p*-MA percentages, regardless of the initial *p*-MA concentration.

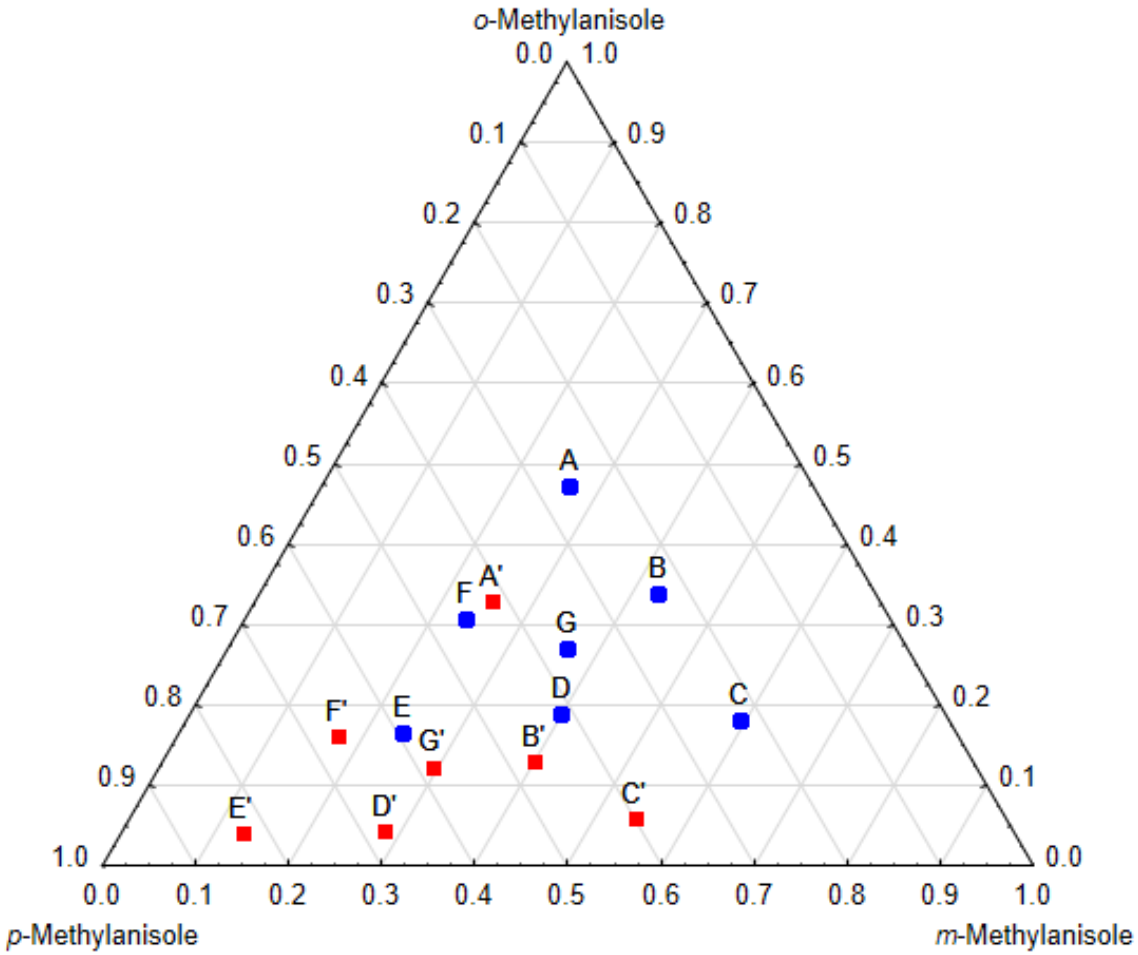

Figure 120: Ternary competition plot obtained from the *p*-MA/*m*-MA/*o*-MA experiments. Blue circles indicate mother liquor compositions, while red squares indicate guest compositions in the.

As the selectivity of DMT towards the methylanisole guests is clearly in favour of *p*-MA, we subsequently thought it interesting to determine if any selectivity changes would occur when the unsubstituted anisole was made to compete with these

methylanisoles in binary mixtures. Figures 121–123 indicate the outcome of these experiments.

Owning to the nature of the curve generated from the anisole/*p*-MA experiments (Figure 121), it is clear that DMT does not display highly selective behaviour in the presence of these two guests. This observation is demonstrated by considering the inclusion complex obtained from a mother liquor composition of approximately 9% anisole, which contained only 13% of this guest, while the complex generated from a mixture with 72% anisole contained only 84% anisole. The average selectivity coefficient in this case was determined to be 1.92.

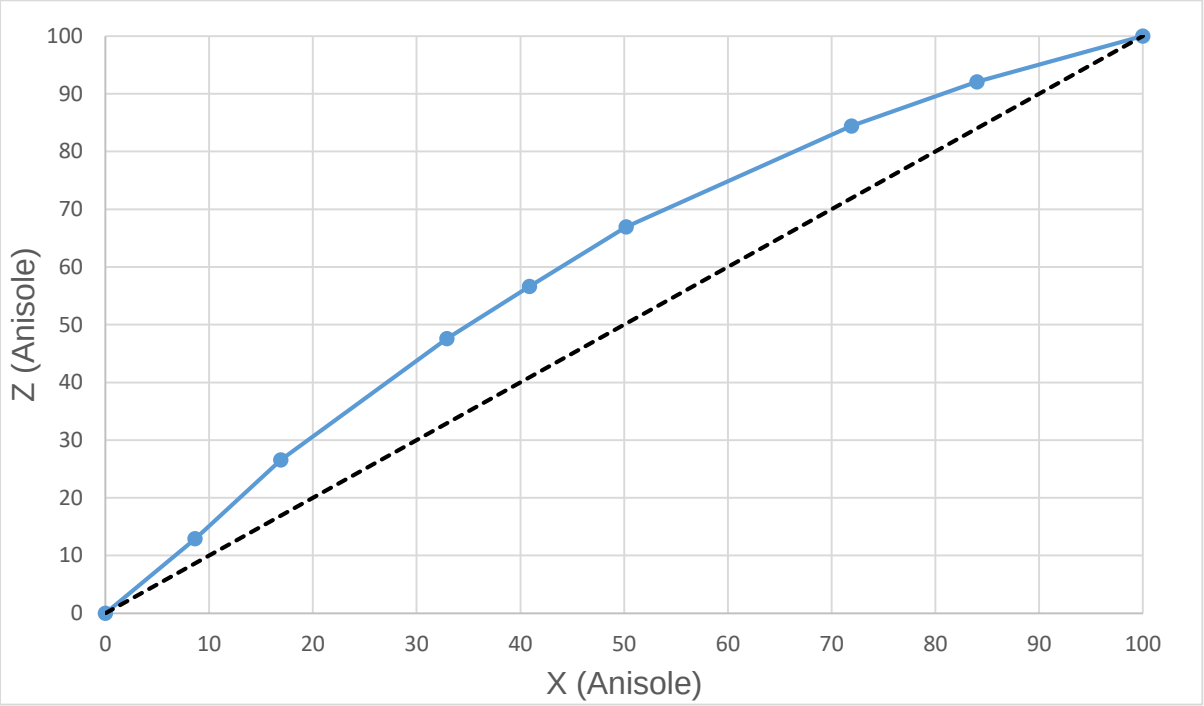

Figure 121: Selectivity curve obtained from the anisole/*p*-MA experiments. Coloured blue is the molar fraction of anisole in the inclusion complex (Z) *vs* the molar fraction of anisole in the mother liquor (X). Black dashes indicate the theoretical line of no selectivity.

In contrast to the anisole/*p*-MA experiment, the selectivity curve obtained from the anisole/*m*-MA experiment (Figure 122) indicates a high selectivity in favour of anisole. From a mother liquor composition of approximately 8% anisole, crystals were obtained

containing ~36% anisole. When DMT was crystallized from a mixture with a mother liquor composition of ~70% aniline (~30% *m*-MA), the crystals comprised ~93% aniline. The average K value for this experiment was found to be 5.89.

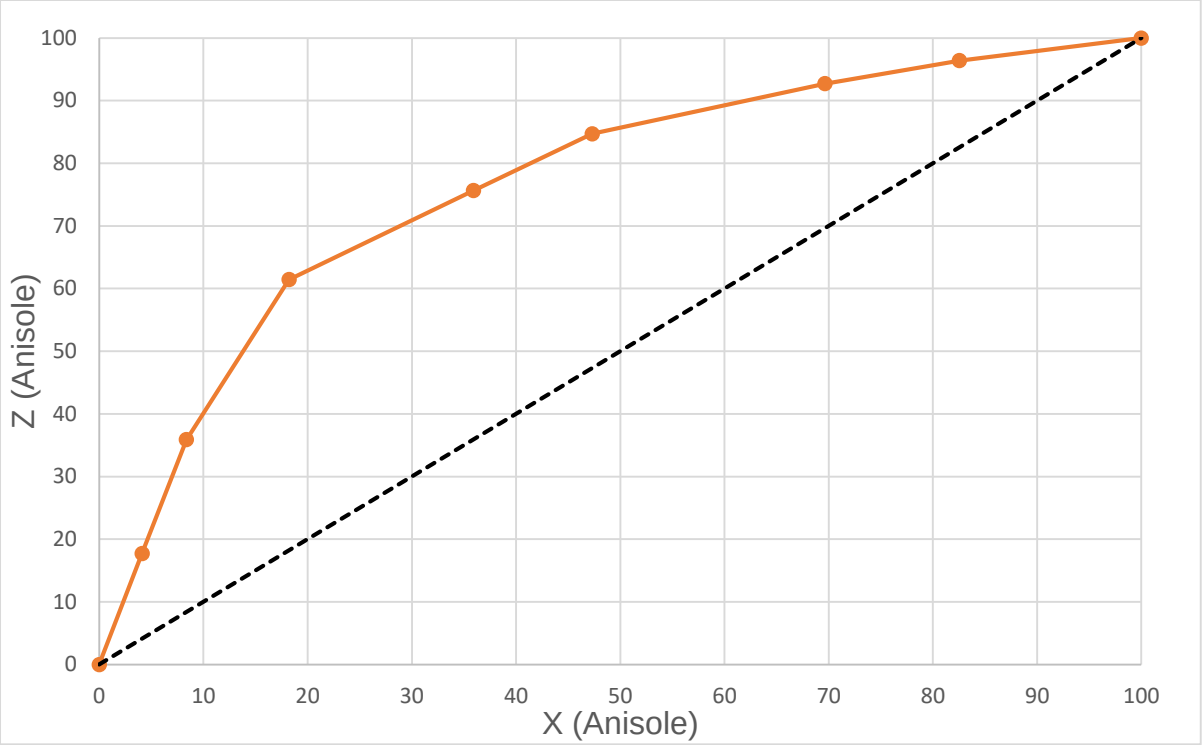

Figure 122: Selectivity curve obtained from the anisole/*m*-MA experiments. Coloured orange is the molar fraction of anisole in the inclusion complex (Z) *vs* the molar fraction of anisole in the mother liquor (X). Black dashes indicate the theoretical line of no selectivity.

The results of the anisole/*o*-MA experiment (Figure 123) are comparable to that of Figure 122 except that higher selectivities are observed for anisole in Figure 123: from a mother liquor composition of 16% anisole and 84% *o*-MA, DMT formed a complex containing ~62% anisole, while an inclusion compound containing 90% anisole was obtained when the mother liquor comprised only 39% anisole. The average K for this experiment was 11.62, significantly higher than for the previous two selectivity curves where anisole was also present as a guest.

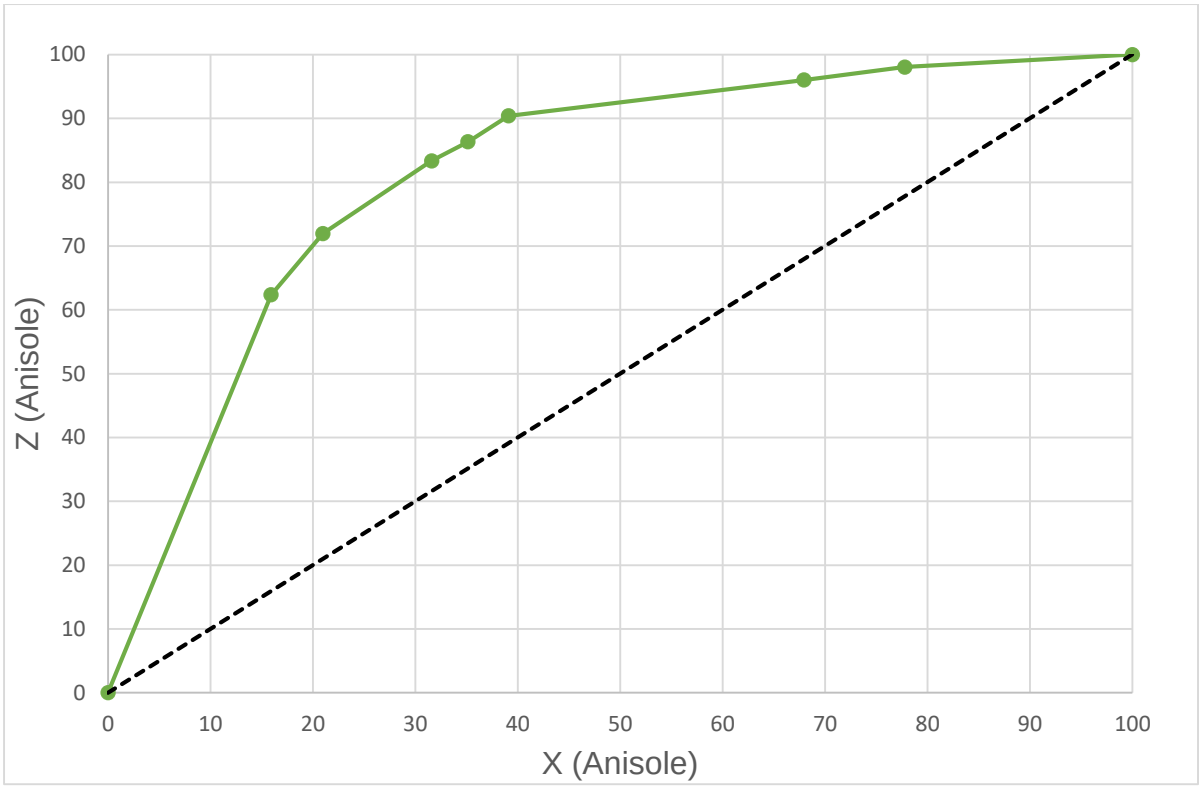

Figure 123: Selectivity curve obtained from the anisole/*o*-MA experiments. Coloured green is the molar fraction of anisole in the inclusion complex (Z) *vs* the molar fraction of anisole in the mother liquor (X). Black dashes indicate the theoretical line of no selectivity.

Careful consideration of the results obtained in the single competition and selectivity curve experiments yielded an overall selectivity order of *p*-MA > *m*-MA > *o*-MA when considering only the methyl-substituted anisole guests. When unsubstituted anisole was added to these experiments, DMT preferentially included this guest, followed by the methyl anisoles in the same order as before, *i.e.*, anisole > *p*-MA > *m*-MA > *o*-MA.

8.4 Thermal Analysis

Once more, thermal analyses were carried out on each inclusion complex. Upon heating, thermal events were monitored through thermogravimetric analysis and differential scanning calorimetry. Figures 124–127 show the TG, DTG and DSC traces obtained for each complex upon heating at 10 °C.min^{-1} under high purity nitrogen as a purge gas.

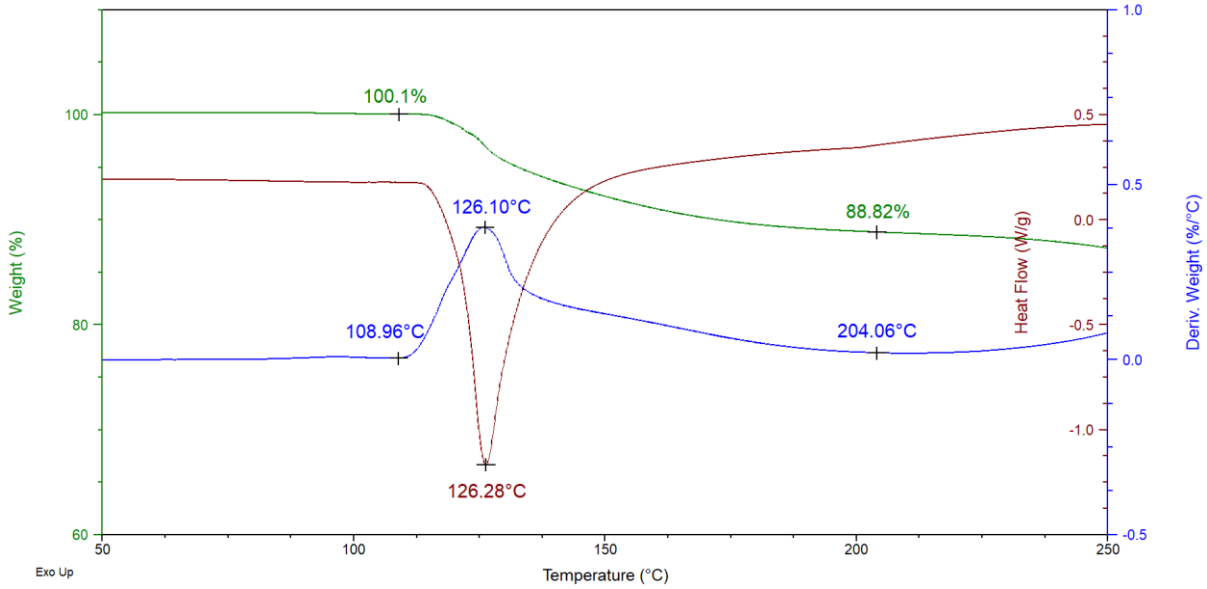

Figure 124: Overlaid TG (green), DTG (blue) and DSC (brown) traces for the 2DMT•anisole complex upon heating at 10 °C.min^{-1}.

The expected mass loss upon removal of all of the guest from a 2:1 DMT•anisole inclusion complex is 10.6%. The TG trace (Figure 124, green) indicates a mass loss of ~11.3% which correlates well with that expected. The onset temperature of the mass loss process was approximately 109.0 °C, while cessation of mass loss occurred at ~204.1 °C (DTG). One endotherm with a peak maximum at 126.3 °C is observed, representing concomitant host melt and guest release events (DSC). Furthermore, the maximum rate of guest release occurred at 126.1 °C (DTG).

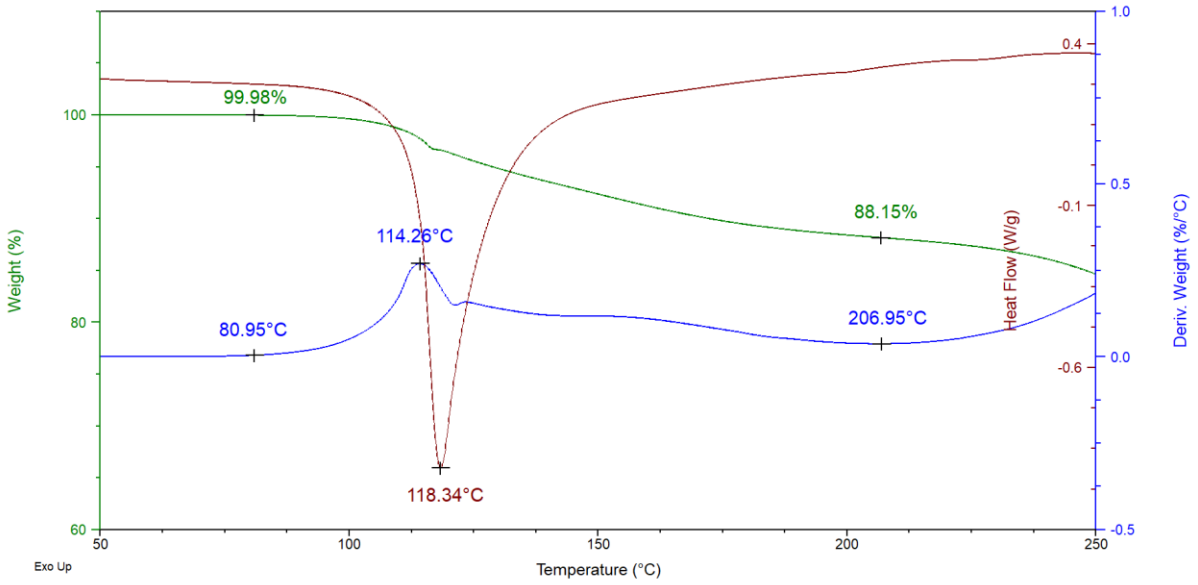

Figure 125: Overlaid TG (green), DTG (blue) and DSC (brown) traces for the 2DMT•*p*-MA complex upon heating at 10 °C.min^{-1}.

The 2:1 DMT•*p*-MA complex experiences an 11.8% mass loss which is in direct agreement with the 11.8% expected for this complex (TG) (Figure 125). The onset of guest release occurred at ~81.0 °C which is significantly lower than that of the more preferred anisole in the 2DMT•anisole complex (DTG). The mass loss experienced a plateaux at ~207.0 °C corresponding to the cessation of guest release, after which the mass loss increased once more due to host decomposition. The single endotherm peak for the simultaneous host melt and guest release events occurred at approximately 118.3 °C (DSC), and the maximum rate of guest release was observed at 114.3 °C (DTG).

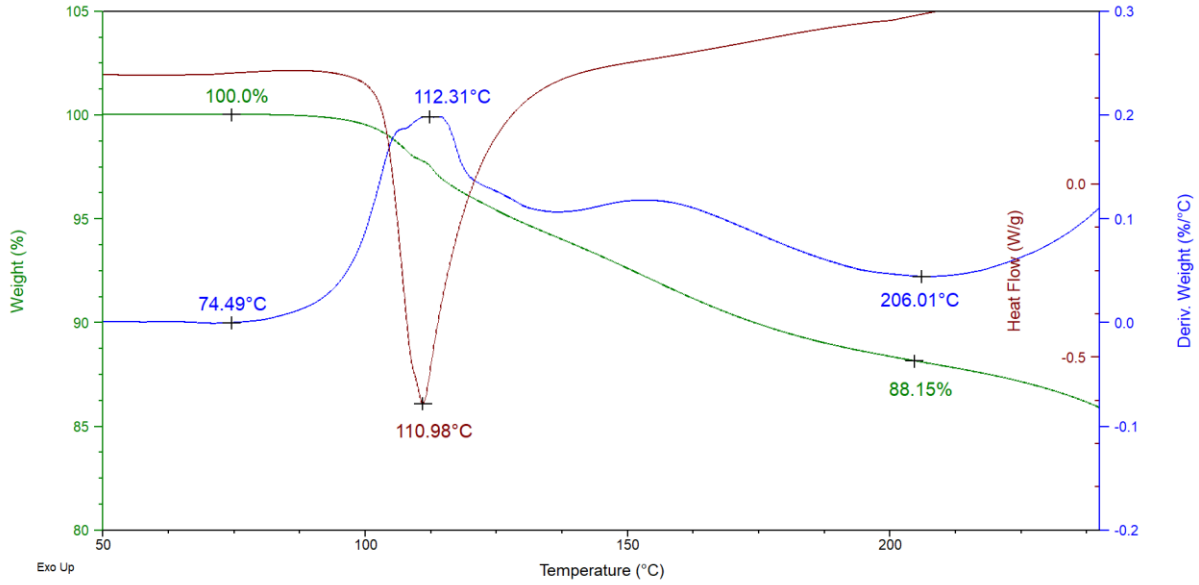

Figure 126: Overlaid TG (green), DTG (blue) and DSC (brown) traces for the 2DMT•*m*-MA complex upon heating at 10 °C.min^{-1}.

The mass loss due to guest release experienced by the 2DMT•*m*-MA complex was observed to be 11.9%, as in the previous case, once more agreeing with the amount required for a 2:1 host:guest inclusion complex (TG) (Figure 126). The guest release process initiated at 74.5 °C (DTG), while the cessation of mass loss due to guest release was determined to occur at ~206.0 °C, as indicated by the inflection of the DTG trace (Figure 126, blue). The maximum rate of guest release was at ~112.3 °C (DTG), and the peak endotherm for both guest release and host melt events occurred at 111.0 °C (DSC).

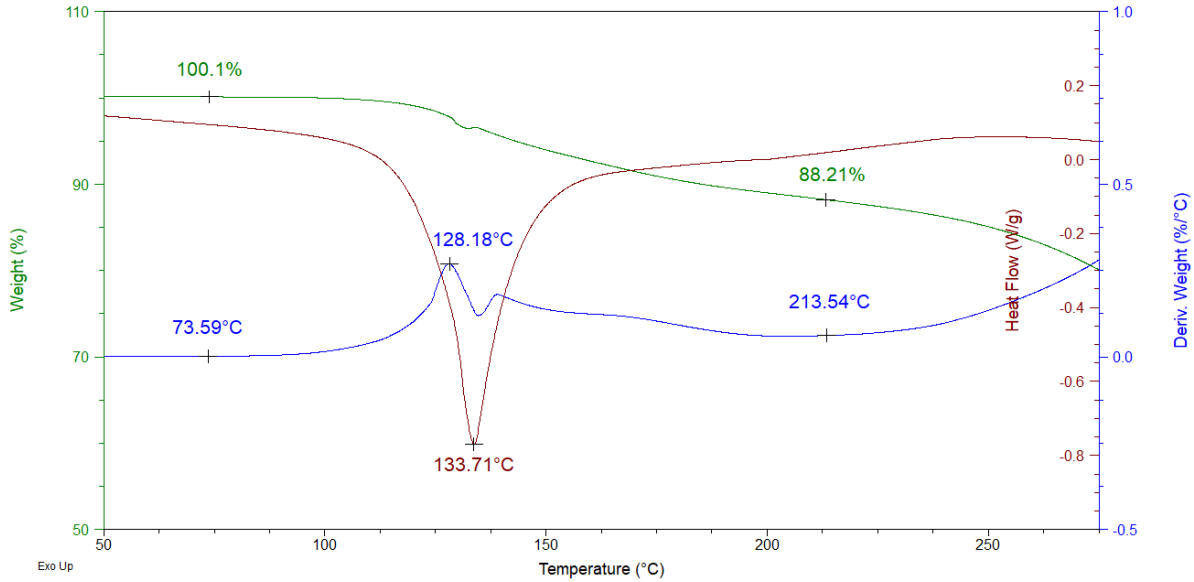

Figure 127: Overlaid TG (green), DTG (blue) and DSC (brown) traces for the 2DMT•*o*-MA complex upon heating at 10 °C.min^{-1}.

Once more, the mass loss due to guest release for the 2:1 DMT•*o*-MA complex (11.9%) agreed with that expected (11.8%) (TG, Figure 127). The onset temperature of mass loss ensued at ~73.6 °C while the maximum rate of mass loss was at ~128.2 °C (DTG). After the mass loss inflection point at ~213.5 °C, host decomposition was responsible for the observed further mass loss. Finally, the endotherm peak for concomitant guest release and host melt occurred at 133.7 °C (DSC).

The relevant thermal data for these experiments are summarized in Table 60. The assessment of the term T_{on}–T_b[160,161] may be considered valid for these experiments as the single crystal X-ray structures for all four inclusion complexes are isostructural. Determination of T_{on}–T_b indicated a thermal stability order of anisole (–44.7 °C) >> *p*-MA (–94.5 °C) > *o*-MA (–94.7 °C) > *m*-MA (–101.0 °C) (Table 60). This is in reasonable agreement with the observed selectivity order (anisole > *p*-MA > *m*-MA > *o*-MA).

Table 60: Summary of the major thermal events observed in the anisole and methylanisole complexes with DMT.

Guest	T_b (°C)	T_{on} (°C)[a]	T_{on}–T_b (°C)	T_p (°C)[b]	T_{end} (°C)[c]	Mass loss % (Expected)
Anisole	153.7	109.0	–44.7	126.1	126.3	11.3 (10.6)
p-Methylanisole	175.5	81.0	–94.5	114.3	118.3	11.8 (11.8)
m-Methylanisole	175.5	74.5	–101.0	112.3	111.0	11.9 (11.8)
o-Methylanisole	171.0	73.6	–97.4	128.2	133.7	11.9 (11.8)

[a]T_{on} is the onset temperature for guest release estimated from the DTG; [b]T_p values were determined from the blue DTG traces; [c]T_{end} values were obtained from the brown DSC traces.

8.5 Single Crystal X-Ray Analysis

The individual inclusion complexes of DMT with anisole and the methylanisole isomers were further analysed by means of single crystal X-ray diffraction. The host framework was found to be isostructural in each case and each complex crystallized in the monoclinic *C*2 crystal system. Figure 128 is a stereoview to show the crystal packing, while Figure 129 shows the unit cells for these complexes. The different guest species suffer various degrees of disorder. In the case of anisole and *m*-MA, the disorder is symmetry-generated, but well modelled. *p*-Methylanisole exhibits two perpendicular axes of rotation, resulting in four overlapping structures. Finally, *o*-MA was badly disordered and the crystal structure was solved with a relatively large wR2 (0.2016). Table 61 lists additional crystallographic data for these complexes.

Table 61: Crystallographic data for the complexes between DMT and the four anisole guests.

	2DMT•Anisole	**2DMT•*p*-MA**	**2DMT•*m*-MA**	**2DMT•*o*-MA**
Chemical formula	$C_{30}H_{30}O_4$	$C_{30}H_{30}O_4$	$C_{30}H_{30}O_4$	$C_{30}H_{30}O_4$
	$\bullet 0.5C_7H_8O$	$\bullet 0.5C_8H_{10}O$	$\bullet 0.5C_8H_{10}0$	$\bullet 0.5C_8H_{10}O$
Formula weight	1017.21	1031.24	1031.24	1031.24
Crystal system	Monoclinic	Monoclinic	Monoclinic	Monoclinic
Space group	*C*2	*C*2	*C*2	*C*2
μ (Mo-Kα)/mm^{-1}	0.080	0.079	0.079	0.080
a/Å	17.3615(9)	17.1882(9)	17.3855(14)	17.4790(14)
b/Å	11.9898(7)	12.2958(7)	12.1202(10)	11.939(1)
c/Å	14.0450(7)	14.1345(8)	14.2982(12)	14.2189(12)
alpha/°	90	90	90	90
beta/°	109.318(2)	109.639(2)	110.411(3)	110.415(3)
gamma/°	90	90	90	90
V/$Å^3$	2758.9(3)	2813.5(3)	2823.7(4)	2780.9(4)
Z	2	2	2	2
F(000)	1084	1100	1100	1100
Temp./K	200	200	200	200

Restraints	1	10	1	11
Nref	6700	6532	7028	6887
Npar	384	332	382	327
R	0.0325	0.0579	0.0371	0.0631
wR2	0.0856	0.1689	0.1004	0.2016
S	1.03	1.05	1.05	1.07
θ min-max/°	2.1, 28.3	1.5, 28.4	2.1, 28.3	1.5, 28.3
Tot. data	25780	28064	49491	51842
Unique data	6700	6532	7028	6887
Observed data [I > 2.0 sigma(I)]	6083	5987	6469	6228
R_{int}	0.017	0.019	0.019	0.019
Dffrn measured fraction θ full	0.999	1.000	0.999	0.998
Min. resd. dens. (e/ Å^3)	–0.17	–0.82	–0.17	–0.80
Max. resd. dens. (e/ Å^3)	0.22	0.56	0.20	0.95

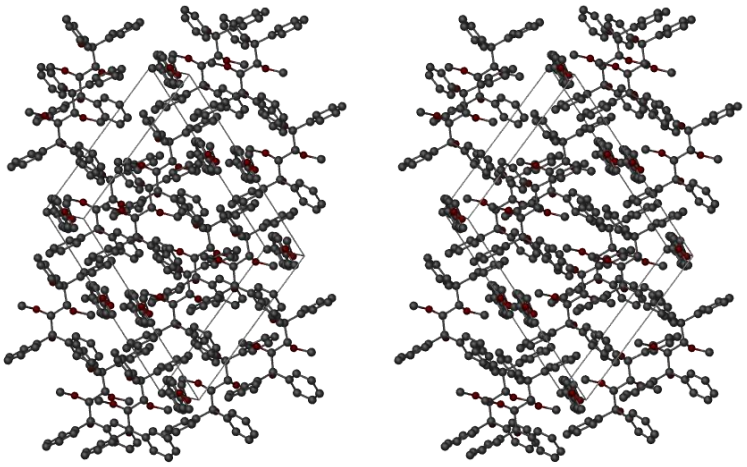

Figure 128: Stereoview of the 2DMT•*p*-MA complex to show the packing in three dimensions, as representative sample

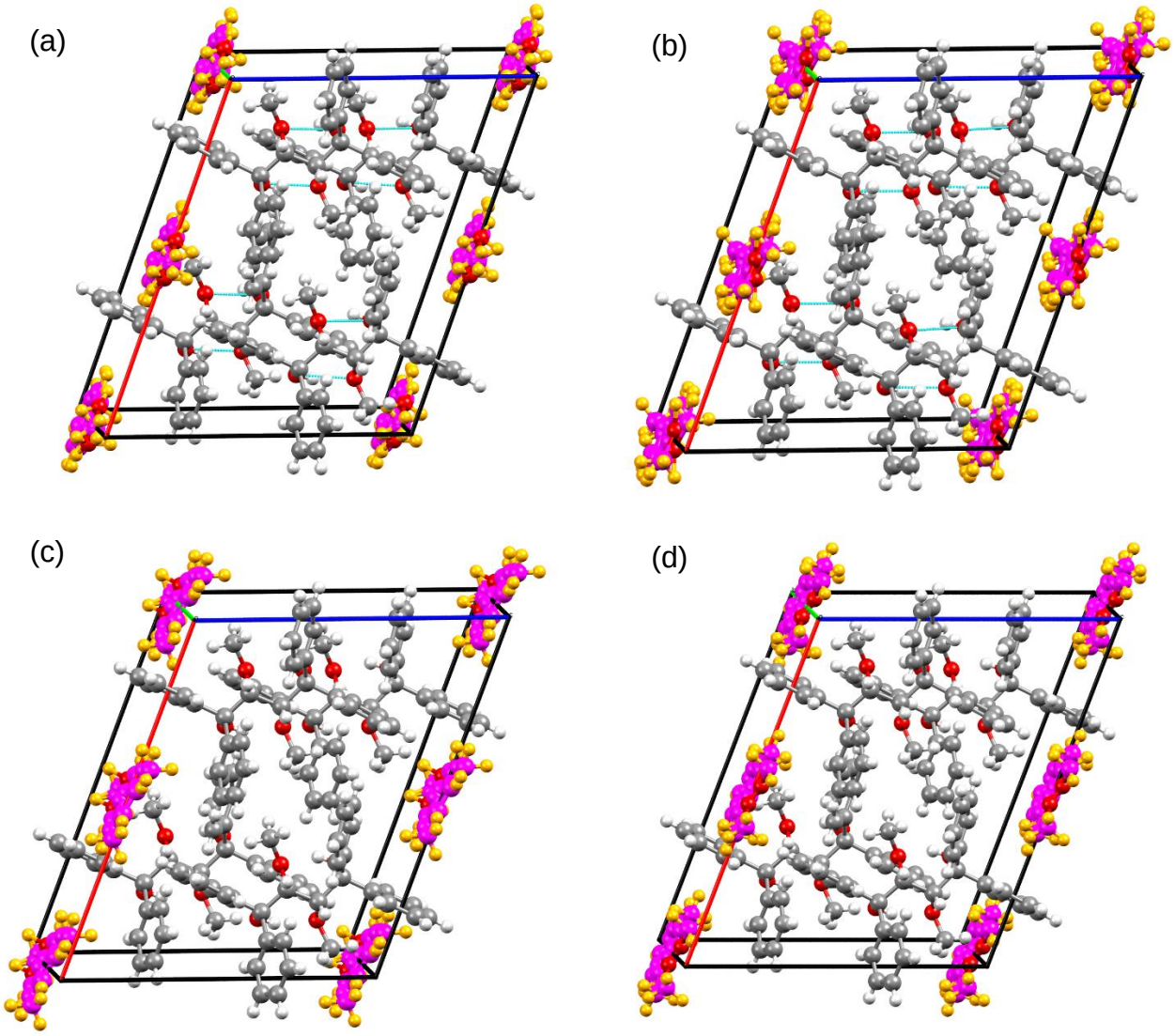

Figure 129: The unit cells for the DMT complexes with anisole and the isomeric methylanisoles; the guests have a magenta carbon framework while the hosts have a grey carbon framework; hydrogen bonding is shown by means of light-blue dashed lines; a) 2DMT•anisole, b) 2DMT•*p*-MA, c) 2DMT•*m*-MA and d) 2DMT•*o*-MA; the isostructural nature of all the host frameworks are clearly evident here.

Hydrogen Bonding

A pair of 1,3- and 2,4- intramolecular classic hydrogen bonding interactions are present between hydroxy and methoxy moieties on the host butane backbone. These interaction types only stabilize the host geometry and are not present between host and guest, and they range between 2.625(2) and 2.680(3) Å, with angles between 139 and 143°. Table 62 lists the individual hydrogen bonding interactions, and Figure 130 shows the hydrogen bonding in the host, with the 2DMT•*p*-MA complex as a representative example.

Table 62: Classic intramolecular hydrogen bonding interactions in the DMT complexes with anisole and the methylanisole guests.

Complex	Non-covalent interaction	Distance (Å) D–A	Angle (°) D-H···A
2DMT•anisole	(host)O-H···O(host methoxy)	2.676(2)	140
	(host)O-H···O(host methoxy)	2.625(2)	141
2DMT•*p*-MA	(host)O-H···O(host methoxy)	2.680(3)	140
	(host)O-H···O(host methoxy)	2.642(3)	143
2DMT•*m*-MA	(host)O-H···O(host methoxy)	2.678(2)	140
	(host)O-H···O(host methoxy)	2.648 (2)	141
2DMT•*o*-MA	(host)O-H···O(host methoxy)	2.677(3)	139
	(host)O-H···O(host methoxy)	2.632(3)	141

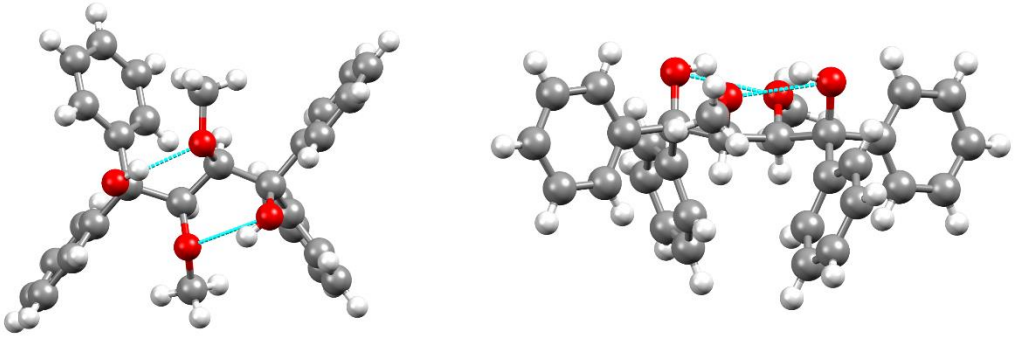

Figure 130: Two views of the host intramolecular hydrogen bonding, depicted with light-blue dashed lines.

Several non-classic intramolecular hydrogen bonding interactions also exist within the host structure in each complex. These manifest between *ortho*-aromatic hydrogens on the phenyl rings of DMT and an adjacent methoxy oxygen atom, and range between 2.651(5) and 2.760(4) Å (100–103°). While all the methyl-substituted anisole-containing complexes exhibit four of these interactions, only three could be identified in the 2DMT•anisole complex. Additionally, intermolecular host–host interactions of this kind were also identified, one each for the complexes with anisole and *o*-MA, and two each in the case of *p*-MA and *m*-MA. These were found to occur between various host aromatic hydrogens and host hydroxy or methoxy oxygens [3.294(5)–3.533(2) Å, 162–171°]. Figure 131 is representative of the interactions involving hydroxy and methoxy oxygens, and Table 63 lists these interactions in detail.

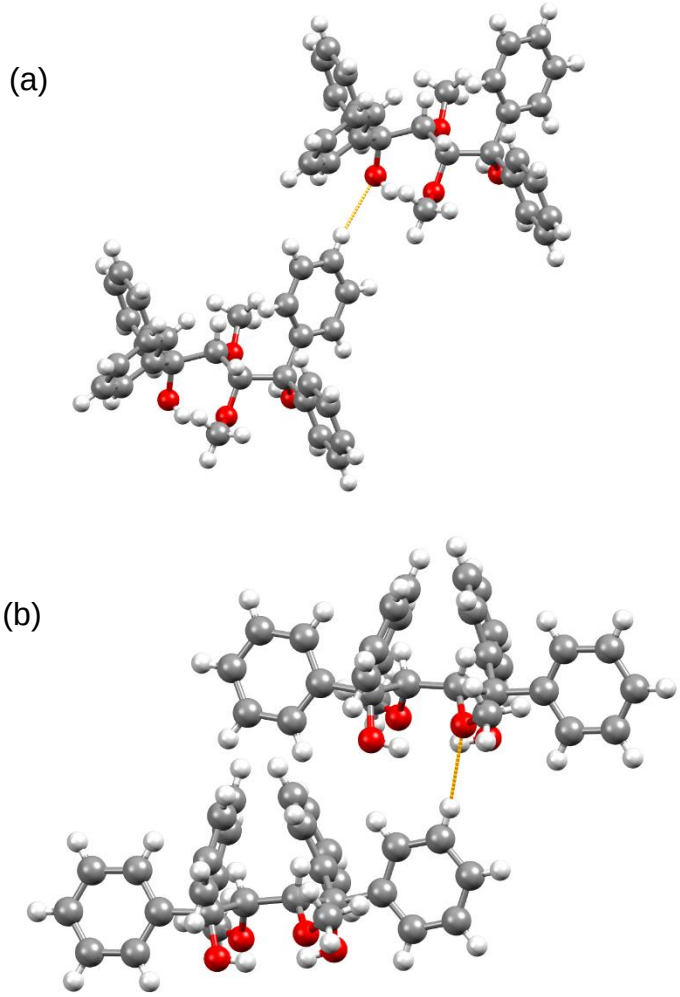

Figure 131: Intermolecular non-classic hydrogen bonding interactions depicted as orange dashes; a) a (host)*p*-ArH···O(host hydroxy) interaction in the 2DMT•anisole complex and b) a (host)*m*-ArH···O(host methoxy) interaction in the 2DMT•*m*-MA complex.

Table 63: Non-classic inter- and intra- molecular hydrogen bonding interactions in the DMT complexes with anisole and the methylanisole guests.

Complex	Non-covalent interaction	Distance (Å) D–A	Angle (°) D-H···A
2DMT•anisole	(host)*o*-ArH···O(host hydroxy)	2.655(2)	102
	(host)*o*-ArH···O(host hydroxy)	2.760(2)	100
	(host)*o*-ArH···O(host hydroxy)	2.656(2)	101
	(host)*p*-ArH···O(host hydroxy)[a]	3.317(3)	169
2DMT•*p*-MA	(host)*o*-ArH···O(host hydroxy)	2.653(4)	102
	(host)*o*-ArH···O(host hydroxy)	2.739(4)	100
	(host)*o*-ArH···O(host hydroxy)	2.760(4)	100
	(host)*o*-ArH···O(host hydroxy)	2.651(5)	102
	(host)*m*-ArH···O(host methoxy)[b]	3.502(4)	166
	(host)*p*-ArH···O(host hydroxy)[a]	3.294(5)	162
2DMT•*m*-MA	(host)*o*-ArH···O(host hydroxy)	2.656(2)	102
	(host)*o*-ArH···O(host hydroxy)	2.754(3)	100
	(host)*o*-ArH···O(host hydroxy)	2.759(3)	100
	(host)*o*-ArH···O(host hydroxy)	2.632(3)	103
	(host)*m*-ArH···O(host methoxy)[b]	3.533(2)	168
	(host)*p*-ArH···O(host hydroxy)[a]	3.327(3)	168
2DMT•*o*-MA	(host)*o*-ArH···O(host hydroxy)	2.663(5)	103
	(host)*o*-ArH···O(host hydroxy)	2.760(4)	100
	(host)*o*-ArH···O(host hydroxy)	2.766(4)	100
	(host)*o*-ArH···O(host hydroxy)	2.667(5)	101
	(host)*p*-ArH···O(host hydroxy) [a]	3.314(6)	171

Symmetry operators: a) –1/2+x, –1/2+y,z; b) 3/2–x, –1/2+y, 1–z

π–π and CH–π Interactions

Various inter- and intra- molecular π–π stacking interactions may be discerned in the DMT complexes with the anisole guests. They are weak, ranging between 4.708(1) and 5.981(3) Å. The intramolecular type within the host occurs between two phenyl rings connected to the same carbon on the butane backbone [4.708(1)–4.875(1) Å], while intermolecular host–host π–π interactions range between 4.708(1)–5.967(2) Å. The strongest intermolecular host–guest interactions of this kind in each complex typically have a length of 4.965(4)–5.558(5) Å. Figure 132 provides various views of these in order to gain a better understanding.

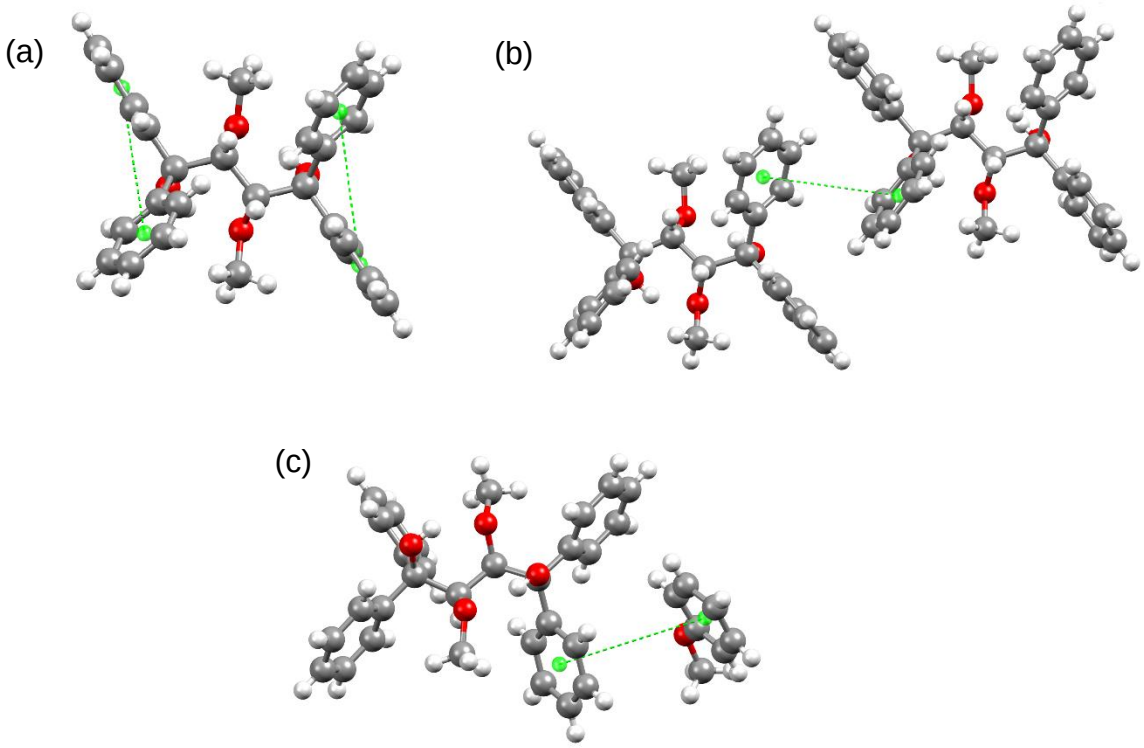

Figure 132: Representative π–π stacking interactions; these are denoted by green dashed lines for a) intramolecular π–π stacking in the host, b) an intermolecular interaction between two host molecules, and c) π–π stacking between host and guest.

Intramolecular CH–π interactions are consistently present between host methoxy hydrogen atoms and a phenyl ring of the same molecule. These vary from 2.76 to 2.96 Å (144–152°). Only the 2DMT•anisole complex displays an intermolecular host–host interaction of this type [(host)*m*-ArH···Cg(host), 2.98 Å, 170°]. The remaining complexes have host–guest CH–π interactions between 2.57 and 2.96 Å (147–171°), and Figure 133 is representative of these interactions, while Table 64 lists them in detail.

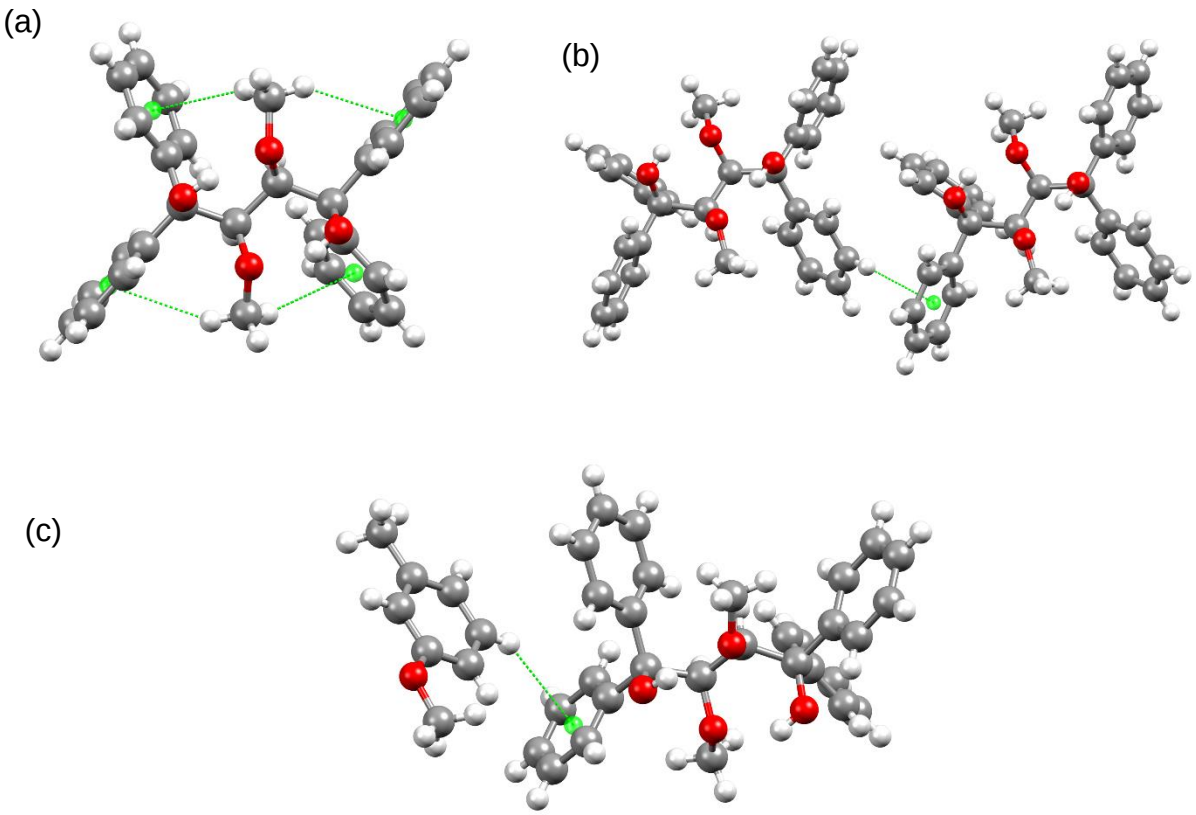

Figure 133: Representative CH–π interactions shown as green dashed lines for a) host–host intramolecular interactions, b) a host–host intermolecular interaction in the 2DMT•anisole complex, and c) a host–guest CH–π interaction.

Table 64: CH–π stabilizing interactions in the host-guest complexes of DMT and the anisole guests.

Complex	Non-covalent interaction	Distance (Å)	Angle (°)	Symmetry operator
2DMT•anisole	(host methoxy)C-H···Cg(host)	2.91	149	x,y,z
	(host methoxy)C-H···Cg(host)	2.86	146	x,y,z
	(host methoxy)C-H···Cg(host)	2.82	145	x,y,z
	(host methoxy)C-H···Cg(host)	2.76	148	x,y,z
	(host)*m*-ArH···Cg(host)	2.98	170	1–x, y, 1–z
2DMT•*p-MA*	(host methoxy)C-H···Cg(host)	2.96	152	x,y,z
	(host methoxy)C-H···Cg(host)	2.86	146	x,y,z
	(host methoxy)C-H···Cg(host)	2.87	145	x,y,z
	(host methoxy)C-H···Cg(host)	2.85	151	x,y,z
	(guest)*m*-ArH···Cg(host)	2.94	171	1–x, y, 1–z
2DMT•*m-MA*	(host methoxy)C-H···Cg(host)	2.94	149	x,y,z
	(host methoxy)C-H···Cg(host)	2.84	147	x,y,z
	(host methoxy)C-H···Cg(host)	2.95	147	x,y,z
	(host methoxy)C-H···Cg(host)	2.90	146	x,y,z
	(guest methyl)C-H···Cg(host)	2.81	171	–1/2+x, –1/2+y, z
	(guest)*m*-ArH···Cg(host)	2.96	147	3/2–x, –1/2+y, –z
2DMT•*o*-MA	(host methoxy)C-H···Cg(host)	2.91	146	x,y,z
	(host methoxy)C-H···Cg(host)	2.85	146	x,y,z
	(host methoxy)C-H···Cg(host)	2.88	144	x,y,z
	(host methoxy)C-H···Cg(host)	2.81	150	x,y,z
	(guest methyl)C-H···Cg(host)	2.57	169	–1/2+x, –1/2+y, z

Short Contacts

Many contacts which are smaller than the sum of the van der Waals radii are present in these complexes (Table 65). They include both host–host and host–guest interaction types. The majority of these result between host aromatic hydrogens or carbons and host hydroxy hydrogens [2.30–2.89 Å, 105–162°]. Host–guest short contacts predominantly involve the guest methoxy or methyl CH_3. The 2DMT•*m*-MA complex has a singular (host)*p*-ArH···*m*-ArC(guest) interaction, while 2DMT•*o*-MA has a significant short contact much shorter than the van der Waals radii of the participating atoms [(host)*o*-ArC···H-C(guest methyl), 2.27 Å and 128°] (Figure 134).

(a)

(b)

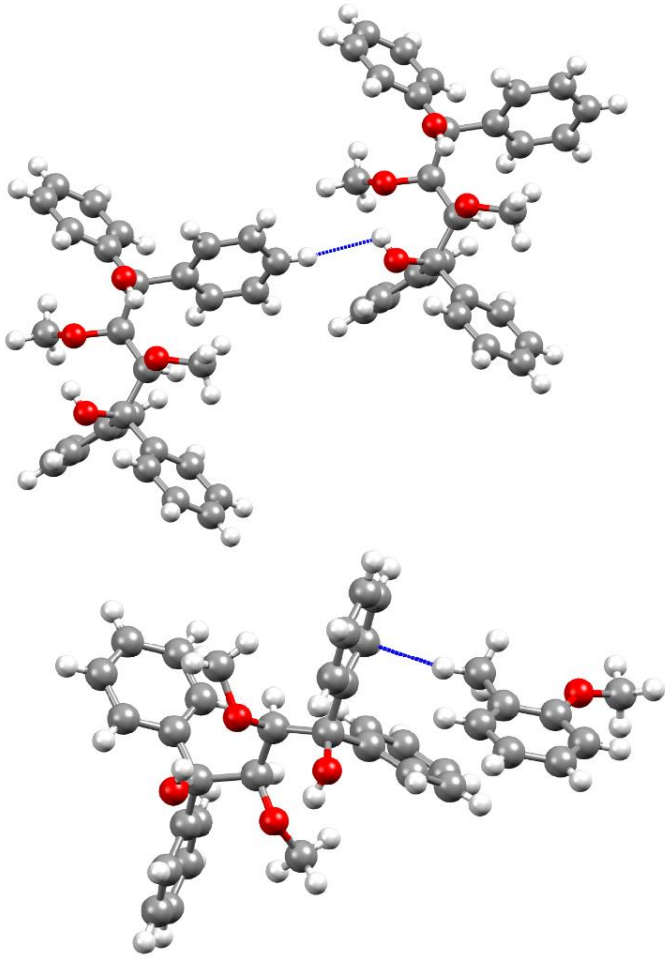

Figure 134: Examples of short contacts (blue) in the DMT complexes with the anisole guests; a) host–host intermolecular short contact between a *para*-aromatic hydrogen and a hydroxy hydrogen, and b) a short host–guest contact in the *o*-MA complex.

Table 65: Summary of the various contacts shorter than the van der Waals radii in the DMT complexes with anisole and the methylanisole isomers.

Complex	Non-covalent interaction	Distance (Å)	Angle (°)	Symmetry operator
2DMT•anisole	(host hydroxy)O-H···*p*-ArH(host)	2.32	108	–1/2+x,1/2+y,z
	(host hydroxy)O-H···*p*-ArH(host)	2.30	148	1/2+x,1/2+y,z
	(host)*p*-ArH··· *m*-ArC(host)	2.89	145	1–x,y,–z
	(host)*p*-ArH···O-C(guest methoxy)	2.66	156	3/2–x,1/2+y,1–z
2DMT•*p*-MA	(host hydroxy)O-H···*p*-ArH(host)	2.32	108	–1/2+x,1/2+y,z
	(host hydroxy)O-H···*p*-ArH(host)	2.38	162	–1/2+x,1/2+y,z
	(host)*p*-ArC···H-C(guest methoxy)	2.81	157	1/2+x,1/2+y,z
	(host)*m*-ArC···H-C(guest methyl)	2.85	110	x,y,z
	(host methoxy)C-H···H-C(guest methoxy)	2.34	135	x,1+y,–z
	(host)*p*-ArH···H-C(guest methoxy)	2.31	153	1/2+x,1/2+y,1+z
2DMT•*m*-MA	(host hydroxy)O-H···*p*-ArH(host)	2.30	105	–1/2+x,1/2+y,z
	(host hydroxy)O-H···*p*-ArH(host)	2.31	149	1/2+x,1/2+y,z
	(host)*p*-ArH···*m*-ArC(host)	2.87	149	1–x,y,–z
	(host)*m*-ArC···H-C(guest methyl)	2.86	105	1/2+x,1/2+y,z
	(host)*m*-ArH···H-C(guest methyl)	2.24	128	1–x,y,–z
	(host)*p*-ArH···*m*-ArC(guest)	2.72	162	3/2–x,1/2+y,1-z
2DMT•*o*-MA	(host hydroxy)O-H···*p*-ArH(host)	2.30	107	–1/2+x,1/2+y,z
	(host hydroxy)O-H···*p*-ArH(host)	2.29	151	1/2+x,–1/2+y,z
	(host methoxy)C-H···H-C(guest methoxy)	2.23	149	1–x,1+y,–z
	(host)*p*-ArH···*m*-ArC(host)	2.87	146	1–x,y,–z
	(host)*o*-ArC···H-C(guest methyl)	2.27	128	1/2+x,1/2+y,z

For ease of comparison, all the significant host–guest interactions obtained from these X-ray diffraction data are summarized in Table 66. The contacts herein listed may aid in elucidating the reasons for the selectivity of DMT observed for these guests.

Table 66: Significant host–guest interactions for the complexes of DMT with anisole and the isomeric methylanisoles.

Interaction	2DMT•anisole	2DMT•*p*-MA	2DMT•*m*-MA	2DMT•*o*-MA
π–π	5.360(5)–5.980(5)Å (10 contacts)	5.187(6)–5.378(6) Å (6 contacts)	4.965(4)–5.354(4) Å (6 contacts)	5.353(7)–5.737(7) Å (8 contacts)
CH–π	None	2.94 Å, 171° (guest)*m*-ArH···Cg(host)	2.81 Å, 171° (guest methyl)C-H···Cg(host) 2.96 Å, 147° (guest)*m*-ArH···Cg(host)	2.57 Å, 169° (guest methyl)C-H···Cg(host)
Short contacts	2.66 Å, 156°, < (host)*p*-ArH···O-C(guest methoxy)	2.81 Å, 157°, < (host)*p*-ArC···H-C(guest methoxy) 2.85 Å, 110°, < (host)*m*-ArC···H-C(guest methyl) 2.34 Å, 135°, < (host methoxy)C-H···H-C(guest methoxy) 2.31 Å, 153°, < (host)*p*-ArH···H-C(guest methoxy)	2.86 Å, 105°, < (host)*m*-ArC···H-C(guest methyl) 2.24 Å, 128°, < (host)*m*-ArH···H-C(guest methyl) 2.72 Å, 162°, < (host)*p*-ArH···*m*-ArC(guest)	2.23 Å, 149°, < (host methoxy)C-H···H-C(guest methoxy) 2.27 Å, 128°, << (host)*o*-ArC···H-C(guest methyl)

*< denotes contacts less than the sum of the van der Waals radii and << denotes contacts less than this sum minus 0.2 Å.

A comparison of host–guest interactions in these complexes does not satisfactorily explain the selectivity order of DMT towards these guests (anisole > *p*-MA > *m*-MA > *o*-MA). All three methyl-substituted guests experience a number of host–guest interactions. Most notably, the number of short contacts in each complex mirror the aforementioned selectivity order [*p*-MA (4) > *m*-MA (3) > *o*-MA (2)]. The preferred guest, anisole, experiences relatively few host–guest contacts and it therefore appears that the preferential selectivity for this guest by DMT may not be as dependent on intermolecular interactions in the solid state. The selectivity order is possibly best explained by considering the shapes of the guests. Anisole and *p*-MA may simply be easier to accommodate within the host crystal during crystallization owing to their symmetrical structure, while *m*-MA and, to a larger extent *o*-MA, are less preferred due to their lack of symmetry. However, we cannot at this stage state confidently that this is the case.

We also investigated the nature of the guest accommodation. As all four complexes were determined to be isostructural, the mode in which the guest is packed within the host framework yielded identical results for each complex. All guests experience discrete cavity occupation in the host crystal as represented in Figure 135.

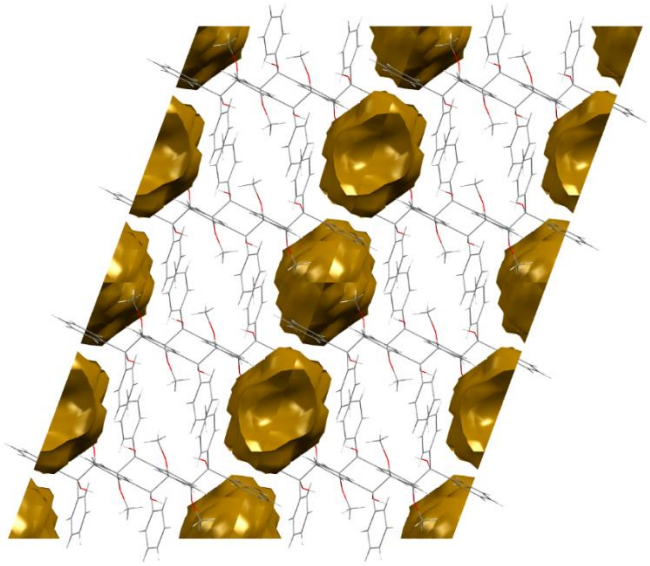

Figure 135: 2DMT•*o*-MA complex, as a representative example, with the guest removed from the packing calculation to show the discrete cavity occupation of the guests.

8.6 Hirshfeld Surface Analysis

An analysis of the two-dimensional plots generated from the Hirshfeld surface of the guest from each complex was performed. Figure 136a–d shows these 2D plots with the relevant structural features. Figure 136a is the fingerprint plot for the 2DMT•anisole complex, and there are three distinct areas that can be identified, that is S1, which represents C···H interactions, and W1 and W2, each ascribed to H···H interactions. The plot for the 2DMT•*p*-MA complex (Figure 136b) displays largely the same pattern of interactions: at S1, C···H interactions dominate, while W1 comprises H···H interactions. It is worth noting that W1 in this case extends closer to the origin of the plot than in the anisole complex, indicative of generally closer H···H interactions in the *p*-MA complex. For the 2DMT•*m*-MA complex (Figure 136c), the area representing of C···H interactions has broadened and is denoted by W1. W2 in this plot points towards a low density area of H···H interactions, while S1 alludes to close H···H interactions. Finally, Figure 136d shows two sharp spikes S1 (C···H interactions) and S2 (H···H interactions). These can be ascribed to the short intermolecular host–guest interactions noted for the 2DMT•*o*-MA complex in Table 66.

The type and number of interactions in all four complexes are comparable (Figure 137). H···H interactions range between 69.9 and 72.6% of the total interactions, while C···H contacts comprise 27.4–29.6% of the total. The 2DMT•*o*-MA complex has an additional 0.9% O···H and 0.1% C···C interactions, while the complex containing *m*-MA experiences 0.1% C···C interactions. Furthermore, the *p*-MA complex has 0.1% O···H and the anisole complex 1.8% of this interaction type. Hirshfeld surface analyses were, therefore, also unable to explain the selectivity order of DMT for the anisole guests, as was the case for SCXRD.

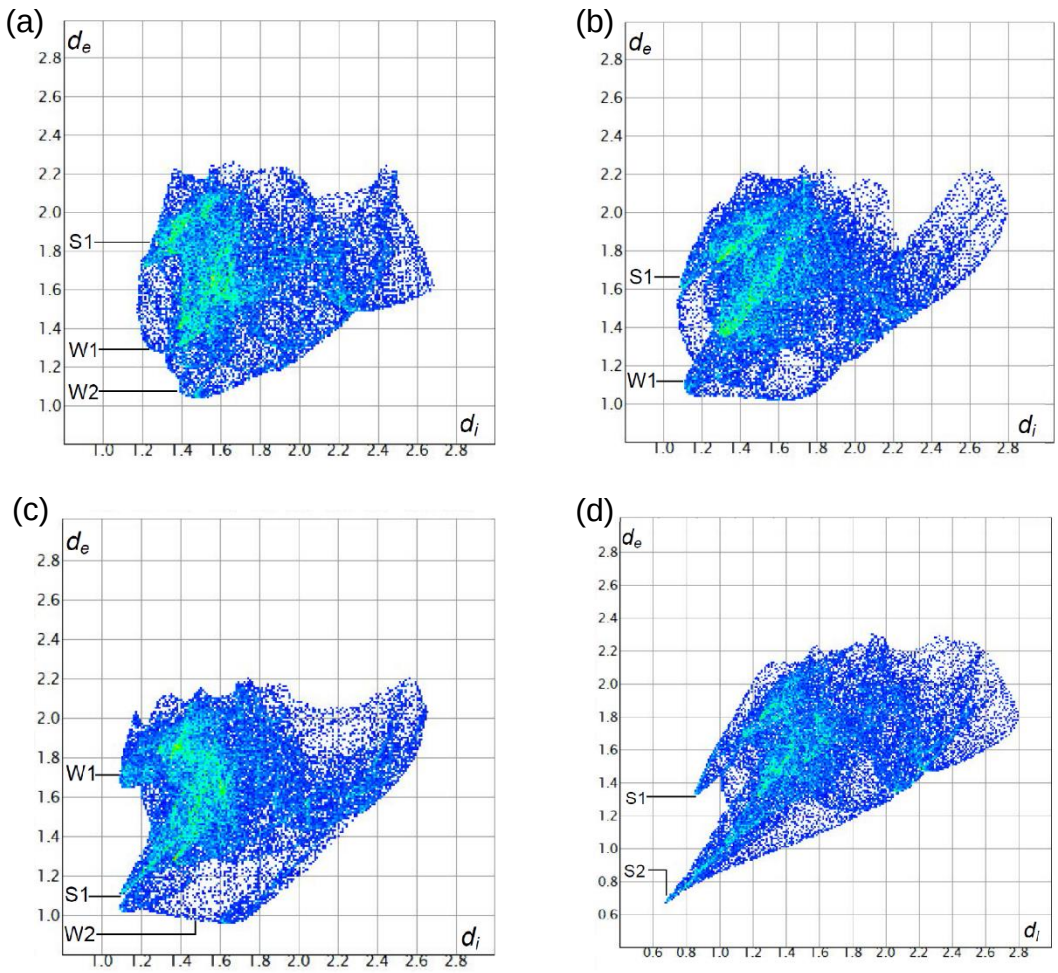

Figure 136: Two-dimensional fingerprint plots obtained from the Hirshfeld surfaces of the guests in the inclusion complexes of a) 2DMT•anisole, b) 2DMT•*p*-MA, c) 2DMT•*m*-MA and d) 2DMT•*o*-MA.

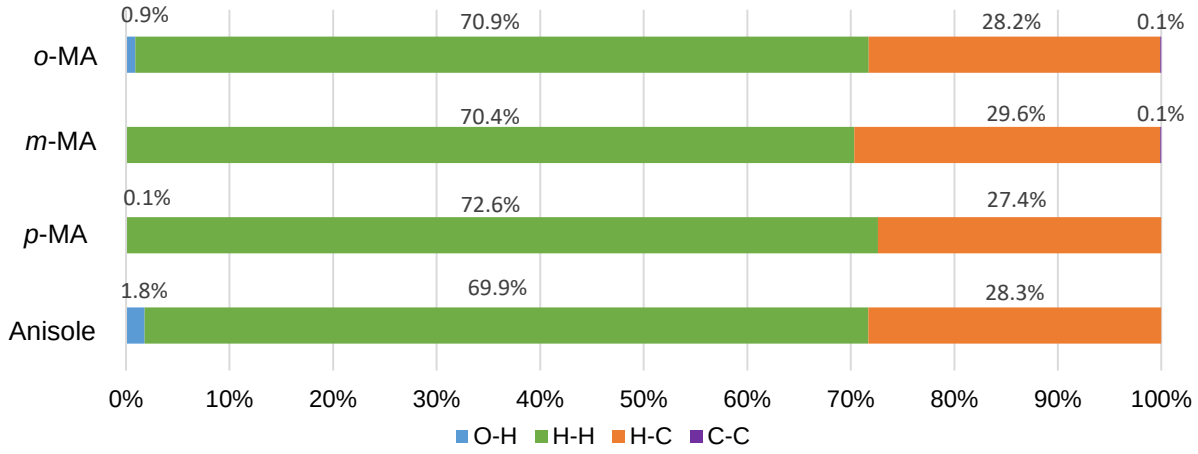

Figure 137: Graphical display showing the percentage and type of intermolecular interactions in each of these complexes.

8.7 Conclusion

This study found that the DMT host compound successfully formed inclusion complexes with anisole and the isomeric methylanisoles. Through competition experiments, it was determined that DMT selectively included anisole over the methylanisoles. *p*-Methylanisole was the second preferred followed by *m*-methylanisole and *o*-methylanisole. Thermal experiments (T_{on}–T_b) were in reasonable agreement with the observed selectivity order of DMT for these guests, while X-ray and Hirshfeld surface analyses were unhelpful in this regard. It was suggested that, perhaps, the symmetrical molecular shapes of preferred guests anisole and *p*-MA allowed for more efficient host–guest packing, compared with the less symmetrical and less preferred *m*-MA and *o*-MA. However, further future work in this regard may provide a better understanding as to how all of these experiments may be related back to the observed selectivity order.

Chapter 9: Inclusion Compounds of DMT (73) with the Cresol Isomers

9.1 Introduction

Cresols are aromatic, methyl-substituted phenol compounds consisting of three isomers, namely *p*-cresol (*p*-CR), *m*-cresol (*m*-CR) and *o*-cresol (*o*-CR). Cresols are traditionally extracted from coal tar, but synthetic routes such as methylation of phenol now experience widespread application. Cresols are prevalent in nature. For example, they are often found in the glands of animals such as male African elephants and beavers.[190,191] Many biological fermentation processes produce *p*-CR as a waste product.[192] Cresols are often employed as precursors in the production of herbicides and epoxy resins (*o*-CR), production of insecticides and disinfectants (*m*-CR) and the synthesis of antioxidants (*p*-CR).[86, 193,194] With a wide variety of applications, it is important to be able to obtain the cresol isomers separately as pure products; however, only *o*-CR can be separated through distillative measures as its boiling point (191.0 °C) is adequately different from that of *m*-CR (202.3 °C) and *p*-CR (202.0 °C).[195] It is therefore of value to investigate sequestration of the cresols through host-guest complexation and, in particular, to determine whether DMT shows any discriminatory behaviour when allowed to recrystallize from mixtures of the cresol isomers.

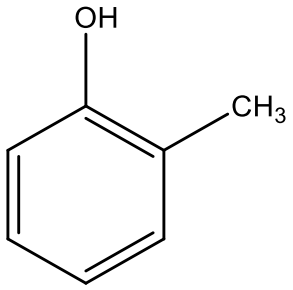

o-CR

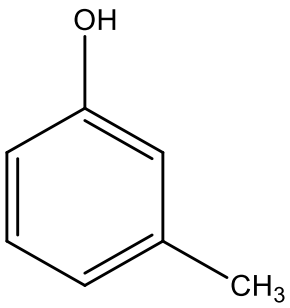

m-CR

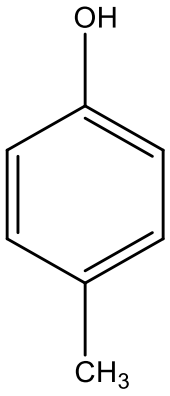

p-CR

9.2 Individual and Equimolar Inclusion Experiments

DMT was independently recrystallized from each of the three cresol isomers after which the crystals were isolated, washed and subjected to ^{1}H-NMR spectroscopy. In each case, DMT formed 2:1 host-guest complexes with these compounds (Table 67).

Table 67: Host:guest ratios of complexes formed during individual recrystallization experiments.*

Guest	Host:guest
p-Cresol	2:1
m-Cresol	2:1
o-Cresol	2:1

*Determined using ^{1}H-NMR spectroscopy with $CDCl_3$ as solvent.

Equimolar competition experiments were performed by allowing DMT to crystallize from various equimolar combinations of the cresol isomers. The solids so-obtained were once more subjected to ^{1}H-NMR spectroscopy whereupon it was found that an overall 2:1 host:guest complex was formed in each case (Table 68). Subsequent GC-MS analysis of these complexes furnished data indicating which isomer was preferentially included (Table 68). When *p*-CR and *m*-CR competed, the latter guest was preferred by 56.8% in comparison with *m*-CR (43.2%). A competition experiment between *p*-CR and *o*-CR resulted in DMT displaying preference for *o*-CR (77.6%), while this guest was also preferred (78.5%) in an experiment involving it and *m*-CR (21.5%). Finally, an experiment involving all three isomers simultaneously resulted in *o*-CR being preferentially included (64.1%) followed by *p*-CR (18.4%) and *m*-CR (17.5%).

Table 68: Competition experiments and H:G ratios obtained.*

***p*-Cresol**	***m*-Cresol**	***o*-Cresol**	**Guest ratios (% Standard deviation)[$]**	**Overall H:G ratio**
X	X		***56.8***:43.2 (1.0)	2:1
X		***X***	22.3:***77.6*** (0.7)	2:1
	X	***X***	21.5:***78.5*** (0.8)	2:1
X	X	***X***	18.4:17.5:***64.1*** (0.6)(1.0)(1.6)	2:1

*Determined using GC-MS; preferred guests are given in bold font face for ease of comparison; [$]experiments were carried out in triplicate, and an average ratio is provided here with % e.s.d.'s in parentheses.

9.3 Host Selectivity Profiles with Changing Guest Concentrations in Binary and Ternary Guest Mixtures

DMT's ability to include and even discriminate between the isomers of cresol at different molar concentrations was subsequently assessed by recrystallizing the host from non-equimolar binary mixtures of these guests. Assessment of the mother liquor and crystal contents allowed for the construction of the selectivity curves in Figures 138–140.

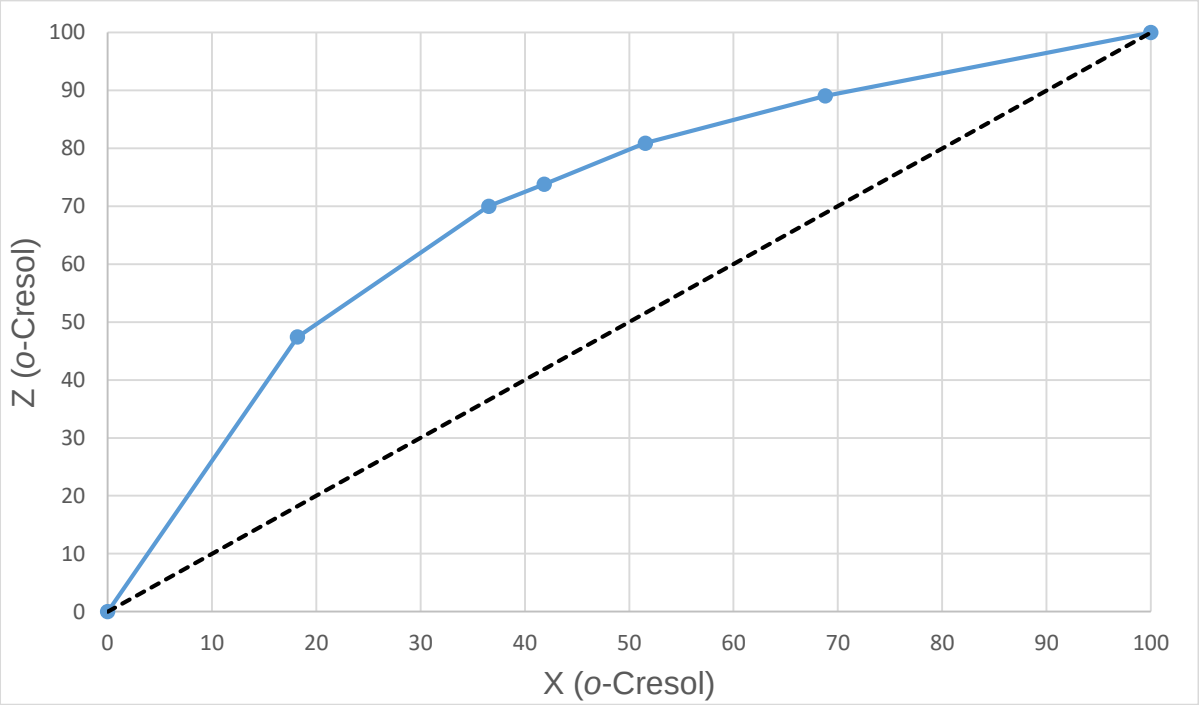

Figure 138: Selectivity curve of *o*-CR *vs* *m*-CR. Coloured blue is the molar fraction of *o*-CR in the inclusion complex (Z) *vs* the molar fraction of *o*-CR in the mother liquor (X). Black dashes indicate the theoretical line of no selectivity.

Figure 138 was obtained from the *o*-CR/*m*-CR experiment and indicated that *o*-CR was consistently preferred by DMT. From a mother liquor composition of ~18.2% *o*-CR, crystals were obtained which contained 47.4% of this guest, while a solid incorporating 89.1% *o*-CR was obtained when DMT was allowed to crystallize from a

mother liquor composed of 68.8% of this guest. K, the average selectivity coefficient for this curve, was calculated to be 3.95.

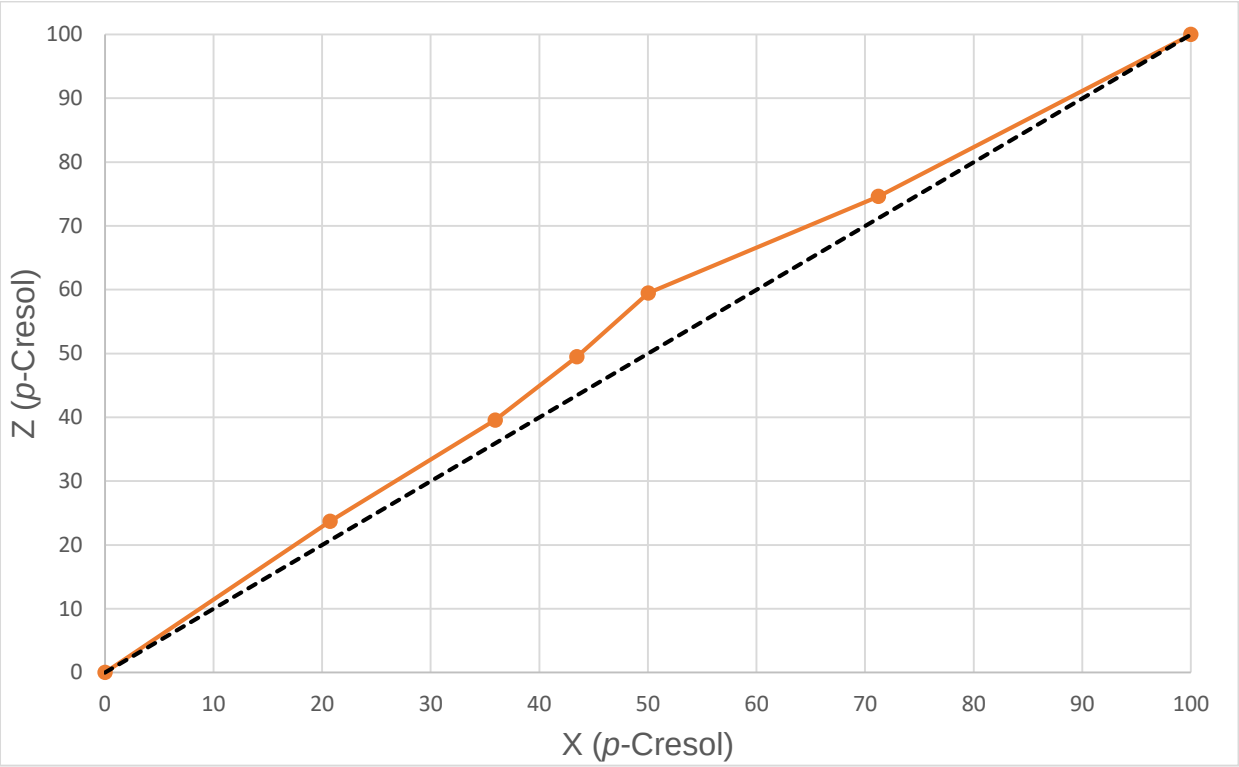

Figure 139: Selectivity curve of *p*-CR *vs* *m*-CR. Coloured orange is the molar fraction of *p*-CR in the inclusion complex (Z) *vs* the molar fraction of *p*-CR in the mother liquor (X). Black dashes indicate the theoretical line of no selectivity.

When *p*-CR was made to compete against *m*-CR, the selectivity curve in Figure 139 resulted. The relatively flat trajectory of the curve, which closely follows the theoretical line of no selectivity, indicates that *p*-CR is only slightly preferred over *m*-CR by DMT. A solid obtained from a mother liquor composition of ~20.7% *p*-CR contained only 23.7% of this guest. Similarly, at higher *p*-CR concentrations (71.2%), the resultant inclusion complex contained 74.6% *p*-CR. K for this curve was, as expected, much lower (1.26) than for the *o*-CR/*m*-CR experiment. This result has already been alluded to when considering the equimolar experiments summarized previously in Table 68, where the host was only somewhat more selective for *p*-CR in the presence of *m*-CR.

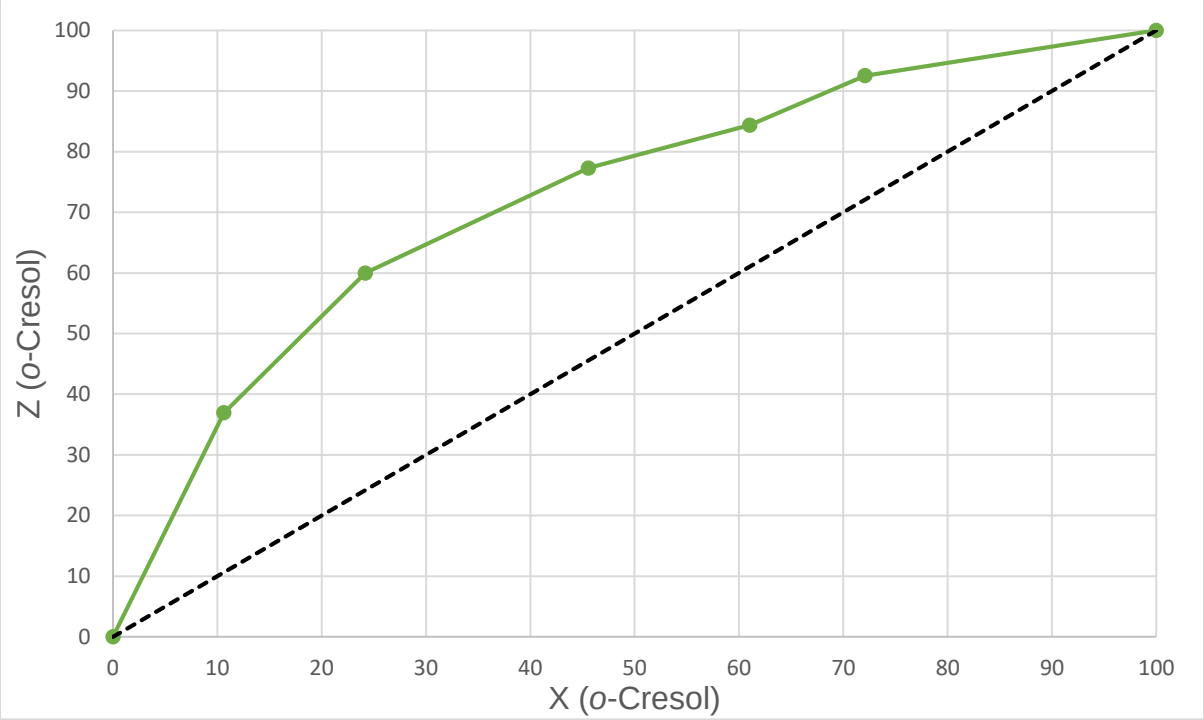

Figure 140: Selectivity curve of *o*-CR *vs* *p*-CR. Coloured green is the molar fraction of *o*-CR in the inclusion complex (Z) *vs* the molar fraction of *o*-CR in the mother liquor (X). Black dashes indicate the theoretical line of no selectivity.

Finally, when *p*-CR was made to compete against *o*-CR in unequal amounts, the selectivity curve in Figure 140 was obtained. DMT preferentially included *o*-CR over the entire molar concentration range investigated. At low *o*-CR mother liquor concentrations (24.2%), the inclusion complex contained ~60% of this guest. Similarly, at a higher *o*-CR mother liquor concentration of ~72.1%, the crystals included 92.5% *o*-CR (and only ~7.5% *p*-CR). The selectivity coefficient for this curve was higher than for the preceding cresol selectivity experiments (K = 4.39).

DMT was recrystallized from ternary mixtures containing all three cresol isomers in various ratios. Figure 141 was constructed after analysing the mother liquor (blue circles) and crystal compositions (red squares). Upon crystallization, the amount of included *o*-CR increased at every data point. The average increase for *o*-CR was ~33.6%. Subsequently, the *p*-CR content of the crystals decreased on average by 15.3%, and the *m*-CR content decreased by 18.3% (on average) relative to the mother liquor composition.

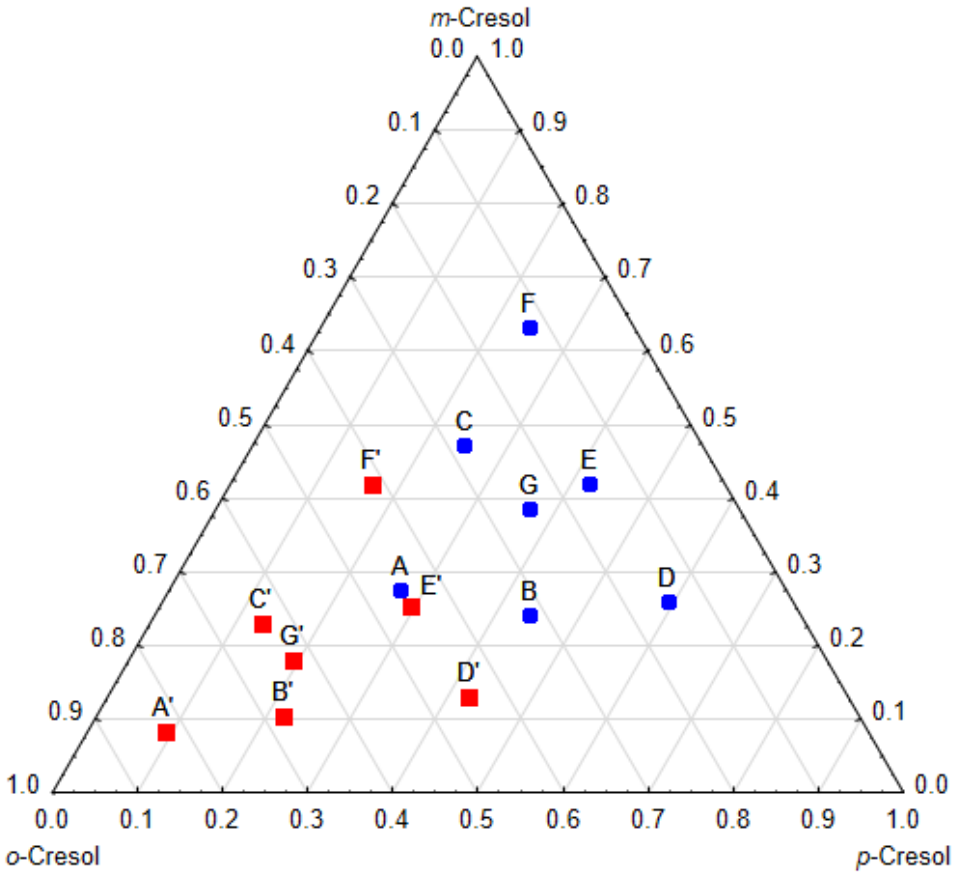

Figure 141: Ternary competition plot obtained from the *p*-CR/*m*-CR/*o*-CR experiments. Blue circles indicate mother liquor compositions, while red squares indicate guest composition in the crystals.

Consideration of the outcome of all of these equimolar and non-equimolar competition and selectivity experiments indicate that DMT has a definite selectivity order for the cresols in the order *o*-CR > *p*-CR > *m*-CR.

9.4 Thermal Analysis

Thermal analysis was again carried out on these complexes between DMT and the cresol isomers. Thermogravimetric analysis and differential scanning calorimetry were used to determine the temperatures at which significant thermal events occurred upon heating. A heating rate of 10 °C.min^{-1} was employed under high purity nitrogen as purge gas. The thermal traces thus obtained are provided in Figures 142–144.

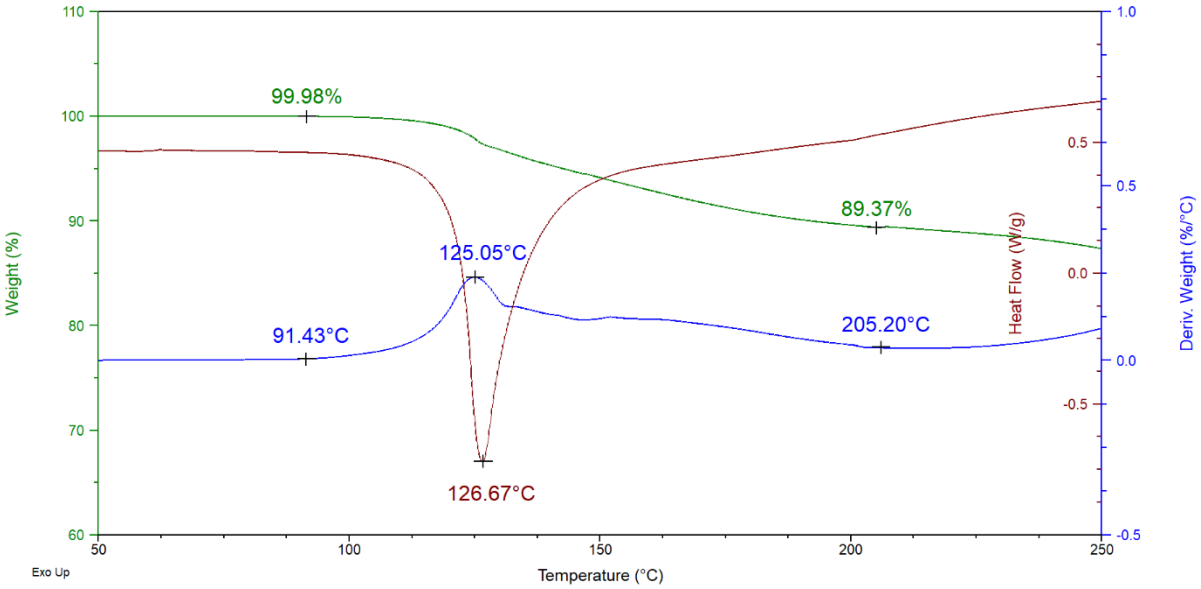

Figure 142: Overlaid TG (green), DTG (blue) and DSC (brown) traces for the 2DMT•*p*-CR complex with heating at 10 °C.min^{-1}.

The DTG trace in Figure 142 (blue) experiences a plateaux at ~205.2 °C, which corresponds to a mass loss of 10.6% (TG). This is in excellent agreement with an expected mass loss of 10.6% for a 2:1 DMT•*p*-CR complex. Mass loss was observed to increase at higher temperatures due to host decomposition. The onset of the mass loss event was determined to occur at ~91.4 °C, while guest release reached a maximum rate at approximately 125.1 °C (DTG). The endotherm peak temperature attributed to the guest release process and host melt was measured at ~126.7 °C.

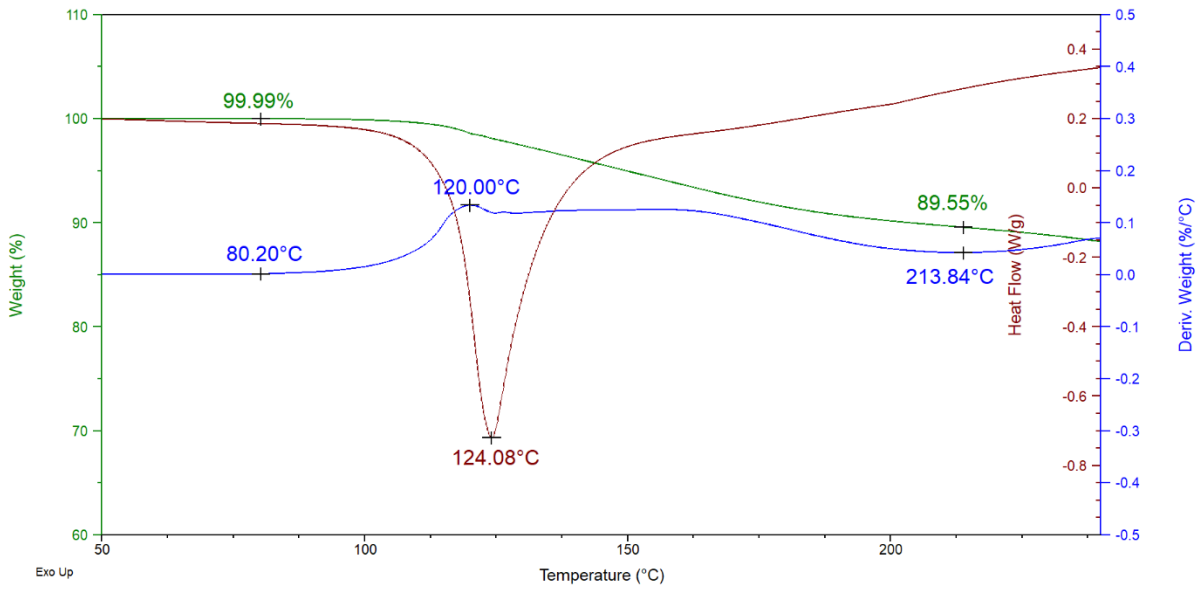

Figure 143: Overlaid TG (green), DTG (blue) and DSC (brown) traces for the 2DMT•*m*-CR complex with heating at 10 °C.min^{-1}.

The 2DMT•*m*-CR complex experienced a mass loss event which initiated at ~80.2 °C. Mass loss reached a maximum rate at ~120.0 °C and continues until approximately 213.8°C (Figure 143, DTG). The total mass loss at this point was calculated to be 10.4% (TG) which correlates well with the expected 10.6% for a 2:1 host:guest complex between DMT and *m*-CR. Lastly, the peak endotherm temperature, T_{end}, in this case, was observed at ~124.1 °C (DSC).

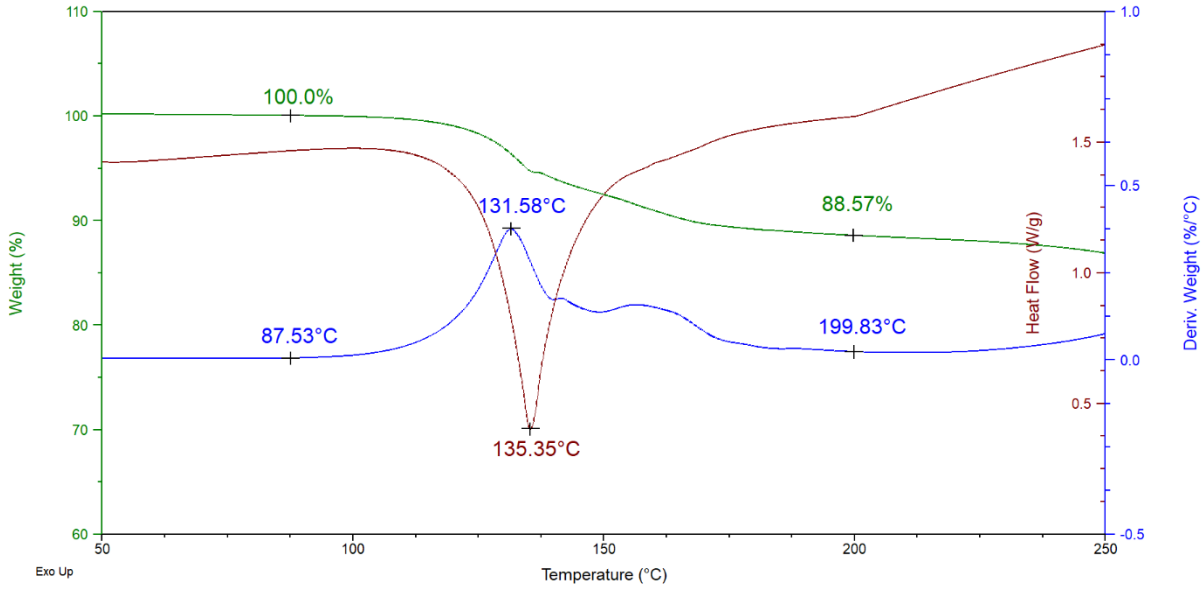

Figure 144: Overlaid TG (green), DTG (blue) and DSC (brown) traces for the 2DMT•*p*-CR complex with heating at 10 °C.min^{-1}.

Finally, the mass loss for the 2DMT•*o*-CR complex was 11.4% (green TG trace, Figure 144). This is in reasonable agreement with the expected 10.6%. The onset temperature for the guest release process was estimated to be ~87.5 °C (DTG), while the maximum rate of guest release occurred at ~131.6 °C. The endotherm peak temperature was approximately 135.4 °C, significantly higher than for the DMT complexes with *p*-CR and *m*-CR.

Table 69 provides a summary of the significant thermal events measured during the course of these thermal experiments. It is gratifying to note that the selectivity order that DMT displays toward these cresol isomers is mirrored by these parameters. As a measure of thermal stability, T_{end}, the endotherm peak temperature, decreases in the order *o*-CR (135.4 °C) > *p*-CR (126.7 °C) > *m*-CR (124.1 °C) indicating that the 2DMT•*o*-CR complex has a higher thermal stability than the *p*-CR complex and the *m*-CR complex, in that order. This trend was copied by T_p, the maximum rate of guest release from the complex [*o*-CR (131.6 °C) > *p*-CR (125.1 °C) > *m*-CR (120.0 °C)]. Furthermore, the measurement of T_{on}–T_b[160,161] becomes less negative in the order *m*-CR (–122.1 °C) < *p*-CR (–110.6 °C) < *o*-CR (–103.5 °C), again signifying that the complex with the more preferred guest has a higher thermal stability, in this case.

Table 69: Summary of the major thermal events observed in the aniline and toluidine complexes with DMT.

Guest	T_b (°C)	T_{on} (°C)[a]	T_{on}–T_b (°C)	T_p (°C)[b]	T_{end} (°C)[c]	Mass loss % (Expected)
p-Cresol	202.0	91.4	–110.6	125.1	126.7	10.6 (10.6)
m-Cresol	202.3	80.2	–122.1	120.0	124.1	10.4 (10.6)
o-Cresol	191.0	87.5	–103.5	131.6	135.4	11.4 (10.6)

[a]T_{on} is the onset temperature for guest release estimated from the DTG; [b]T_p values were determined from the blue DTG traces; [c]T_{end} values were obtained from the brown DSC traces;

9.5 Single Crystal X-Ray Analysis

Single crystals of the inclusion complexes of DMT with the cresols were subjected to X-ray diffraction experiments. The data from these (Table 70) indicated that all three of the complexes are isostructural, having crystallized in the monoclinic *C*2 crystal system. In each case, the guests are disordered around a two-fold rotational axis. In the case of the 2DMT•*p*-CR complex, it was not possible to determine the position of the hydroxyl hydrogen atom and it was placed in a calculated position. As a result, information regarding potential hydrogen bond formation by this guest could not be acquired.

Table 70: Crystallographic data for the complexes between DMT and the three cresol isomers.

	2DMT•*p*-CR	**2DMT•*m*-CR**	**2DMT•*o*-CR**
Chemical formula	$C_{30}H_{30}O_4$ •0.5C_8H_8O	$C_{30}H_{30}O_4$ •0.5C_8H_{10}	$C_{30}H_{30}O_4$ •0.5C_7H_8O
Formula weight	1017.21	1017.21	1017.21
Crystal system	Monoclinic	Monoclinic	Monoclinic
Space group	*C*2	*C*2	*C*2
μ (Mo-Kα)/mm^{-1}	0.080	0.080	0.080
a/Å	17.3436(12)	17.3219(9)	17.3665(8)
b/Å	12.0126(8)	12.0646(6)	11.9235(6)
c/Å	14.0767(10)	14.1378(7)	14.1752(7)
alpha/°	90	90	90
beta/°	110.152(3)	110.136(2)	109.802(2)
gamma/°	90	90	90
V/$Å^3$	2753.2(3)	2774.0(2)	2761.7(2)
Z	2	2	2
F(000)	1084	1084	1084
Temp./K	200	200	200
Restraints	2	6	6

Nref	6817	6398	6816
Npar	372	342	342
R	0.0343	0.0370	0.0369
wR2	0.0894	0.0989	0.1022
S	1.03	1.05	1.03
θ min-max/°	2.1, 28.3	2.1, 28.4	2.1, 28.4
Tot. data	28811	22385	54587
Unique data	6817	6398	6816
Observed data [I > 2.0 sigma(I)]	6125	5667	6283
R_{int}			
Dffrn measured fraction θ full	0.020	0.018	0.018
	0.998	0.998	0.995
Min. resd. dens. (e/ Å^3)	–0.18	–0.25	–0.25
Max. resd. dens. (e/ Å^3)	0.18	0.21	0.29

Figure 145a–c shows the three unit cells for these complexes, and Figure 146 is a stereoview of the 2DMT•*p*-CR complex, as a representative example, to better depict the host–guest packing.

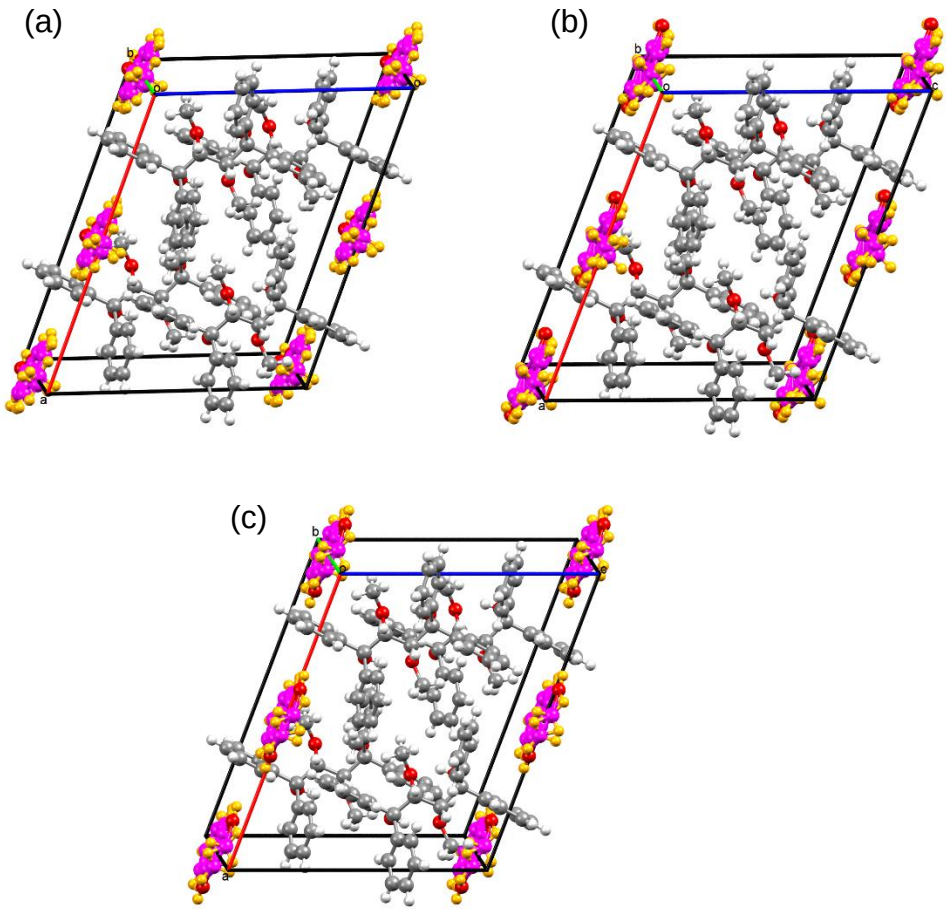

Figure 145: The unit cells for the DMT complexes with a) *p*-CR, b) *m*-CR and c) *o*-CR. Isostructural host frameworks are clearly evident here.

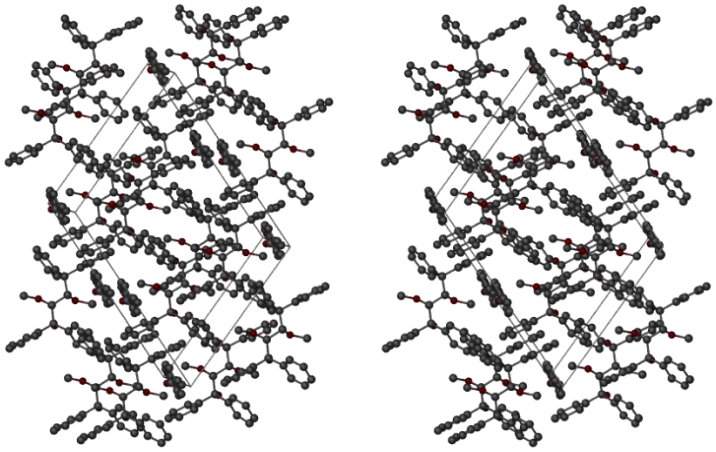

Figure 146: Stereoview of the 2DMT•*p*-CR complex to show packing in three dimensions, as a representative example.

Hydrogen bonding interactions

A pair of 1,3- and 2,4- intramolecular classic hydrogen bonds are observed in each of these DMT complexes with the cresols. They all occur between a hydroxy hydrogen atom and a methoxy oxygen atom. They range in distance between 2.625(2) and 2.678(2) Å with angles 138–141°. Table 71 lists these interactions in more detail while Figure 147 shows representative views of these interactions in the 2DMT•*p*-CR complex.

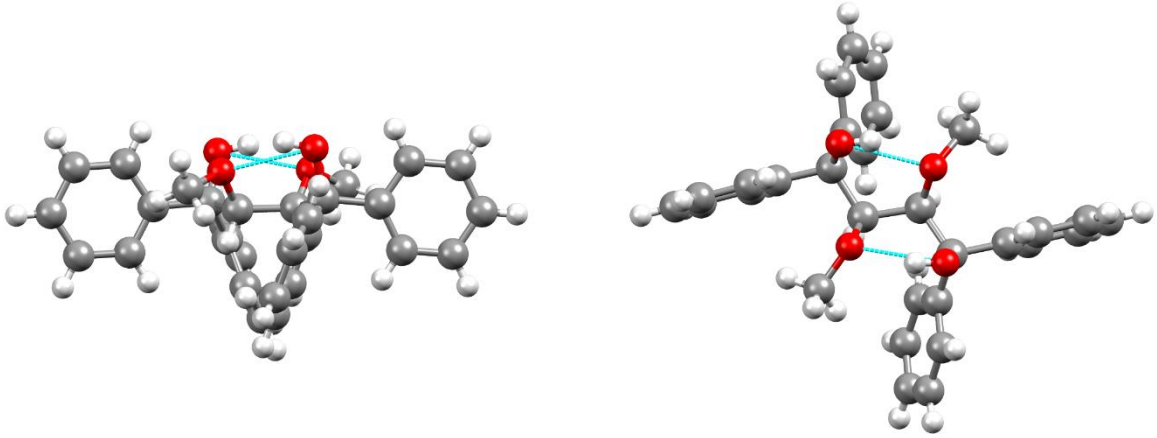

Figure 147: Two views of the host intramolecular hydrogen bonding, depicted with light-blue dashed lines (as in the 2DMT•*p*-CR complex).

Table 71: Classic intermolecular hydrogen bonding interactions in the DMT complexes with the cresols.

Complex	Non-covalent interaction	Distance (Å) D–A	Angle (°) D-H···A
2DMT•*p*-CR	(host)O-H···O(host methoxy)	2.678(2)	140
	(host)O-H···O(host methoxy)	2.635(2)	141
2DMT•*m*-CR	(host)O-H···O(host methoxy)	2.670(2)	140
	(host)O-H···O(host methoxy)	2.625(2)	140
2DMT•*o*-CR	(host)O-H···O(host methoxy)	2.676(2)	138
	(host)O-H···O(host methoxy)	2.629(2)	141

Non-classic hydrogen bonding interactions are also evident in these complexes. They present as both intra- and inter- molecular interactions involving only host molecules. A single exception to this is an (host)*p*-ArH···O(guest hydroxy) interaction in the 2DMT•*o*-CR complex [3.437(5) Å, 172°, Figure 148]. Intramolecular interactions of this type occur between a host *ortho*-aromatic hydrogen and an adjacent host hydroxy oxygen atom [2.646(3)–2.765(2) Å, 100–102°]. The remaining interactions are intermolecular in nature between two host molecules. These involve a *meta*- or *para*-aromatic hydrogen of one host and a hydroxy or methoxy oxygen atom of another host (Table 72).

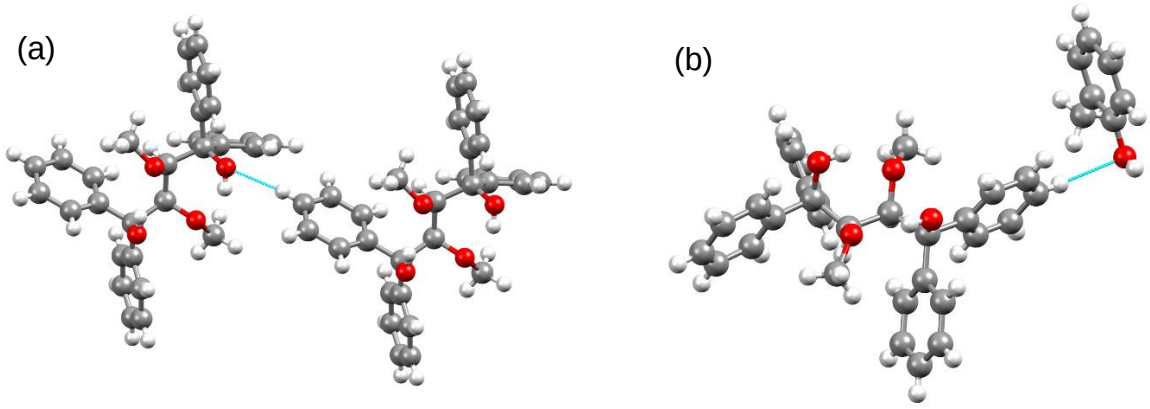

Figure 148: Non-classic hydrogen bonding interactions depicted by means of light-blue dashes in the 2DMT•*o*-CR complex; a) (host)*p*-ArH···O(host hydroxy); b) (host)*p*-ArH···O(guest hydroxy).

Table 72: Non-classic inter- and intra- molecular hydrogen bonding interactions in the DMT complexes with the cresols.

Complex	Non-covalent interaction	Distance (Å) D–A	Angle (°) D-H···A
2DMT•*p*-CR	(host)*o*-ArH···O(host hydroxy)	2.659(2)	102
	(host)*o*-ArH···O(host hydroxy)	2.762(2)	100
	(host)*o*-ArH···O(host hydroxy)	2.765(2)	100
	(host)*o*-ArH···O(host hydroxy)	2.659(2)	101
	(host)*m*-ArH···O(host methoxy)[a]	3.517(2)	168
	(host)*p*-ArH···O(host hydroxy)[b]	3.284(3)	168
2DMT•*m*-CR	(host)*o*-ArH···O(host hydroxy)	2.653(3)	102
	(host)*o*-ArH···O(host hydroxy)	2.757(3)	100
	(host)*o*-ArH···O(host hydroxy)	2.646(3)	102
	(host)*p*-ArH···O(host hydroxy)[b]	3.297(4)	166
2DMT•*o*-CR	(host)*o*-ArH···O(host hydroxy)	2.652(2)	102
	(host)*o*-ArH···O(host hydroxy)	2.755(3)	100
	(host)*o*-ArH···O(host hydroxy)	2.761(3)	100
	(host)*o*-ArH···O(host hydroxy)	2.652(3)	101
	(host)*p*-ArH···O(host hydroxy)[b]	3.312(3)	170
	(host)*p*-ArH···O(guest hydroxy)[b]	3.437(5)	172

Symmetry operators: a) 3/2–x,–1/2+y,1–z; b) –1/2+x,–1/2+y,z

π–π and CH–π interactions

As expected in systems rich in aromatic moieties, π–π stacking interactions are plentiful, albeit that they are relatively weak in nature. The interactions between host molecules range between 4.731(1) and 5.997 Å. In turn, host–gest stacking interactions vary in length between 5.206(3)–5.836(2) Å. Figure 149 depicts examples of these interactions from the 2DMT•*m*-CR complex.

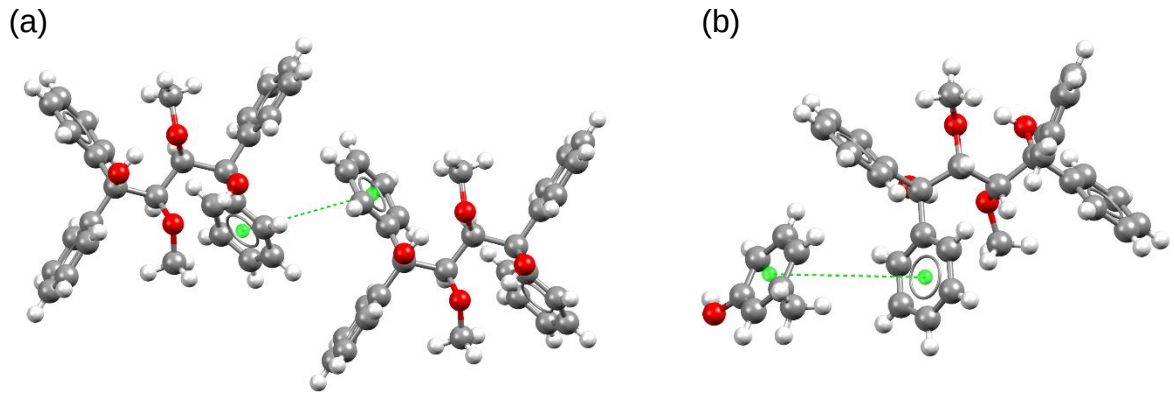

Figure 149: Representative π–π stacking interactions in the 2DMT•*m*-CR complex; a) an intermolecular host–host interaction; b) an intermolecular host–guest interaction.

CH–π stabilizing interactions within these complexes present predominantly as intramolecular contacts between a host methoxy hydrogen and an adjacent phenyl ring (2.80–2.94 Å, 146–151°). Each complex has four of these interactions. Furthermore, the 2DMT•*m*-CR complex has one (host)*m*-ArH···Cg(host) interaction (2.95 Å, 170°), while the DMT complex with *o*-CR as guest has an (host)*m*-ArH···Cg(host) interaction (2.97 Å, 170°) and a (guest hydroxy)O-H···Cg(host) interaction of 2.70 Å and 173° (Figure 150). For a more detailed insight, these interactions are listed in Table 73.

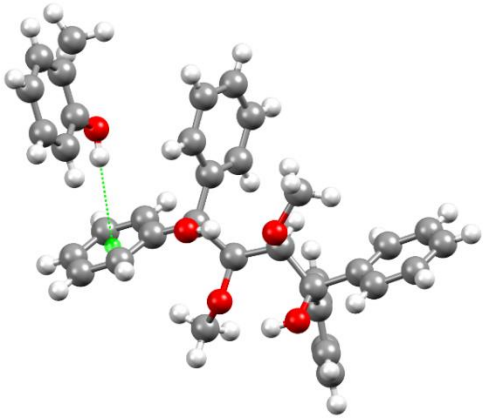

Figure 150: CH–π stabilizing interactions between host and guest in the 2DMT•*o*-CR complex. The interaction is depicted as a green dashed line.

Table 73: C-H–π stabilizing interactions in the host-guest complexes of DMT and the cresols.

Complex	Non-covalent interaction	Distance (Å)	Angle (°)	Symmetry operator
2DMT•*p*-CR	(host methoxy)C-H···Cg(host)	2.85	147	x,y,z
	(host methoxy)C-H···Cg(host)	2.92	150	x,y,z
	(host methoxy)C-H···Cg(host)	2.85	145	x,y,z
	(host methoxy)C-H···Cg(host)	2.84	151	x,y,z
2DMT•*m*-CR	(host methoxy)C-H···Cg(host)	2.94	149	x,y,z
	(host methoxy)C-H···Cg(host)	2.86	147	x,y,z
	(host methoxy)C-H···Cg(host)	2.80	146	x,y,z
	(host methoxy)C-H···Cg(host)	2.84	147	x,y,z
	(host)*m*-ArH···Cg(host)	2.95	170	1–x, y, 1–z
2DMT•*o*-CR	(host methoxy)C-H···Cg(host)	2.89	149	x,y,z
	(host methoxy)C-H···Cg(host)	2.85	147	x,y,z
	(host methoxy)C-H···Cg(host)	2.83	145	x,y,z
	(host methoxy)C-H···Cg(host)	2.81	150	x,y,z
	(host)*m*-ArH···Cg(host)	2.97	170	1–x, y, 1–z
	(guest hydroxy)O-H···Cg(host)	2.70	173	–1/2+x,–1/2+y,z

Short Contacts

Host–host contacts shorter than the van der Waals radii of the participating atoms range between 2.24 and 2.89 Å (144–171°) (Table 74). These contacts present either as a (host hydroxy)O-H···*p*-ArH(host) or (host)*p*-ArH···*m*-ArC(host) interaction. The 2DMT•*p*-CR complex lacks intermolecular host–guest short contacts whereas the DMT complexes with *m*-CR and *o*-CR both have two host–guest short contact interactions. These present between a host aromatic carbon and the guest hydroxy oxygen atom, and between a host aromatic hydrogen and guest hydroxy oxygen atom (2.13–3.09 Å, 102–172°, Table 74). Figure 151 shows some of these contacts for a better understanding.

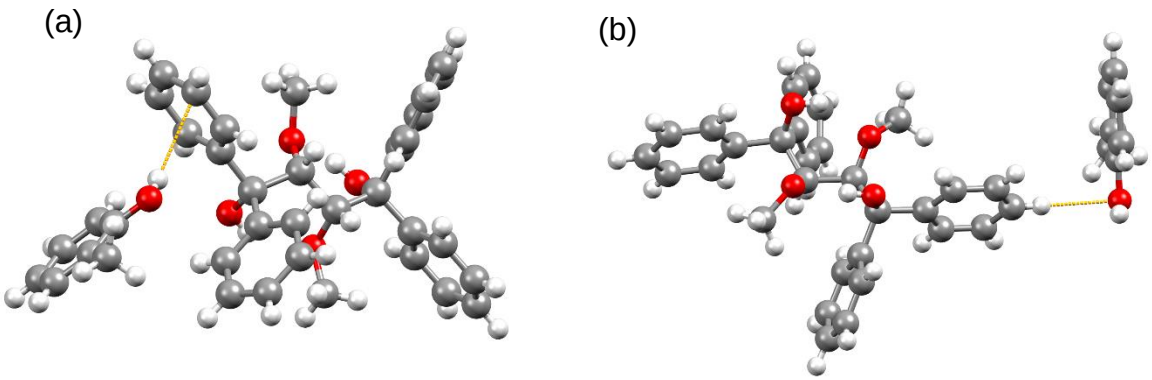

Figure 151: Short host–guest contacts in the complex of DMT•*o*-CR; a) (host)*m*-ArC···H-O(guest hydroxy) and b) (host)*p*-ArH···O-C(guest hydroxy).

Table 74: Summary of the various contacts shorter than the van der Waals radii found in the DMT complexes with the cresol guests.

Complex	Non-covalent interaction	Distance (Å)	Angle (°)	Symmetry operator
2DMT•*p*-CR	(host hydroxy)O-H···*p*-ArH(host)	2.30	167	–1/2+x,1/2+y,z
	(host hydroxy)O-H···*p*-ArH(host)	2.29	148	1/2+x,1/2+y,z
	(host)*p*-ArH···*m*-ArC(host)	2.85	144	1–x,y,–z
2DMT•*m*-CR	(host hydroxy)O-H···*p*-ArH(host)	2.30	170	–1/2+x,1/2+y,z
	(host hydroxy)O-H···*p*-ArH(host)	2.32	146	1/2+x,1/2+y,z
	(host)*p*-ArH···*m*-ArC(host)	2.89	144	1–x,y,–z
	(host)*o*-ArC···O-C(guest hydroxy)	3.09	102	1/2+x,1/2+y,z
	(host)*m*-ArH···H-O(guest hydroxy)	2.13	106	1–x,y,–z
2DMT•*o*-CR	(host hydroxy)O-H···*p*-ArH(host)	2.24	171	–1/2+x,1/2+y,z
	(host hydroxy)O-H···*p*-ArH(host)	2.28	150	1/2+x,1/2+y,z
	(host)*p*-ArH···*m*-ArC(host)	2.86	148	1–x,y,–z
	(host)*m*-ArC···H-O(guest hydroxy)	2.51	143	1/2+x,1/2+y,z
	(host)*p*-ArH···O-C(guest hydroxy)	2.49	172	1/2+x,1/2+y,1+z

Table 75: Significant host–guest interactions for the complexes of DMT with the cresol guests.

Interaction	2DMT•*p*-CR	2DMT•*m*-CR	2DMT•*o*-CR
π–π	5.261(6)–5.797(6) Å (8 contacts)	5.206(3)–5.836(2) Å (7 contacts)	5.328(2)–5.887(2) Å (8 contacts)
CH–π	None	None	2.70 Å, 173° (guest hydroxy)O-H···Cg(host)
Short contacts	None	3.09 Å, 102°, < (host)*o*-ArC···O-C(guest hydroxy) 2.13 Å, 106°, < (host)*m*-ArH···H-O(guest hydroxy)	2.51 Å, 143°, < (host)*m*-ArC···H-O(guest hydroxy) 2.49 Å, 172°, < (host)*p*-ArH···O-C(guest hydroxy)

*< denotes contacts less than the sum of the van der Waals radii and << denotes contacts less than this sum minus 0.2 Å

Table 75 contains a summary of the host–guest interactions measured in these complexes, in order to more readily identify significant interactions within these complexes that contribute to the selective behaviour of DMT towards the cresols. These contacts are skewed towards the more preferred *o*-CR guest in terms of both number and strength. For example, this guest experiences a CH–π interaction with the host which is absent in the less preferred complexes. In addition, this complex has two contacts that are much shorter (denoted by <<) than the van der Waals radii of the participating atoms. In contrast, the 2DMT•*m*-CR complex has two notable short contacts of which only one is significantly shorter than the van der Waals radii of the participating atoms, while *p*-CR does not experience these interaction types. Only π–π stacking interactions retain *p*-CR in the host crystal.

Finally, a comparison of the mode of packing in all three host-guest complexes with the cresol isomers was performed by disregarding the guest molecules in the packing calculation. As these complexes are isostructural, it was not surprising that the guests are held in discrete cavities in each case (Figure 152).

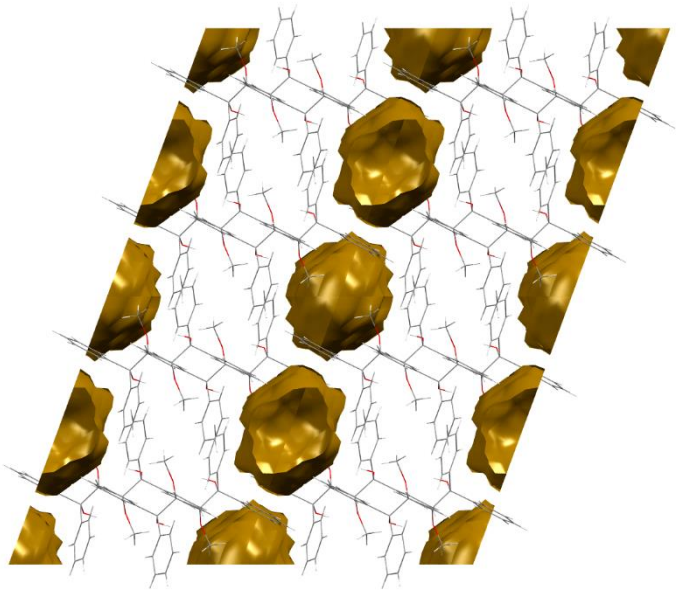

Figure 152: The discrete cavity-guest packing mode in the 2DMT•*p*-CR complex as representative example of the guest packing in all of the complexes with the cresol guests.

9.6 Hirshfeld Surface Analysis

As has become customary, Hirshfeld surface analysis was employed to better visualize the magnitude of contacts present in these DMT complexes with the cresol isomers. Figure 153a shows the two-dimensional fingerprint plot obtained for the 2DMT•*p*-CR complex. The four distinct features that occur closest to the origin of the fingerprint plot include the spikes S1 and S2 (C···H and H···H interactions, respectively) as well as broader wing-like areas W1 and W2, both indicative of H···H interactions between host and guest. The fingerprint plot for the 2DMT•*m*-CR complex (Figure 153b) contains only two broad wing areas W1 and W2, both of which represent H···H interactions. C···H interactions are found scattered throughout the plot at further d_e and d_i distances. The 2DMT•*o*-CR complex fingerprint (Figure 153c) displays a sharp spike, S1, indicative of C···H interactions. The broad W1 area is indicative of H···H interactions as usual, whereas S2 represents very prominent O···H interactions, a feature that is absent in the preceding two plots. Figure 154 quantifies the different types of interactions observed in each complex. In all three complexes, the number of H···H interactions are approximately equal (~67–68%). The second most numerous are of the C···H type. While they do not differ significantly from one another, they do increase from least preferred to most preferred guest [*m*-CR (23.4%) < *p*-CR (26.8%) < *o*-CR (29.2%)]. Furthermore, both O···C and O···H interactions (while few in comparison with H···H and C···H) also decrease in this same order.

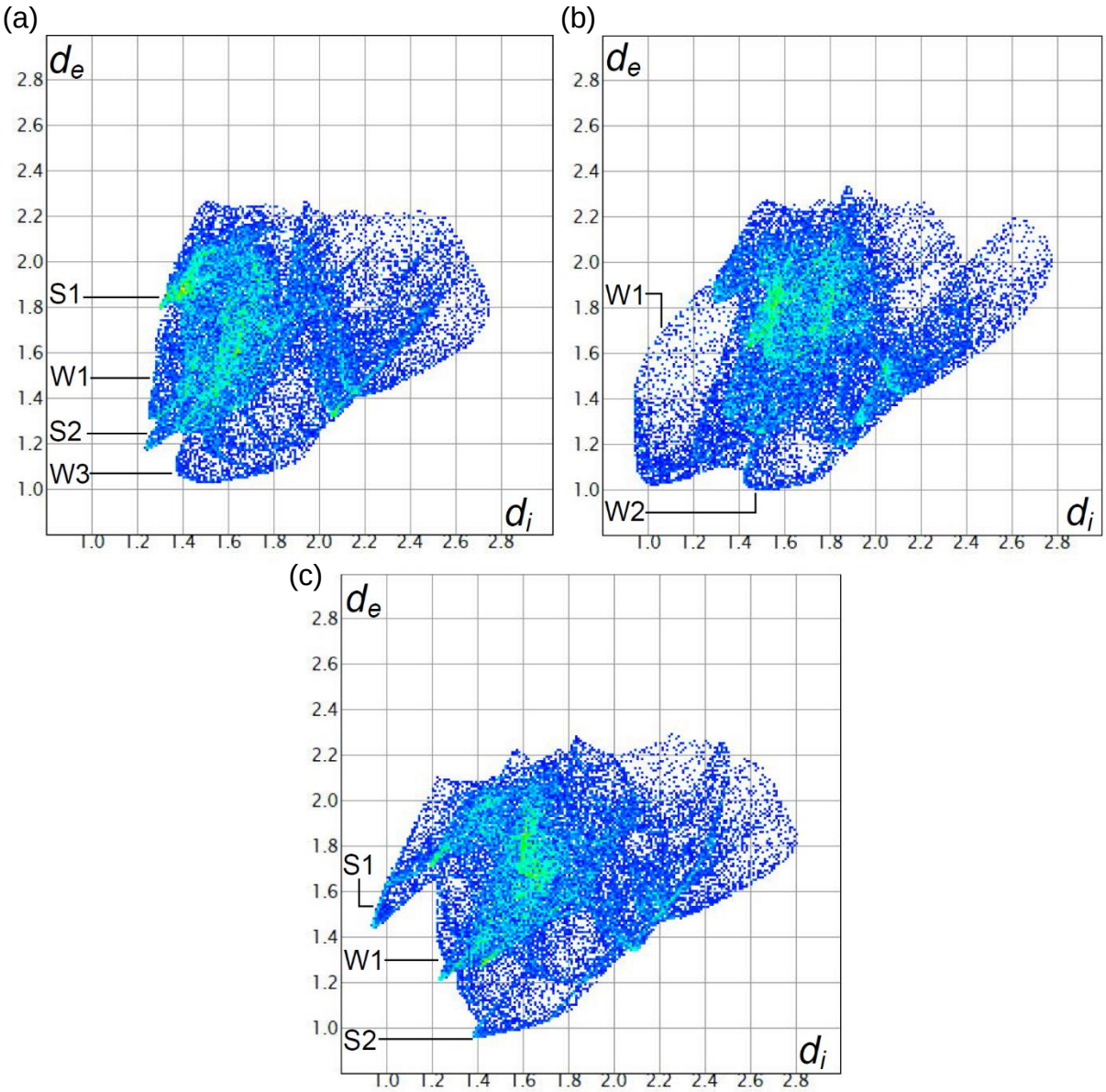

Figure 153: Two-dimensional fingerprint plots obtained from Hirshfeld surfaces for the inclusion complexes of a) 2DMT•*p*-CR, b) 2DMT•*m*-CR, and c) 2DMT•*o*-CR.

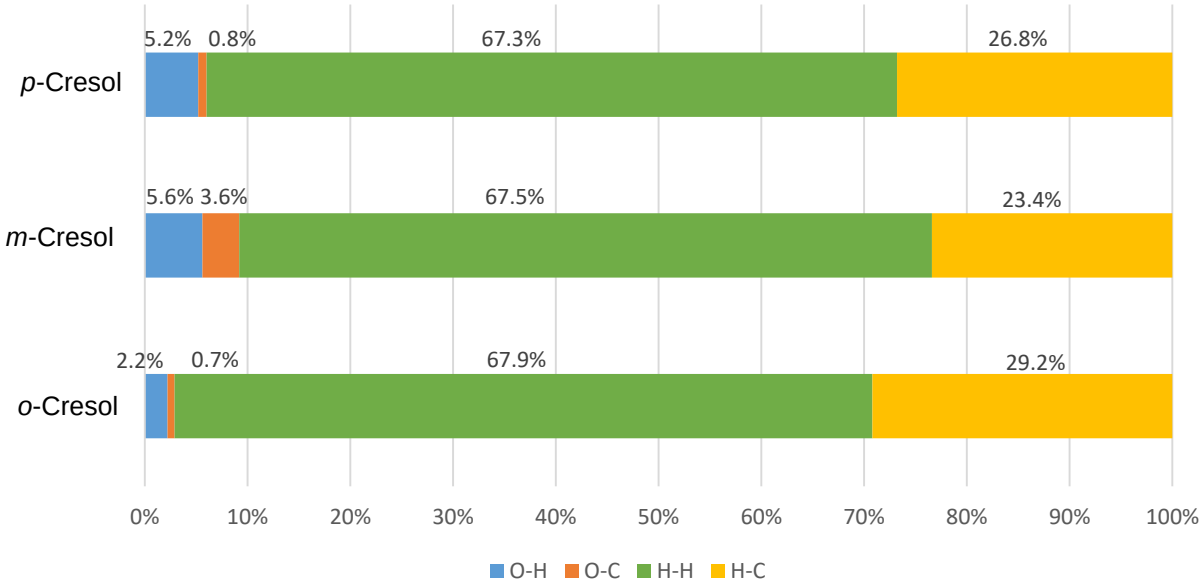

Figure 154: Graphical display showing the percentage and type of intermolecular interactions in each complex.

9.7 Conclusion

Through these experiments, it was shown that DMT successfully formed inclusion complexes with the isomeric cresol compounds. The host:guest ratio was 2:1 in each case. DMT showed discriminatory behaviour towards the inclusion of these guests when crystallized from binary and ternary mixtures. *o*-CR was selectively included above the more difficult to separate *m*-CR and *p*-CR isomers. Furthermore, DMT showed very similar selectivity for *m*-CR and *p*-CR, with the latter only slightly preferred. Thermal analyses of the complexes confirmed the selectivity order displayed by DMT. Consideration of the various parameters (T_{end}, T_p and T_{on}–T_b) indicated a thermal stability order of *o*-CR > *p*-CR > *m*-CR which is in direct accordance with the aforementioned selectivity order. Single crystal X-ray analysis showed the presence of numerous significant interactions between the host and *o*-CR while the less preferred guests experienced fewer of these. Hirshfeld surface analysis indicated a correlation between the relative amount of C···H interactions between host and guest and the selectivity order: the most preferred guest experienced fewer of these interactions (*o*-CR, 23.4%) while the least preferred guest experienced more

(*m*-CR, 29.2%). Overall, this work shows some promise for the possible future application of this host in the separation of the cresol isomers, more especially *o*-CR from the *m*- and *p*- isomers.

Chapter 10: Miscellaneous

10.1 Other Inclusions

In addition to the guest compounds successfully included by DMT in Chapters 3–9, the host's ability to form complexes with a variety of other, unrelated compounds was also assessed. These are comprised of aromatic, heterocyclic and aliphatic compounds. Table 76 lists these compounds and their inclusion result as determined through ^{1}H-NMR spectroscopy.

Table 76: Miscellaneous inclusion compounds of DMT.

Guest	H:G	Guest	H:G
Acetonitrile	*a*	Cyclohexanone	2:1
Acetophenone	2:1	Diethyl ether	*a*
Adamantane*b*	–	Dioxane	*a*
Anthracene*b*	–	DMF	*a*
Benzene	2:1	Ethanol	–
p-Bromoanisole	*a*	Ethyl acetate	*a*
4-Bromobenzotrifluoride	2:1	Iodobenzene	2:1
Bromocyclohexane	2:1	Isobutylbenzene	2:1
Bromomesitylene	–	Limonene	2:1
1-Bromonaphthalene	*a*	Methanol	–
2-Bromo-p-xylene	2:1	Menthol*b*	–
p-Bromotoluene*b*	*a*	Mesitylene	–
2-Butanol	–	Methylcyclohexane	2:1
Camphor*b*	–	2-Methylcyclohexanone	*a*
2-Chlorobenzaldehyde	*a*	3-Methylcyclohexanone	*a*
4-Chlorobenzaldehyde*b*	*a*	4-methylcyclohexanone	*a*
Chlorobenzene	2:1	2-Methylpyridine	*a*
p-Chloroiodobenzene*b*	–	3-Methylpyridine	*a*
2-Chloronitrobenzene*b*	*a*	4-Methylpyridine	*a*

3-Chloronitrobenzene[b]	[a]	Morpholine	[a]
4-Chloronitrobenzene[b]	[a]	Naphthalene[b]	–
2-Chlorophenol	[a]	Phenol[b]	[a]
3-Chlorophenol	[a]	Piperidine	[a]
4-Chlorophenol[b]	[a]	2-Propanol	–
4-Chlorotoluene	[a]	Pyridine	[a]
Citronellol	–	Tetrahydrofuran	[a]
Cyclohexane	2:1	Tetralin	2:1
Cyclohexene	2:1	Thymol[b]	[a]
Decalin	2:1	Vanilin[b]	–

A hyphen (–) is indicative that no inclusion complex formed according to ^{1}H-NMR. [a]difficult to crystallize. [b]guest was a solid at room temperature, and required a co-solvent (ethanol) for dissolution.

From the inclusion experiments listed in Table 76 it is interesting to note that DMT either did not form inclusion compounds with potential guests which are solids at room temperature, or had difficulty crystallizing from them. In cases such as the chloronitrobenzene isomers, phenol and thymol (where they have relatively low melting points) no host, guest or complex crystallized upon standing when DMT was dissolved in the melted guest or together with a co-solvent. Compounds with a relatively high melting point (such as adamantane, anthracene, camphor and naphthalene) crystallized out of solution with a co-solvent upon standing without forming a host-guest complex. As the alcohols methanol, ethanol and 2-propanol were also not included, they were deemed as appropriate co-solvents in which to dissolve DMT and potential solid guests. Furthermore, DMT failed to crystallize from non-aromatic solvents such as acetonitrile, diethyl ether, dioxane and ethyl acetate. Basic compounds such as morpholine, pyridine and the methylpyridines also failed to produce any solid.

DMT formed inclusion complexes with many substituted phenyl compounds such as acetophenone, the halobenzenes and isobutylbenzene. DMT also included some alicyclic compounds such as cyclohexanone (but failed to crystallize from the methylcyclohexanones), cyclohexane, cyclohexene and decalin. In all cases where a host-guest complex formed, the host:guest ratio was 2:1.

10.2 Computational Analysis

A conformational search was performed on DMT at a molecular mechanics level using the MMFF force field. From this search, it was observed that the group of lowest energy conformers (**a**) adopted a butane backbone with *anti* geometry. The two hydroxy groups and the two methoxy groups were arranged *syn* on the butane backbone with 1,3- and 2,4- hydrogen bonding interactions between the hydroxy and methoxy moieties stabilizing their arrangement. The second lowest energy conformer family (**b**), while having the same basic arrangement, had a smaller butane dihedral angle and, as a result, this conformer experienced greater 1,2- and 3,4- hydrogen bond stabilization. The next conformer group, which was significantly less stable (**c**), had the butane backbone arranged in a *gauche* conformation, with the hydroxy groups *anti* to the methoxy groups, and the methoxy methyl groups *anti* relative to one other. In this group of conformers, a 1,4- hydrogen bond prevails. Table 77 shows the computed energies and structural parameters of conformers **a**–**c**.

Subsequent refinement of the geometry of these three lower energy conformers were performed at the DFT level (RB3LYP/6-31G*). These refinements, done in vacuo, resulted in the reversal of the stability order for conformers **a** and **b**. Further refinement at the RB3LYP/6-311G* level resulted in a reversion of the stability order, albeit with a small energy difference.

The ideal hydrogen bond has a linear D–H···A arrangement, but, geometric constraints within the DMT molecule makes this impossible. Regardless, hydrogen bonding is still identifiable through consideration of the donor O–H bond direction relative to the acceptor oxygen, as well as the distance between these interacting atoms (ranging between 1.62–2.09 Å, intermediate strength).

The electrostatic potential surfaces were computed for the optimized DFT structures. These surfaces assist in indicating the degree of hydrogen bonding interactions. The positive polarity typically associated with the hydroxy hydrogens on C(1) and C(4) is spread out in Figure 155a due to their participation in 1,3- and 2,4- hydrogen bonding. In contrast, the concentrated positive charge on the hydroxy hydrogen in Figure 155c is indicative of that hydroxy acting only as a hydrogen bond acceptor.

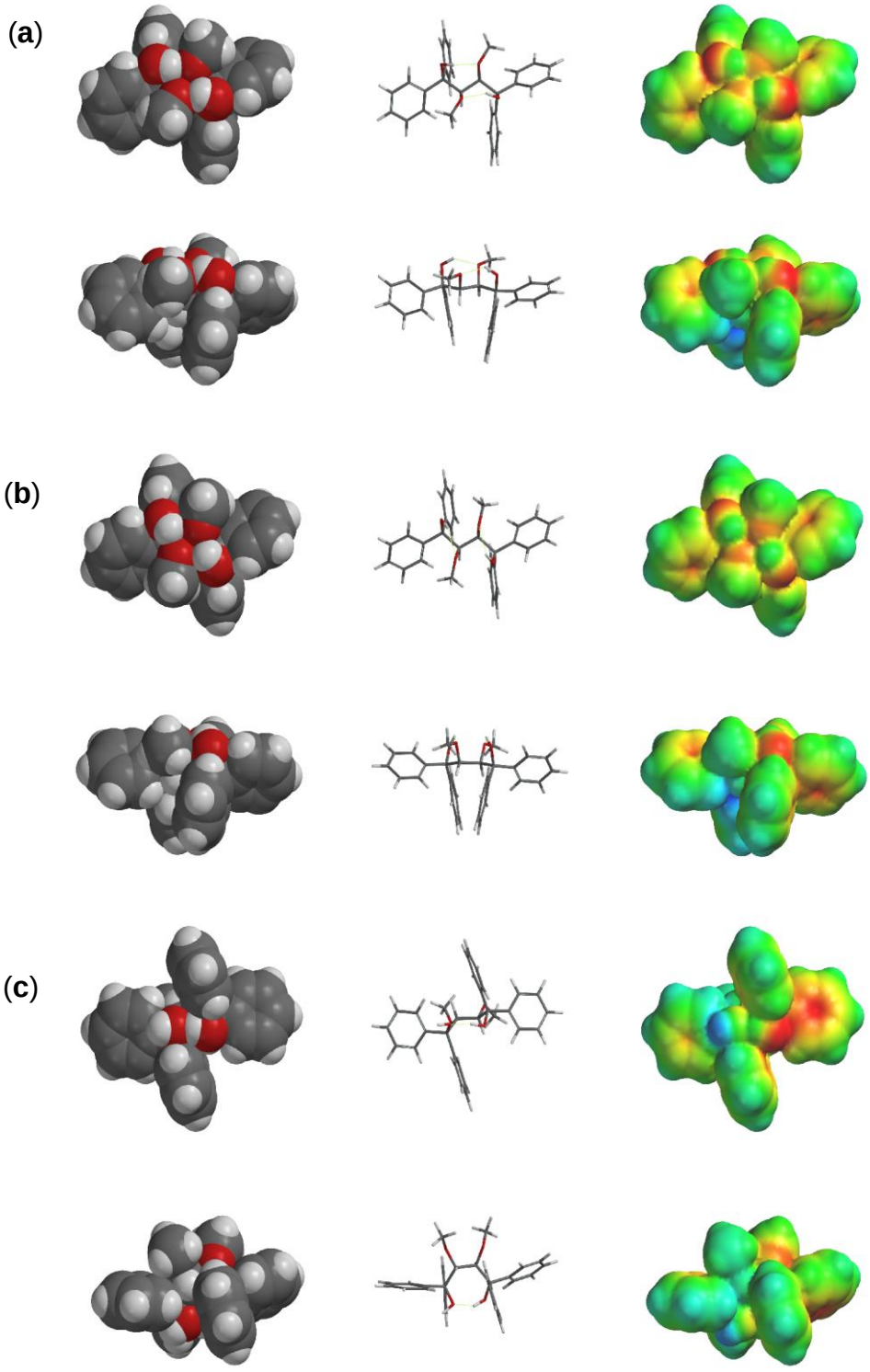

Figure 155: Perspectives of the DFT-optimised structures a–c and their electrostatic potential surfaces. Colours near red represent large negative electrostatic potentials, while near blue represent large positive values.

Table 77: Computed energies and structural parameters in conformers a–c of DMT.

Computational level and conformers	Energy ($kJ.mol^{-1}$)	E_{rel} ($kJ.mol^{-1}$)	Hydrogen bonding relationships, DH···A distances and D···A distances (Å)*			Torsion angle (°)
			1,2	1,3	1,4	C1,C2,C3,C4
MMFF						
a	865.98	0		1.911, 2.685		–175.12
b	866.1	0.12	2.086, 2.724			–168.81
c	870.38	4.4			1.619, 2.516	–59.75
DFT (RB3LYP/6-31G*)						
a	–3838736.02	1.44		1.864, 2.726		–179.05
b	–3838737.46	0	2.035, 2.645			–162.63
c	–3838731.52	5.94			1.774, 2.696	–62.1
DFT (RB3LYP/6-311G*)						
a	–3839581.42	0		1.870, 2.715		179.54
b	–3839580.44	0.98	2.053, 2.645			–162.85
c	–3839575.95	5.47			1.762, 2.679	–63.61

*Due to the symmetrical nature of these conformers, distances reported for 1,2- and 1,3- intramolecular interactions are equal to those of 3,4- and 2,4- intramolecular interactions.

10.3 DMT Single Crystal X-Ray Analysis

Suitable crystals of DMT without any guest present for X-ray analysis were obtained through the slow crystallization of the host from citronellol. DMT crystallized in the tetragonal $I4_1$ space group. Table 78 lists crystallographic data for this crystal while Figure 156 shows the unit cell and Figure 157 a stereoview of the packing.

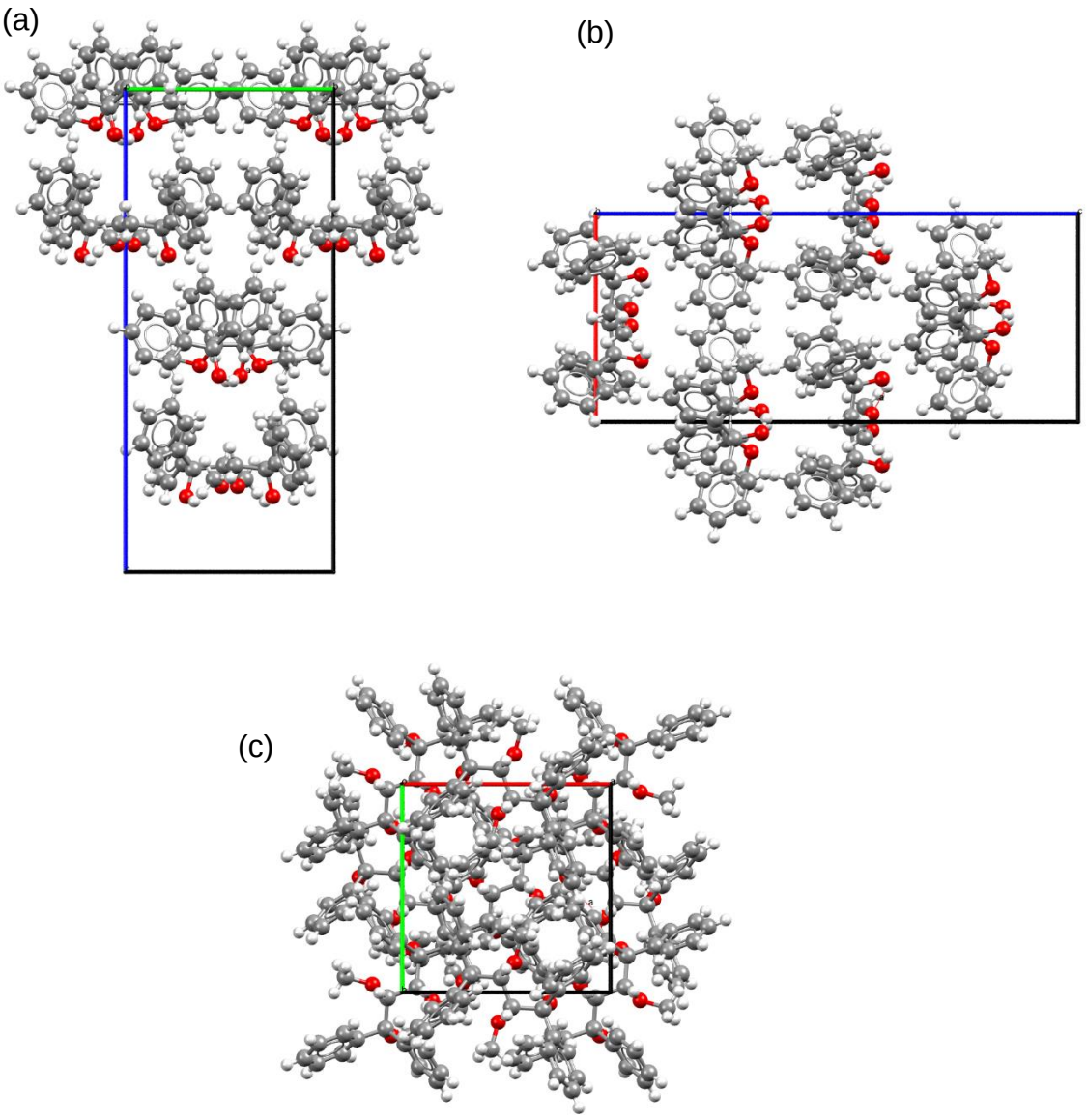

Figure 156: Unit cell of DMT in the absence of guest; a) view down the crystallographic 'a' axis; b) view down the crystallographic 'b' axis, and c) view down the crystallographic 'c' axis.

Table 78: Crystallographic data for DMT in the absence of guest.

Parameter	DMT
Chemical formula	$C_{30}H_{30}O_4$
Formula weight	454.54
Crystal system	Tetragonal
Space group	$I4_1$
μ (Mo-Kα)/mm^{-1}	0.078
a/Å	10.2823(6)
b/Å	10.2823(6)
c/Å	23.8173(17)
alpha/°	90
beta/°	90
gamma/°	90
V/Å ^{3}	2518.1(3)
Z	4
F(000)	968
Temp./K	200
Restraints	1
Nref	3129
Npar	156
R	0.0307
wR2	0.0826
S	1.09
θ min-max/°	2.2, 28.3
Tot. data	39639
Unique data	3129
Observed data [I > 2.0 sigma(I)]	2982
R_{int}	0.020
Dffrn measured fraction θ full	1.000
Min. resd. dens. (e/ $Å^3$)	–0.13
Max. resd. dens. (e/ $Å^3$)	0.16

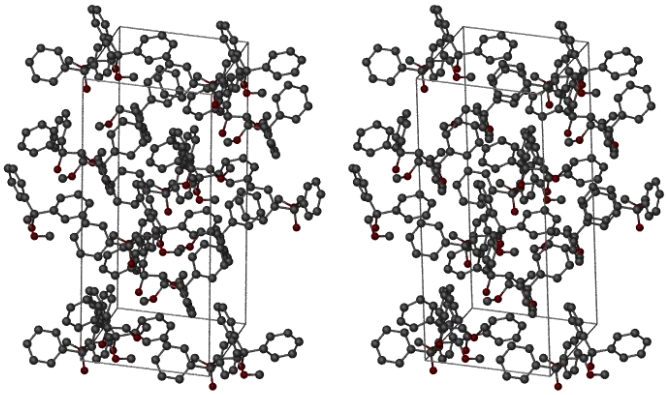

Figure 157: Stereoview of the DMT packing.

The host experiences four intermolecular π–π stacking interactions, three of which are relatively weak [5.084(1)–5.865(1) Å]. The fourth is significantly shorter at 4.267(1) Å (Figure 158).

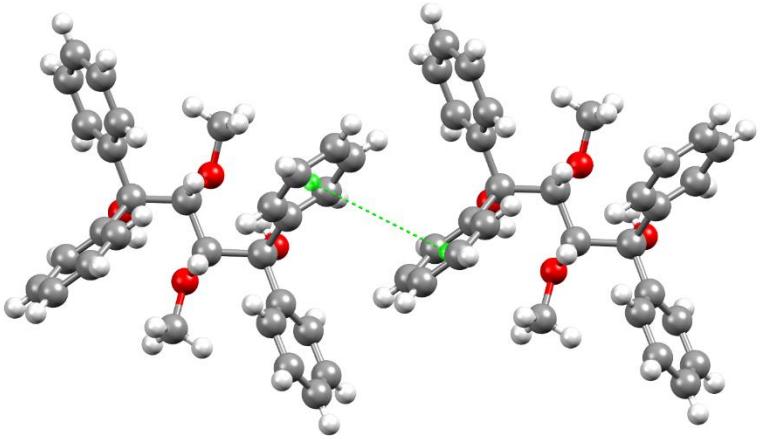

Figure 158: Shortest intermolecular stacking interaction between host molecules.

In addition to a CH–π interaction between hosts, two short contacts are present that stabilize the crystal packing. These include a (host)*m*-ArH···*o*-ArC(host) and a (host hydroxy)C-O···*o*-ArH(host) interaction summarized in Table 79. Figure 159 depicts these short contacts.

Table 79: Prominent intermolecular interactions experienced by DMT.

Interaction	DMT
π–π	4.267(1)–5.865(1) Å (4 contacts)
CH–π	2.79 Å, 166° (host)*m*-ArH···Cg(host)
Short contacts	2.80 Å, 162°, < (host)*m*-ArH···*o*-ArC(host) 2.70 Å, 146°, < (host hydroxy)C-O···*o*-ArH(host)

*< denotes contacts less than the sum of the van der Waals radii

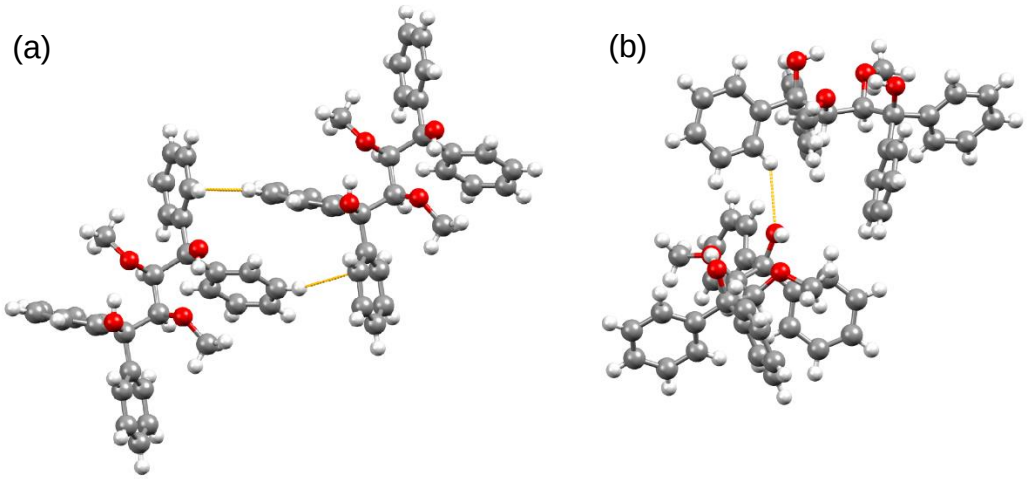

Figure 159: Prominent short contacts between DMT molecules; a) (host)*m*-ArH···*o*-ArC(host) and b) (host hydroxy)C-O···*o*-ArH(host).

The host geometry is slightly different from that of the computed conformers. While resembling conformer **a** with 1,3- and 2,4- intramolecular hydrogen bonds clearly evident, there are significant differences in DH···A and D···A distances. In the crystal structure, these values are 2.02 and 2.70 Å, respectively while they were computed to be 1.87 and 2.72 Å. The torsion angle was measured to be 165.38° which is closer to

that of conformer **b** than **a**. These differences may be ascribed to the intermolecular interactions DMT experiences with other host molecules within the crystal, since computations were carried out in vacuo and thus did not take these into account.

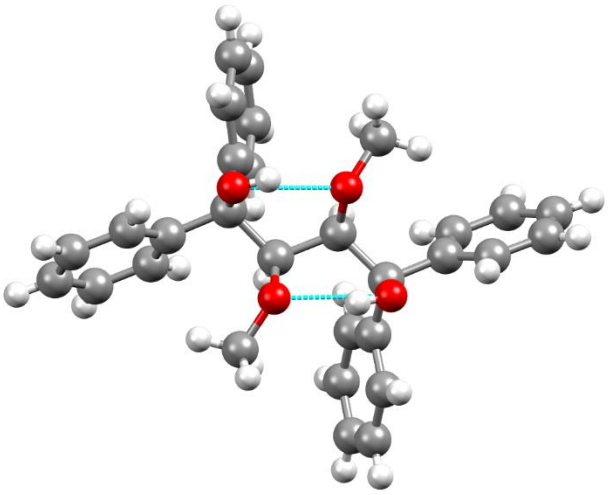

Figure 160: Crystal structure conformation of DMT resembles the computed 'a' conformer.

10.4 Isostructurality of Inclusion Compounds

As noted throughout this work, the host crystal lattice is isostructural across all the X-ray structures analysed. The uncomplexed crystal structure, however, is not isostructural, as is evident from the differing crystal systems and space groups for complexed (monoclinic, *C*2) and uncomplexed (tetragonal, $I4_1$) DMT. Figure 161 also shows the simulated powder X-ray diffraction (PXRD) traces of selected host-guest complexes as well as that of uncomplexed DMT. From this figure, it is clear that the inclusion complexes all share the same peaks, with minor differences in 2Θ values and intensities ascribed to small geometrical differences induced as a result of the presence of different guest species in each complex. The PXRD trace of DMT alone (dark blue) is significantly different to the traces of the inclusion complexes.

The crystal packing similarity calculation routine of the software package was used to generate best-fit superimposed crystal structures obtained by least-squares analysis.

Mercury All the crystal structures available were compared to that of the arbitrarily chosen 2DMT•aniline complex. As a representative sample, the packing overlay of the host from this complex, and the host from the 2DMT•toluene complex is shown in Figure 162. A molecular cluster size of 15 molecules was compared in each case. The similarity calculations allow for the numerical determination of the similarity in PXRD traces between crystal structures as well as the root mean square (RMS) deviation of distances between equivalent atoms in each structure. Table 80 lists these values for ease of comparison from which it can be seen that there is a high PXRD similarity between all the inclusion complexes (> 0.986), whereas the PXRD of DMT on its own has a similarity of only 0.86. In addition, the RMS values are quite low for all the inclusion complexes (0.037–0.316 Å), and higher for DMT on its own (0.534 Å). Similarly, a packing overlay of the host molecules from the inclusion complexes result in all 15 host molecules matching with the host molecules from the reference complex, whereas only four out of the fifteen host molecules from the packing of DMT on its own overlaps with the reference complex (Figure 163). These considerations allow us to state with confidence that the host structures are isostructural in each inclusion complex analysed in this work.

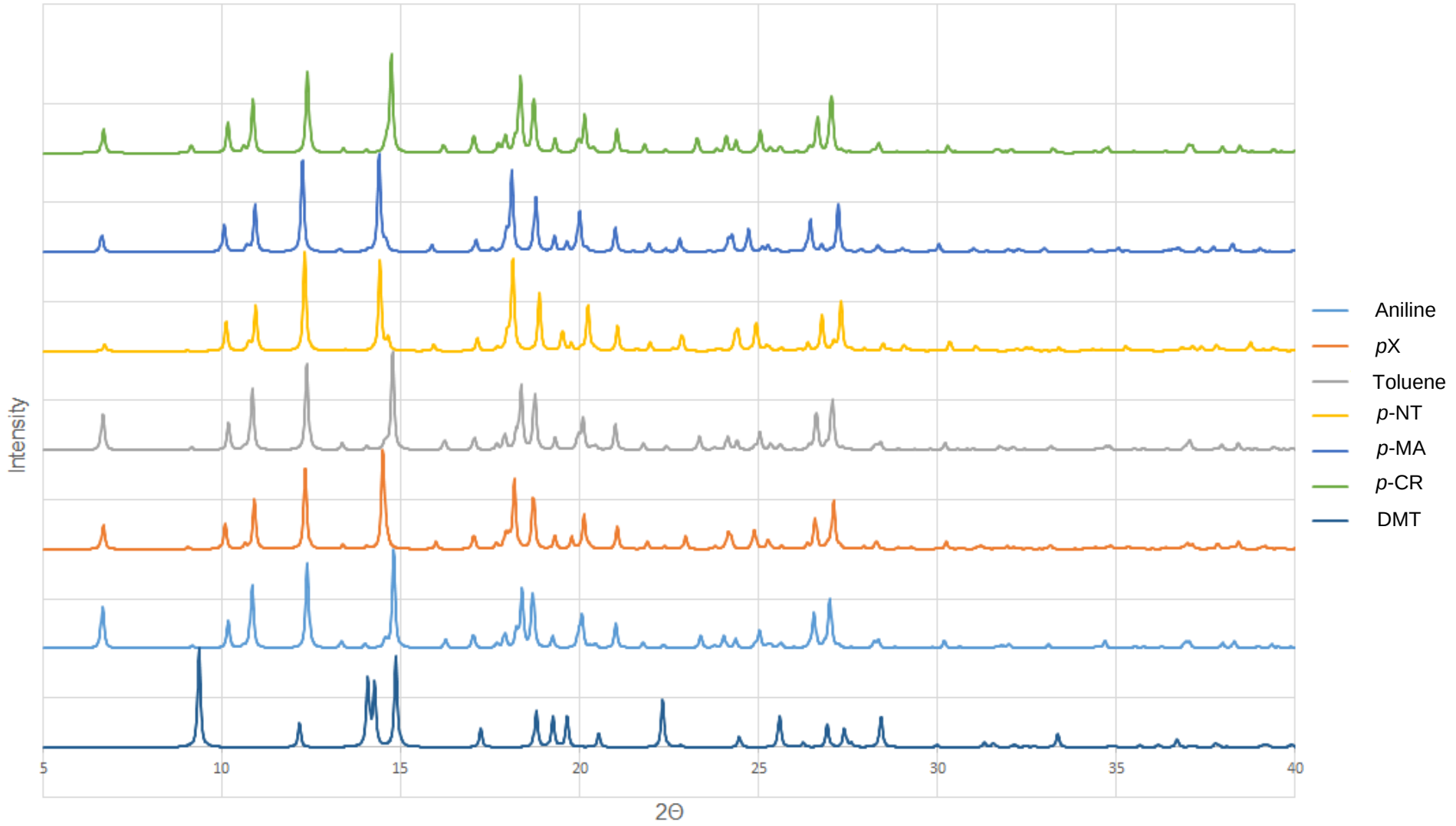

Figure 161: Overlaid PXRD traces of selected inclusion complexes of DMT and uncomplexed DMT.

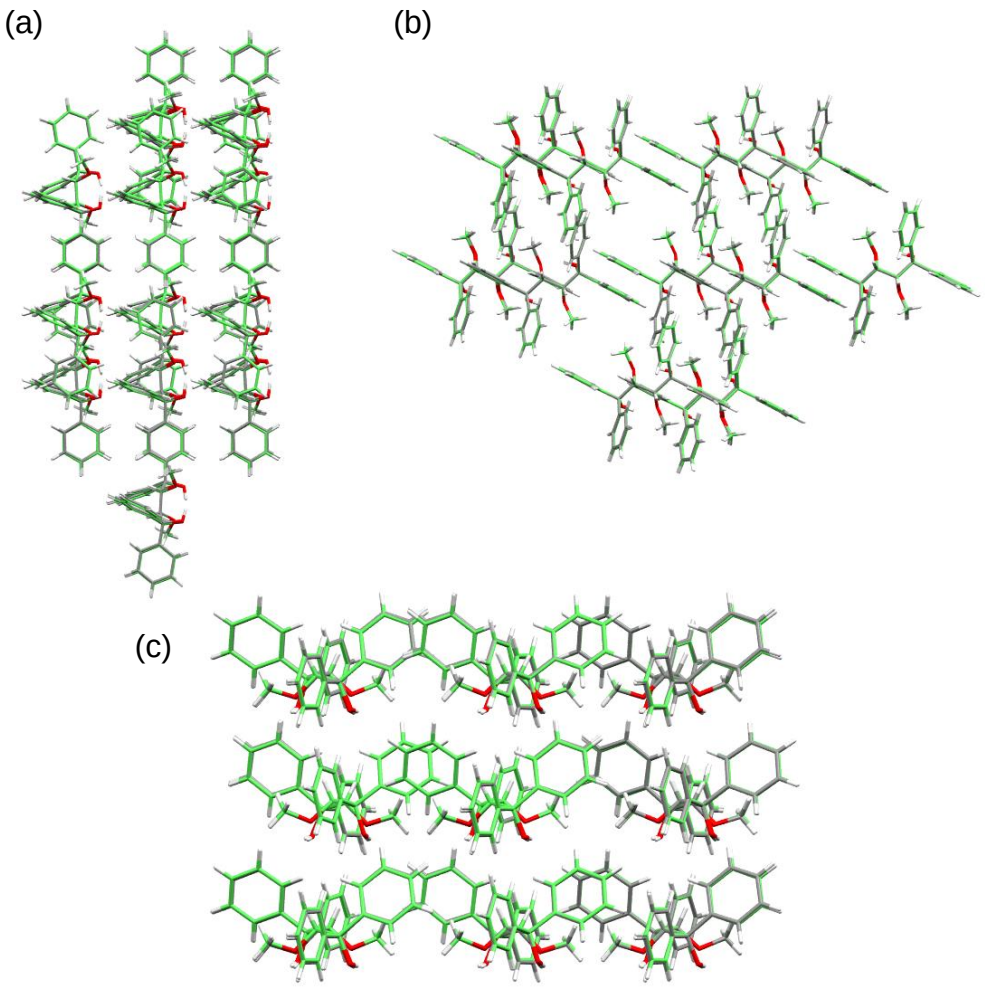

Figure 162: Molecular overlay of the aniline (grey) and toluene (green) complexes of DMT as a representative example. Shown here are perspectives from the crystallographic 'a', 'b' and 'c' axes.

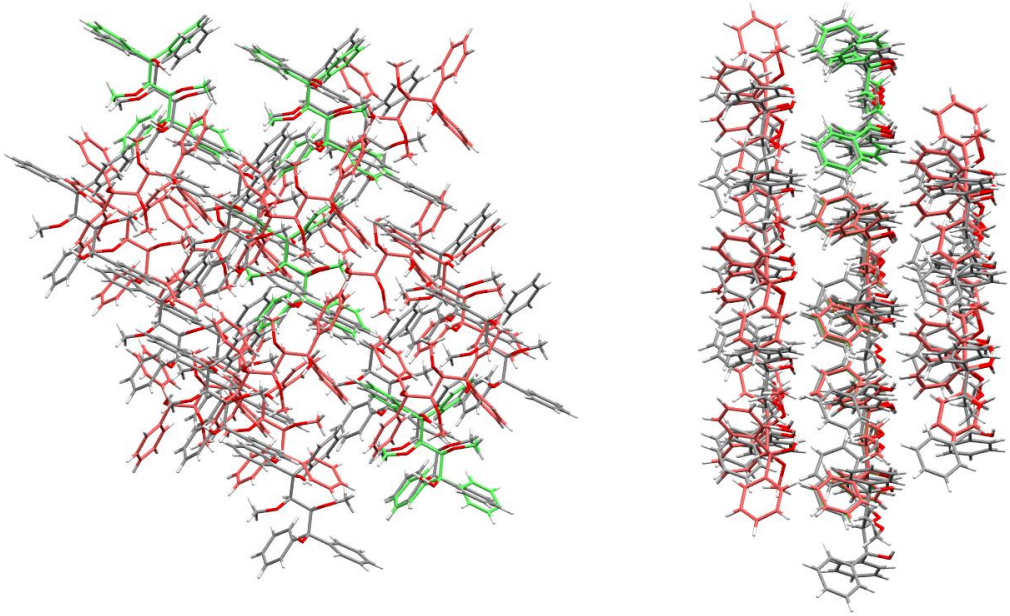

Figure 163: Two perspectives of the overlay of the host packing of the aniline complex (grey) and DMT without guest (red and green) to show the mismatch between the host packing. DMT moleules in green match with the those in the aniline complex, and those in red do not.

Table 80: Structural similarity parameters of various inclusion complexes of DMT and DMT with no guest, relative to the 2DMT•aniline complex.

Comparison Complex	Number of molecules in common	Root mean square (Å)	PXRD similarity
2DMT•NMA	15 out of 15	0.078272	0.999098
2DMT•DMA	15 out of 15	0.159599	0.994658
2DMT•*p*-TD	15 out of 15	0.0851057	0.998303
2DMT•*m*-TD	15 out of 15	0.0652789	0.999165
2DMT•*o*-TD	15 out of 15	0.0900049	0.998997
2DMT•*p*X	15 out of 15	0.12098	0.996563
2DMT•*m*X	15 out of 15	0.0765458	0.998487
2DMT•*o*X	15 out of 15	0.120657	0.998338
2DMT•Toluene	15 out of 15	0.0370017	0.999693
2DMT•EB	15 out of 15	0.124454	0.996894
2DMT•Cumene	15 out of 15	0.316248	0.986236
2DMT•Nitrobenzene	15 out of 15	0.156778	0.996876
2DMT•*p*-NT	15 out of 15	0.208439	0.99276
2DMT•*m*-NT	15 out of 15	0.132075	0.997445
2DMT•*o*-NT	15 out of 15	0.144301	0.99619
2DMT•Anisole	15 out of 15	0.0981025	0.998758
2DMT•*p*-MA	15 out of 15	0.17927	0.993617
2DMT•*m*-MA	15 out of 15	0.15116	0.995947
2DMT•*o*-MA	15 out of 15	0.0723148	0.998796
2DMT•*p*-CR	15 out of 15	0.0493357	0.999473
2DMT•*o*-CR	15 out of 15	0.0579767	0.999473
2DMT•*m*-CR	15 out of 15	0.0564023	0.999035
DMT	4 out of 15	0.53442	0.858473

Chapter 11: Conclusion and Future Work

11.1 Conclusion

DMT, as a host compound, was readily synthesised through Grignard addition reaction with diethyl L-tartrate, the product of which was selectively methylated to produce the title compound (DMT) in good yield. It displayed excellent ability to include monocyclic aromatic molecules as guests. It formed inclusion complexes with compounds such as the isomers of nitrobenzene, aniline, anisole, toluene, ethylbenzene and cumene. DMT also included halo-aromatic compounds and a select few alicyclic guests such as cyclohexane, cyclohexene and cyclohexanone. A 2:1 host:guest ratio was consistently preferred in each case.

DMT failed to form complexes with straight- or branched- chain alcohols such as methanol, ethanol, 2-propanol and 2-butanol. Furthermore, it did not include compounds such as acetonitrile, diethyl ether, morpholine or ethyl acetate.

The main focus of this research project was to determine whether the title host compound was able to discriminate between isomers or related compounds through selective enclathration. Isomers used in this investigation were *para*-, *meta*- and *ortho*- isomers of anisole, toluidine, nitrotoluene, cresol and xylene, as well as related compounds including ethylbenzene, cumene, *N*-methylaniline and *N,N*-dimethylaniline. Selective inclusion by DMT was observed to varying degrees in all experiments attempted (Table 81 summarizes the outcome of these). DMT consistently showed selectivity for one guest over another from both equimolar and non-equimolar guest mixtures, with the exception being the nitrobenzene/p-NT experiment and the m-NT/o-NT experiment (Chapter 7) for which DMT showed a concentration dependent selectivity profile.

Table 81: Summary of DMT's selectivity order.

Chapter	1st preferred	2nd preferred	3rd preferred	4th preferred
3	*N,N*-Dimethylaniline	*N*-Methylaniline	Aniline	
4	*p*-Xylene	Ethylbenzene	*o*-Xylene	*m*-Xylene
5	*p*-Toluidine	*o*-Toluidine	*m*-Toluidine	Aniline
6	Toluene	Ethylbenzene	Cumene	
7*	*p*-Nitrotoluene	Nitrobenzene	*o*-Nitrotoluene	*m*-Nitrotoluene
8	Anisole	*p*-Methylanisole	*m*-Methylanisole	*o*-Methylanisole
9	*o*-Cresol	*p*-Cresol	*m*-Cresol	

*DMT's selectivity towards Nitrobenzene/*p*-NT, and *o*-NT/*m*-NT guest pairs varied according to concentration.

In experiments dealing with aniline and the *N*-methylated aniline compounds, DMA was preferred over NMA, followed by aniline. Similarly, when aniline competed with the toluidine isomers, *p*-TD was most preferred, followed by *o*-TD, *m*-TD and lastly aniline again. When DMT was recrystallized from mixtures of the xylene isomers and EB, *p*X was selected for, followed by EB, *o*X and *m*X, while EB was again second most preferred when it competed against toluene (most preferred) and cumene (least preferred). Unsubstituted anisole was selected preferentially over *p*-MA, *m*-MA and *o*-MA in that order. Regarding the cresols, DMT was significantly selective for *o*-CR when competing with both *p*-CR and *m*-CR.

Thermal analyses were performed on all suitable host-guest complexes in this study. Analysis of the terms T_{on}–T_b (valid due to the isostructurality of host packing) yielded results mirroring the selectivity order displayed by DMT in some cases, but not all. A notable exception was the measurement of this parameter for complexes with least preferred aniline which was significantly higher relative to the more preferred guests

NMA and DMA (Chapter 3) as well as the toluidine isomers (Chapter 5). Consideration of T_p and T_{end} values, where possible, were also often in accordance with the host's selectivity orders, indicating that the host selectivity is, possibly, dependent on the thermal stabilities of the complexes.

Single crystal X-ray analysis of these host-guest complexes showed that, in all cases, the geometries of the host compounds were largely stabilized by intramolecular 1,3- and 2,4- hydrogen bonds. Guest compounds were situated in discrete cavities formed in the host crystal, and experienced host–guest interactions such as π–π stacking, CH–π interactions and other short contacts. None of the guests participated in classic hydrogen bond interactions with the host.

Finally, Hirshfeld surface analysis was conducted on each host-guest complex to ascertain if there was any quantitative interaction type between host and guest that contributed to the observed selectivity orders displayed by the host. This form of analysis did not yield consistent trends with regards to selectivity orders, but depending on the host system, decreases in the H···H interaction percentage correlated with reduced selectivity (Chapter 3 and Chapter 5); decreases in the amount of C···H interactions had the same effect (Chapter 6 and 9). The absence of a trend in the nitrobenzene/nitrotoluene experiments (Chapter 7) may have been indicative of the host's concentration-dependent selectivity behaviour observed for some of these guest mixtures.

11.2 Future Work

As improvements to the selectivity, or indeed changes to the selectivity orders, displayed by DMT remains attractive, there is opportunity to, in future, modify DMT in order to improve the selective behaviour.

The synthetic route of DMT allows for modifications to be made to both the phenyl moieties of DMT as well as the methoxy and hydroxy groups. Plausible derivatives of DMT include adding substituents onto the phenyl rings by substituting bromobenzene in the Grignard reaction for compounds that will yield methyl-, methoxy- or bulkier naphthyl- substituted solids, by using *o*- and *p*- bromotoluene, *o*- and *p*- bromoanisole and 1-bromonaphthalene in these reactions (Scheme 9).

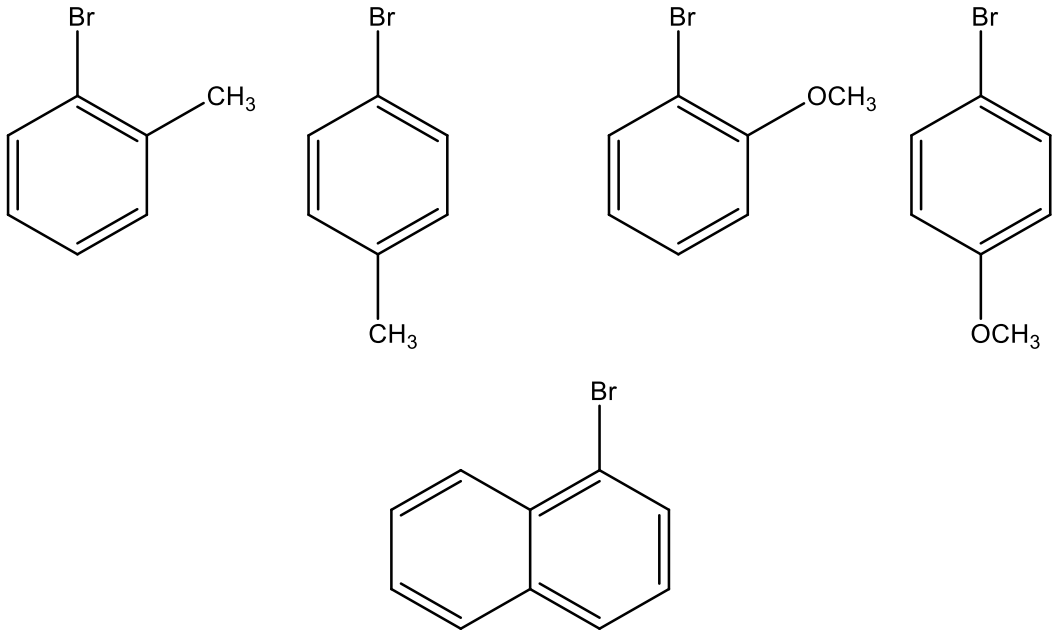

Scheme 9: Variety of bromo compounds to be used in Grignard reactions for further derivatization of DMT.

Furthermore, the position of the methoxy moieties may be varied from the secondary position to the tertiary position, thereby allowing for the retention of the chiral secondary hydroxy sensor groups in TETROL, which may find improved application in isomer separation, or indeed in the resolution of racemates. This may be achieved through the reaction pathway as proposed by Xie *et al* through a selective 2,3-cylosulfitation step (Scheme 10).[199]

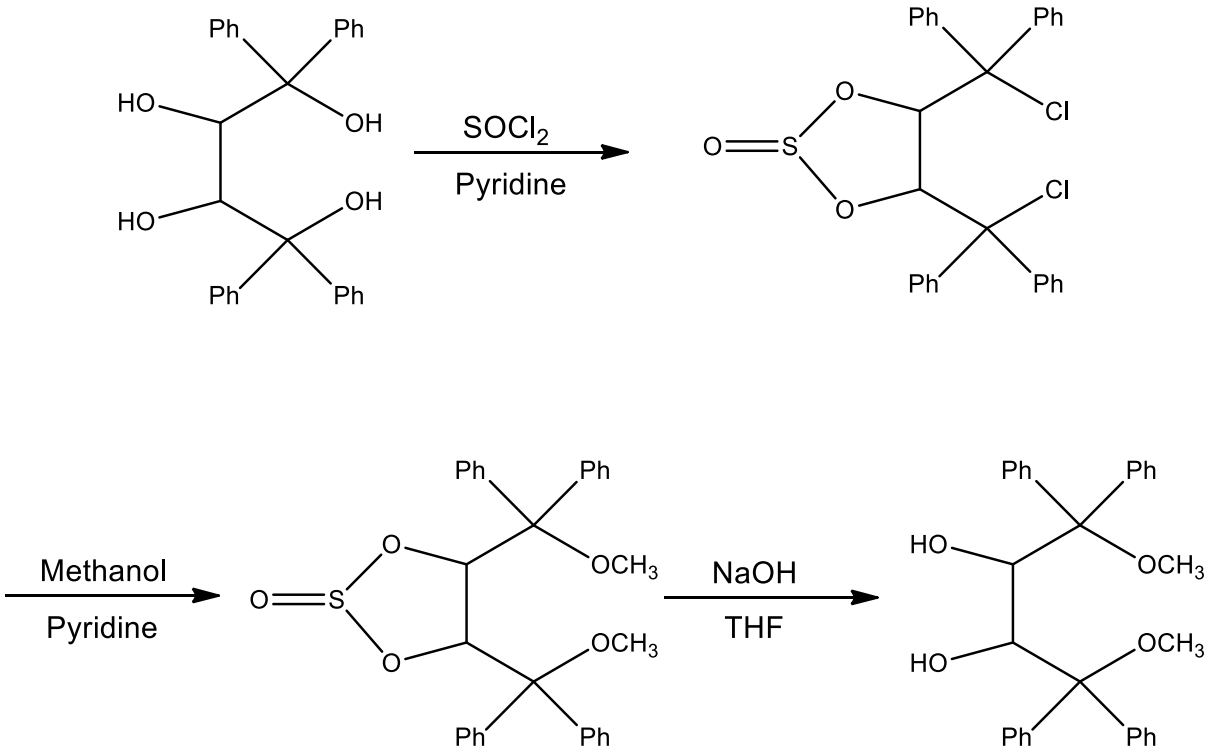

Scheme 10: Proposed synthetic pathway towards 1,4-dimethoxy-1,1,4,4-tetraphenylbutane-2,3-diol through a cyclic sulfite intermediate.

References

1. McMurry, J., *Organic Chemistry 8th Edition*. Belmont, California, USA, 2010.
2. Cooper, C., *Organic Chemist's Desk Reference, 2nd Edition*. Taylor & Francis: Boca Raton, Florida, USA, 1995.
3. Bruice, P. Y., *Organic Chemistry*. Pearson/Prentice Hall: Upper Saddle River, New Jersey, USA, 2004.
4. Carey, F. A., *Organic Chemistry*. McGraw-Hill: New York, USA, 2000.
5. Sasaki, S.; Igawa, K.; Konishi, G.-i., The effect of regioisomerism on the solid-state fluorescence of bis(piperidyl)anthracenes: structurally simple but bright AIE luminogens. *J. Mater. Chem. C* **2015**, *3* (23), 5940–5950.
6. Armstrong, D. W., Optical isomer separation by liquid chromatography. *Anal. Chem.* **1987**, *59* (2), 84A–91A.
7. Chhabra, N.; Aseri, M. L.; Padmanabhan, D., A review of drug isomerism and its significance. *Int. J. App. Basic Med. Res.* **2013**, *3* (1), 16–18.
8. Agranat, I.; Caner, H.; Caldwell, J., Putting chirality to work: the strategy of chiral switches. *Nat. Rev. Drug Discov.* **2002**, *1* (10), 753–768.
9. Lim, S. A., Ethambutol-associated optic neuropathy. *Ann. Acad. Med. Singapore* **2006**, *35* (4), 274–278.
10. Thomas, J. P.; Baughn, C. O.; Wilkinson, R. G.; Shepherd, R. G., A new synthetic compound with antituberculous activity in mice: ethambutol (dextro-2, 2′- (ethylenediimino)-di-1-butanol). *Am. Rev. Respir. Dis.* **1961**, *83* (6), 891–893.
11. Saito, S.; Michishita, T.; Maeda, S., Separation of meta- and para- xylene mixture by distillation accompanied by chemical reactions. *J. Chem. Eng. Jpn.* **1971**, *4* (1), 37–43.
12. Shiau, L.-D.; Wen, C.-C.; Lin, B.-S., Separation and purification of p-xylene from the mixture of m-xylene and p-xylene by distillative freezing. *Ind. Eng. Chem. Res.* **2005**, *44* (7), 2258–2265.
13. Cheng, C., Solid-liquid-vapor multiple phase transformation process with coupled absorption-melting operations. Google Patents: 1992.
14. Cheng, C.; Cheng, S. W., Distillative freezing process for separating volatile mixtures and apparatuses for use therein. Google Patents: 1984.

15. Kaur, B.; Srivastava, R., Simultaneous determination of epinephrine, paracetamol, and folic acid using transition metal ion-exchanged polyaniline–zeolite organic–inorganic hybrid materials. *Sensors Actuators B: Chem.* **2015**, *211*, 476–488.
16. Sun, N.-N.; Yan, B., Rapid and facile ratiometric detection of CO32− based on heterobimetallic metal-organic frameworks (Eu/Pt-MOFs). *Dyes and Pigments* **2017**, *142*, 1–7.
17. Ma, J.; Yao, Z.; Hou, L.; Lu, W.; Yang, Q.; Li, J.; Chen, L., Metal organic frameworks (MOFs) for magnetic solid-phase extraction of pyrazole/pyrrole pesticides in environmental water samples followed by HPLC-DAD determination. *Talanta* **2016**, *161*, 686–692.
18. Kang, Z.; Ding, J.; Fan, L.; Xue, M.; Zhang, D.; Gao, L.; Qiu, S., Preparation of a MOF membrane with 3-aminopropyltriethoxysilane as covalent linker for xylene isomers separation. *Inorg. Chem. Commun.* **2013**, *30*, 74–78.
19. Alaerts, L.; Séguin, E.; Poelman, H.; Thibault-Starzyk, F.; Jacobs, P. A.; De Vos, D. E., Probing the lewis acidity and catalytic activity of the metal–organic framework [Cu3(btc)2] (BTC=benzene-1,3,5-tricarboxylate). *Chem. Eur. J.* **2006**, *12* (28), 7353–7363.
20. Loiseau, T.; Serre, C.; Huguenard, C.; Fink, G.; Taulelle, F.; Henry, M.; Bataille, T.; Férey, G., A Rationale for the large breathing of the porous aluminum terephthalate (MIL-53) upon hydration. *Chem. Eur. J.* **2004**, *10* (6), 1373–1382.
21. Barthelet, K.; Marrot, J.; Riou, D.; Férey, G., A breathing hybrid organic–inorganic solid with very large pores and high magnetic characteristics. *Angew. Chem. Int. Ed.* **2002**, *41* (2), 281–284.
22. Alaerts, L.; Kirschhock, C. E. A.; Maes, M.; van der Veen, M. A.; Finsy, V.; Depla, A.; Martens, J. A.; Baron, G. V.; Jacobs, P. A.; Denayer, J. F. M.; De Vos, D. E., Selective ddsorption and separation of xylene Isomers and ethylbenzene with the microporous vanadium(IV) terephthalate MIL-47. *Angew. Chem. Int. Ed.* **2007**, *46* (23), 4293–4297.
23. Steed, J. W.; Atwood, J. L., *Supramolecular Chemistry*, John Wiley & Sons, Ltd, USA, 2009; pp 1–48.
24. Weber, E.; Josel, H.-P., A proposal for the classification and nomenclature of host-guest-type compounds. *J. Inclusion Phenom.* **1983**, *1* (1), 79–85.

25. Eißmann, D.; Katzsch, F.; Weber, E., Synthesis and solvent sorption characteristics of new types of tartaric acid, lactic acid and TADDOL derived receptor compounds. *Tetrahedron* **2015**, *71* (40), 7695–7705.
26. Ooyama, Y.; Yoshida, K., Solid-state photophysical properties and functional characteristics of heterocyclic quinol-type fluorescent hosts with clathrate-forming ability. *J. Synth. Org. Chem Jpn.* **2009**, *67* (4), 337–348.
27. Ooyama, Y.; Yoshida, K., Heterocyclic quinol-type fluorophores. Dramatic solid-state fluorescence enhancement behaviour of imidazoanthraquinol-type clathrate hosts upon inclusion of various kinds of organic solvent molecules. *New J. Chem.* **2005**, *29* (9), 1204–1212.
28. Yoshida, K.; Ooyama, Y.; Tanikawa, S.; Watanabe, S., Heterocyclic quinol-type fluorophores. Part 2. Solid-state fluorescence enhancement behaviour of benzofurano[3,2-b]naphthoquinol-type clathrate hosts upon inclusion of amine molecules. *J. Chem. Soc. Perkin Trans 2* **2002**, (3), 708–714.
29. Rahemi, V.; Vandamme, J. J.; Garrido, J. M. P. J.; Borges, F.; Brett, C. M. A.; Garrido, E. M. P. J., Enhanced host–guest electrochemical recognition of herbicide MCPA using a β-cyclodextrin carbon nanotube sensor. *Talanta* **2012**, *99*, 288–293.
30. Kurzątkowska, K.; Sayin, S.; Yilmaz, M.; Radecka, H.; Radecki, J., Calix[4]arene derivatives as dopamine hosts in electrochemical sensors. *Sensors Actuators B: Chem.* **2015**, *218*, 111–121.
31. Seebach, D.; Beck, A. K.; Heckel, A., TADDOLs, their derivatives, and TADDOL analogues: versatile chiral auxiliaries. *Angew. Chem. Int. Ed. Engl.* **2001**, *40* (1), 92–138.
32. Lusi, M.; Barbour, L. J., Solid–vapor sorption of xylenes: prioritized selectivity as a means of separating all three isomers using a single substrate. *Angew. Chem. Int. Ed.* **2012**, *51* (16), 3928–3931.
33. Nassimbeni, L. R.; Bathori, N. B.; Patel, L. D.; Su, H.; Weber, E., Separation of xylenes by enclathration. *Chem. Commun.* **2015**, *51* (17), 3627–3629.
34. Caira, M. R.; Nassimbeni, L. R.; Vujovic, D.; Toda, F., Separation of xylenols by inclusion. *J. Phys. Org. Chem.* **2000**, *13* (1), 75–79.
35. Kuhn, R.; Stoecklin, F.; Erni, F., Chiral separations by host-guest complexation with cyclodextrin and crown ether in capillary zone electrophoresis. *Chromatographia* **1992**, *33* (1), 32–36.

36. Seeman, J. I.; Secor, H. V.; Armstrong, D. W.; Timmons, K. D.; Ward, T. J., Enantiomeric resolution and chiral recognition of racemic nicotine and nicotine analogs by beta-cyclodextrin complexation. Structure-enantiomeric resolution relationships in host-guest interactions. *Anal. Chem.* **1988**, *60* (19), 2120–2127.
37. Bortolini, O.; Fantin, G.; Fogagnolo, M.; Maietti, S., Resolution of organic racemates via host-guest enantioselective inclusion complexation in bile acid derivatives. *Arkivoc* **2006**, *2006* (6), 40–48.
38. Legrand, S.; Heikkinen, H.; Nicholls, I. A.; Root, A.; Svenson, J.; Unelius, C. R., Preparation, characterization and application of a stationary chromatographic phase from a new (+)-tartaric acid derivative. *Tetrahedron Lett.* **2010**, *51* (17), 2258–2261.
39. Wenzel, T. J.; Wilcox, J. D., Chiral reagents for the determination of enantiomeric excess and absolute configuration using NMR spectroscopy. *Chirality* **2003**, *15* (3), 256–270.
40. Yi, J.; Du, G.; Yang, Y.; Li, Y.; Li, Y.; Guo, F., Chiral discrimination of natural isoflavanones using (*R*)- and (*S*)-BINOL as the NMR chiral solvating agents. *Tetrahedron: Asymmetry* **2016**, *27* (22), 1153–1159.
41. Nageswara Rao, R.; Santhakumar, K., Cyclodextrin assisted enantiomeric recognition of emtricitabine by 19F NMR spectroscopy. *New J. Chem.* **2016**, *40* (10), 8408–8417.
42. Lee, J.-W.; Choi, K. J.; Lee, Y.; Yoon, J.-H., Spectroscopic identification and conversion rate of gaseous guest-loaded hydroquinone clathrates. *Chem. Phys. Lett.* **2012**, *528*, 34–38.
43. Lee, J.-W.; Kang, S.-P.; Yoon, J.-H., Highly selective enclathration of ethylene from gas mixtures. *J. Phys. Chem. C* **2014**, *118* (12), 6059–6063.
44. Adams, J. E.; Cox, J. R.; Christiano, A. J.; Deakyne, C. A., Molecular dynamics of host−guest complexes of small gas molecules with calix[4]arenes. *J. Phys. Chem. A* **2008**, *112* (30), 6829–6839.
45. Annunziata, L.; Albunia, A. R.; Venditto, V.; Mensitieri, G.; Guerra, G., Polymer/gas clathrates for gas storage and controlled release. *Macromolecules* **2006**, *39* (26), 9166–9170.
46. Neiner, D.; Okamoto, N. L.; Condron, C. L.; Ramasse, Q. M.; Yu, P.; Browning, N. D.; Kauzlarich, S. M., Hydrogen encapsulation in a silicon clathrate type I

structure: Na5.5(H2)2.15Si46: Synthesis and characterization. *J. Am. Chem. Soc.* **2007**, *129* (45), 13857–13862.

47. Han, K. W.; Lee, Y.-J.; Jang, J. S.; Jeon, T.-I.; Park, J.; Kawamura, T.; Yamamoto, Y.; Sugahara, T.; Vogt, T.; Lee, J.-W.; Lee, Y.; Yoon, J.-H., Fast and reversible hydrogen storage in channel cages of hydroquinone clathrate. *Chem. Phys. Lett.* **2012**, *546*, 120–124.
48. Strobel, T. A.; Hester, K. C.; Koh, C. A.; Sum, A. K.; Sloan, E. D., Properties of the clathrates of hydrogen and developments in their applicability for hydrogen storage. *Chem. Phys. Lett.* **2009**, *478* (4), 97–109.
49. Ogawa, N.; Takahashi, C.; Yamamoto, H., Physicochemical characterization of cyclodextrin–drug interactions in the solid state and the effect of water on these interactions. *J. Pharm. Sci.* **2015**, *104* (3), 942–954.
50. Zhang, J.; Ma, P. X., Cyclodextrin-based supramolecular systems for drug delivery: Recent progress and future perspective. *Adv. Drug Del. Rev.* **2013**, *65* (9), 1215–1233.
51. Wenz, G., An Overview of host-guest chemistry and its application to nonsteroidal anti-inflammatory drugs. *Clin. Drug Investig.* **2000**, *19* (2), 21–25.
52. Mandelcorn, L., Clathrates. *Chem. Rev.* **1959**, *59*, 827–839.
53. Bensouilah, N.; Boutemeur-Kheddis, B.; Bensouilah, H.; Meddour, I.; Abdaoui, M., Host-guest complex of nabumetone: β-cyclodextrin: quantum chemical study and QTAIM analysis. *J. Incl. Phenom. Macrocycl. Chem.* **2017**, 1–16.
54. Saha, A.; Nayak, S. K.; Chattopadhyay, S.; Mukherjee, A. K., Study of charge transfer interactions of a resorcin[4]arene with [60]- and [70]fullerenes by the absorption spectrometric method. *J. Phys. Chem. A* **2004**, *108* (40), 8223–8228.
55. Sarmentero, M. A.; Ballester, P., Molecular inclusion of organometallic sandwich complexes within hybrid cavitand-resorcin[4]arene receptors. *Org. Biomol. Chem.* **2007**, *5* (18), 3046–3054.
56. Ballester, P.; Shivanyuk, A.; Far, A. R.; Rebek, J., A synthetic receptor for choline and carnitine. *J. Am. Chem. Soc.* **2002**, *124* (47), 14014–14016.
57. Eckel, R.; Ros, R.; Decker, B.; Mattay, J.; Anselmetti, D., Supramolecular chemistry at the Ssngle-molecule level. *Angew. Chem. Int. Ed.* **2005**, *44* (3), 484–488.

58. Menozzi, D.; Biavardi, E.; Massera, C.; Schmidtchen, F.-P.; Cornia, A.; Dalcanale, E., Thermodynamics of host–guest interactions between methylpyridinium salts and phosphonate cavitands. *Supramol. Chem.* **2010**, *22* (11–12), 768–775.
59. Schnatwinkel, B.; Rekharsky, M. V.; Brodbeck, R.; Borovkov, V. V.; Inoue, Y.; Mattay, J., Thermodynamic aspects of the host–guest chemistry of pyrogallol[4]arenes and peralkylated ammonium cations. *Tetrahedron* **2009**, *65* (13), 2711–2715.
60. Kroto, H. W.; Heath, J. R.; O'Brien, S. C.; Curl, R. F.; Smalley, R. E., C60: Buckminsterfullerene. *Nature* **1985**, *318* (6042), 162–163.
61. Muck-Lichtenfeld, C.; Grimme, S.; Kobryn, L.; Sygula, A., Inclusion complexes of buckycatcher with C60 and C70. *Phys. Chem. Chem. Phys.* **2010**, *12* (26), 7091–7097.
62. Sygula, A.; Fronczek, F. R.; Sygula, R.; Rabideau, P. W.; Olmstead, M. M., A Double concave hydrocarbon buckycatcher. *J. Am. Chem. Soc.* **2007**, *129* (13), 3842–3843.
63. Le, V. H.; Yanney, M.; McGuire, M.; Sygula, A.; Lewis, E. A., Thermodynamics of host–guest interactions between fullerenes and a buckycatcher. *J. Phys. Chem. B* **2014**, *118* (41), 11956–11964.
64. Greene, L.; Elzey, B.; Franklin, M.; Fakayode, S. O., Analyses of polycyclic aromatic hydrocarbon (PAH) and chiral-PAH analogues-methyl-beta-cyclodextrin guest-host inclusion complexes by fluorescence spectrophotometry and multivariate regression analysis. *Spectrochim. Acta A* **2017**, *174*, 316–325.
65. Harata, K., Structural aspects of stereodifferentiation in the solid state. *Chem. Rev.* **1998**, *98* (5), 1803–1828.
66. Hapiot, F.; Tilloy, S.; Monflier, E., Cyclodextrins as supramolecular hosts for organometallic complexes. *Chem. Rev.* **2006**, *106* (3), 767–781.
67. Hu, T.; Na, W.; Yan, X.; Su, X., Sensitive fluorescence detection of ATP based on host-guest recognition between near-infrared β-Cyclodextrin-CuInS2 QDs and aptamer. *Talanta* **2017**, *165*, 194–200.
68. Lu, S.; Wang, A.; Ma, Y. J.; Xuan, H. Y.; Zhao, B.; Li, X. D.; Zhou, J. H.; Zhou, L.; Wei, S. H., Cyclodextrin type dependent host-guest interaction mode with

phthalocyanine and their influence on photodynamic activity to cancer. *Carbohydr. Polym.* **2016**, *148*, 236–242.

69. Michalska, P.; Wojnicz, A.; Ruiz-Nuno, A.; Abril, S.; Buendia, I.; Leon, R., Inclusion complex of ITH12674 with 2-hydroxypropyl-beta-cyclodextrin: Preparation, physical characterization and pharmacological effect. *Carbohydr. Polym.* **2017**, *157*, 94–104.
70. You, Q.; Zhang, P.; Bai, S.; Huang, W.; Jia, Z.; Zhou, C.; Li, D., Supramolecular linear polymer formed by host–guest interactions of β-cyclodextrin dimers and polyacrylamide end-capped with adamantane. *Colloids Surf. Physicochem. Eng. Aspects* **2015**, *484*, 130–135.
71. Lacour, M.; Sterkers, O., Histamine and Betahistine in the Treatment of Vertigo. *CNS Drugs* **2001**, *15* (11), 853–870.
72. Tang, K.-T.; Chao, Y.-H.; Chen, D.-Y.; Lim, Y.-P.; Chen, Y.-M.; Li, Y.-R.; Yang, D.-H.; Lin, C.-C., Betahistine attenuates murine collagen-induced arthritis by suppressing both inflammatory and Th17 cell responses. *Int. Immunopharmacol.* **2016**, *39*, 236–245.
73. Sokolova, L.; Hoerr, R.; Mishchenko, T., Treatment of vertigo: A randomized, double-blind trial comparing efficacy and safety of ginkgo biloba extract EGb 761 and Betahistine. *Int. J. Otolaryngol.* **2014**, *2014* (682439).
74. Maeda, H.; Iga, Y.; Nakayama, H., Characterization of inclusion complexes of betahistine with β-cyclodextrin and evaluation of their anti-humidity properties. *J. Incl. Phenom. Macrocycl. Chem.* **2016**, *86* (3), 337–342.
75. Sharipov, R. A.; Sharapov, K. S.; Kemelbekov, U. S.; Volynkin, V. A.; Yu, V. K.; Panyushkin, V. T.; Praliev, K. D., The structure and pharmacological properties of the 4-acetoxy-1-(2-ethoxyethyl)-4-phenylpiperidine inclusion complex with β-cyclodextrin. *J. Incl. Phenom. Macrocycl. Chem.* **2016**, 1–8.
76. Pedersen, C. J., Cyclic polyethers and their complexes with metal salts. *J. Am. Chem. Soc.* **1967**, *89* (10), 2495–2496.
77. Pedersen, C. J., Cyclic polyethers and their complexes with metal salts. *J. Am. Chem. Soc.* **1967**, *89* (26), 7017–7036.
78. Luo, X.; Guo, B.; Luo, J.; Deng, F.; Zhang, S.; Luo, S.; Crittenden, J., Recovery of lithium from wastewater using development of Li ion-imprinted polymers. *ACS Sustain. Chem. Eng.* **2015**, *3* (3), 460–467.

79. Sun, D.; Zhu, Y.; Meng, M.; Qiao, Y.; Yan, Y.; Li, C., Fabrication of highly selective ion imprinted macroporous membranes with crown ether for targeted separation of lithium ion. *Sep. Purif. Technol.* **2017**, *175*, 19–26.
80. Torrejos, R. E. C.; Nisola, G. M.; Song, H. S.; Han, J. W.; Lawagon, C. P.; Seo, J. G.; Koo, S.; Kim, H.; Chung, W.-J., Liquid-liquid extraction of lithium using lipophilic dibenzo-14-crown-4 ether carboxylic acid in hydrophobic room temperature ionic liquid. *Hydrometallurgy* **2016**, *164*, 362–371.
81. Ghildiyal, N.; Pant, G. J. n.; Rawat, M. S. M.; Singh, K., Spectral investigation of the effect of anion on the stability of non covalent assemblies of 2,3,5,6,8,9,11,12-octahydro-1,4,7,10,13-benzopentaoxacyclopentadecine (benzo-15-crown-5) with sodium halides. *Spectrochim. Acta A* **2017**, *171*, 507–514.
82. Duncanson, P.; Griffiths, D. V.; Miller, J. R., Synthesis and studies of the 15-crown-5 complex of the sodium salt of 2-nitroimidazole. *Tetrahedron* **1997**, *53* (38), 13177–13182.
83. Niederhauser, T. L.; Brown, B. R.; Ziemer, S. P.; Sargent, J. D.; Woolley, E. M., Thermodynamics of complexation of aqueous 18-crown-6 with potassium ion: apparent molar volumes and apparent molar heat capacities of aqueous 18-crown-6 and of the (18-crown-6 + potassium chloride) complex at temperatures (278.15 to 393.15) K, at molalities (0.02 to 0.3) mol.kg^{-1}, and at the pressure 0.35 MPa. *J. Chem. Thermodyn.* **2004**, *36* (12), 1067–1077.
84. Zaeni, A.; Behrens, U.; Liebing, P.; Olbrich, F.; Edelmann, F. T., Preparative and structural investigation of crown ether adducts of potassium fluorenides. *J. Organomet. Chem.* **2017**, *830*, 141–145.
85. Fonari, M. S.; Simonov, Y. A.; Kravtsov, V. C.; Lipkowski, J.; Ganin, E. V.; Yavolovskii, A. A., Hydrogen bonding assemblies in host–guest complexes with 18-crown-6. *J. Mol. Struct.* **2003**, *647* (1–3), 129–140.
86. Ullmann, F.; Bohnet, M., *Ullmann's Encyclopedia of Industrial Chemistry*. Wiley-VCH: 2003, USA.
87. Gutsche, C. D., *Calixarenes revisited*. The Royal Society of Chemistry: 1998, Cambridge, United Kingdom.
88. Demircan, E.; Eymur, S.; Demir, A. S., Proline–calixarene thiourea host–guest complex catalyzed enantioselective aldol reactions: from nonpolar solvents to the presence of water. *Tetrahedron: Asymmetry* **2014**, *25* (5), 443–448.

89. Atwood, J. L.; Barbour, L. J.; Heaven, M. W.; Raston, C. L., Association and orientation of C70 on complexation with calix[5]arene. *Chem. Commun.* **2003**, (18), 2270–2271.
90. McMahon, G.; O'Malley, S.; Nolan, K.; Diamond, D., Important calixarene derivatives – their synthesis and applications. *Arkivoc* **2003**, *2003* (vii).
91. Morales, A.; Santana, A.; Althoff, G.; Melendez, E., Host–guest interactions between calixarenes and Cp_2NbCl_2. *J. Organomet. Chem.* **2011**, *696* (13), 2519–2527.
92. Basílio, N.; Piñeiro, Á.; Da Silva, J. P.; García-Río, L., Cooperative assembly of discrete stacked aggregates driven by supramolecular host–guest complexation. *J. Org. Chem.* **2013**, *78* (18), 9113–9119.
93. Chao, J.; Li, Z.; Liu, Y.; Zhang, Y.; Guo, Z.; Zhang, B.; Wang, X., Investigation of the inclusion interaction of *p*-sulfonatocalix[6]arene with trimebutine maleate. *J. Mol. Liq.* **2016**, *213*, 173–178.
94. Perret, F.; Coleman, A. W., Biochemistry of anionic calix[n]arenes. *Chem. Commun.* **2011**, *47* (26), 7303–7319.
95. Qin, Z.; Guo, D.-S.; Gao, X.-N.; Liu, Y., Supra-amphiphilic aggregates formed by p-sulfonatocalix[4]arenes and the antipsychotic drug chlorpromazine. *Soft Matter* **2014**, *10* (13), 2253–2263.
96. Wang, K.; Zhang, H.-Q.; Xing, S.-Y.; Wang, X.-G.; Dou, H.-X.; Cui, J.-H., Distorted cone conformation and unique packing structure of *p*-sulfonatocalix[5]arene via complexation of *N*-methyl-*N*′-(naphthalen-2-ylmethyl)-4,4′-bipyridinium. *Tetrahedron* **2016**, *72* (41), 6558–6565.
97. Alves, M. M.; Gonçalves, M. P.; Rocha, C. M. R., Effect of ferulic acid on the performance of soy protein isolate-based edible coatings applied to fresh-cut apples. *Food Sci. Technol.* **2017**, *80*, 409–415.
98. Hassanzadeh, P.; Arbabi, E.; Atyabi, F.; Dinarvand, R., Ferulic acid exhibits antiepileptogenic effect and prevents oxidative stress and cognitive impairment in the kindling model of epilepsy. *Life Sci.* **2017**, *179*, 9–14.
99. Chao, J.; Wang, H.; Song, K.; Wang, Y.; Zuo, Y.; Zhang, L.; Zhang, B., Host-guest inclusion system of ferulic acid with *p*-Sulfonatocalix[n]arenes: Preparation, characterization and antioxidant activity. *J. Mol. Struct.* **2017**, *1130*, 579–584.

100. Basílio, N.; Francisco, V.; García-Río, L., Independent pathway formation of guest–host in host ternary complexes made of ammonium salt, calixarene, and cyclodextrin. *J. Org. Chem.* **2012**, *77* (23), 10764–10772.
101. Hosseinzadeh, R.; Seichter, W.; Sanaeishoar, T.; Weber, E., Synthesis and supramolecular behaviour of 2,7-dibromo-9-alkynylfluorenols. *Supramol. Chem.* **2007**, *19* (6), 353–364.
102. Barton, B.; Betz, R.; Caira, M. R.; Hosten, E. C.; McCleland, C. W.; Pohl, P. L.; Taljaard, B., Clathrates of novel ethylenediamine derivatives: thermal, X-ray crystallographic and conformational analysis of inclusion complexes of *N,N′*-bis(5-phenyl-5-dibenzo[a,d]cycloheptenyl)ethylenediamine and its 10,11-dihydro analogue. *Tetrahedron* **2016**, *72* (47), 7536–7551.
103. Tanaka, K.; Hori, K.; Tsuyuhara, S.; Motoki, S.; Shide, S.; Arakawa, R.; Caira, M. R., Role of halogen bonding in clathrate formation of tetra- and hexasalicylides derived from halogenated salicylic acids. *Tetrahedron* **2013**, *69* (3), 1120–1127.
104. Okeke, E. B.; Soldatov, D. V., Coordination and inclusion compounds formed by addition of quinoline (Q) or isoquinoline (Iq) to a metal(II) dibenzoylmethanate (Co, Ni, Zn, Cd). *J. Therm. Anal. Calorim.* **2010**, *100* (3), 801–810.
105. Shen, Y.; Xue, H.; Wei, Y.-Q.; Shen, M.; Xu, R.-C.; Wang, X.; Shen, X.; Zhu, D.-R., Syntheses, structures and inclusion properties of supramolecular dibenzotetraaza[14]annulene hosts for aromatic ring. *J. Incl. Phenom. Macrocycl. Chem.* **2016**, *86* (3), 191–199.
106. Toda, F.; Tanaka, K.; Nagamatsu, S.; Mak, T. C. W., X-ray analysis of trans-9, 10-dihydroxy-9,10-diphenyl-9,10-dihydroanthracene and Its 1:2 molecular complex with methanol, and structural comparison with the related 1:1 ethanol and 1:1 1,4-butanediol adducts. *Isr. J. Chem.* **1985**, *25* (3-4), 346–352.
107. Toda, F.; Tanaka, K.; Mak, T. C. W., Structure of a 1:1 molecular complex of trans-9,10-dihydroxy-9,10-diphenyl-9,10-dihydroanthracene with ethanol. *Tetrahedron Lett.* **1984**, *25* (13), 1359–1362.
108. Li-feng, C.; Rees, L. V. C., Temperature-programmed desorption of hydrocarbons from ZSM-5, ZSM-11, and Theta-1; part 1. *n*-hexane and *n*-octane. *Zeolites* **1988**, *8* (4), 310–316.

109. Toda, F.; Tanaka, K.; Mak, T. C. W., Interaction of dihydroxy host systems with glycols. A comparative study of the crystal structures of 1:1 molecular complexes of 1,4-butanediol with 2,5-bis(4-chlorophenyl)hydroquinone andtrans-9,10-dihydroxy-9,10-diphenyl-9,10-dihydroanthracene. *J. Inclusion Phenom.* **1985**, *3* (3), 225–233.
110. Bond, D. R.; Nassimbeni, L. R.; Toda, F., Complexation with diol host compounds. Part 1. Structures of the 1:2 molecular complexes oftrans-9, 10-dihydroxy-9,10-diphenyl-9,10-dihydroanthracene with acetophenone and with 3-methylcyclopentanone. *J. Inclusion Phenom. Mol. Recognit. Chem.* **1989**, *7* (6), 623–635.
111. Bond, D. R.; Caira, M. R.; Harvey, G. A.; Nassimbeni, L. R.; Toda, F., Complexation with diol host compounds. 5. Structures and thermal analyses of inclusion compounds of trans-9,10-dihydroxy-9,10-diphenyl-9,10-dihydroanthracene with 2-butanone, 4-vinylpyridine, 4-methylpyridine and 2-methylpyridine. *Acta Crystallographica Section B* **1990**, *46* (6), 771–780.
112. Bond, D. R.; Nassimbeni, L. R.; Toda, F., Complexation with diol host compounds. Part 3. Molecular inclusion of 4-methylcyclohexanone and 2-methylcyclohexanone by the host,trans-9,10-dihydroxy-9,10-diphenyl-9,10-dihydroanthracene. *J. Crystallogr. Spectrosc. Res.* **1989**, *19* (5), 847–859.
113. Caira, M. R.; Nassimbeni, L. R.; Schubert, W.-D.; Toda, F., Complexation with diol host compounds. Part 9. Structures and thermal analyses of inclusion compounds of *trans*-9,10-dihydroxy-9,10-diphenyl-9,10-dihydroanthracene with acetonitrile and 3-hydroxypropionitrile. *Thermochim. Acta* **1992**, *206*, 265–271.
114. Coetzee, A.; R. Nassimbeni, L.; Su, H., Desolvation of trans-9,10-dihydroxy-9,10-diphenyl-9,10-dihydroanthracene•cyclohexanone: kinetic compensation effect. *J. Chem. Res. S.* **1998**, (12), 740–741.
115. Weber, E.; Nitsche, S.; Wierig, A.; Csöregh, I., Inclusion compounds of diol hosts featuring two 9-hydroxy-9-fluorenyl or analogous groups attached to linear spacer units. *Eur. J. Org. Chem.* **2002**, *2002* (5), 856–872.
116. Weber, E.; Wierig, A.; Skobridis, K., Crystalline diol hosts featuring a bulky biphenyl framework – host synthesis and formation of inclusion compounds. *J. prakt. Chem.* **1996**, *338* (1), 553–557.

117. de Vries, E. J. C.; Nassimbeni, L. R.; Weber, E., Inclusion of amides by a fluorenyl diol host. *J. Incl. Phenom. Macrocycl. Chem.* **2009**, *63* (3), 203–210.
118. Bourne, S. A.; Corin, K.; Cruickshank, D. L.; Davson, J.; Nassimbeni, L. R.; Su, H.; Weber, E., Enclathration of bases by a fluorenyl host: structure, stability and selectivity. *New J. Chem.* **2011**, *35* (7), 1556–1561.
119. Skobridis, K.; Theodorou, V.; Alivertis, D.; Seichter, W.; Weber, E.; Csöregh, I., Crystalline complexes of 2,2′-bis(9-hydroxy-9-fluorenyl)biphenyl host with oligofunctional and conjugate functional group guests. *Supramol. Chem.* **2007**, *19* (6), 373–382.
120. Ji, B.-M.; Deng, D.-S.; Wang, W.-Z.; Miao, S.-B., Hydrogen bond-directed co-crystals of (±)-1,1′-binaphthalene-2,2′-diol with aromatic diimines: Structures and selectivity. *J. Mol. Struct.* **2009**, *937* (1–3), 107–115.
121. Ji, B.; Miao, S.; Deng, D., Molecular recognition and supramolecular self-assemblies of (±)-2,2′-dihydroxy-1,1′-binaphthyl with aromatic aza compounds. *Struct. Chem.* **2008**, *19* (2), 265–268.
122. Biradha, K.; Mahata, G., Enclathration of aromatic molecules by the O−H···N supramolecular adducts of racemic-bis-β-naphthol and 4,4‘-bipyridine. *Cryst. Growth Des.* **2005**, *5* (1), 61–63.
123. Imai, Y.; Kido, S.; Kamon, K.; Kinuta, T.; Sato, T.; Tajima, N.; Kuroda, R.; Matsubara, Y., A charge-transfer complex of 10,10‘-dihydroxy-9,9‘-biphenanthryl and methylviologen as a visual inclusion host system. *Org. Lett.* **2007**, *9* (24), 5047–5050.
124. Hart, H.; Lin, L. T. W.; Ward, D. L., Molecular design for hosts in crystalline host-guest complexes. *J. Am. Chem. Soc.* **1984**, *106* (14), 4043–4045.
125. Toda, F.; Akagi, K., Molecular complexes of acetylene alcohols with n- and χ-donors. *Tetrahedron Lett.* **1968**, *9* (33), 3695–3698.
126. Bacsa, J.; Caira, M. R.; Jacobs, A.; Nassimbeni, L. R.; Toda, F., Complexation with diol host compounds. Part 33. Inclusion and separation of pyridines by a diol host compound. *Cryst. Eng.* **2000**, *3* (4), 251–261.
127. Weber, E.; Skobridis, K.; Wierig, A.; Nassimbeni, L. R.; Johnson, L., Complexation with diol host compounds. Part 10. Synthesis and solid state inclusion properties of bis(diarylhydroxymethyl)-substituted benzenes and biphenyls; X-ray crystal structures of two host polymorphs and of a non-functional host analogue. *J. Chem. Soc. Perkin Trans 2* **1992**, (12), 2123–2130.

128. Katzsch, F.; Weber, E., Crystalline inclusion properties of new pyridine and thiophene modified wheel-and-axle diol hosts. *CrystEngComm* **2015**, *17* (13), 2737–2753.
129. Katzsch, F.; Gruber, T.; Weber, E., Crystalline inclusion of wheel-and-axle diol hosts featuring benzo[b]thiophene units as a lateral construction element. *Cryst. Growth Des.* **2015**, *15* (10), 5047–5061.
130. Skobridis, K.; Paraskevopoulos, G.; Theodorou, V.; Seichter, W.; Weber, E., Crystalline host–guest complexes of constitutionally isomeric diol hosts. A structural case study. *Cryst. Growth Des.* **2011**, *11* (12), 5275–5288.
131. Jetti, R. K. R.; Xue, F.; Mak, T. C. W.; Nangia, A., 4-Tritylbenzoic acid. A molecular scaffold for wheel-and-axle host-guest inclusion compounds with a supramolecular axis. *J. Chem. Soc. Perkin Trans 2* **2000**, (6), 1223–1232.
132. Hu, X.; Shan, Z.; Li, W., Second example for the heterocomplexation of chiral diols and complete disproportionation of enantiomers for non-racemic 2,3-O-cyclohexylidene-1,1,4,4-tetraphenylthreitols. *J. Fluorine Chem.* **2010**, *131* (4), 505–509.
133. Shan, Z.; Xiong, Y.; Yi, J.; Hu, X., Heterocomplexation of a chiral dipeptide and quantitative enantiomeric enrichment of nonracemic 1,1′-bi-2-naphthol. *J. Org. Chem.* **2008**, *73* (22), 9158–9160.
134. Bagi, P.; Juhász, K.; Timári, I.; Kövér, K. E.; Mester, D.; Kállay, M.; Kubinyi, M.; Szilvási, T.; Pongrácz, P.; Kollár, L.; Karaghiosoff, K.; Czugler, M.; Drahos, L.; Fogassy, E.; Keglevich, G., A study on the optical resolution of 1-isopropyl-3-methyl-3-phospholene 1-oxide and its use in the synthesis of borane and platinum complexes. *J. Organomet. Chem.* **2015**, *797*, 140–152.
135. Barton, B.; Hosten, E. C.; Jooste, D. V., Comparative investigation of the inclusion preferences of optically pure versus racemic TADDOL hosts for pyridine and isomeric methylpyridine guests. *Tetrahedron*.
136. Shan, Z.; Hu, X.; Zhou, Y.; Peng, X.; Li, Z., A convenient approach to C2-chiral 1,1,4,4-tetrasubstituted butanetetraols: Direct alkylation or arylation of enantiomerically pure diethyl tartrates. *Helv. Chim. Acta* **2010**, *93* (3), 497–503.
137. Barton, B.; Caira, M. R.; Hosten, E. C.; McCleland, C. W., A computational, X-ray crystallographic and thermal stability analysis of TETROL and its pyridine and methylpyridine inclusion complexes. *Tetrahedron* **2013**, *69* (41), 8713–8723.

138. Barton, B.; Caira, M. R.; Hosten, E. C.; McCleland, C. W.; Weitz, S., Clathrates of TETROL: further aspects of the selective inclusion of methylcyclohexanones in their energetically unfavorable axial methyl conformations. *J. Org. Chem.* **2015**, *80* (14), 7184–7192.
139. Barton, B.; Caira, M. R.; Hosten, E. C.; McCleland, C. W.; Weitz, S., Clathrates of TETROL: selective inclusion of methylcyclohexanones in their energetically unfavorable axial methyl conformations. *Chem. Commun.* **2014**, *50* (87), 13353–13355.
140. Pohl, P. L. TETROL and Derivatives: Synthesis, Host-Guest Properties and Racemate Resolutions. Masters Dissertation, Nelson Mandela Metropolitan University, 2015.
141. Seebach, D.; Kalinowski, H.-O.; Bastani, B.; Crass, G.; Daum, H.; Dörr, H.; Dupreez, N. P.; Ehrig, V.; Langer, W.; Nüssler, C.; Oei, H.-A.; Schmidt, M., Herstellung von hilfsstoffen für die asymmetrische synthese aus weinsäure. addition von butyllithium an aldehyde in chiralem medium. *Helv. Chim. Acta* **1977**, *60* (2), 301–325.
142. Teller, H.; Flügge, S.; Goddard, R.; Fürstner, A., Enantioselective gold catalysis: Opportunities provided by monodentate phosphoramidite ligands with an acyclic TADDOL backbone. *Angew. Chem. Int. Ed.* **2010**, *49* (11), 1949–1953.
143. Toda, F.; Tanaka, K.; Stein, Z.; Goldberg, I., Structure and inclusion characteristics of (*R,R*)-(–)-2,3-dimethoxy-1,1,4,4-tetraphenylbutane-1,4-diol. *J. Chem. Soc. Perkin Trans 2* **1993**, (12), 2359–2361.
144. *Bruker AXS, APEX2 SADABS and SAINT*, Madison, WI, 2010.
145. Sheldrick, G., SHELXT - Integrated space-group and crystal-structure determination. *Acta Crystallogr. A* **2015**, *71* (1), 3–8.
146. Sheldrick, G., Crystal structure refinement with SHELXL. *Acta Crystallogr. C* **2015**, *71* (1), 3–8.
147. Hubschle, C. B.; Sheldrick, G. M.; Dittrich, B., ShelXle: a Qt graphical user interface for SHELXL. *J. Appl. Crystallogr.* **2011**, *44* (6), 1281–1284.
148. Becker, H., *Organicum: practical handbook of organic chemistry*. Pergamon Press; Addison Wesley Pub. Co., Reading, Mass.: 1973.
149. Turner, M. J.; McKinnon, J. J.; Wolff, S. K.; Grimwood, D. J.; Spackman, P. R.; Jayatilaka, D.; Spackman, M. A. *CrystalExplorer17*, 2017.

150. Wavefunction, *Spartan'10*, Irvine, CA.
151. Narayanan, S.; Deshpande, K., Aniline alkylation over solid acid catalysts. *Appl. Catal., A.* **2000**, *199* (1), 1–31.
152. Seayad, A.; Ahmed, M.; Klein, H.; Jackstell, R.; Gross, T.; Beller, M., Internal olefins to linear amines. *Science* **2002**, *297* (5587), 1676–1678.
153. Ivanova, I. I.; Pomakhina, E. B.; Rebrov, A. I.; Hunger, M.; Kolyagin, Y. G.; Weitkamp, J., Surface species formed during aniline methylation on zeolite H–Y investigated by in situ MAS NMR spectroscopy. *J. Catal.* **2001**, *203* (2), 375–381.
154. Boot, M. D.; Tian, M.; Hensen, E. J. M.; Mani Sarathy, S., Impact of fuel molecular structure on auto-ignition behavior – Design rules for future high performance gasolines. *Prog. Energy Combust. Sci.* **2017**, *60* (Supplement C), 1–25.
155. Bandyopadhyay, R.; Singh, P. S.; Rao, B. S., Formation of *N*-methylaniline by transalkylation of aniline with *N,N*-dimethylaniline over zeolite beta. *Appl. Catal., A.* **1997**, *155* (1), 27–39.
156. Iranpoor, N.; Firouzabadi, H.; Nowrouzi, N.; Khalili, D., Selective mono- and di-*N*-alkylation of aromatic amines with alcohols and acylation of aromatic amines using Ph3P/DDQ. *Tetrahedron* **2009**, *65* (19), 3893–3899.
157. Nehate, M.; Bokade, V. V., Selective *N*-alkylation of aniline with methanol over a heteropolyacid on montmorillonite K10. *Appl Clay Sci.* **2009**, *44* (3), 255–258.
158. Gaikar, V. G.; Mandal, T. K.; Kulkarni, R. G., Adsorptive separations using zeolites: Separation of substituted anilines. *Sep. Sci. Technol.* **1996**, *31* (2), 259–270.
159. Yebeutchou, R. M.; Dalcanale, E., Highly selective monomethylation of primary amines through host−guest product sequestration. *J. Am. Chem. Soc.* **2009**, *131* (7), 2452–2453.
160. Barbour, L. J.; Caira, M. R.; Nassimbeni, L. R., Enclathration of diethyl ether. *J. Chem. Soc. Perkin Trans 2* **1993**, (8), 1413–1414.
161. Caira, M. R.; Nassimbeni, L. R.; Niven, M. L.; Schubert, W.-D.; Weber, E.; Dorpinghaus, N., Complexation with hydroxy host compounds. Part 1. Structures and thermal analysis of a suberol-derived host and its host-guest complexes with dioxane and acetone. *J. Chem. Soc. Perkin Trans 2* **1990**, (12), 2129–2133.

162. Akbari, A.; Alavi, S. M., The effect of cesium and antimony promoters on the performance of Ti-phosphate-supported vanadium(V) oxide catalysts in selective oxidation of *o*-xylene to phthalic anhydride. *Chem. Eng. Res. Des.* **2015**, *102* (Supplement C), 286–296.
163. Bierkandt, T.; Hemberger, P.; Oßwald, P.; Köhler, M.; Kasper, T., Insights in *m*-xylene decomposition under fuel-rich conditions by imaging photoelectron photoion coincidence spectroscopy. *Proc. Combust. Inst.* **2017**, *36* (1), 1223–1232.
164. Fadzil, N. A. M.; Rahim, M. H. A.; Maniam, G. P., A brief review of *para*-xylene oxidation to terephthalic acid as a model of primary C–H bond activation. *Chin. J. Catal.* **2014**, *35* (10), 1641–1652.
165. Hossain, M. M.; Atanda, L.; Al-Yassir, N.; Al-Khattaf, S., Kinetics modeling of ethylbenzene dehydrogenation to styrene over a mesoporous alumina supported iron catalyst. *Chem. Eng. J.* **2012**, *207* (Supplement C), 308–321.
166. Long, X.-l.; Wang, Z.-h.; Wu, S.-q.; Wu, S.-m.; Lv, H.-f.; Yuan, W.-k., Production of isophthalic acid from *m*-xylene oxidation under the catalysis of the $H_3PW_{12}O_{40}$/carbon and cobalt catalytic system. *Ind. Eng. Chem. Res.* **2014**, *20* (1), 100–107.
167. Zhang, B.; Xiu, G.; Chen, J.; Yang, S., Detonation and deflagration characteristics of *p*-Xylene/gaseous hydrocarbon fuels/air mixtures. *Fuel* **2015**, *140* (Supplement C), 73–80.
168. Devi, R. N.; Edgar, M.; Gonzalez, J.; Slawin, A. M. Z.; Tunstall, D. P.; Grewal, P.; Cox, P. A.; Wright, P. A., Structural studies and computer simulation of the inclusion of aromatic hydrocarbons in a zinc 2,6-naphthalene dicarboxylate framework compound. *J. Phys. Chem. B* **2004**, *108* (2), 535–543.
169. Vermoortele, F.; Maes, M.; Moghadam, P. Z.; Lennox, M. J.; Ragon, F.; Boulhout, M.; Biswas, S.; Laurier, K. G. M.; Beurroies, I.; Denoyel, R.; Roeffaers, M.; Stock, N.; Düren, T.; Serre, C.; De Vos, D. E., *p*-Xylene-selective metal–organic frameworks: A case of topology-directed selectivity. *J. Am. Chem. Soc.* **2011**, *133* (46), 18526–18529.
170. Caroline English, J.; Bhat, V. S.; Ball, G. L.; McLellan, C. J., Establishing a total allowable concentration of o-toluidine in drinking water incorporating early lifestage exposure and susceptibility. *Regul. Toxicol. Pharm.* **2012**, *64* (2), 269–284.

171. Hwang, J. J.; Soto, C.; Lafaurie, D.; Stephen, M.; Sarno, D. M., Porous microspheres of polyaniline, poly(*o*-toluidine), and poly(*m*-toluidine) prepared from double emulsions stabilized by toluidine isomers as the single surfactant. *J. Colloid Interface Sci.* **2017**, doi: 10.1016/j.jcis. 2017.11.029
172. Wu, J.; Weir, M. D.; Zhang, Q.; Zhou, C.; Melo, M. A. S.; Xu, H. H. K., Novel self-healing dental resin with microcapsules of polymerizable triethylene glycol dimethacrylate and *N,N*-dihydroxyethyl-*p*-toluidine. *Dent. Mater.* **2016**, *32* (2), 294–304.
173. *Ullmann's Encyclopedia of Industrial Chemistry*. John Wiley & Sons, USA, 2003.
174. McHedlov-Petrossyan, N. O.; Kamneva, N. N.; Al-Shuuchi, Y. T. M.; Marynin, A. I.; Shekhovtsov, S. V., The peculiar behavior of fullerene C60 in mixtures of 'good' and polar solvents: Colloidal particles in the toluene–methanol mixtures and some other systems. *Colloids Surf. Physicochem. Eng. Aspects* **2016**, *509* (Supplement C), 631–637.
175. Wang, D.; Nie, L.; Shao, X.; Yu, H., Exposure profile of volatile organic compounds receptor associated with paints consumption. *Sci. Total Environ.* **2017**, *603–604* (Supplement C), 57–65.
176. Zhang, Y.; Wang, W.; Wang, Y.-B., The nature of the noncovalent interactions between fullerene C60 and aromatic hydrocarbons. *Comput. Theor. Chem* **2017**, *1122*, 34–39.
177. Karpińska, M.; Wlazło, M.; Domańska, U., Investigation on the ethylbenzene/styrene separation efficiency with ionic liquids in liquid–liquid extraction. *Chem. Eng. Res. Des.* **2017**, *128* (Supplement C), 214–220.
178. Zou, Y.; Jiang, H.; Liu, Y.; Gao, H.; Xing, W.; Chen, R., Highly efficient synthesis of cumene via benzene isopropylation over nano-sized beta zeolite in a submerged ceramic membrane reactor. *Sep. Purif. Technol.* **2016**, *170* (Supplement C), 49–56.
179. Han, S.-J.; Zhang, Y.; Kim, I.; Chay, K.-O.; Yoon, H. J.; Jang, D. I.; Yang, S. Y.; Park, J.; Woo, H. A.; Park, I.; Lee, S.-R., Redox regulation of the tumor suppressor PTEN by the thioredoxin system and cumene hydroperoxide. *Free Radical Biol. Med.* **2017**, *112* (Supplement C), 277–286.
180. Wang, Y.; Saebø, S.; Pittman, C. U., The structure of aniline by ab initio studies. *Comput. Theor. Chem* **1993**, *281* (2), 91–98.

181. Bikelytė, G.; Härtel, M.; Stierstorfer, J.; Klapötke, T. M.; Pimerzin, A. A.; Verevkin, S. P., Benchmark properties of 2-, 3- and 4-nitrotoluene: Evaluation of thermochemical data with complementary experimental and computational methods. *J. Chem. Thermodyn* **2017**, *111* (Supplement C), 271–278.
182. Wang, B.; Wu, Y.; Jiang, B.; Song, H.; Li, W.; Jiang, Y.; Wang, C.; Sun, L.; Li, Q.; Li, A., Optimized degradation removal of 2-nitrotoluene by combination of cathodic reduction and electro-oxidation process. *Electrochim. Acta* **2016**, *219* (Supplement C), 509–515.
183. Sangeetha, K.; Guru Prasad, L.; Mathammal, R., Structural elucidation and physicochemical properties of an organic NLO crystal: 4-Nitrotoluene-2-sulphonic acid dihydrate. *J. Mol. Struct.* **2017**, doi: 10.1016/ j.molstruc.2017.11.048.
184. Kumar, A.; Kumar, P.; Paul, S.; Jain, S. L., Visible light assisted reduction of nitrobenzenes using $Fe(bpy)_3^{+2}$/rGO nanocomposite as photocatalyst. *Appl. Surf. Sci.* **2016**, *386* (Supplement C), 103–114.
185. Sharma, D.; Mishra, S., Chemical reactivity of coal under Friedel-Crafts reaction conditions: Effect of nature of solvent, alkylating agent and catalyst on extractability of coal through a complex series reaction (ATD 3 reaction). *Fuel* **1995**, *74*, 913–916.
186. Reddy, B. M.; Rao, K. N.; Reddy, G. K.; Bharali, P., Characterization and catalytic activity of V_2O_5/Al_2O_3-TiO_2 for selective oxidation of 4-methylanisole. *J. Mol. Catal. A: Chem.* **2006**, *253* (1), 44–51.
187. Sladojevich, F.; Michaelides, I. N.; Darses, B.; Ward, J. W.; Dixon, D. J., Expedient route to the functionalized calyciphylline A-type skeleton via a Michael addition–RCM strategy. *Org. Lett.* **2011**, *13* (19), 5132–5135.
188. Kedrowski, B. L.; Hoppe, R. W., A Concise synthesis of (±)-cacalol. *J. Org. Chem.* **2008**, *73* (13), 5177–5179.
189. Bianco, G. G.; Ferraz, H. M. C.; Costa, A. M.; Costa-Lotufo, L. V.; Pessoa, C.; de Moraes, M. O.; Schrems, M. G.; Pfaltz, A.; Silva, L. F., (+)- and (−)-Mutisianthol: First total synthesis, absolute configuration, and antitumor activity. *J. Org. Chem.* **2009**, *74* (6), 2561–2566.
190. Kioko, J.; Taylor, K.; Milne, H. J.; Hayes, K. Z.; Kiffner, C., Temporal gland secretion in African elephants (*Loxodonta africana*). *Mamm Biol.* **2017**, *82* (Supplement C), 34–40.

191. Tang, R.; Webster, F. X.; Müller-Schwarze, D., Phenolic compounds from male castoreum of the North American beaver, *Castor canadensis*. *J. Chem. Ecol.* **1993**, *19* (7), 1491–1500.
192. Usha, S. P.; Gupta, B. D., Urinary *p*-cresol diagnosis using nanocomposite of ZnO/MoS_2 and molecular imprinted polymer on optical fiber based lossy mode resonance sensor. *Biosens. Bioelectron.* **2018**, *101* (Supplement C), 135–145.
193. Wang, C.-S.; Liao, Z.-K., Synthesis of high purity *o*-cresol formaldehyde novolac epoxy resins. *Polym. Bull.* **1991**, *25* (5), 559–565.
194. Hanada, H., Phenolic antioxidant 2,6-di-*tert*-butyl-*p*-cresol (vitamin E synthetic analogue) does not inhibit 1,1'-dimetyl-4,4'-bipyridium dichloride (paraquat)-induced structural chromosomal damage in cultured leukocytes of the dark-spotted-frog Pelophylax (Rana) nigromaculatus. *Hereditas* **2012**, *149* (5), 173–177.
195. Kondapaneni, R. V.; Virendra, U.; Vedantam, S., Study of effect of parameters on separation of cresol isomers. *J. Environ. Chem. Eng.* **2017**, *5* (5), 5280–5284.
196. Bruno, I. J.; Cole, J. C.; Edgington, P. R.; Kessler, M.; Macrae, C. F.; McCabe, P.; Pearson, J.; Taylor, R., New software for searching the Cambridge Structural Database and visualizing crystal structures. *Acta Crystallogr. B* **2002**, *58* (3 Part 1), 389–397.
197. Macrae, C. F.; Bruno, I. J.; Chisholm, J. A.; Edgington, P. R.; McCabe, P.; Pidcock, E.; Rodriguez-Monge, L.; Taylor, R.; van de Streek, J.; Wood, P. A., Mercury CSD 2.0 - new features for the visualization and investigation of crystal structures. *J. Appl. Crystallogr.* **2008**, *41* (2), 466–470.
198. Taylor, R.; Macrae, C. F., Rules governing the crystal packing of mono- and dialcohols. *Acta Crystallogr. B* **2001**, *57* (6), 815–827.
199. Xie, J.-S.; Hu, X.-Y.; Shan, Z.-X.; Zhou, Z.-Q., A Straightforward and practical approach to chiral inducer: (2*R*,3*R*)-1,4-dimethoxy-1,1,4,4-tetraphenylbutane-2,3-diol. *Aust. J. Chem.* **2015**, *68* (6), 995–998.